

Trinity College Dublin
Coláiste na Tríonóide, Baile Átha Cliath
The University of Dublin

Smurfit Institute of Genetics
School of Genetics and Microbiology

# Investigating Immune and Vascular Mechanisms in Glaucoma

A thesis submitted to Trinity College Dublin, the University of Dublin for the Degree of Doctor of Philosophy

2026

**Jeff Henderson**

Under the supervision of Professor Matthew Campbell

**Declaration**

I declare that this thesis has not been submitted as an exercise for a degree at this or another university and it is entirely my own work, except where noted below:

Dr. Ester Reina Torres, Trinity College Dublin, performed the intracameral injection of IL-18 and subsequent measurement of outflow facility in Figure 3.2.11.

Dr. Paul Cassidy, Trinity College Dublin, performed outflow facility measurement in *Asc*$^{-/-}$ and *Il18*$^{-/-}$ mice in Figures 3.2.13 and 3.2.14.

Dr. Avril Reddy, Trinity College Dublin, generated the supplementary C57BL/6J control RNA-seq dataset used in Chapter 5 (Method 2.13).

I agree to deposit this thesis in the University's open access institutional repository or allow the library to do so on my behalf, subject to Irish Copyright Legislation and Trinity College Library conditions of use and acknowledgment.

I consent to the examiner retaining a copy of the thesis beyond the examining period, should they so wish (EU GDPR May 2018).



Jeff Henderson

**Acknowledgements**

They say that it takes a village to raise a child. In much the same way, it takes a lab to raise a scientist. I have been fortunate to work with some amazing people over the past 4 years, without whom this project would not have been possible.

Firstly, I would like to thank my supervisor, Prof. Matthew Campbell for giving me the opportunity to conduct my PhD research in his lab. His mentorship, both academically and professionally, has been invaluable, providing me with a strong foundation for the next stage of my scientific career. The Campbell lab has been an extremely supportive and motivating environment to work, which is a testament to his leadership and drive.

I would also like to give a special thanks to the lab's resident glaucoma expert and all-round problem solver, Dr. Jeffrey O'Callaghan. His technical expertise, seemingly infinite patience, and willingness to help at every stage have been instrumental to getting this project over the line.

I would also like to extend thanks to other members of the Campbell Lab who have helped me along the way. Thank you to Dr. Natalie Hudson for being incredibly helpful with all things animal-related. Thank you to Drs. Avril Reddy and Kieva Byrne for serving as a great role models to me over the years, right back to supervising my undergraduate project. Avril, thank you in particular for always coming to my assistance whenever I walked into the lab looking lost. A big thank you to my office co-habitants Dr. Chris Greene and Adam McGlinchey. Our coffee runs were scientifically stimulating and great craic in equal measure and I will look back on them very fondly. Thank you as well to all members of the lab past and present who I haven't mentioned by name here. In addition to being great colleagues, you have been wonderful friends, and for that I am most grateful.

I would also like to thank the people in my life outside of the lab whose support has been just as important in making this work possible. Thank you to my parents, Elena and Maurice, my sister, Sophie, and my brother, Matthew. Your support has gotten me to this point in my life and I feel incredibly lucky to have you in my corner. Thank you as well to all my Carnew St friends and my partner Talia for getting me through some of the harder days. I love you all very much.

**Summary**

Glaucoma is a group of optic neuropathies characterised by progressive retinal ganglion cell (RGC) degeneration. It is the leading cause of irreversible blindness worldwide, affecting upwards of 80 million people. Elevated intraocular pressure (IOP) is the only modifiable risk factor for the disease, and current treatments therefore focus on reducing IOP, most commonly with topical medications. However, these medications are suboptimal, as they do not address the underlying cause of IOP elevation, which is increased resistance to aqueous humour (AH) outflow through the conventional outflow pathway. Additionally, many patients respond inadequately, and adherence to long-term dosing schedules is often poor, thus limiting the effectiveness of these interventions. Surgical procedures are available for treatment resistant cases, but these are invasive and carry significant risk of complications. Importantly, existing treatments do not target the root cause of vision loss: RGC death. There is therefore a need both for new therapies that more effectively lower IOP by reducing conventional outflow resistance, and for neuroprotective strategies that directly prevent RGC degeneration. Progress in both of these areas has been limited by an incomplete understanding of the disease's pathophysiology.

The first objective of this project, addressed in Chapter 3 was to determine whether modulation of inflammatory pathways in the anterior segment can alter AH outflow and therefore IOP in glaucoma. In DBA/2J mice, the anterior chamber displayed a pro-inflammatory profile with increased infiltration of activated myeloid-lineage cells, upregulation of the inflammasome receptors NLRP3 and AIM2, and elevated levels of IL-1β and IL-18. These findings are consistent with canonical inflammasome activation and loss of ocular immune privilege, suggesting that sterile inflammation contributes to elevated IOP in this model. Intracameral injection of canonical inflammasome effector cytokines produced opposing effects on outflow facility, with IL-18 reducing and IL-1β enhancing outflow. Outflow facility was increased in *Asc*$^{-/-}$ mice relative to wild-type controls, indicating that under physiological conditions, canonical inflammasome activation decreases outflow facility. To assess the role of non-canonical signalling, caspase-11-deficient (*Casp11*$^{-/-}$) mice were subjected to dexamethasone-induced ocular hypertension (OHT), developing higher IOP and reduced outflow facility relative to wild-type controls, indicating a potential protective role for caspase-11. Collectively, these

findings establish inflammation as a modulator of AH outflow and highlight the canonical inflammasome as potential therapeutic target for lowering IOP.

The second objective of this project, addressed in Chapters 4 and 5, was to determine whether retinal vascular dysfunction is a feature of glaucoma, its timing in relation to RGC loss, and underlying mechanisms. In Chapter 4, IOP, retinal vascular integrity, and retinal structure were examined in DBA/2J mice and in mice with dexamethasone-induced OHT. Fundus fluorescein angiography (FFA) revealed increased retinal vascular leakage in DBA/2J mice from 6 months of age, coinciding with inner retinal thinning on optical coherence tomography (OCT), while dexamethasone-treated mice showed increased leakage after 4 weeks, preceding inner retinal thinning. These findings indicate that vascular leakage is an early consequence of OHT and may precede RGC degeneration. Immunostaining showed reduced Mfsd2a levels, but unchanged claudin-5 levels, in the inner retina of both models, implicating increased transcytosis as the mechanism of leakage. In Chapter 5, analysis of RNA-seq data from microbead OHT and optic nerve crush (ONC) models revealed *Cav1* upregulation and transcriptional signatures of endothelial activation, inner blood-retinal barrier (iBRB) dysfunction, and innate immune activation in both models. These findings further highlight increased transcytosis and vascular dysfunction as common features of murine glaucoma and point to retinal inflammation as a mediating mechanism. In the microbead model, a biphasic inflammatory response was observed, with an early upregulation of innate immune signalling, an intermediate phase of partial resolution with vascular remodelling signatures, and a later resurgence of innate immune activation coinciding with RGC loss. The presence of vascular dysfunction signatures in the ONC model indicated that RGC degeneration itself can exacerbate vascular dysfunction, suggesting a self-reinforcing cycle of inflammation and vascular leakage once neurodegeneration is established.

In summary, this thesis provides evidence that dysregulated inflammation and retinal vascular dysfunction contribute to the pathophysiology of glaucoma. It establishes sterile inflammation as a regulator of AH outflow and identifies the canonical inflammasome as a potential therapeutic target for IOP control. It also provides evidence that retinal vascular dysfunction is a common and potentially causal mediator of RGC loss across multiple models of glaucoma. Ultimately, this work supports the view of glaucoma as a systemic disease that leads to a loss of ocular homeostasis, rather than a disease of elevated IOP or RGC loss in isolation.

**Publications arising from this work**

Henderson, J., O'Callaghan, J., & Campbell, M. (2024). Gene therapy for glaucoma: Targeting key mechanisms. *Vision research*, *225*, 108502. **(Appendix 3)**

Table of contents

*Declaration* ..... *3*

*Acknowledgements* ..... *5*

*Summary* ..... *6*

*Publications arising from this work* ..... *8*

*Table of contents* ..... *9*

*Table of figures* ..... *13*

*Glossary of abbreviations* ..... *15*

*Chapter 1: General Introduction* ..... *18*

1.1 The eye and visual transduction ..... 19

1.2 AH flow dynamics ..... 21

AH production ..... 23

Outflow resistance generation ..... 24

1.3 Glaucoma ..... 27

Subtypes of glaucoma ..... 29

Primary OAG ..... 29

Normal tension glaucoma ..... 30

Primary ACG ..... 31

Secondary glaucoma ..... 33

Effect of OHT on RGCs ..... 35

1.4 Current treatments for glaucoma ..... 40

IOP lowering medications ..... 41

Surgical interventions ..... 42

1.5 Mouse models of glaucoma ..... 44

DBA/2J ..... 45

Dexamethasone-induced OHT ..... 46

Microbead-induced OHT ..... 47

ONC ..... 48

1.6 Project aims ..... 49

*Chapter 2: Materials and Methods* ..... *51*

2.1 Animals ..... 52

2.2 Dissection of murine anterior segments for immunostaining ..... 52

2.3 Immunostaining of murine anterior segments ..... 53

2.4 Dexamethasone-induced OHT ..... 54

2.5 IOP measurement ..... 55

2.6 Measurement of outflow facility ..... 55

2.7 Intracameral injection ..... 56

2.8 In vivo retinal imaging ..... 56

2.9 Quantification of retinal layer thickness from OCT ..... 57

2.10 Quantification of retinal vascular leakage from FFA ..... 57

2.11 Biotin permeability assay ..... 57

2.12 Immunostaining of retinal cryosections ..... 58

2.13 RNA-seq of C57BL/6J control mice ..... 59

2.14 RNA seq analysis ..... 60

2.15 Statistical analysis ..... 61

*Chapter 3: Investigating the role of inflammation in regulating AH outflow* ..... *62*

3.1 Introduction ..... 63

3.1.1 Innate immunity and sterile inflammation ..... 63

3.1.2 Inflammasomes and pyroptosis ..... 63

3.1.3 Sterile inflammation and outflow resistance ..... 67

3.1.4 Chapter aims ..... 68

3.2 Results ..... 70

3.2.1 Immunohistochemical profiling of the anterior chamber in glaucomatous mice ..... 70

3.2.2 Dissecting canonical and non-canonical inflammasome signalling in AH outflow regulation ..... 87

3.3 Discussion ..... 97

3.3.1 Pro-inflammatory profile in the anterior uvea of DBA/2J mice ..... 97
3.3.2 Canonical inflammasome activation decreases outflow facility ..... 98
3.3.3 Potential protective role of caspase-11 in steroid induced glaucoma ..... 100
3.3.4 Conclusions ..... 101

*Chapter 4: Investigating iBRB integrity in mouse models of glaucoma ..... 103*

4.1 Introduction ..... 104
4.1.1 The blood-retinal barrier ..... 104
4.1.2 TJs control paracellular transport ..... 106
4.1.3 Caveolin-mediated transcytosis at the iBRB ..... 108
4.1.4 The vascular theory of glaucoma ..... 108
4.1.5 The iBRB in glaucoma ..... 109
4.1.6 Chapter aims ..... 110

4.2 Results ..... 111
4.2.1 Early subretinal fluid accumulation and BRB dysfunction in DBA/2J mice . 111
4.2.2 iBRB leakage precedes structural RGC loss in mice with dexamethasone-induced OHT ..... 120
4.2.3 Immunostaining for iBRB components in OHT models ..... 125

4.3 Discussion ..... 131
4.3.1 Existence of iBRB leakage in OHT models ..... 131
4.3.2 Temporal relationship between IOP elevation, retinal vascular leakage, and RGC loss ..... 132
4.3.3 Outer retinal abnormalities in DBA/2J mice ..... 134
4.3.4 Mechanism of vascular leakage ..... 134
4.3.5 Conclusions ..... 136

*Chapter 5: Transcriptomic profiling of the iBRB in glaucoma ..... 137*

5.1 Introduction ..... 138
5.1.1 NVU activation contributes to loss of iBRB integrity ..... 138
5.1.2 Immune cell infiltration into the CNS ..... 139
5.1.3 Inflammation and RGC death in glaucoma ..... 140
5.1.4 Chapter aims ..... 141

5.2 Results ..... 142
5.2.1 Early vascular expression changes in mice with microbead-induced OHT ... 142

5.2 Vascular expression changes in the ONC model those mirror those in the microbead induced OHT model ..... 154
5.3 Discussion ..... 164
5.3.1 Upregulation of *Cav1* supports transcytosis-mediated iBRB leakage mechanism ..... 164
5.3.2 Early endothelial activation in microbead-induced OHT ..... 165
5.3.3 Biphasic inflammatory response in the retina following OHT ..... 167
5.3.4 Late iBRB-associated expression changes in ONC mirror microbead model 168
5.3.5 Conclusions ..... 169
*Chapter 6 General Discussion* ..... *170*
6.1 Inflammation as an IOP regulating mechanism ..... 171
6.2 Inflammation as a therapeutic target for IOP control ..... 173
6.3 Retinal vascular dysfunction as a feature of glaucoma ..... 174
6.4 Challenges in targeting the retinal vasculature for neuroprotection ..... 177
6.5 Glaucoma as a systemic disease ..... 178
6.6 Limitations and future directions ..... 179
6.7 Conclusion ..... 181
*Bibliography* ..... *182*
*Appendix 1: DEG list for RNA-seq analysis* ..... *233*
*Appendix 2: GSEA output tables* ..... *246*
*Appendix 3: Publications arising from this work* ..... *260*

**Table of figures**

Figure 1.1| Anatomy of the eye ..... 20
Figure 1.2| Histology of the retina ..... 21
Figure 1.3| AH flow dynamics ..... 23
Figure 1.4| Structure of the conventional outflow pathway ..... 26
Figure 1.5| Outflow resistance and elevated IOP in glaucoma ..... 33
Figure 1.6| Glaucomatous neurodegeneration ..... 38
Figure 3.1.1| Two signal model of NLRP3 inflammasome signalling ..... 66
Figure 3.2.1 | Regions of the anterior chamber analysed by immunostaining ..... 70
Figure 3.2.2| F4/80 immunostaining in DBA/2J anterior segments ..... 72
Figure 3.2.3| CD11b immunostaining in DBA/2J anterior segments ..... 74
Figure 3.2.4| CD68 immunostaining in DBA/2J anterior segments ..... 76
Figure 3.2.5| NLRP3 immunostaining in DBA/2J anterior segments ..... 78
Figure 3.2.6| AIM2 immunostaining in DBA/2J anterior segments ..... 80
Figure 3.2.7| NLRP1 immunostaining in DBA/2J anterior segments ..... 82
Figure 3.2.8| NLRC4 immunostaining in DBA/2J anterior segments ..... 83
Figure 3.2.9| IL-1β immunostaining in DBA/2J anterior segments ..... 85
Figure 3.2.10| IL-18 immunostaining in DBA/2J anterior segments ..... 86
Figure 3.2.11| Outflow facility following intracameral injection of IL-18 ..... 88
Figure 3.2.12| Outflow facility following intracameral injection of IL-1β ..... 89
Figure 3.2.13| Outflow facility in *Il18* $^{-/-}$ mice ..... 91
Figure 3.2.14| Outflow facility in *Asc*$^{-/-}$ mice ..... 92
Figure 3.2.15| IOP in *Casp11*$^{-/-}$ mice following dexamethasone treatment ..... 94
Figure 3.2.16| Outflow facility in *Casp11*$^{-/-}$ mice following dexamethasone treatment ..... 96
Figure 4.1.1| Anatomical location of BRBs ..... 105
Figure 4.1.2| Molecular structure of TJs at the iBRB ..... 107
Figure 4.2.1| Schematic of in vivo imaging protocol in DBA/2J mice ..... 111
Figure 4.2.2| IOP measurement in DBA/2J mice ..... 112
Figure 4.2.3| Fundus images of DBA/2J mice ..... 113
Figure 4.2.4| OCT scans in 3-month old DBA/2J mice ..... 114
Figure 4.2.5| OCT scans in 6-month old DBA/2J mice ..... 115
Figure 4.2.6| FFA in 3-month old DBA/2J mice ..... 116
Figure 4.2.7| FFA in 6-month old DBA/2J mice ..... 117

Figure 4.2.8| Correlation between IOP and cumulative FFA intensity in 6 month old DBA/2J mice ..... 118
Figure 4.2.9| Ex vivo biotin extravasation in 9-month old DBA/2J mice ..... 119
Figure 4.2.10| In vivo imaging protocol in mice with dexamethasone-induced OHT..... 120
Figure 4.2.11| IOP progression in mice with dexamethasone-induced OHT..... 121
Figure 4.2.12| OCT scans of mice with dexamethasone-induced OHT..... 122
Figure 4.2.13| FFA in dexamethasone-treated mice..... 123
Figure 4.2.14| Correlation between IOP elevation and final FFA intensity in dexamethasone-induced OHT..... 124
Figure 4.2.15 | Claudin-5 immunostaining in OHT models ..... 126
Figure 4.2.16 | VE-Cadherin immunostaining in OHT models ..... 128
Figure 4.2.17 | Mfsd2a immunostaining in OHT models ..... 130
Figure 5.2.1| Outline of groups for RNA-seq analysis of microbead-induced OHT model ..... 142
Figure 5.2.2 | PCA of microbead-induced OHT samples ..... 143
Figure 5.2.3| Differential gene expression at 3 days post-OHT induction..... 144
Figure 5.2.4| Differential gene expression at 2 weeks post-OHT induction..... 145
Figure 5.2.5| Differential gene expression at 6 weeks post-OHT induction..... 146
C)..... 150
Figure 5.2.6| GSEA plots for microbead-induced OHT model..... 150
Figure 5.2.7| Gene plots of markers of iBRB dysfunction in microbead-induced OHT model..... 152
Figure 5.2.8| Gene plots of RGC markers in microbead-induced OHT model ..... 153
Figure 5.2.9| Outline of groups for RNA-seq analysis of ONC model..... 154
Figure 5.2.10 | PCA of ONC samples ..... 155
Figure 5.2.11| Differential gene expression at 3 days post-ONC injury ..... 156
Figure 5.2.12| Differential gene expression at 2 weeks post-ONC injury ..... 157
Figure 5.2.13| GSEA plots for ONC model ..... 160
Figure 5.2.14| Gene plots of markers of iBRB dysfunction in ONC model..... 162
Figure 5.2.15| Gene plots of RGC markers in ONC model ..... 163

**Glossary of abbreviations**

| | |
|---|---|
| ACAID | Anterior chamber-associated immune deviation |
| ACG | Angle-closure glaucoma |
| AH | Aqueous humour |
| AQP | Aquaporin |
| BBB | Blood-brain barrier |
| BDNF | Brain-derived neurotrophic factor |
| BRB | Blood-retinal barrier |
| Cav-1 | Caveolin 1 |
| CNTF | Ciliary neurotrophic factor |
| CNS | Central nervous system |
| CSF | Cerebrospinal fluid |
| DAMP | Damage associated molecular pattern |
| DEG | Differentially expressed gene |
| ECM | Extracellular matrix |
| ER | Endoplasmic reticulum |
| FFA | Fundus fluorescein angiography |
| GC | Glucocorticoid |
| GDNF | Glial cell-line derived neurotrophic factor |
| GO | Gene Ontology |
| GR | Glucocorticoid receptor |
| GSDMD | Gasdermin-D |
| GSEA | Gene set enrichment analysis |
| GWAS | Genome-wide association studies |
| iBRB | Inner blood-retinal barrier |
| IL | Interleukin |
| IOP | Intraocular pressure |
| IPL | Inner plexiform layer |
| JAM | Junctional adhesion molecule |
| JCT | Juxtacanalicular tissue |
| LC | Lamina cribrosa |
| LGN | Lateral geniculate nucleus |

| | |
|---|---|
| LPI | Laser peripheral iridotomy |
| LPS | Lipopolysaccharide |
| MAVS | Mitochondrial antiviral signalling protein |
| MIGS | Minimally invasive glaucoma surgery |
| MMP | Matrix metalloproteinase |
| NES | Normalised enrichment score |
| NGF | Nerve growth factor |
| NLR | NOD-like receptor |
| NTG | Normal tension glaucoma |
| NVU | Neurovascular unit |
| OAG | Open-angle glaucoma |
| oBRB | Outer blood-retinal barrier |
| OCT | Optical coherence tomography |
| OHT | Ocular hypertension |
| ONC | Optic nerve crush |
| ONH | Optic nerve head |
| OPL | Outer plexiform layer |
| PACG | Primary angle closure glaucoma |
| PAMPs | Pathogen associated molecular patterns |
| PAS | Peripheral anterior synechiae |
| PBS | Phosphate buffered saline |
| PCA | Principal component analysis |
| PDGFB | Platelet derived growth factor subunit B |
| PDS | Pigment dispersion syndrome |
| PEX | Pseudoexfoliation syndrome |
| PEXG | Pseudoexfoliative glaucoma |
| POAG | Primary open angle glaucoma |
| PRR | Pathogen recognition receptor |
| REC | Retinal endothelial cell |
| RGC | Retinal ganglion cell |
| RNFL | Retinal nerve fibre layer |
| ROS | Reactive oxygen species |
| RPE | Retinal pigment epithelium |

| | |
|---|---|
| SC | Schlemm’s canal |
| SCEC | Schlemm’s canal endothelial cell |
| SLT | Selective laser trabeculoplasty |
| TAMP | TJ-associated marvel protein |
| TEM | Transendothelial migration |
| TGF-β | Transforming growth factor-β |
| TJ | Tight junction |
| TM | Trabecular meshwork |
| TNF | Tumour necrosis factor |
| VEGF | Vascular endothelial growth factor |
| VST | Variance stabilised transformation |
| ZO | Zona occludens |

# Chapter 1: General Introduction

## 1.1 The eye and visual transduction

The eye is a highly specialised sensory organ that enables vision, one of the most important senses for humans and many animals. By capturing light and converting it into electrical signals, the eye facilitates the processing and interpretation of visual information in the brain, forming images. The human eyeball comprises three primary layers: the outermost supporting layer, which includes the cornea, the sclera, and their transitional zone known as the limbus; the middle uveal layer, which forms the vascular core of the eye and consists of the iris, ciliary body, and choroid; and the innermost layer, the retina (Kels et al., 2015). The human eye can be further subdivided into three chambers: the anterior chamber, the posterior chamber, and the vitreous cavity. The anterior chamber is located between the posterior surface of the cornea and the anterior surface of the iris and lens. This chamber is filled with aqueous humour (AH), a clear fluid with a high rate of turnover that provides nutrients to the avascular tissues of the front of the eye, and mechanical support through maintaining intraocular pressure (IOP). Behind the anterior chamber lies the posterior chamber, which is bordered by the posterior surface of the iris at the front, the anterior surface of the zonular fibres at the back, the crystalline lens at its centre, and the ciliary processes at its periphery. The vitreous cavity is enclosed by the zonular fibres, the ciliary body, and the posterior surface of the crystalline lens on its anterior side, while its posterior boundary is formed by the retina and the optic nerve (Fig. 1.1). The vitreous cavity is filled with vitreous humour, an optically clear gelatinous substance with a low turnover rate that provides shape to the eye and maintains optical clarity (Kels et al., 2015).

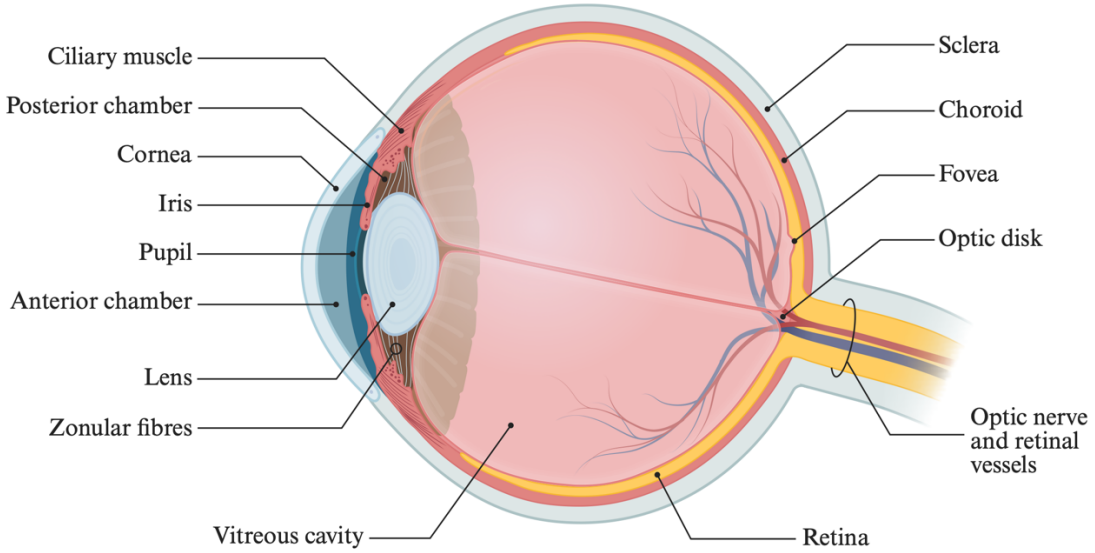



**Figure 1.1| Anatomy of the eye**

*Schematic of the human eye with key anatomical features highlighted. Created with BioRender.*

The visual process begins as light enters the eye through the cornea, traversing the anterior chamber and passing through the pupil and the lens. From there, the light travels through the vitreous humour and ultimately reaches the retina, a specialised tissue at the back of the eye responsible for capturing and transmitting visual information. The retina, considered a peripheral extension of the central nervous system (CNS), originates during embryonic development as an outpocketing of brain neural tissue (London et al., 2013). It contains a variety of specialised neurons, including photoreceptor cells, which detect light and initiate the visual signalling process. The macula is a structure positioned at the centre of the retina and is crucial for high-acuity central vision. The fovea is a small pit within the macula that is densely packed with cone photoreceptors responsible for colour perception and sharp vision. Rod and cone photoreceptors in the outer retina interact with photons through pigments stored in the membranous disks of their outer segments. In darkness, photoreceptors are depolarised and continuously release glutamate at synapses in the outer plexiform layer (OPL). Absorption of photons leads to hyperpolarisation of the photoreceptor membrane, resulting in a reduction in neurotransmitter release, which is detected by bipolar cells. These bipolar cells serve as intermediaries, transmitting signals to the synapses of retinal ganglion cells (RGCs) in the inner plexiform layer (IPL). RGCs then carry the action potentials generated by these signals out of the retina. Their axons

converge at the optic nerve head (ONH) to form the optic nerve, which transmits the signals to the brain for higher-level processing (Fig. 1.2). Additionally, horizontal cells in the retina facilitate lateral interactions in the OPL, while amacrine cells perform similar functions in the IPL, which enhance the contrast sensitivity of the system.

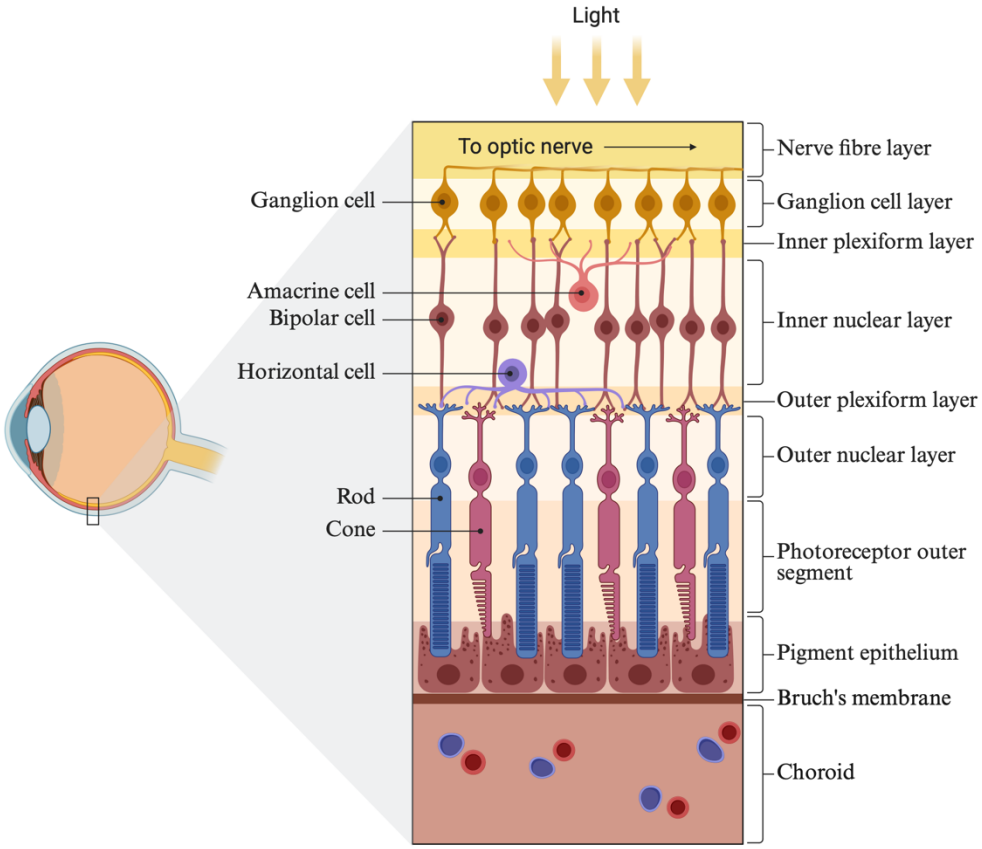



**Figure 1.2| Histology of the retina**

*Schematic cross section of the mammalian retina. Light enters from the anterior side and passes through successive retinal layers. Key cell types involved in visual transduction, as well as retinal layers, are highlighted. Created with BioRender.*

### 1.2 AH flow dynamics

AH is a clear fluid that is secreted from the ciliary epithelium, a bilayer of cells located on the surface of the ciliary processes that project from the ciliary body. The lens and cornea are avascular, as they must remain transparent to allow for light transmission. With a low protein concentration and an optical density similar to that of water, AH serves as a

surrogate for blood in these structures, supplying them with nutrients, removing waste metabolic products, and permitting inflammatory cells and mediators to circulate in the eye under pathological conditions. The flow of AH is also important for providing shape to the globe of the eye via the generation of IOP (Goel et al., 2010; To et al., 2002). AH moves from the posterior chamber to the anterior chamber of the eye via the pupil. Here, a temperature gradient gives rise to a convective flow pattern, downwards from the cooler corneal surface and upwards from the warmer interior of the eye (Heys & Barocas, 2002). IOP is controlled by the dynamic balance between AH production (inflow) and its drainage (outflow) through two key pathways at the iridocorneal angle. The first pathway, the conventional outflow pathway, involves AH passing through the trabecular meshwork (TM), crossing the inner wall of Schlemm's canal (SC) into its lumen, followed by drainage through collector channels into aqueous veins that ultimately drain into the episcleral venous circulation (Goel et al., 2010)**.** The unconventional outflow pathway encompasses all non-trabecular AH outflow. Unconventional flow passes through the interstitial spaces between ciliary muscle fibres and into the supraciliary and suprachoroidal spaces (Fig. 1.3). From these spaces, AH can either be resorbed by orbital vessels (the uveoscleral pathway) or drained through the vortex veins via the choroid (the uveovortex pathway) (Johnson et al., 2017). The conventional outflow pathway is predominant in humans, accounting for approximately 85% of AH outflow (Bill & Phillips, 1971). This predominance becomes more pronounced with age (Toris et al., 1999).

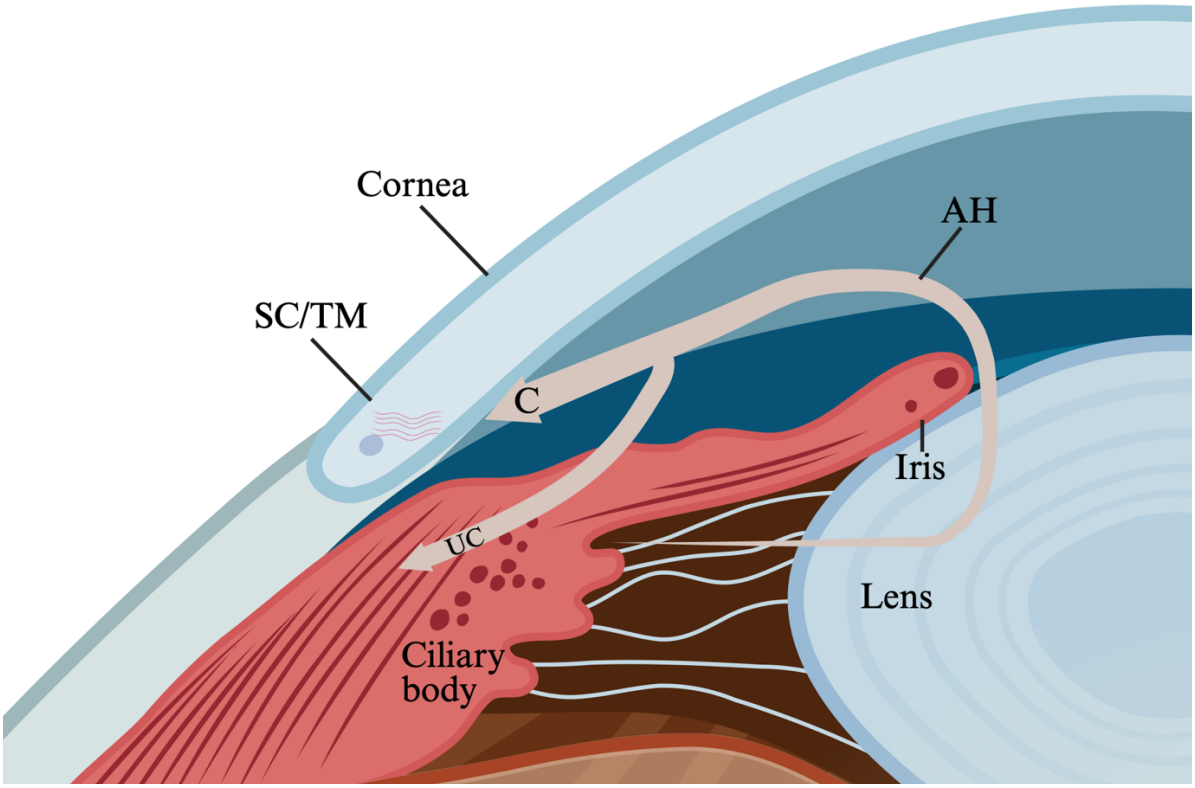



**Figure 1.3| AH flow dynamics**

*Upon secretion from the ciliary body, AH moves from the posterior to the anterior chamber of the eye via the pupil. A temperature gradient causes AH to move downwards from the corneal surface, where it is drained via either the conventional outflow pathway (C) or the unconventional outflow pathway (UC). The conventional outflow pathway, involves AH passing through the TM, crossing the inner wall of SC into its lumen. Unconventional flow passes through the interstitial spaces between ciliary muscle fibres into the supraciliary and suprachoroidal spaces. Created with BioRender. Adapted from Henderson et al. (2024) and O'Callaghan, Cassidy, et al. (2017).*

## AH production

AH is derived from plasma and enters the posterior chamber after traversing the capillary endothelium, the stroma of the ciliary processes, and the ciliary epithelial bilayer. The blood-aqueous barrier is formed primarily by tight junctions (TJs) between non-pigmented epithelial cells of the ciliary epithelium. TJs between endothelial cells in ciliary processes, in the iris vasculature, and between SC endothelial cells (SCECs) also contribute to the blood-aqueous barrier (Coca-Prados, 2014). AH formation involves diffusion,

ultrafiltration, and active secretion. Diffusion allows lipid-soluble molecules to move passively along their concentration gradient, while ultrafiltration permits limited movement of water and small solutes across the fenestrated endothelial lining of ciliary capillaries into the stroma. In contrast to these passive mechanisms, active secretion is the predominant mechanism, accounting for 80-90% of AH production. This process occurs primarily in the non-pigmented epithelial cells facing the posterior chamber (Goel et al., 2010).

Active transport involves the selective movement of ions and other solutes across the ciliary epithelium, primarily transcellularly via membrane-embedded transport proteins. This process is responsible for generating the electrochemical gradients that ultimately drive AH formation. Multiple transporters mediate the movement of ions such as $Cl^-$, $HCO_3^-$, and $Na^+$, in addition to biomolecules such as ascorbic acid and amino acids, across the epithelial layer (Goel et al., 2010). Aquaporins (AQPs) facilitate rapid water movement across the epithelium in response to these ion-driven osmotic gradients. Among these, AQP1 and AQP4 have been shown to contribute to AH secretion (Yamaguchi et al., 2006). Once secreted, AH consists primarily of water and carries ions, carbohydrates, amino acids, proteins, and dissolved gases. A key difference between AH and plasma is the significantly lower protein concentration in AH, which contains ~200-fold less protein. In contrast, glucose and urea levels in AH are approximately 80% of their plasma concentrations (Goel et al., 2010).

**Outflow resistance generation**

The rate of AH outflow via the conventional outflow pathway is the primary determining factor of IOP, with increased resistance to outflow giving rise to ocular hypertension (OHT). While many components of the conventional outflow pathway are involved in the generation of outflow resistance, their precise contributions have not been fully resolved. The filtering portion of the TM is divided into three consecutive regions: the uveal meshwork, which is located nearest to the anterior chamber; the corneoscleral meshwork, which is central; and the juxtacanalicular/cribriform meshwork (JCT), which is in direct contact with the inner wall of SC (Fig. 1.4) (Abu-Hassan et al., 2014). The uveal and corneoscleral meshworks are highly porous networks of connective tissue beams (lamellae), on which TM cells reside. Openings range from 25-75 μm at the proximal side of the uveal meshwork and gradually become smaller towards the distal side, ranging from 2-15 μm in the deeper layers of the corneoscleral meshwork (Johnson, 2006). As a

consequence of their large fenestrations, the contribution of these regions to outflow resistance is negligible (Grant, 1963). Rather, due to the phagocytic qualities of their resident TM cells, these layers serve as pre-filters, removing large debris from the AH before it reaches the less porous JCT and SC, where it could lead to blockage and pathological changes in outflow resistance (Stamer & Clark, 2017).

The JCT, in contrast, is composed of a loosely arranged extracellular matrix (ECM) in which a small number of JCT TM cells are embedded (Tamm, 2009). JCT TM cells are functionally and anatomically distinct from those of the uveal and corneoscleral meshwork, displaying fibroblastic and smooth-muscle-like properties (Patel et al., 2020; Stamer & Clark, 2017). They are responsible for remodelling the ECM and regulating the contractile tone of the JCT in response to a variety of stimuli (Keller & Acott, 2013). After passing through the JCT, AH then reaches the inner wall of SC. SC is a unique vessel that displays properties of both blood and lymphatic vessels and facilitates flow of AH in the basal to apical direction (Kizhatil et al., 2014; Patel et al., 2020). The endothelial cells of SC's inner wall (SCECs) lie on a discontinuous basement membrane and are attached by TJs (Gong et al., 1996; Grierson et al., 1978). These TJs contribute to outflow resistance, as underscored by the fact that double knockdown of tricellulin and ZO-1 via intracameral injection of siRNA leads to transient increases outflow facility in mice (Tam et al., 2017). Although it had been a matter of debate for several years, it is now widely accepted that AH passes across the inner wall of SC via transendothelial pores in giant vacuoles, which are outpouchings of SCECs that form at high pressure (Pedrigi et al., 2011). Interestingly, the pore density on SCECs is reduced in glaucomatous eyes, relative to healthy eyes, indicating that pore density may be an important determinant of outflow resistance (Johnson et al., 2002).

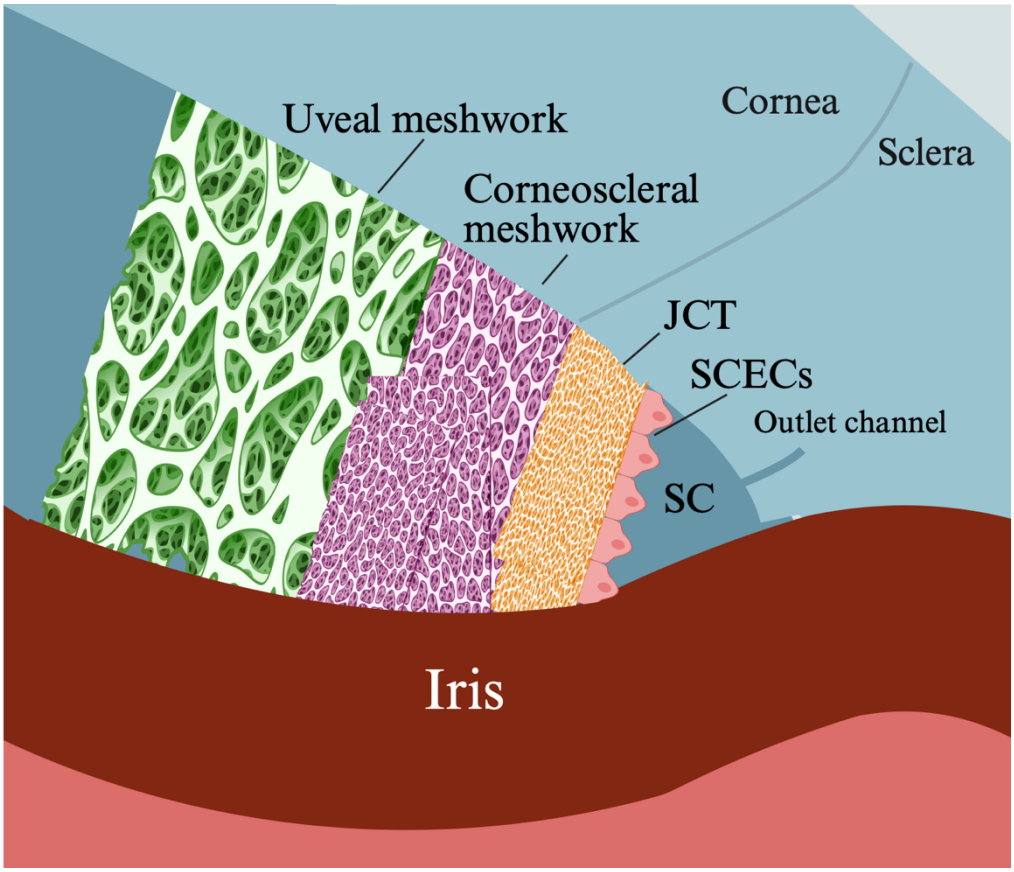



**Figure 1.4| Structure of the conventional outflow pathway**

*Schematic showing the three layers of the TM: Uveal meshwork, corneoscleral meshwork and JCT. The JCT is in direct contact with SCECs, which line SC. AH flows through the TM into SC, where it then drains into episcleral veins via outlet channels. Created with BioRender.*

Early experiments using micro-cannulation to measure the pressure in various structures of the conventional outflow pathway indicated that the majority of outflow resistance lies within 14 µm upstream of SC's inner wall (Mäepea & Bill, 1989, 1992). Since then, a large body of evidence has grown to suggest that the site of outflow resistance is located somewhere along the JCT, the basement membrane of SC, and its inner wall. However, to date, studies have not been able to attribute the bulk of this resistance to any one of these components. This is referred to as the 'paradox of outflow resistance generation' (Overby et al., 2009). It has been postulated that this paradox may be explained by a synergistic model, in which the total resistance generated by the outflow tissue as a whole is greater than that generated by any component in isolation. The leading synergistic model is the 'funnelling model'. According to this model, the association of the JCT with SC's inner wall, in conjunction with the discrete nature of permeable pores on the latter, means that

AH will flow in a non-uniform pattern through the JCT, as flow patterns converge or 'funnel' on a given pore. Consequently, there will be a reduction in the effective area available for flow through the JCT, increasing the effective hydraulic resistance in this region (Overby et al., 2009). One prediction of this model is that outflow resistance would decrease if the JCT and the inner wall of SC were to pull away from one another, as this would lead to a more uniform flow through the JCT. Support for this comes from the 'washout effect'. When bovine eyes are perfused at high pressures, outflow facility increases over time and this increase in facility has been shown to correlate with the degree of separation between the JCT and the SC inner wall. This can be reversed by perfusing eyes at 0 mmHg for one hour, allowing the JCT and SC to associate once more (Overby et al., 2002). The funnelling model could also explain the segmental outflow pattern observed in tracer studies, whereby AH flows through only a fraction of the total area of SC inner wall, as flow may preferentially occur at regions where the JCT is separated from the inner wall (Hann et al., 2005). Further evidence for the funnelling model comes from the fact that that Rho kinase inhibitors increase outflow facility by increasing the separation between the JCT and the SC inner wall (Lu et al., 2008).

### 1.3 Glaucoma

Glaucoma is a group of optic neuropathies characterised by progressive RGC degeneration. Affecting upwards of 80 million people, glaucoma is the leading cause of irreversible blindness worldwide (Tham et al., 2014). While the pathogenesis of glaucoma is not well understood, risk factors include age, family history, and elevated IOP (Weinreb et al., 2014). The normal IOP range in adults is 10-21 mmHg, with IOP values exceeding 21 mmHg being classified as hypertensive (Khaw et al., 2004). There is an established link between OHT and glaucomatous RGC death, as pressure build-up in the anterior chamber leads to excess force being exerted on the retina and the ONH. The ONH is the region where RGC axons converge, creating a depression in the retina known as the optic disk. This area forms a blind spot as it lacks photoreceptors. These axons pass through pores in the lamina cribrosa (LC), a fenestrated, three-dimensional network of load-bearing trabeculae, many of which contain capillaries, that provides structural and nutrient support to the RGC axons as they leave the eye on their path to the brain (Downs & Girkin, 2017). Glaucoma can be broadly classed into what is termed open-angle glaucoma (OAG) and angle-closure glaucoma (ACG). These forms are distinguished based on the state of the

angle between the iris and the cornea (the iridocorneal angle). This is the site of AH drainage, which, when obstructed, leads to increases in IOP. In OAG, drainage is restricted despite the irideocorneal angle remaining open. Contrastingly in ACG, elevated IOP occurs as a direct result of the iris becoming displaced and obstructing the irideocorneal angle. Glaucoma can be further broken down into primary and secondary forms. In primary glaucoma, elevations in IOP are idiopathic, while in secondary glaucoma, OHT is caused by known factors such as systemic disease, trauma, or treatment with corticosteroids (Weinreb et al., 2014).

**Clinical presentation**

Although elevated IOP is linked to glaucoma, OHT alone is neither necessary nor sufficient for a glaucoma diagnosis. The prevalence of OHT in POAG varies significantly across ethnic groups, with an average of 50% of cases having IOPs within the normal range (Kim & Park, 2016; Sommer et al., 1991; Wang et al., 2011). Furthermore, many individuals with elevated IOP never develop glaucoma, even after years of monitoring (Weinreb et al., 2014). Adult-onset OAG often presents asymptomatically in its early stages, with approximately 50% of affected individuals unaware of their condition (McCann et al., 2020). As the disease progresses, patients initially experience difficulties with peripheral vision, followed by central vision impairment, eventually leading to challenges in performing daily activities (Ramulu et al., 2013; Ramulu et al., 2014). Without treatment, this progression can result in irreversible blindness. In contrast, acute ACG is a medical emergency characterised by a rapid increase in IOP. Symptoms include blurred vision, halos around lights, eye pain, nausea, and vomiting, with the potential for rapid onset blindness. Individuals with a narrow iridocorneal angle are at the highest risk for ACG. This risk can be assessed using gonioscopy or anterior segment imaging techniques such as spectral-domain optical coherence tomography (OCT) or ultrasound biomicroscopy (Stein et al., 2021).

Diagnostic tests for glaucoma include perimetry, gonioscopy, IOP measurement, and corneal thickness measurement (allows for true IOP to be ascertained from measured IOP, which can be influenced by corneal properties), and ONH and retinal nerve fibre layer (RNFL) evaluation using OCT and fundus photography. Perimetry assesses visual field loss, which typically begins in the periphery and progresses toward the centre, although

some patients may experience early central vision loss. Sequential perimetry results allow clinicians to monitor changes in visual fields and guide further management of the disease. Structural evaluation of the ONH and RNFL using OCT and fundus photography helps detect glaucomatous damage. Disease progression is often evidenced by increased thinning of the RNFL on sequential OCT scans or by expansion of ONH cupping. Structural damage in specific regions of the ONH or RNFL is frequently associated with corresponding functional loss seen on perimetry (Stein et al., 2021). Recent advances in machine-learning modelling techniques are promising tools for glaucoma management. These models can help identify patients likely to experience disease progression, predict future visual field loss, and determine individualised target IOP levels to stabilise the disease. When combined with established diagnostic methods, these innovations offer significant potential for improving detection, monitoring, and treatment outcomes in glaucoma care (Garcia, Lavieri, et al., 2019; Garcia, Nitta, et al., 2019).

## Subtypes of glaucoma

### Primary OAG

Primary OAG (POAG) is the most prevalent subtype of glaucoma, accounting for 74% of all glaucoma cases worldwide (Quigley & Broman, 2006). As its name suggests, POAG is anatomically defined by the presence of an open iridocorneal angle. In POAG, OHT results from molecular and cellular defects within the conventional outflow pathway, leading to reduced AH outflow (Fig. 1.5). Under physiological conditions, AH outflow is dynamically regulated by interactions between TM cells and SCECs that control cell contractility, ECM turnover, and cell-cell junction integrity via autocrine and paracrine signalling. This allows the outflow tissues to respond to fluctuations in IOP and maintain pressure homeostasis (Stamer & Acott, 2012). Disruption of these pathways leads to the sustained elevation of outflow resistance characteristic of POAG. Local bioactive molecules play an important role in this process. Lipid-derived signalling molecules, for example prostaglandins, mediate TM and SCEC contractility and cell-cell junctions over short timescales, while longer-term effects involve changes in ECM turnover (Bahler et al., 2008; Stamer et al., 2010). Cytokines also regulate AH outflow. Notably, transforming growth factor-β (TGF-β) levels are elevated in the AH of glaucoma patients, while perfusion of human eyes with TGF-β results in a gradual but substantial reduction in outflow facility over several days (Gottanka et al., 2004; Tripathi et al., 1994). This effect is mediated, at least in part, by dysregulation of ECM homeostasis in the JCT, where TGF-β promotes fibrosis-like

changes through increased synthesis and deposition of ECM components (Fuchshofer et al., 2003; Fuchshofer & Tamm, 2009; Zhavoronkov et al., 2016). As cytokines both contribute to and arise from inflammatory processes, chronic low-grade inflammation may play an important role in driving ECM remodelling and increased outflow resistance in POAG. This concept is explored further in Chapter 3. Small signalling molecules, such as nucleotides, also regulate outflow. Mechanical stretch of TM cells induced by IOP fluctuations stimulates the release of ATP into the extracellular space (Li et al., 2011; Li et al., 2012). Extracellular ATP can directly enhance outflow facility through the activation of potassium channels (Gu & Wiley, 2006), or be metabolised to adenosine by exoenzymes. Activation of adenosine A1 receptors within the conventional outflow pathway has been shown to rapidly increase outflow facility in cultured bovine eyes via matrix metalloproteinase (MMP) activation, promoting degradation of ECM components within the TM and junctions between SCECs, reducing outflow resistance (Crosson et al., 2005; O'Callaghan, Cassidy, et al., 2017). Collectively, these signalling pathways function to maintain IOP within a narrow range that does not compromise optic nerve integrity. In POAG, this homeostatic capacity is frequently lost, leading to a chronic elevation of IOP.

**Normal tension glaucoma**

Although distinct in presentation, normal-tension glaucoma (NTG) is classified as a subset of POAG due to the presence of an open iridocorneal angle. In NTG, optic nerve damage and characteristic glaucomatous visual field loss occur despite IOP remaining within the statistically normal range (Lee et al., 1998). Several hypotheses have been proposed to explain the pathophysiology of NTG. One suggestion is that certain individuals are more sensitive to normal fluctuations in IOP, such that IOPs within the normal range induce mechanical stress on axons within the LC, leading to damage. Supporting evidence includes the variation in NTG prevalence across ethnic groups, with epidemiological studies showing that NTG accounts for 20-40% of POAG cases in European and African populations, but 47-92% in Asian populations (Klein et al., 1992; Salvetat et al., 2023; Zhao et al., 2019). Additionally, reducing IOP has been shown to slow NTG progression in some, but not all, patients, indicating that IOP is not the sole cause of NTG progression (Anderson, 2003; Group, 1998). Another hypothesis attributes NTG to vascular dysregulation. Studies have shown that systemic hypotension, particularly nocturnal low blood pressure, is more common in NTG patients (Hayreh et al., 1994; Meyer et al., 1996).

Circadian fluctuations in mean ocular perfusion pressure have also been identified as a risk factor for visual field defect progression in NTG (Choi et al., 2007). Reduced systemic blood pressure decreases ocular perfusion pressure, which in turn leads to diminished blood supply to optic nerve fibres. This is particularly pertinent in individuals with significant nighttime blood pressure dips (Killer & Pircher, 2018). An abnormally high pressure gradient across the LC has also been proposed as a contributing mechanism. IOP exerts an anterograde force on the LC, counterbalanced by cerebrospinal fluid (CSF) pressure from the posterior side. When CSF pressure is low, it may mimic the effects of OHT on the ONH and LC, contributing to RGC death (Jonas & Wang, 2013). Another potential mechanism is impaired CSF circulation within the subarachnoid space surrounding the optic nerve. CSF is recycled approximately four times daily to maintain the microenvironment of neural tissue (Simon & Iliff, 2016). Reduced CSF turnover, leading to elevated levels of amyloid-β and tau, has been implicated in Alzheimer's disease (Tarasoff-Conway et al., 2015). A decline in CSF dynamics may similarly contribute to NTG by increasing the concentration of toxic proteins around the optic nerve. An age-related overlap between glaucoma and Alzheimer's disease has been observed, supporting this hypothesis (Cesareo et al., 2015; Mancino et al., 2018). Additionally, tracer studies have demonstrated reduced concentrations of contrast-loaded CSF in the subarachnoid space of the optic nerve in NTG patients (Killer et al., 2012). Furthermore, NTG patients exhibit narrower optic canal diameters compared to controls, suggesting a predisposition to bottlenecks in CSF movement from the intracranial to orbital subarachnoid space (Killer & Pircher, 2018; Pircher et al., 2017).

**Primary ACG**

Primary ACG (PACG) is characterised by elevated IOP resulting from mechanical obstruction of the TM. Unlike POAG, angle closure is the primary cause of disease in PACG, with OHT arising as a secondary consequence (Fig. 1.5). Angle closure occurs either when the peripheral iris presses against the TM (appositional closure) or forms adhesions with it (synechial closure). PACG can be classified into acute and chronic forms based on the speed of onset. In acute PACG, the iris quickly and completely blocks the TM, leading to a sudden increase in IOP. Chronic PACG has a more gradual onset, with the iris slowly covering the TM portion by portion, leading to peripheral anterior synechiae (PAS). Initially, the PAS may be discrete and multi-centred. However, they progressively expand

and fuse, leading to a gradual elevation in IOP over time. Like POAG, chronic PACG is generally asymptomatic and painless, as the eyes have sufficient time to adapt (Sun et al., 2017). PACG eyes generally have characteristic anatomical features including a small cornea, shallow anterior chamber, thick lens, an anteriorly positioned lens, and a short axial length (Lowe, 1970; Marchini et al., 1998). These features all contribute to a crowded anterior segment and a narrow iridocorneal angle. There are several mechanisms that can cause the progression of a narrow anterior chamber angle to a closed one. These can be divided into two types: pupillary block and non-pupillary block. Pupillary block is the most common mechanism of angle closure. In pupillary block, resistance to AH flow occurs in space between the lens and the posterior surface of the iris. This resistance creates a pressure differential between the posterior and anterior chambers. The posterior chamber pressure rises, causing the peripheral iris to be pushed forward. The forward movement of the iris then narrows or completely closes the angle, and can lead to the formation of PAS if iris apposition to the TM occurs for a long period of time (Quigley et al., 2003; Tarongoy et al., 2009). Non pupillary block factors include plateau iris and ciliary block. In plateau iris, the peripheral iris is displaced forward due to an anteriorly positioned or thickened ciliary body, which pushes it towards the TM. Plateau iris may cause persistent angle closure, even after a laser peripheral iridotomy (LPI) has relieved pupillary block. Plateau iris is found in about one third of Asian PACG eyes that have undergone LPI (Kumar et al., 2008; Kumar et al., 2009). Another major mechanism is ciliary block. Also called aqueous misdirection, this rare mechanism occurs when AH is misdirected posteriorly into or around the vitreous cavity, causing the ciliary body, lens, and iris to move forward. This results in a shallow anterior chamber and angle closure (Luntz & Rosenblatt, 1987; Ng & Morgan, 2012). The majority of eyes with PACG have more than one mechanism underlying angle closure including pupillary block and plateau iris configuration (Shabana et al., 2012; Sun et al., 2017).

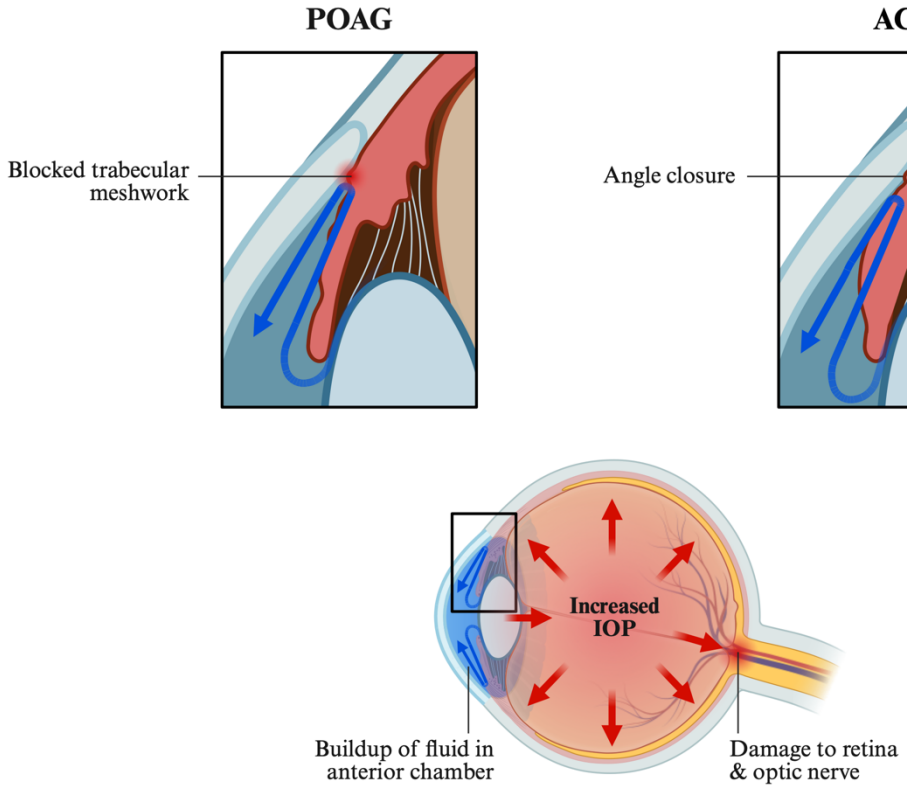



**Figure 1.5| Outflow resistance and elevated IOP in glaucoma**

*Top: Schematic showing resistance AH outflow (blue) in POAG (left) and in ACG (right). Bottom: Schematic showing the consequence of outflow resistance: elevated IOP and damage to the optic nerve and retina. Created with BioRender.*

### Secondary glaucoma

Secondary glaucoma refers to a type of glaucoma that develops as a result of another underlying condition, injury, or medication. These conditions disrupt AH outflow in the eye, leading to OHT and potential optic nerve damage as in primary glaucoma. The iridocorneal angle in secondary glaucoma may be open or closed (Mueller et al., 2024). The most common cause of secondary glaucoma is pseudoexfoliation syndrome (PEX), an age-related connective tissue disorder characterised by the deposition of fibrillar material in the ECM of various organs. In the eye, PEX material is found in the anterior segment structures and conjunctiva (Mueller et al., 2024; Ritch & Schlötzer-Schrehardt, 2001; Streeten et al., 1987). This material, along with pigment liberated from the iris, which is a hallmark of PEX, can accumulate in the TM, increasing resistance to AH outflow. Initial

deposits act as a focal point for the aggregation of serum proteins, such as albumin (Küchle et al., 1996), further exacerbating TM obstruction. The resulting rise in IOP gradually leads to glaucomatous optic neuropathy, a condition known as pseudoexfoliative glaucoma (PEXG) (Mueller et al., 2024). Pigment dispersion syndrome (PDS) is another common cause of secondary glaucoma. PDS is characterised by the shedding of pigment granules from the iris that occurs due to atypical contact between the iris and the zonules of the lens. As in PEXG, these pigment granules can subsequently deposit in the TM, increasing AH outflow resistance and resulting in OHT, and subsequently optic neuropathy, if left untreated. This is known as pigmentary glaucoma (Scuderi et al., 2019).

Iatrogenic glaucoma is another common form of secondary glaucoma. Certain medications, whether administered locally to the eye or systemically, can elevate IOP and lead to optic neuropathy if not addressed. Most drugs that list glaucoma as a contraindication or adverse effect are associated with inducing acute ACG (Razeghinejad et al., 2011). The mechanism involves stimulation of the sympathetic or inhibition of the parasympathetic nervous system, resulting in pupil dilation. In patients with narrow angles, this dilation can lead to pupillary block, further reducing the depth of the anterior chamber and causing obstruction of the TM, leading to an increase in outflow resistance and elevated IOP, (Razeghinejad et al., 2011). Such medications primarily trigger glaucoma in individuals with preexisting risk factors for angle closure, such as advanced age, hyperopia, a narrow iridocorneal angle or a family history for angle closure glaucoma (Lachkar & Bouassida, 2007). Examples of drugs associated with angle-closure glaucoma include sulfonamide-derived medications (Lee et al., 2007), tricyclic antidepressants (Ritch et al., 1994), monoamine oxidase inhibitors (Richa & Yazbek, 2010), and the anti-parkinsonian drug trihexyphenidyl (Friedman & Neumann, 1972).

Treatment with glucocorticoids (GCs) can also lead OHT in a subset of patients, which, if left untreated, may progress to iatrogenic glaucoma. In contrast to the aforementioned drugs, glaucoma induced by GCs more closely resembles POAG in its clinical presentation. GC therapy over weeks to months can elevate IOP in certain individuals in the absence of gonioscopic changes. If untreated, this OHT can result in glaucomatous optic neuropathy. The development of GC-induced OHT depends on factors such as the duration of therapy, the potency and physicochemical properties of the GC, the route of administration, and individual susceptibility (Overby & Clark, 2015). Early studies investigated the prevalence

of OHT following topical GC use for 4-6 weeks. These studies found that approximately 5% of individuals were high responders, experiencing significant IOP elevation, while approximately one-third had more modest increases (Armaly, 1963a; Becker, 1965). Notably, almost all patients with POAG were classified as high responders (Armaly, 1963b), pointing to a potential mechanistic overlap between steroid-induced glaucoma and POAG. Responder rates are higher in patients exposed to high intraocular levels of GCs with approximately half of individuals implanted with devices for sustained intravitreal GC delivery developing OHT (Bollinger et al., 2011; Kiddee et al., 2013). In most cases, steroid-induced IOP elevation is transient and reversible upon discontinuation of therapy, provided the GC has not been used for more than a year. Typically, IOP normalises within 2 to 4 weeks after stopping the medication (Tripathi et al., 1999). However, any vision loss resulting from GC-induced OHT is irreversible.

**Effect of OHT on RGCs**

The existence of NTG suggests that OHT is not the sole cause of glaucomatous optic neuropathy. However, it remains the only modifiable risk factor for the disease. The precise mechanism by which elevated IOP leads to RGC degeneration is not yet fully understood. Several hypotheses have been proposed, including mechanical damage, impaired axonal transport and oxidative stress. These factors likely interact in complex ways, with their relative contributions varying based on the individual and the specific subtype of glaucoma.

The principal site of insult to RGC cells in glaucoma is the laminar region of the ONH (Fig. 1.6). This can be attributed to the fact that the LC is a weak point in the posterior wall of the eye from a biomechanical standpoint, as it is approximately one-third the thickness of the sclera and only comprises around 40% of the total tissue volume in the laminar region of the ONH. Thus the LC must support the ONH against mechanical strain caused by IOP elevation, while also providing a pathway for RGC axons to leave the eye (Downs & Girkin, 2017). Early scanning electron microscopy studies of glaucomatous ONHs showed that the first structural evidence of damage was in the backward collapse of the anterior LC, followed by a prominent bowing of the whole structure (Quigley et al., 1981). Recent OCT-based studies of the ONH have explored changes in neural tissue thickness in prelaminar regions, along with alterations in LC position, shape, and thickness in glaucomatous eyes. One study found that, in patients with asymmetric glaucoma, the LC was positioned more posteriorly within the scleral canal in the glaucomatous eye compared

to the contralateral eye (Jeoung et al., 2016). Additionally, the LC is displaced further posteriorly in high-tension glaucoma compared to NTG, suggesting that IOP-related mechanical strain plays a key role in LC remodelling (L. Li et al., 2016). Furthermore, after surgical IOP reduction, the LC moves anteriorly in glaucomatous eyes, and eyes that sustain this anterior displacement over time exhibit a slower rate of progressive RNFL thinning (Lee & Kim, 2015).

Beyond direct mechanical stress, OHT in glaucoma may also disrupt the essential neurotrophic support that RGCs rely on for survival. Neurotrophins are a family of proteins that support the survival, growth, and differentiation of neurons and include nerve growth factor (NGF), brain derived neurotrophic factor (BDNF), ciliary neurotrophic factor (CNTF), and glial cell line-derived neurotrophic factor (GDNF), among others. Of the neurotrophins, BDNF and its receptor, TrkB, have emerged as potentially important mediators of glaucomatous RGC degeneration. Axonal transport of BDNF is disrupted in rodent and primate models of OHT (Pease et al., 2000; Quigley et al., 2000). Additionally, there is growing evidence of impaired BDNF signalling in human glaucoma, with reduced levels being observed in the ONH, tear film, and serum of glaucoma patients, relative to controls (Ghaffariyeh et al., 2009; Gupta et al., 2014; Oddone et al., 2017). Given the potential role of BDNF signalling in glaucoma development, its application as a neuroprotective agent has been explored. Early studies demonstrated that intravitreal injections of recombinant BDNF could delay RGC death in a rat hypertension model and an optic nerve crush (ONC) model in cats (Chen & Weber, 2001; Ko et al., 2001). However, this approach has limited clinical application due to the need for multiple injections for lasting neuroprotection. To address this, gene therapy strategies using viral vectors to deliver transgenes encoding BDNF or TrkB have been explored as a means of providing longer lasting neuroprotective effects and have demonstrated some efficacy in rodent models of glaucoma (Henderson et al., 2024).

Oxidative stress represents another potential contributor to RGC death in glaucoma. Oxidative stress is an imbalance in redox homeostasis, whereby pro-oxidative processes that generate reactive oxygen species (ROS) overcome intrinsic antioxidant defence mechanisms. This leads to DNA, protein and lipid damage in addition to mitochondrial dysfunction which further induces ROS generation. In particular, RGCs are highly susceptible to oxidative damage owing to their high metabolic demand, high lipid and

glutamate content, and limited capacity for regeneration (Hurley et al., 2022). Various animal studies suggest that oxidative stress plays a major role in glaucomatous neurodegeneration (Mittag et al., 2000; Moreno et al., 2004; Ozdemir et al., 2009). Additionally, POAG patients display lower antioxidant capacity in the AH and serum relative to cataract controls and this is associated with a higher level of visual field damage, lower RGC numbers, and increased cup-to-disk ratio (Abu-Amero et al., 2013; Asano et al., 2017; Nucci et al., 2013; Tanito et al., 2016). Considering this, the potential of antioxidants as neuroprotective molecules has been explored. For example, rapamycin, a synthetic antioxidant and autophagy-inducing agent that relieves oxidative stress by inhibiting mTor, has been shown to increase survival of RGCs in a rat chronic hypertension model (Su et al., 2014).

While the mechanisms above highlight RGC-intrinsic pathways of OHT-induced loss, there is also evidence that elevated IOP may contribute to RGC damage indirectly through its effects on other retinal cell types, including the retinal vasculature. This concept will be explored in Chapters 4 and 5.

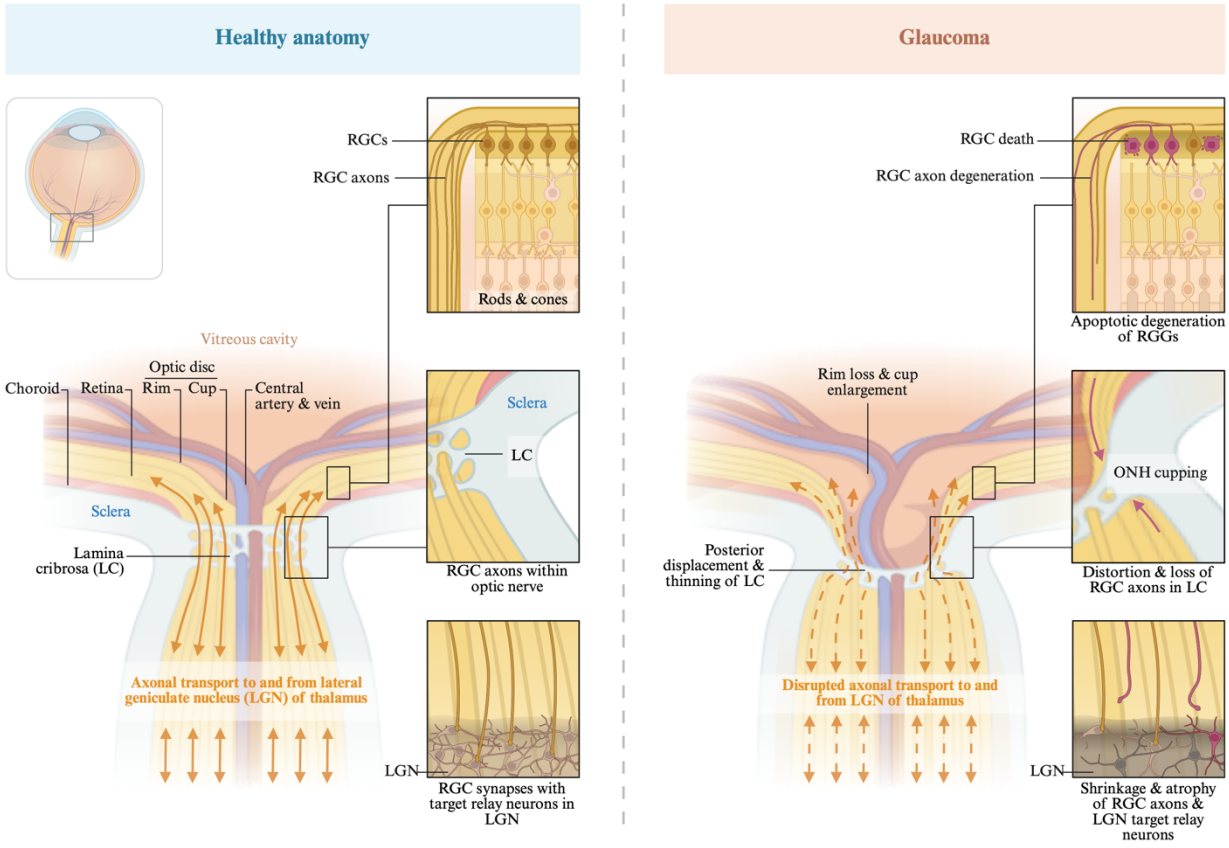



**Figure 1.6| Glaucomatous neurodegeneration**

*Schematic of the optic disc in healthy (left) and glaucomatous (right) eyes. In health, retinal RGC axons converge at the neuroretinal rim, surrounding the central cup, and pass through the LC to form the optic nerve projecting to the lateral geniculate nucleus (LGN). In glaucoma, elevated IOP displaces and thins the LC, deepening the cup and narrowing the rim. These changes disrupt axonal transport, trigger RGC apoptosis, and ultimately cause optic nerve degeneration with atrophy of LGN relay neurons. Created with Biorender. Adapted from Weinreb et al. (2014).*

## Genetics

Glaucoma can develop at any age. Cases occurring before the age of 40 are classified as early-onset glaucoma and typically follow an autosomal dominant Mendelian inheritance pattern. These forms are caused by rare genetic variants with large biological effects. In contrast, late-onset glaucoma is generally multifactorial, arising from common risk variants at multiple loci with smaller effect sizes, along with contributions from environmental factors (Wiggs & Pasquale, 2017).

First identified in 1997, *MYOC*, encoding myocilin, was the first gene to be linked with POAG (Stone et al., 1997). *MYOC*-associated glaucoma displays an autosomal dominant inheritance pattern, leading to earlier onset compared to cases with complex inheritance. *MYOC* mutations account for 2-4% of overall POAG cases and 10-30% of juvenile-onset cases (Menaa et al., 2011). *MYOC* is highly expressed in TM cells as well as in various ocular and non-ocular tissues (Karali et al., 2000; Takahashi et al., 1998). Deletion or overexpression of *Myoc* in mice does not lead to any observable phenotype, indicating that myocilin has a minimal role in IOP regulation under normal conditions (Gould et al., 2004; Kim et al., 2001). This is further supported by the fact that null mutations in *MYOC* are equally prevalent in glaucoma patients and controls (Pang et al., 2002). Most disease-causing mutations in *MYOC* are missense variants located in the third exon, which encodes the olfactomedin domain. Among these, *P370L* and *Y347H*, are linked to the most severe phenotypes (Wiggs & Pasquale, 2017). Such mutations lead to a gain of function phenotype, with mutant myocilin forming detergent insoluble aggregates and accumulating in the endoplasmic reticulum (ER), resulting in ER stress (Joe et al., 2003; Liu & Vollrath, 2004; Yam et al., 2007). Chronic ER stress in TM cells results in cell death, ultimately elevating IOP (Joe et al., 2003; Zode et al., 2011). The Tg-*MYOC*$^{Y437H}$ mouse model, expressing the human Y437H allele, associated with severe early onset glaucoma, replicates human disease features including reduced MYOC secretion, elevated IOP after 3 months, and RGC loss after 4 months (Zode et al., 2011).

Rare mutations involving two genes, *OPTN* (encoding optineurin) and *TBK1* (encoding Tank-binding protein-1), are associated with an early onset form of NTG with an autosomal dominant inheritance pattern (Fingert et al., 2011; Rezaie et al., 2002). The E50K *OPTN* missense mutation and copy number variations in TBK1 are associated with severe disease manifestation before the age of 40 (Aung et al. 2005). Optineurin is expressed in various tissues, including the heart, brain, liver, kidney, and notably in ocular structures such as the TM, non-pigmented ciliary epithelium, and retina (Rezaie & Sarfarazi, 2005). Both OPTN and TBK1 play crucial roles in autophagy and NF-κB signaling, with their encoded proteins known to interact (Fingert et al., 2016; Minegishi et al., 2013; Richter et al., 2016; Sudhakar et al., 2009; Wiggs & Pasquale, 2017). Optineurin functions as a negative regulator of NF-κB, a process modulated by TBK1 (Sudhakar et al., 2009). The E50K *OPTN* mutation enhances the interaction between TBK1 and OPTN, potentially increasing NF-κB activity and promoting cell death (Morton et al., 2008). Phosphorylation of optineurin by TBK1

also promotes the induction of autophagy and this interaction is enhanced by the E50K mutation (Minegishi et al., 2013; Wild et al., 2011). Mutations in *OPTN* have also been linked to amyotrophic lateral sclerosis (ALS), suggesting a potential shared pathophysiological mechanism with NTG (Cirulli et al., 2015).

While the above loci were identified through linkage studies, such studies are less effective at detecting variants with smaller biological effects that contribute to adult-onset glaucoma risk. Genome-wide association studies (GWAS) have been successfully utilised for this purpose, uncovering genomic loci associated with POAG (Bailey et al., 2016; Burdon et al., 2011; Chen et al., 2014; Choquet et al., 2018; Thorleifsson et al., 2010), NTG (Wiggs et al., 2012), PXG (Aung et al., 2015; Thorleifsson et al., 2007), and PACG (Khor et al., 2016; Vithana et al., 2012). To date, GWAS have identified 329 genetic loci associated with POAG (Singh et al., 2025). These loci are involved in diverse biological processes including the ECM organisation, cytokine signalling, lipid metabolism, membrane biology, regulation of cell division, autophagy, and ocular development (Wiggs, 2015). Although POAG susceptibility has a strong genetic component with heritability estimated to be 13-81%, the proportion of variance explained by known common variants remains limited, despite increasing substantially in recent years (from 9.4% in 2021 to 14.1% in 2023) (Gharahkhani et al., 2021; Han et al., 2023; Singh et al., 2025). To address this challenge of "missing heritability", the incorporation of endophenotypes has been successfully used to identify novel disease-associated loci (Bonnemaijer et al., 2019; Craig et al., 2020; Han et al., 2023). Recent advances in machine learning have further enhanced this approach by enabling more accurate phenotyping of ONH traits, thereby increasing the power of GWAS to detect associated genetic loci (Alipanahi et al., 2021).

### 1.4 Current treatments for glaucoma

As it is the only modifiable risk factor for the disease, all available glaucoma treatments focus on reducing IOP. Large multicentre clinical trials have shown that reducing IOP is efficacious in both preventing and slowing the progression of glaucoma, including NTG (Anderson, 2003; Group, 1998; Heijl et al., 2002; Kass et al., 2002). Current guidelines from the American Academy of Ophthalmology Preferred Practice Pattern state that an initial reduction of 20-30% in IOP is a suitable target for slowing disease progression. This

target should be achieved using the fewest possible medications while minimising adverse effects (Gedde et al., 2021).

**IOP lowering medications**

For decades, IOP lowering medications have been the first-line therapy for most glaucoma patients. These medications work by either reducing AH production, or increasing its outflow. Among them, prostaglandin analogues are the most effective and consequently the most commonly prescribed (T. Li et al., 2016; Lindén & Alm, 1999). Prostaglandin analogues reduce IOP primarily by enhancing uveoscleral outflow through activation of prostanoid receptors in the ciliary muscle, leading to relaxation of muscle bundles and increasing intermuscular spaces that facilitate AH drainage. Over longer timescales, they agents also promote ECM remodelling through upregulation of MMPs, further reducing tissue resistance to outflow (Gaton et al., 2001; Winkler & Fautsch, 2013). Prostaglandin analogues may also modestly increase conventional outflow by reducing TM cell contractility and increasing ECM turnover (Winkler & Fautsch, 2013). Prostaglandin analogues offer the advantages of once-nightly dosing and minimal systemic side effects. However, they can cause local adverse effects, including eyelash elongation and darkening, orbital fat loss, iris pigmentation, and uveitis (Gedde et al., 2021). Additionally, because these medications primarily act on the unconventional outflow pathway, concerns exist regarding their long-term efficacy. Many patients eventually require combination therapy to achieve target IOP reductions (Schmier et al., 2014). The recently approved latanoprostene bunod may address this issue by targeting both the conventional and unconventional outflow pathways. It is a nitric oxide-donating prostanoid receptor agonist that is metabolised into latanoprost acid, an $F_{2\alpha}$ prostaglandin analogue, and butanediol mononitrate. Nitric oxide is subsequently released from butanediol mononitrate. While latanoprost acid primarily increases uveoscleral outflow as described for prostaglandin analogues, nitric oxide induces relaxation of the conventional outflow tissues via cyclic GMP-dependent signalling (Cavet et al., 2014). Compared with timolol over 3 months of follow-up, latanoprostene bunod has superior IOP-lowering efficacy and a comparable safety profile (Bailey et al., 2016; Weinreb et al., 2016). Second-line IOP-lowering medications include carbonic anhydrase inhibitors and β-blockers, both of which reduce IOP by inhibiting AH production. Carbonic anhydrase inhibitors act on the ciliary epithelium, reducing bicarbonate ion formation and impairing the osmotic gradient

required for AH secretion (Aslam & Gupta, 2025). β-blockers suppress sympathetic stimulation of β-adrenergic receptors in the ciliary epithelium, leading to decreased cyclic AMP signalling and reduced aqueous secretion (Brooks & Gillies, 1992; Polansky et al., 1989). However, β-blockers are associated with systemic side effects such as bradycardia, hypotension, and heart failure (Han et al., 2008). Recently introduced, Rho kinase inhibitors lower IOP by enhancing conventional outflow. Rho kinase inhibitors reduce conventional outflow resistance by decreasing SCEC stiffness, which increases pore formation at the inner wall and diminishes the funnelling effect that limits AH drainage. Additionally, Rho kinase inhibition alters cytoskeletal organisation and focal adhesion dynamics, weakening attachments between SCECs and the JCT, further expanding outflow spaces and decreasing the magnitude of the funnelling effect. (Tanna & Johnson, 2018). Netarsudil, a Rho kinase inhibitor approved by the US Food and Drug Administration in 2017, has shown IOP-lowering efficacy comparable to timolol but with a higher incidence of adverse effects (Kahook et al., 2019; Serle et al., 2018; Wagner et al., 2022). While topical eyedrops are the least invasive therapeutic option, adherence to dosing schedules poses a significant challenge, resulting in poor compliance that limits the real-world effectiveness of these treatments. Fewer than half of patients with glaucoma use medications as prescribed after one year (Schwartz & Quigley, 2008). Barriers to adherence include difficulty with eye drop administration, intolerable adverse effects, and cost of medications (Robin & Muir, 2019).

**Surgical interventions**

When topical medications fail to sufficiently reduce IOP, or if vision loss persists despite well-controlled IOP, surgical interventions are indicated. One such intervention is laser trabeculoplasty, which involves targeting the TM with lasers to increase outflow facility. Laser types include argon, micropulse, and selective laser trabeculoplasty (SLT) and excimer trabeculotomy (Stein et al., 2021). SLT was first introduced in 1995 and was approved by the FDA in 2001. It succeeded argon laser trabeculectomy and had the advantage of using a shorter pulse duration, which minimised heat dissipation and collateral damage to surrounding tissues (Garg & Gazzard, 2018; Latina & Park, 1995). SLT is a short, outpatient procedure with a quick recovery time and a strong safety profile. Given the challenges of patient non-compliance with topical medication regimens, some studies suggest that SLT may be a more cost-effective first-line treatment (Stein et al., 2012). A

clinical trial comparing SLT to medication as an initial therapy found that SLT is equally effective at lowering IOP and more cost-efficient than long-term medication use. SLT also had no sight-threatening complications, and patients initially treated with SLT experienced fewer medication-related side effects compared to those who started with medication. After three years, nearly 75% of patients randomised to SLT required no additional medications to maintain IOP control. However, approximately 15% of SLT patients required further IOP-lowering interventions within the first year (Gazzard et al., 2019; Stein et al., 2021). Laser trabeculoplasty is not recommended for certain glaucoma types, such as ACG, and some patients may require retreatment to sustain its effects. Nevertheless, SLT can be particularly beneficial for patients who struggle with medication adherence or experience difficulty tolerating topical treatments.

If medical and laser treatments fail to sufficiently reduce IOP, incisional surgeries are typically performed. These include trabeculectomy, tube shunt implantation, and minimally invasive glaucoma surgeries (MIGS). Trabeculectomy has been the gold standard in glaucoma surgery for decades. It involves creating a partial-thickness scleral flap and excising a segment of the TM to establish an alternative drainage route from the anterior chamber to the subconjunctival space. Tube shunt implantation, on the other hand, uses glaucoma drainage devices to create a permanent sclerotomy, directing AH into the subconjunctival space (Wagner et al., 2022). Trabeculectomy and tube shunt implantation remain the most effective procedures for lowering IOP. A randomised clinical trial comparing these surgeries found similar outcomes in IOP reduction and the need for additional IOP-lowering medications five years post-surgery. However, patients who received a tube shunt had a lower risk of surgical failure and reoperation compared to those who underwent trabeculectomy (Gedde et al., 2010). This has led to tube shunt implantation becoming the preferred surgical option in recent years (Vinod et al., 2017). Both procedures carry risks, including bleeding, inflammation, cataract formation, corneal swelling, hypotony, and IOP elevation due to scar tissue formation. Therefore, they are generally reserved for patients who do not respond to medications or laser treatments (Gedde et al., 2012).

MIGS are a newer alternative that lower IOP with minimal disruption to the sclera or conjunctiva. They work by improving AH drainage into SC, the suprachoroidal space, or the subconjunctival space, sometimes with an implanted device, or by selectively reducing

aqueous production (Fellman et al., 2020). Unlike traditional bleb-based procedures, MIGS are relatively simple to perform, requiring surgical skills similar to those used in modern cataract surgery. This allows cataract surgeons who are not glaucoma specialists to perform them. MIGS are also less invasive and have a favourable safety profile compared to traditional incisional surgeries (Pereira et al., 2021). Although MIGS are generally less effective at lowering IOP than trabeculectomy or tube shunts, they are well-suited for early to moderate glaucoma. However, some patients require multiple MIGS procedures to achieve adequate IOP reduction. While long-term safety and efficacy data on MIGS is still limited, several short-term studies have reported promising results up to 2 years post-surgery (Ahmed et al., 2020; Rosdahl & Gupta, 2020; Samuelson et al., 2019; Stein et al., 2021)

### 1.5 Mouse models of glaucoma

As with many conditions, studying the pathophysiology of glaucoma directly in human patients is challenging. For this reason, animal models that recapitulate key features of the disease are used to investigate disease mechanisms and therapies. While glaucoma can be modelled in several species, rodent models are particularly attractive for exploratory research, as they are small in size, have a short life span, and can be easily manipulated experimentally, while still having a similar ocular structure and physiology to that of humans (Johnson & Tomarev, 2010). For example, mice have comparable IOP levels and AH turnover rates to humans (Aihara et al., 2003; Savinova et al., 2001). Furthermore, like humans, mice have a well-developed TM and SC, and display both conventional and unconventional AH outflow pathways (Lindsey & Weinreb, 2002; D. R. Overby et al., 2014). Most rodent models of glaucoma rely on optic nerve damage mediated by OHT, which may arise through genetic alterations or be experimentally induced by chemical, surgical, or mechanical means. Other approaches, such as the ONC model, bypass IOP elevation altogether, instead focusing directly on RGC degeneration through mechanical insult to the optic nerve (Tang et al., 2011). While these systems have provided valuable insights into the disease process, they often fall short of reproducing a ‘true’ glaucomatous phenotype. Many do not recapitulate all clinical hallmarks or follow the disease course observed in humans. Consequently, there is no “perfect” model of glaucoma, with the most appropriate choice depending on the research question at hand. Four mouse models of glaucoma are particularly relevant to this project: DBA/2J, dexamethasone-induced OHT,

microbead-induced OHT, and ONC. The phenotypes, benefits, and drawbacks of each of these models will be discussed in the current section.

**DBA/2J**

The DBA/2J mouse is one of the most extensively characterised glaucoma models. First described in 1998, the strain develops a progressive iris disease involving pigment dispersion and stromal atrophy, which ultimately leads to OHT and glaucoma-like features such as ONH cupping, RGC loss, and visual impairment (John et al., 1998; Libby et al., 2005). The pathology is driven by loss-of-function mutations in two melanosomal protein-encoding genes, *Gpnmb* and *Tyrp1*. Mutant *Gpnmb* promotes pigment dispersion, while mutant *Tyrp1* causes stromal atrophy. Together these mutations permit toxic intermediates of pigment production to leak from melanosomes (Anderson et al., 2002). There is also a systemic component to the DBA/2J pathology. IOP elevation is preceded by a breakdown of ocular immune privilege, and can be attenuated by reconstituting DBA/2J bone marrow with that from mice of the same background carrying the wild-type *Gpnmb* allele. This can be attributed to the fact that *Gpnmb* is also expressed in bone marrow-derived cells (Anderson et al., 2008; Mo et al., 2003). Current understanding therefore suggests a two-step pathological sequence. Initially, melanosomal dysfunction mediated by mutant *Tyrp1* and *Gpnmb* induces mild iris damage, causing pigment and other cellular debris to be released into the anterior chamber. Next, due to *Gpnmb* deficiency, bone marrow-derived immune cells respond abnormally to this debris, triggering an inflammatory attack on the iris, resulting in iris atrophy and subsequent elevation of IOP (Anderson et al., 2008). The ultimate cause of IOP elevation in the DBA/2J model remains unclear. Whether the rise in pressure is driven primarily by physical blockage of the outflow pathways by pigment, by remodelling of the TM and SC, or by a combination of both processes, is not yet well established. It must also be noted that due to a frameshift mutation in the *C5* gene, DBA/2J mice do not express a functional complement component C5 protein (Wetsel et al., 1990). However, this deficiency is reported to play a protective role, with restoration of C5 activity leading to earlier and more severe RGC loss (Howell et al., 2013).

Advantages of the DBA/2J strain as a glaucoma model include the fact that, as a congenital model, its disease develops spontaneously, thereby avoiding the variability introduced by surgical or chemical procedures. Additionally, the DBA/2J mouse more closely resembles the natural course of human glaucoma compared to inducible models, exhibiting a gradual,

age-related rise in IOP accompanied by progressive RGC loss (Inman et al., 2006). However, it also associated with several limitations. The course of both IOP elevation and RGC loss is not entirely predictable and has been reported to vary between groups. IOP elevation has been reported as early as 4 months of age (Scholz et al., 2008), but is generally found to be elevated between 6 and 9 months of age, with 8-9 months of age being reported to represent a transition to OHT for many mice (Inman et al., 2006; Libby et al., 2005; Turner et al., 2017). The strain also develops corneal calcifications that may confound IOP measurement by tonometry, and can obscure in vivo retinal imaging (Turner et al., 2017). RGC loss has been reported to begin between 7 and 9 months of age, with most optic nerves being severely damaged by 12 months of age (Inman et al., 2006; Libby et al., 2005). RGC loss independent of IOP has been reported in the model, which can confound studies investigating the relationship between IOP and RGC loss in the model (Turner et al., 2017; Wang & Dong, 2016).

**Dexamethasone-induced OHT**

As mentioned in Section 1.3, prolonged treatment with GCs can lead to OHT in human patients, which can further progress to iatrogenic glaucoma if left untreated (Bollinger et al., 2011). For this reason, animal models of GC-induced OHT have been developed in an attempt to understand GC-induced glaucoma, and POAG more generally. Relevant to this project is the widely-used dexamethasone-induced OHT model, in which mice are fitted with subcutaneous micro-osmotic pumps that systemically release dexamethasone over a period of 4 weeks. This leads to elevations in IOP within 2 weeks of implantation, which coincides with a significant decrease in outflow facility, increased ECM in the JCT, a more pronounced basement membrane underlying the inner wall of SC, and an increased number of myofibroblasts along the outflow pathway (Darryl R. Overby et al., 2014; Whitlock et al., 2010). The precise mechanism by which GCs induce OHT is not fully understood. However, evidence suggests that it may be related to the downstream expression patterns of the GC receptor (GR). GR is spliced into two alternative isoforms: GRα and GRβ. GRα is a transcription factor that translocates to the nucleus when bound to GCs. GRα homodimers then control the transcription of numerous genes by binding to glucocorticoid response elements. On the other hand, GRβ cannot bind to GCs but can dimerise with GRα, thereby serving as an antagonist to GC-mediated gene regulation. It is therefore hypothesised that the ratio of these isoforms may influence the susceptibility of TM cells

to GCs. Indeed, TM cell lines derived from healthy individuals express higher levels of GRβ than glaucomatous TM cells (Zhang et al., 2005). Furthermore, overexpression of GRβ in the TM of mouse eyes inhibits GC-induced OHT (Patel et al., 2018). Interestingly, there appears to be significant overlap in the mechanisms underlying GC-induced glaucoma and that caused by mutant *MYOC*. Firstly, GCs induce the expression of *MYOC* in TM cells (Clark et al., 2001). Furthermore, as in mice with *MYOC* mutations, mice with dexamethasone-induced OHT express markers of ER stress in the TM, and their OHT can be alleviated via treatment with ER stress suppressor 4-phenyl butyric acid (Zode et al., 2011; Zode et al., 2014). Aside from the TM, there is also evidence that GCs increase the expression of TJs by SC endothelial cells (Underwood et al., 1999).

Advantages of using the dexamethasone-induced OHT model include the fact that it is inducible and produces a rapid increase in IOP which shortens experimental timelines and facilitates longitudinal studies. Importantly, the osmotic minipump approach does not require direct ocular manipulation, thereby avoiding potential confounding factors introduced in other models. Moreover, it is a one-time surgical procedure and does not require repeated daily administrations, as is the case with topical dosing (Zode et al., 2014). However, systemic administration of dexamethasone also has several drawbacks. The implantation of osmotic minipumps is invasive, and systemic exposure can result in significant weight loss, leading to relatively high dropout rates (Whitlock et al., 2010). In addition, RGC loss is not reported in this model; however, the short timeframe of systemic dexamethasone treatment means that RGC loss is likely to be minimal. By contrast, topical dexamethasone administration for 6 weeks has been shown to cause a significant reduction in pattern electroretinography responses, as well as loss of RGCs and optic nerve axons (Zode et al. 2014).

**Microbead-induced OHT**

While dexamethasone-induced OHT represents a manipulation of physiological processes to elevate IOP, the injection of material into the anterior chamber to directly obstruct AH outflow provides an even more direct and rapid means of inducing OHT. In this regard, obstruction of the TM via intracameral injection of microparticles has a long track record in experimental glaucoma research (Morgan & Tribble, 2015). Early approaches included injection of glutaraldehyde treated autologous red blood cells into the anterior chamber.

The increased rigidity of these modified cells caused TM occlusion and sustained IOP elevation in both rabbits and primates (Quigley & Addicks, 1980). In the past two decades, the availability of high quality microbeads with diameters matching the pores in the TM has facilitated the induction of OHT in various species. The relatively small anterior chamber of the rodent eye is particularly well-suited to this approach (Morgan & Tribble, 2015). In mice, a wide range of injection parameters and techniques have been described, as summarised in Morgan and Tribble (2015). The choice of bead size is an important practical consideration in microbead models: larger beads are easier to view and manipulate but they carry a greater risk of occluding the injection cannula. The protocol most relevant to this project is the "4+1" mixture, originally described by Cone et al. (2012). This involves injection of 4 µl of a bead mixture (2 µl of 6 µm beads and 2 µl of 1 µm beads), followed by 1 µl of viscoelastic solution, which was shown to produce the highest IOP elevation and optic nerve damage over a 28-week period compared with other bead combinations. This approach was later adopted by Keuthan et al. (2023) to generate the RNA-seq dataset analysed in Chapter 5.

Advantages of using microbeads to induce OHT include the fact that it allows for rapid and controlled induction of IOP elevation. OHT can be induced in days, and the degree of IOP elevation can be controlled by manipulating bead size. Thus, it is particularly useful for studying the effect of IOP on RGCs and the retina (Morgan & Tribble, 2015). Limitations include the fact that IOP elevation is transient, and can require more than one injection to sustain IOP for long enough to induce RGC loss (Biswas & Wan, 2019). Additionally, the degree of RGC loss can be quite low, with RGC loss being as low as 7-12% at 4 to 12 weeks after injection in some paradigms (Claes et al., 2021; Cone et al., 2010). Lastly, the intracameral injection of microbeads can lead to complications such as increased inflammation in the anterior chamber, corneal neovascularization, ulceration and endophthalmitis in a minority of animals (Biswas & Wan, 2019).

**ONC**

While the aforementioned models involve secondary damage to RGCs as a result of elevated IOP, in some experimental contexts, it may be desirable to induce a specific insult to RGCs in the absence of OHT. The ONC model is widely used in this regard. In this model, a mechanical injury is applied to RGC axons, triggering a retrograde degenerative

response termed Wallerian degeneration, which ultimately leads to RGC loss (Johnson & Tomarev, 2010). The procedure is relatively simple to perform in mice. A temporal canthotomy and blunt dissection are performed to expose the optic nerve, which is then crushed with a calibrated cross-action forceps to deliver a consistent amount of force. The severity of injury can be controlled by modifying the force or duration of the crush (Johnson & Tomarev, 2010). RGC degeneration begins rapidly, with survival reported to decline to 47% at one week and 27% at two weeks post-injury, respectively (Johnson & Tomarev, 2010; Levkovitch–Verbin et al., 2000). The death of RGCs in the ONC model is progressive, involving both primary injury and a second wave of degeneration. Thus, not all axons are damaged by the procedure itself. Instead, many are lost due to downstream factors in the resulting neurotoxic environment. This makes the ONC model ideal for studying neuroprotective interventions (Johnson & Tomarev, 2010).

Advantages of the ONC model include its simplicity, reproducibility, and reliability in inducing RGC loss, a feature that is often more variable in OHT models. However, several drawbacks limit its translational relevance. The ONC model does not replicate the pathophysiology of human glaucoma, as it bypasses IOP elevation. Additionally, because the injury is acute and severe, it does not reflect the chronic, slowly progressing nature of glaucomatous neurodegeneration. As a result, it does not allow the opportunity to study gradual stress responses in RGCs prior to degeneration, which is an important aspect of glaucoma pathophysiology.

### 1.6 Project aims

This introduction section has outlined the current state of glaucoma research, including its clinical subtypes, genetic underpinnings, and available treatments. It has also examined the pathophysiology of OHT and its relationship to RGC loss, as well as the animal models used to study these processes. It is evident that while treatment options exist for glaucoma, they are suboptimal. Current therapies focus exclusively on lowering IOP, often by indirect means that do not directly address the underlying resistance to outflow in the conventional outflow pathway. There is therefore an unmet need both for more effective IOP-lowering treatments that act on the conventional outflow pathway and for therapies that directly protect RGCs. A major barrier to progress in both areas is an incomplete understanding of the disease's pathophysiology. To address this gap, this PhD project aimed to investigate

the pathophysiology of glaucoma at both the front and back of the eye through two broad objectives. The first, addressed in Chapter 3, was to examine whether immune pathways in the anterior segment can influence AH outflow and thereby regulate IOP. The second, examined across Chapters 4 and 5, was to determine whether retinal vascular dysfunction represents an early and potentially causal factor in RGC degeneration across multiple mouse models of glaucoma.

# Chapter 2: Materials and Methods

## 2.1 Animals

Mice were purchased from Jackson Laboratory and subsequently bred and housed in a specific-pathogen-free unit at the Smurfit Institute of Genetics, Trinity College Dublin. Animals were maintained under standard conditions with ad libitum access to food and water and a 12-hour light/dark cycle. All procedures were conducted in accordance with institutional regulations and approved by the Health Products Regulatory Authority, which oversees the implementation of EU Directive 2010/63/EU on the protection of animals used for scientific purposes. All mice were bred on a C57BL/6J background, with the exception of DBA/2J mice. For immunostaining experiments in Chapters 3 and 4, DBA/2J and C57BL/6J mice were between 9 and 12 months of age. For perfusion experiments in Chapter 3, *Casp11*$^{-/-}$ mice, *Il18*$^{-/-}$ mice, *Asc*$^{-/-}$ mice, as well as C57BL/6J mice subject to intracameral injection to IL-18 and Il-1β were between 3 and 6 months of age. For Fundus fluorescein angiography (FFA) and OCT analyses in Chapter 4, cohorts of DBA/2J mice and age matched controls were examined at 3, 6 and 9 months of age. Mice subject to dexamethasone-induced OHT and naïve controls were between 3 and 6 months of age. Body weight in dexamethasone-treated mice was monitored regularly, and animals were euthanised if they lost > 10% of body weight in a single week or > 20% across the 4-week experimental period. Approximately equal numbers of male and female mice were used for all experiments.

## 2.2 Dissection of murine anterior segments for immunostaining

Animals were sacrificed by cervical dislocation and eyes were quickly enucleated. Eyes were fixed in 4% paraformaldehyde for 1 hour at room temperature. The vitreous body was dissected from the eye and the lens removed. Anterior segments were washed in phosphate-buffered saline (PBS), before being placed in sucrose solutions of incrementally increasing concentration (10% and 20% until the tissue sank to the bottom of the container, and 30% overnight at 4 $^{o}$C). Anterior segments were then snap frozen in Optimal Cutting Temperature compound (OCT, VWR, 361603E) by immersion in liquid nitrogen. 12 µm sections were taken on charged polylysine slides (Menzel-Gläser) using a Leica Microsystems CM 1900 cryostat. Slides were stored at -20$^{o}$C prior to immunostaining.

### 2.3 Immunostaining of murine anterior segments

Slides were allowed to thaw for 10 min at room temperature. A hydrophobic barrier was drawn around the sections using a PAP pen (Sigma Aldrich Z672548). Slides were then washed 3 times in PBS, followed by a blocking step for 1 hour at room temperature in a solution containing 5% normal goat serum, 1% bovine serum albumin, and 0.1% Triton X-100 in PBS. Sections were incubated in primary antibody overnight at 4 $^{o}$C. Sections were then washed 3 times in PBS before being incubated in secondary antibody for 2 hours at room temperature**.** A list of all the antibodies used and their dilutions is provided in Table 2.1. Two further PBS washes were performed after the secondary antibody incubation, followed by counterstaining with DAPI (1:3000) for 30 seconds. Slides were washed once more in PBS, before mounting slides in Aqua Poly/Mount (Polysciences, Inc) and gently applying coverslips. Slides were imaged on a Zeiss LSM 710 confocal microscope. The signal intensity of each marker in the corneal epithelium, corneal stroma, corneal endothelium, iris, and ciliary body was measured by quantifying the mean grey value following selection using the freehand selection tool in ImageJ.

| Antibody | Supplier | Dilution |
|---|---|---|
| Rat Anti-CD68 (ab53444) | Abcam | 1:500 |
| Rat Anti-CD11b (14-0112-82) | Thermo Fisher Scientific | 1:200 |
| Rat Anti-F4/80 (ab6640) | Abcam | 1:100 |
| Rabbit Anti-NLRP3 (15101) | Cell Signalling | 1:200 |
| Rabbit Anti-AIM2 (20590-1-AP) | Proteintech | 1:100 |
| Rabbit Anti-NLRC4 (PA5-72908) | Thermo Fisher Scientific | 1:100 |
| Rabbit Anti-NLRP1 (NBP1-54899) | Novus Biologicals | 1:200 |
| Rabbit Anti-IL-1β (ab9722) | Abcam | 1:200 |
| Rabbit Anti-IL-18 (ab71495) | Abcam | 1:500 |
| Goat anti-rabbit, Cy3 conjugated (A-10520) | Thermo Fisher Scientific | 1:500 |
| Goat anti-rat, Alexa Fluor 555 conjugated (A-21434) | Thermo Fisher Scientific | 1:500 |

**Table 2.1| List of antibodies used for immunostaining of murine anterior segments**

### 2.4 Dexamethasone-induced OHT

Animals were weighed the day prior to surgery. Osmotic pumps (Alzet, model 1004) were filled with water-soluble dexamethasone (D2915; Sigma-Aldrich) reconstituted in sterile PBS to achieve a delivery rate of 2 mg/kg/day, calculated using Alzet's online formulation calculator (https://www.alzet.com/formulating-the-solution/). Mice were anesthetised with 3% isoflourane in oxygen at a rate of 1 litre/min, and baseline IOP was measured as described in Section 2.5. Animals then received subcutaneous injections of meloxicam (5 mg/kg) for analgesia. The surgical site was shaved, and a 1 cm dorsal incision was made inferiorly along the midline from the base of the scapula. A subcutaneous pocket was created on one side of the animal by blunt dissection with sterile scissors, and the pump was inserted into the pocket with the flow moderator directed posteriorly and placed as far from the incision as possible. The wound was closed using surgical adhesive (Surgibond, RayVet). Mice were treated with dexamethasone for 4 weeks. Following pump implantation, mice were singly housed to prevent wound interference from cage mates. To

mitigate dexamethasone-induced weight loss, their diet was supplemented with a high-calorie nutritional shake (Complan).

### 2.5 IOP measurement

Mice were placed in a chamber and anesthetised with 3% isoflurane in oxygen at 1 litre/min for 2 minutes. Following this, mice were transferred to a head-holder with an inlet to the isoflurane vaporiser and an outlet to the scavenger. IOP was measured with a rebound tonometer (TonoLab), with measurements being taken from minute 3 to minute 8, alternating eyes each minute. IOP measurements were taken at the same time each day for each experiment. The first measurement from the first mouse each day was taken from the right eye; this was alternated for each subsequent mouse. Each IOP measurement was an average of 6 individual readings, with 3 measurements being taken in total at each timepoint. Values were imported to an excel sheet and all post-processing was conducted through MATLAB. A Shapiro-Wilks test was used to test for normality. As the resulting distribution was non-normal, the median IOP measurement at each time point was used to fit a line and interpolate IOP at minute 5 to account for the IOP-lowering effect of anaesthesia over time (Jia et al., 2000). In Chapter 3, IOP measurements were obtained at baseline and weeks 1-3. A week 4 measurement was not taken in this experiment, as isoflurane anaesthesia induces transient reductions in IOP that could confound outflow measurements (Jia et al., 2000). In Chapter 4, IOP was measured at baseline and weeks 1-4.

### 2.6 Measurement of outflow facility

Outflow facility was measured using the iPerfusion system as described in Sherwood et al. (2016). Pairs of eyes were perfused in parallel using two identical, independent perfusion systems. Each perfusion system consists of an automated pressure reservoir, a thermal flow sensor (SLG64-0075, Sensiron) and a wet-wet differential pressure transducer (PX409, Omegadyne). This allows for the desired pressure to be applied, while simultaneously measuring the flow rate out of the system. Mice were sacrificed by cervical dislocation and eyes were enucleated. Following enucleation, eyes were secured to a pedestal using a small drop of cyanoacrylate glue. Filtered (0.2 μm, GVS Filter Technology) PBS was added to the reservoir containing the eye, which was maintained at 35$^{o}$C by a heating element linked to a temperature sensor. The perfusate consisted of 5.5 mM glucose in filtered PBS. The

anterior chamber of the eye was cannulated with a bevelled needle (NF33BV NanoFil, World Precision Instruments) using a stereomicroscope and a micromanipulator. Eyes were perfused 30 mins at 8 mmHg as a preconditioning step.

Eyes were then perfused at incrementally increasing pressure steps ranging from 4.5 to 21 mmHg, while recording flow rate and pressure. Flow (Q) and pressure (P) were averaged over 4 minutes, once eyes had stabilised to a given pressure. A power law model of the form:

$$Q = C_r \left(\frac{P}{P_r}\right)^{\beta} P$$

was fit to the data using weighted power law regression, yielding values for $C_r$, the reference facility at reference pressure $P_r$ = 8 mmHg, which corresponds to the physiological pressure drop across the outflow pathway and $\beta$, a nonlinearity parameter that describes the pressure-dependent increase in facility observed in murine eyes (Sherwood et al., 2016).

### 2.7 Intracameral injection

Mice were anesthetised using 3% isoflurane in oxygen at a rate of 1 litre/min. Pupils were dilated with phenylephrine and tropicamide. Under a dissection microscope, a glass needle (0.1mm diameter) was used to puncture the cornea at the corneoscleral junction, parallel and anterior to the iris, removing the AH by capillary action. A needle was then connected to a 10 µL Hamilton syringe and re-introduced through the initial puncture site. A 1.5 µL bolus of IL-18 (50 ng/mL) or IL-1β (133ng/mL) in sterile PBS was injected into the anterior chamber, followed by 1 µL of air to create a vacuum. This process was repeated for the contralateral eye, using sterile PBS as a control. After 48 hours (IL-18) or 72 hours (IL-1β), mice were sacrificed by cervical dislocation and eyes were enucleated for ex vivo measurement of outflow facility.

### 2.8 In vivo retinal imaging

FFA and spectral domain OCT (SD-OCT) imaging was performed using the Micron IV imaging system. Following administration of 1% tropicamide and 2.5% phenylephrine to induce pupil dilation, mice were anesthetised with a mixture of ketamine and domitor. Baseline Fundal images were taken. OCT imaging was performed using the REVEAL

software (Micron). Following this, mice were injected intraperitoneally with sodium fluorescein (2 mg/mL) at the same volume/weight (100 µL/20 g) to visualise blood vessels. FFA images were then taken on the DISCOVER software (Micron) every 30 seconds for 10 minutes to assess the extravasation of fluorescein from the retinal vasculature.

### 2.9 Quantification of retinal layer thickness from OCT

Retinal layer thickness was quantified from OCT scans by measuring the average thickness across eight evenly spaced regions on a central B-scan image intersecting the optic nerve head, using ImageJ. IPL+RNFL thickness as opposed to RNFL thickness alone, was measured as a proxy of RGC degeneration, as the RNFL is thin and not easily distinguishable from the IPL, thus could lead to segmentation errors and increased variability. Choroidal thickness was measured as the distance from the RPE to the outside of the globe.

### 2.10 Quantification of retinal vascular leakage from FFA

Fluorescein extravasation quantifications were performed using a novel, proprietary software, Fluorescent Ocular Vascular Analysis Software (FOVAS), developed by Dr. Jeffrey O'Callaghan in the Campbell lab. The software allows for semi-automatic registration of retinal vasculature across multiple images taken over the course of a 10-minute FFA procedure. This registration accounts for movement of the mouse during imaging and allows for the creation of a Maximum Intensity Projection (MIP) of all images taken. For mouse images, large macro-vessels can then be masked to allow for specific characterisation of microvascular changes occurring in each retina. Furthermore, a timepoint is set, to which all raw fluorescein values are normalised to account for variations in perfusion rates across experimental animals. Fluorescein leakage was quantified by summing the fluorescence intensity outside the major retinal vessels at each timepoint, including only those timepoints that were available across all eyes. The distribution of cumulative intensity on FFA images was assessed using the Anderson-Darling test and found to be non-parametric. As a result, comparisons between DBA/2J and C57BL/6J mice were made using a Mann-Whitney test, while a Wilcoxon matched-pairs signed-rank test was used for the comparison of leakage before and after dexamethasone-induced OHT.

### 2.11 Biotin permeability assay

Mice were injected intravenously through the tail vein with 2mg/mL EZ-Link Sulfo-NHS-Biotin (600 Da). Eyes were enucleated 5 minutes after biotin injection and immersion fixed

in 4% paraformaldehyde (PFA, pH 7.4) for one hour at 4°C. Retinal wholemounts were taken by cutting along the limbus to remove the anterior segment, and making four additional cuts so that the retina lay flat. Retinas were cryoprotected by sequential incubations in 10%, 20%, and 30% sucrose and frozen in OCT freezing medium (OCT, VWR, 361603E). Retinas were incubated with Cy3-conjected streptavidin (1:200) overnight at 4°C to label Sulfo-NHS-Biotin. Biotin leakage was visualised on a Zeiss Apotome 3 fluorescent microscope. Permeability was assessed by normalising the mean fluorescence intensity in 10 regions of interest inside vessels to the mean of 10 regions of interest outside vessels across the retina in ImageJ.

### 2.12 Immunostaining of retinal cryosections

Mouse retinal cryosections (12-µm thick) were fixed with methanol for 10 minutes at -20°C, washed three times in PBS, and blocked/permeabilised with 5% normal goat serum and 0.5% Triton X-100 in PBS for 30 minutes at room temperature. A list of the antibodies used is provided in Table 2.2. Sections were incubated in primary antibody at 4°C overnight. Sections were then washed 3 times for 5 minutes each in PBS and incubated with the following secondary antibody for 2 hours at room temperature. Following 3 additional PBS washes, sections were counterstained with DAPI (1:3000) for 30 seconds and mounted with Aqua Poly/Mount (Polysciences, Inc). Images were acquired using a Zeiss Apotome 3 fluorescent microscope. Identical acquisition settings were used to acquire images for each comparison. Image processing was performed in ImageJ (NIH). Quantification of vascular marker immunostaining was performed following blinding and randomisation of all images. Using ImageJ, each image was thresholded in the red and green channels to maximise vascular signal while minimising background noise. The percentage area of each channel was then measured, and the vascular marker of interest was normalised to the percentage area of isolectin-IB4 staining.

| Antibody | Supplier | Dilution |
|---|---|---|
| Mouse anti-claudin-5, Alexa Fluor 488 conjugated (352588) | Thermo Fisher Scientific | 1:200 |
| Rat anti-VE-Cadherin (ab282277) | Abcam | 1:200 |
| Rabbit anti-Mfsd2a (80302) | Cell Signalling | 1:200 |
| Isolectin-IB4 Alexa Fluor 568 conjugated | Thermo Fisher Scientific | 1:300 |
| Goat anti-rabbit IgG, Cy3 conjugated (A-10520) | Thermo Fisher Scientific | 1:500 |
| Goat anti-Rat IgG, Cy3 conjugated (A-10522) | Thermo Fisher Scientific | 1:500 |

**Table 2.2| Antibodies used for immunostaining of retinal cryosections**

### 2.13 RNA-seq of C57BL/6J control mice

Eyes were enucleated from 20-week-old C57BL/6J mice after which the neuroretina was carefully isolated. Individual retinas were placed into 350µL RNeasy Lysis Buffer (Buffer RLT, Qiagen) with 1% v/v β-mercaptoethanol, snap-frozen in liquid nitrogen, and stored at -70 °C until RNA isolation. Prior to isolation, retinal samples were thawed on ice and homogenised by repeated passage through a 21-gauge needle attached to a 1mL syringe (approximately 10 passes). Lysates were centrifuged at 12,000g for 5 minutes at 4 °C and the supernatant was then used for total RNA isolation using the RNeasy Mini kit (Qiagen), following the manufacturer's instructions. Genomic DNA was removed via on-column DNase I digestion (12 min, Qiagen) and RNA was eluted in 50µL RNase-free water.

RNA samples were analysed on a TapeStation 2200 (Agilent Technologies) and samples with an RNA integrity number (RIN) value >7 and ribosomal RNA ratio > 1 were used for library preparation and RNA-seq. 100 ng RNA was used for the Watchmaker RNA Library Preparation Kit (Watchmaker Genomics) . RNA-seq with 100 bp paired-end reads and more than 20 million reads per sample was performed on a NovaSeq X platform (Illumina).

### 2.14 RNA seq analysis

RNA-seq data from retinas of C57BL/6J mice aged 2-4 months subjected to microbead-induced OHT or ONC, as well as naïve mice, generated by Keuthan et al. (2023), were accessed through the Gene Expression Omnibus (Accession number: GSE241782) and collated with in-house RNA-seq data outlined in the previous section. Raw FASTQ files were trimmed using Cutadapt (via Trim Galore**)** to remove adapter sequences and low-quality bases. Trimmed reads were aligned to the Gencode GRCm39 mouse reference genome using STAR, and the resulting BAM files were sorted and indexed using Samtools. Gene- and transcript-level quantification was performed using RSEM, and count matrices were imported into R using tximport**.** Differential expression analysis was conducted with DESeq2 (v1.38.3), including batch correction by modelling sample origin as a covariate in the design formula. For visualisation of sample relationships, variance-stabilising transformation (VST) was applied to the raw count data using the vst() function in DESeq2. VST values were then processed with ComBat (from the svapackage) to adjust for technical differences between datasets. Principal component analysis (PCA) was performed on the corrected VST matrix to assess global expression patterns. Genes were considered differentially expressed if they exhibited an absolute $\log_2$ fold change > than 0.58 and an adjusted $p$ value < 0.05, using the Benjamini-Hochberg correction for multiple testing. Volcano plots were generated to visualise the distribution of DEGs based on these thresholds.

Gene set enrichment analysis (GSEA) was performed using the clusterProfiler R package and the org.Mm.eg.db annotation database. Genes were ranked using the product of -log10($p$ value) and the sign of the $\log_2$ fold change. Redundant gene identifiers were resolved by retaining the entry with the highest absolute ranking score. Enrichment analysis of Gene Ontology (GO) Biological Process terms was conducted using the gseGO() function with default normalisation and a $p$ value cutoff of 0.05. The top five positively and negatively enriched GO terms were visualised using bar plots of normalised enrichment scores.

For individual gene plots, VST-normalised counts were extracted and visualised using ggplot2. Gene-level significance was determined using DESeq2's Wald test, with adjusted $p$ values < 0.05 considered significant.

## 2.15 Statistical analysis

In Chapter 3, anterior segment inflammatory marker signals were compared between DBA/2J and C57BL/6J mice using an unpaired Student's *t*-test. For IOP in dexamethasone-treated mice, weeks 1-3 were compared to baseline using a Friedman test with Dunn's correction for multiple comparisons, and the final timepoint was compared between groups using a Mann-Whitney test. Outflow facility in *Casp11*$^{-/-}$, *Asc*$^{-/-}$, *Il18*$^{-/-}$, and intracameral IL-1β injection experiments was analysed using an unpaired weighted *t*-test, while outflow following intracameral IL-18 injection was compared between treated and untreated eyes using a paired weighted *t*-test.

In Chapter 4, IOP between DBA/2J and C57BL/6J mice was compared using a Mann-Whitney test. Retinal thickness and biotin permeability between strains were assessed with unpaired *t*-tests, while cumulative FFA intensity was compared using a Mann-Whitney test. In dexamethasone-treated mice, IOP (weeks 1-4) was analysed against baseline using a Friedman test with Dunn's correction. Retinal thickness was assessed with a paired *t*-test, and cumulative FFA intensity was compared to baseline using a Wilcoxon matched-pairs signed rank test. For all immunostaining analyses, groups were compared using unpaired *t*-tests.

Statistical analyses for Chapter 5 are detailed in Section 2.14.

Unless otherwise stated, $p$ values $< 0.05$ were considered to be significant.

# Chapter 3: Investigating the role of inflammation in regulating AH outflow

## 3.1 Introduction

### 3.1.1 Innate immunity and sterile inflammation

Inflammation is critical for the protection of hosts against invasive pathogens. When infection occurs, a cascade of signals is activated that leads to the recruitment of innate immune cells such as dendritic cells, macrophages, and neutrophils. In turn, these cells phagocytose pathogens and produce additional cytokines and chemokines that lead to the activation of lymphocytes and the adaptive immune response. In addition to eradicating infection, inflammation also plays a role in the healing of tissue in response to trauma or injury in the absence of pathogens. This form of inflammation is termed sterile inflammation. Sterile inflammation, similar to that caused by pathogens, is characterised by the recruitment of innate immune cells and the production of pro-inflammatory cytokines and chemokines, in particular tumour necrosis factor (TNF) and cytokines of the interleukin (IL)-1 family, such as IL-1α, IL-1β, and IL-18 (Chen & Nuñez, 2010). The innate immune system can initiate inflammation in the absence of pathogens due to the ability of pathogen recognition receptors (PRRs) to recognise molecules that are not of pathogenic origin, but rather, would normally be sequestered within cells. When cells undergo necrosis, or otherwise lose plasma membrane integrity, these molecules are released from cells and bind to PRRs. Such molecules are termed damage-associated molecular patterns (DAMPs) (Rock et al., 2010). DAMPs are primarily recognised by PRRs such as Toll-like receptors (TLRs) and C-type lectins, which often converge on common signalling pathways, such as the activation of the NF-κB and AP-1 transcription factors, which then drive the expression of pro-inflammatory cytokines and chemokines. A subset of intracellular PRRs, the NOD-like receptors (NLRs), together with AIM2 (absent in melanoma 2), and pyrin, act as the sensor portion of large multimeric signalling complexes termed inflammasomes. Inflammasomes play a central role in sterile inflammation by mediating the activation of cysteine aspartate protease, caspase-1(Broz & Dixit, 2016; Schroder & Tschopp, 2010).

### 3.1.2 Inflammasomes and pyroptosis

To date, five receptor proteins have been confirmed to assemble inflammasomes: NLRP1, NLRP3, NLRC4, AIM2, and pyrin. Although the upstream signalling events that lead to activation are distinct for each receptor, they ultimately converge on a shared pathway

involving sensor activation, oligomerisation, and the recruitment of the adaptor protein ASC. ASC contains a pyrin domain and a caspase recruitment domain, thus serving as a bridge between the inflammasome sensor and caspase-1. This interaction leads to the conversion of caspase-1 into its catalytically active form, which then executes downstream effector functions including cleavage of pro-IL-1β and pro-IL-18 into their active forms, as well as cleavage of gasdermin-D (GSDMD). GSDMD pore formation in the plasma membrane induces a regulated form of inflammatory cell death termed pyroptosis (Broz & Dixit, 2016; He et al., 2015).

Among the inflammasomes, NLRP3 is the most extensively characterised in the context of age-related eye disease (Mugisho & Green, 2022). Its activation is commonly described by a two-signal model, in which an initial priming step (signal 1) induces NF-κB-dependent upregulation of NLRP3 and pro-IL-1β, followed by a second signal (signal 2) that promotes inflammasome assembly and caspase-1 activation (Bauernfeind et al., 2009). In the glaucomatous outflow pathway, endogenous cytokines such as TNF could provide signal 1, while DAMPs generated by mechanical strain, oxidative stress, and age-related tissue degeneration, such as extracellular ATP, mitochondrial dysfunction associated signals, and particulate ECM debris, are likely candidates for signal 2 activation (Fig. 3.1.1) (Ma et al., 2024; Swanson et al., 2019).

Although less well studied in the context of ocular disease, other inflammasomes could plausibly contribute to sterile inflammation in the outflow tissues. AIM2, which is activated by direct binding of cytosolic double-stranded DNA (Kumari et al., 2020), may respond to host-derived nuclear or mitochondrial DNA released following oxidative damage or cellular stress in TM cells. Similarly, NLRP1, which can be activated in response to intracellular stressors including oxidative stress and protein folding stress (Ball et al., 2022; Liao & Mogridge, 2013; Orth-He et al., 2023), may respond to ER stress in TM cells, which has been shown to contribute to outflow resistance in murine glaucoma models (Zode et al., 2011; Zode et al., 2014). While NLRC4 activation has been classically associated with sensing bacterial flagellin and components of type III secretion systems (Amer et al., 2006; Suzuki et al., 2007), it has also been reported to be expressed in microglia of the CNS, where it contributes to sterile inflammation in response to lysophosphatidylcholine, a lipid-derived DAMP (Freeman et al., 2017). It is thus plausible that NLRC4 activation could occur in myeloid-lineage cells in the outflow tissues in response to modified lipids, which

is potentially relevant given the role of lipid mediators in maintaining IOP homeostasis (Rognon et al., 2025).

While the above inflammasomes signal through caspase-1, a distinct non-canonical inflammasome pathway also exists. In this pathway, murine caspase-11 (human caspases-4 and -5) functions as both a sensor and an effector, leading directly to cleavage of GSDMD and the induction of pyroptosis (Downs et al., 2020). Unlike caspase-1, caspase-11 does not directly process the pro-inflammatory cytokines pro-IL-1β or pro-IL-18 (Ramirez et al., 2018). Nevertheless, capase-11 activation can lead to mature IL-1β and IL-18 formation indirectly, as active GSDMD forms pores in the cell membrane, leading potassium efflux, which in turn activates the NLRP3 inflammasome (Rühl & Broz, 2015). While the most well understood mechanism of caspase-11 activation is via interaction with intracellular LPS, its activation has been observed in astrocytes in sterile inflammatory settings such as ischemia-reperfusion injury (Wan et al., 2024). Interestingly, this appears to be mediated by ER stress, which is a known contributor to outflow resistance in mouse models of OHT (Fradejas et al., 2010; Zode et al., 2011; Zode et al., 2014).

The ultimate consequences of pyroptosis are cell dysfunction and proinflammation. The resulting inflammatory signals are propagated to other cells of the immune system, which can cause a cascade of further inflammation. While sterile inflammation can be beneficial for tissue repair and wound healing, an imbalance of these processes can lead to a chronic, deleterious, pro-inflammatory environment. This is particularly evident during ageing, wherein cells undergo a variety of pathological processes including proteostasis breakdown, mitochondrial dysfunction, altered intercellular communication and senescence (López-Otín et al., 2013). This leads to the phenomenon of inflammageing: a state of sterile, non-resolving, low-grade, and chronic inflammation that progressively increases with age (Feldman et al., 2015). Given that ageing is the primary risk factor for the most prevalent diseases of the developed world (Niccoli & Partridge, 2012), it is plausible that inflammageing plays a role in many of these conditions. The following section will address the potential relevance of sterile inflammation in the context of outflow resistance in glaucoma.

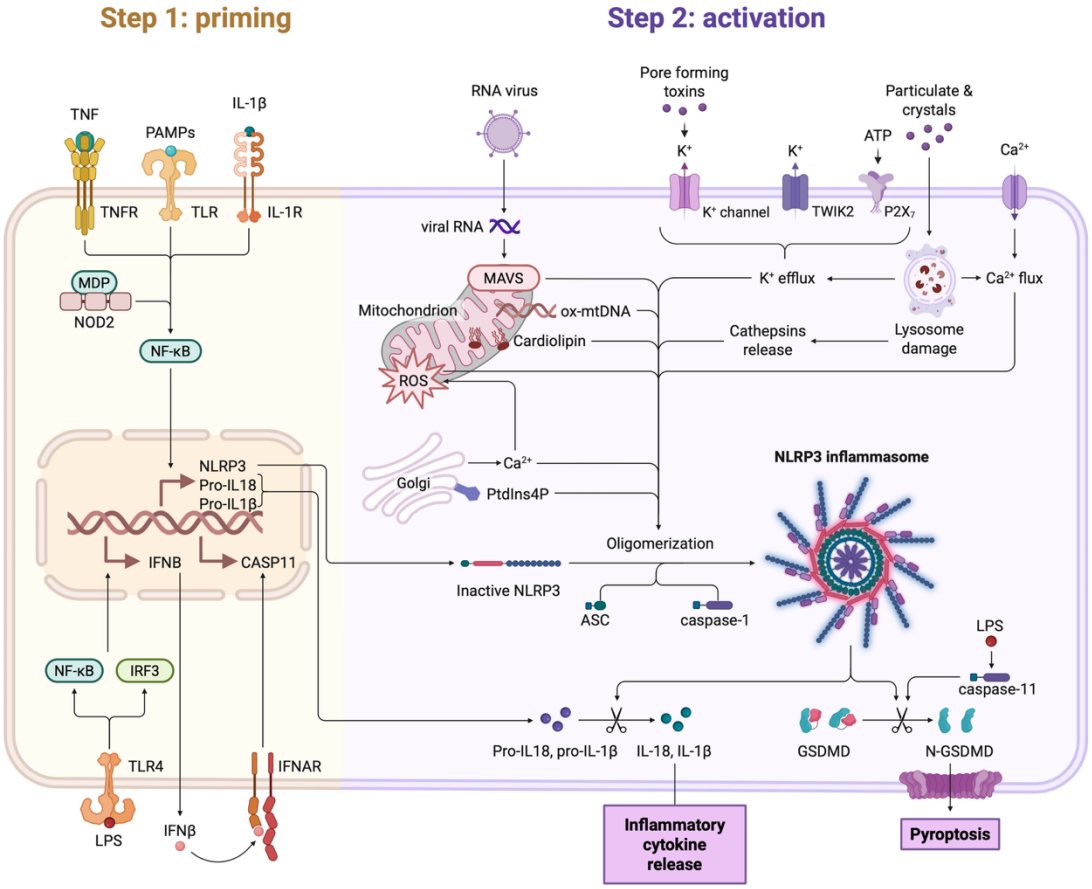



**Figure 3.1.1| Two signal model of NLRP3 inflammasome signalling**

*Step 1 (priming) is triggered by cytokines or pathogen-associated molecular patterns (PAMPs), inducing NF-κB-mediated transcription of canonical and non-canonical inflammasome components. Step 2 (activation) is initiated by diverse PAMPs or DAMPs including particulates, crystals, and ATP, that drive upstream events such as $K^+$ efflux, $Ca^{2+}$ flux, lysosomal disruption, mitochondrial ROS generation, cardiolipin exposure, Ox-mtDNA release. RNA viruses activate NLRP3 through mitochondrial antiviral signalling protein (MAVS). Inflammasome assembly activates caspase-1, which cleaves pro-IL-1β and pro-IL-18, and processes GSDMD to form membrane pores, inducing pyroptosis. Cytosolic LPS directly activates caspase-11, which also cleave GSDMD to trigger pyroptosis. Created in BioRender. Adapted from Swanson et al. (2019)*

### 3.1.3 Sterile inflammation and outflow resistance

The eye is an immune-privileged environment. This was first described in the 1940s, when it was demonstrated that skin allografts survive when placed within the anterior chamber of rabbits that had previously been immunised to reject them (Medawar, 1948). It was later shown that placement of a foreign antigen into the anterior chamber leads to system-wide tolerance of that antigen, a phenomenon known as 'anterior chamber-associated immune deviation' (ACAID) (Kaplan & Streilein, 1977). This process is mediated by F4/80+ macrophages that migrate to the spleen and present the ocular inoculated antigen to B cells, NK cells, CD4 and CD8+ T cells (D'orazio & Niederkorn, 1998; Lin et al., 2005; Sonoda & Stein-Streilein, 2002). The ACAID-inducing properties of macrophages are conferred upon them by immunosuppressive factors present in the AH. This is demonstrated by the fact that macrophages derived from the peritoneum can assume these properties when exposed to AH in vitro. The same effect can be achieved by treating macrophages with TGF-β2, which is present in the AH, indicating that it plays a role in this process (Wilbanks & Wayne Streilein, 1992). Other peptides in the AH, such as calcitonin gene-related peptide and alpha-melanocyte-stimulating hormone, also suppress the inflammatory activity of macrophages (Taylor et al., 1998; Taylor, 2005).

It is clear from the above that there is a high threshold in the AH microenvironment that must be overcome to induce an inflammatory response. This can be considered as a trade-off: while it leaves the ocular environment more susceptible to infection, this risk is far outweighed by the potentially catastrophic consequences of a dysregulated immune response in the eye, given the limited regenerative capacity of retinal neurons (Streilein, 1996). Nevertheless, this does occur in the case of uveitis, characterised by inflammation of the uveal tract, which consists of the pigmented vascular structures of the eye including the iris, ciliary body, and the choroid. Mouse models of uveitis display a loss of ocular immune privilege, including an increase in the concentration of inflammatory cytokines in the AH and a loss of ACAID (K. Ohta et al., 2000; Kouichi Ohta et al., 2000). Notably, ~10% of patients with uveitis develop uveitic glaucoma (Kalogeropoulos & Sung, 2018; Neri et al., 2004). Like POAG, patients with uveitic glaucoma display decreased outflow facility and increased IOP, culminating in optic nerve damage and visual field loss (Alaghband et al., 2019; Kalogeropoulos & Sung, 2018). While the pathophysiology of uveitic glaucoma is unknown, and likely differs between subtypes, it is associated with

increased levels of cytokines, chemokines, and immune cells in the AH (Norose et al., 1994; Sijssens et al., 2007; Verma et al., 1997). The decreased outflow facility in these patients may thus be caused by: **1)** a physical blockage of the outflow pathway due to increased protein concentration, inflammatory cells and debris in uveitic eyes; **2)** the inflammatory environment leading to expression changes in, or damage to the TM and SC; or **3)** some combination of both (Kalogeropoulos & Sung, 2018).

While uveitis represents an outright form of inflammatory glaucoma, there is also evidence that chronic inflammation may contribute to increased outflow resistance in other forms of glaucoma. TM cells have been shown to release a variety of cytokines in response to mechanical stress, including IL-1α, IL-1β, IL-6, and TNF-α (Alvarado et al., 2005; Baudouin et al., 2021; Liton et al., 2005). Additionally, perfusion of porcine eyes with IL-1α and IL-1β leads to increased outflow facility, which is associated with an upregulation of MMPs -3 and -9 (Birke et al., 2011). In increase in outflow facility has similarly been shown in rats upon intracameral injection of IL-1α (Kee & Seo, 1997). It has been proposed that this may represent an autocrine-feedback mechanism in the TM, whereby mechanical stress caused by elevations in IOP leads to the secretion of cytokines by TM cells to restore normal IOP (Baudouin et al., 2021). Furthermore, there are now several studies that have shown an altered cytokine profile in the AH and TM of human eyes with POAG, relative to healthy controls (Burgos-Blasco et al., 2020; Chua et al., 2012; Takai et al., 2012; Taurone et al., 2015; Zhang et al., 2019). The above findings highlight the inflammatory environment of the anterior chamber as a potential contributing mechanism to the development of outflow resistance in glaucoma. Given that age is a major risk factor for glaucoma, and is associated with a dysregulation of inflammation, it is plausible that this altered inflammatory environment could lead to pathological changes in the outflow tissues, culminating in decrease outflow facility and increased IOP.

### 3.1.4 Chapter aims

The central question that this chapter aimed to address is whether modulation of inflammatory pathways in the anterior segment can influence AH outflow and IOP in glaucoma. To this end, there were three primary objectives: 1) to characterise the immune profile of the anterior segment in glaucomatous murine eyes; 2) to uncover the roles of the canonical and non-canonical inflammasomes in regulating outflow facility; and 3) to

investigate the plausibility of manipulating the sterile inflammatory response to regulate outflow facility in murine eyes. Three lines of investigation were pursued. Firstly immunostaining was performed for myeloid-lineage cell markers, inflammasome receptors, and cytokines in the anterior segment of aged DBA/2J mice, to determine whether the glaucomatous eye displays an altered immune profile. Secondly, the effects of canonical inflammasome activation, and its downstream effectors IL-1β and IL-18, on outflow facility were examined. Lastly, the role of caspase-11 in modulating AH outflow was investigated in dexamethasone-induced OHT to assess the contribution of non-canonical inflammasome activation to AH outflow. These approaches were designed to assess both the pathological contribution of inflammation to outflow resistance and the potential for targeted inflammatory modulation as a therapeutic strategy.

## 3.2 Results

### 3.2.1 Immunohistochemical profiling of the anterior chamber in glaucomatous mice

To assess whether modulation of inflammation is a viable strategy to enhance AH outflow in glaucoma, the first part of this chapter aimed to characterise the immune profile of the anterior chamber in a mouse model of the disease. Immunostaining was performed on anterior segment cryosections from aged DBA/2J mice (9-12 months old) and age-matched C57BL/6J controls, targeting immune cell markers, inflammasome components, and downstream cytokines. Expression was quantified in three corneal layers (epithelium, stroma, and endothelium), as well as in the iris and ciliary body, both of which are components of the uveal tract (Fig. 3.2.1).

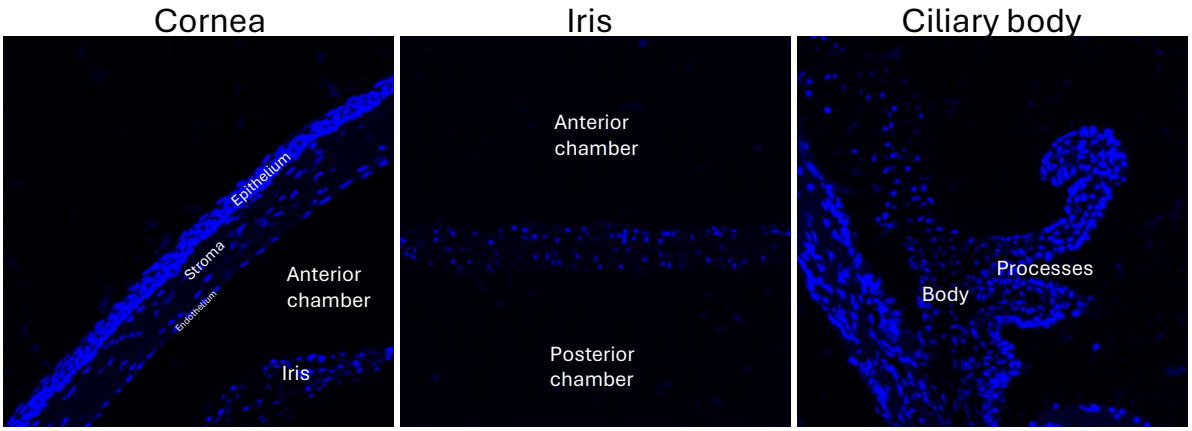



**Figure 3.2.1 | Regions of the anterior chamber analysed by immunostaining**
*Representative images of DAPI-stained anterior segments from C57BL/6J mice illustrating the normal cellular architecture of the analysed regions. Following immunostaining for inflammatory markers, expression was quantified in the three corneal layers (epithelium, stroma, and endothelium) (left), the iris (middle) and ciliary body (right).*

The anterior segment of the eye, particularly the uveal tract, contains resident macrophages and dendritic cells that contribute to the maintenance of ocular immune privilege through mechanisms such as ACAID (McMenamin, 1997; Streilein, 1996). Under pathological conditions, these cells can become immunologically activated, promoting local inflammation and potentially impairing AH outflow. To explore differences in the immune cell profile between healthy and glaucomatous eyes, immunostaining was performed for three monocyte-lineage markers: F4/80, CD68, and CD11b.

Immunostaining for F4/80, a well-established marker of murine tissue-resident macrophages, revealed minimal immunoreactivity in the corneas of both C57BL/6J and DBA/2J mice. Similarly, little to no signal was detected in the iris of C57BL/6J mice; however, in DBA/2J mice, clear F4/80 expression was present in the iris, which also appeared enlarged, consistent with the pigment dispersion phenotype of this model. In the ciliary body, weak F4/80 staining was detected in C57BL/6J mice, whereas a subset of DBA/2J mice exhibited a visibly stronger signal, along with apparent structural atrophy relative to controls (Fig. 3.2.2A).

Quantitative analysis showed no significant differences in F4/80 expression between strains the corneal epithelium (Fig. 3.2.2B; $p = 0.2341$), corneal stroma (Fig. 3.2.2C; $p = 0.7091$), or corneal endothelium (Fig. 3.2.2D; $p = 0.4456$). In the iris, F4/80 signal was significantly higher in DBA/2J mice, with a mean increase of approximately 20-fold relative to controls (Fig. 3.2.2E; $p = 0.0270$). In the ciliary body, elevated F4/80 expression was observed in roughly half of the DBA/2J eyes, while the remainder showed minimal change compared to controls. As a result, the group-level increase was not significant (Fig. 3.2.2F; $p = 0.1952$)

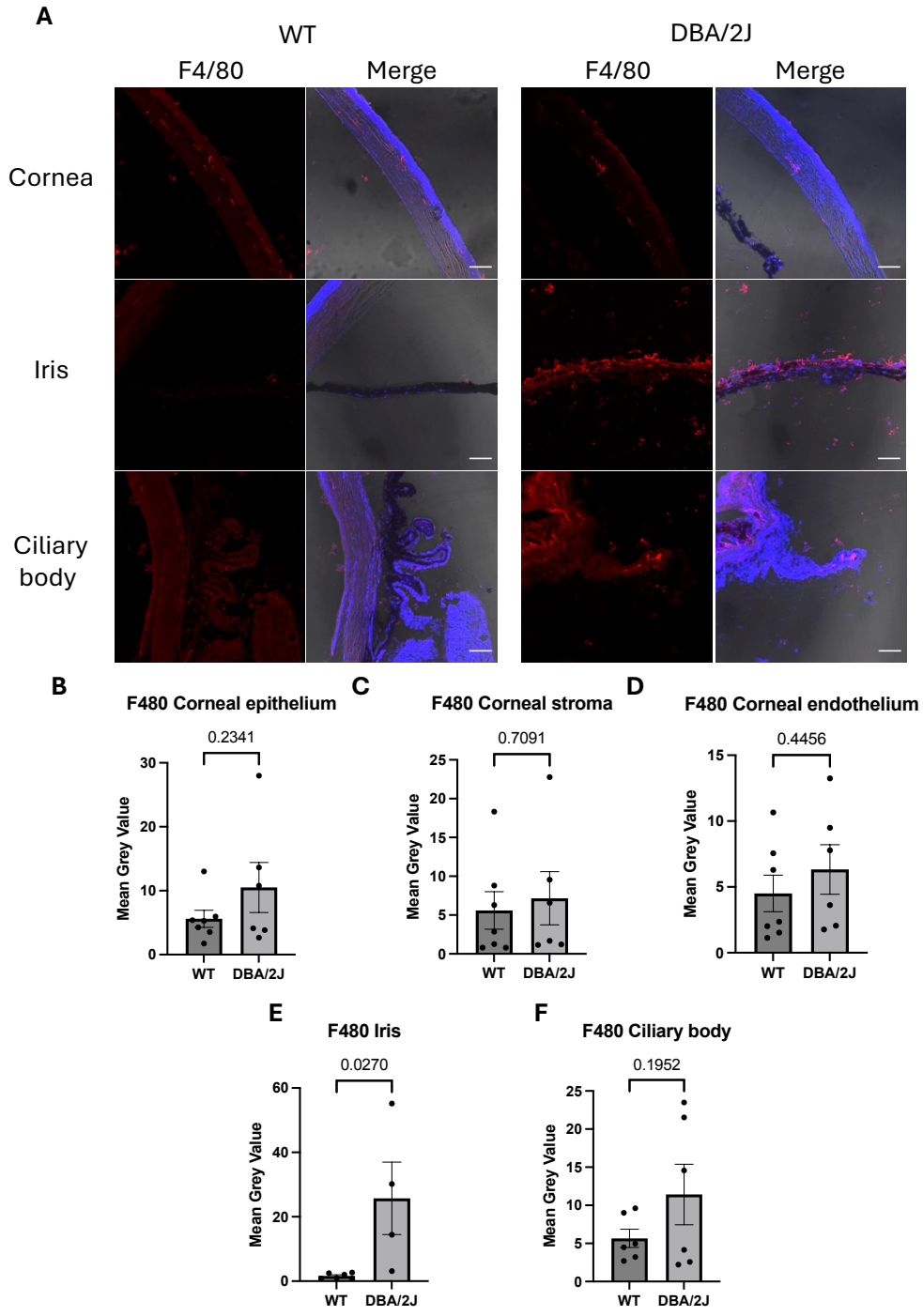



**Figure 3.2.2| F4/80 immunostaining in DBA/2J anterior segments**

***(A)*** *Representative images showing F4/80 immunostaining (red) in the cornea, iris, and ciliary body, in addition to merged images with brightfield and DAPI (grey/blue). Scale bar = 50 µm.* ***(B-F)*** *Quantification of F4/80 signal intensity in the corneal epithelium, corneal stroma, corneal endothelium, iris, and ciliary body. Mean grey values were*

*measured and compared between groups using an unpaired Student's t-test. n = 7 WT ; 6 DBA/2J (Cornea), n = 6 WT ; 4 DBA/2J (Iris), n = 6 WT ; 6 DBA/2J (Ciliary body)*

Immunostaining for CD11b, a widely used marker of myeloid-lineage cells, revealed minimal signal in the corneas of C57BL/6J mice. In DBA/2J mice, the corneal epithelium and stroma similarly showed little immunoreactivity, but a subset exhibited clear CD11b staining in the corneal endothelium. Similar to the pattern observed with F4/80, CD11b signal in the iris was low in C57BL/6J mice but appeared more pronounced in DBA/2J mice, with a globular staining pattern being observed. In the ciliary body, sparse pockets of signal were detected in C57BL/6J mice, while DBA/2J mice showed more widespread CD11b staining (Fig. 3.2.3A).

Quantification of CD11b expression revealed no significant difference between groups in the corneal epithelium (Fig. 3.2.3B; $p = 0.2662$) or corneal stroma (Fig. 3.2.3C; $p = 0.5710$). In the corneal endothelium, CD11b signal appeared elevated in DBA/2J mice, although this trend was driven largely by two mice with higher expression levels and did not reflect a consistent group-wide change (Fig. 3.2.3D; $p = 0.0908$). In the iris, CD11b expression was markedly higher in DBA/2J mice, with an approximately 10-fold increase in mean signal relative to controls (Fig. 3.2.3E; $p = 0.0243$). A similar pattern was observed in the ciliary body, where CD11b signal was also elevated in DBA/2J mice (Fig. 3.2.3F; $p = 0.0336$).

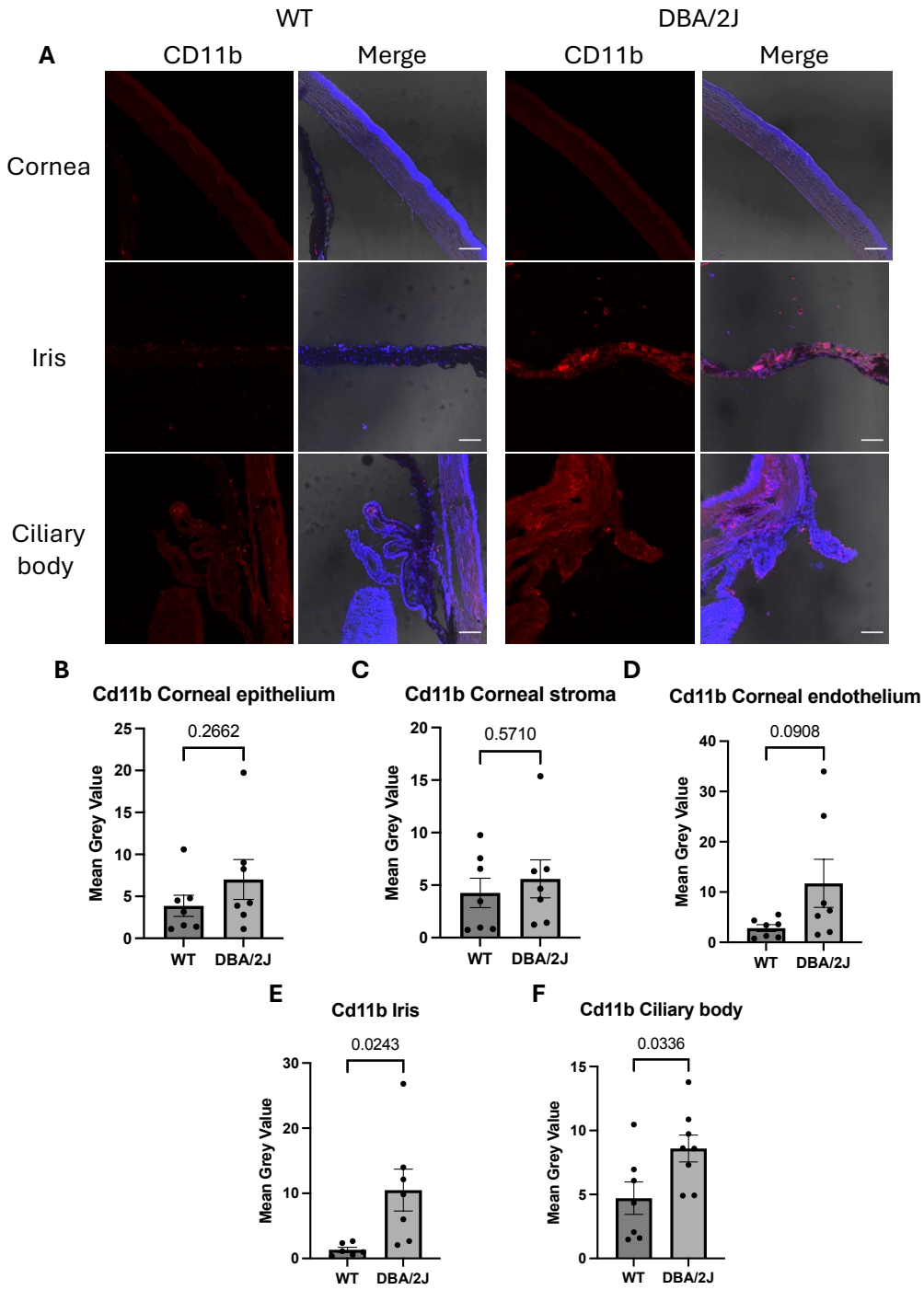



**Figure 3.2.3| CD11b immunostaining in DBA/2J anterior segments**

***(A)*** *Representative images showing CD11b immunostaining (red) in the cornea, iris, and ciliary body, with merged images with brightfield and DAPI (grey/blue). Scale bar = 50 µm.* ***(B-F)*** *Quantification of CD11b signal intensity in the corneal epithelium, corneal stroma, corneal endothelium, iris, and ciliary body. Mean grey values were measured and compared between groups using an unpaired Student's t-test. n = 7 per group (Cornea), n = 6 WT; 7 DBA/2J (Iris), n = 7 WT; 8 DBA/2J (Ciliary body).*

Immunostaining for CD68, a marker of phagocytic myeloid cells, showed minimal signal in the corneas of both C57BL/6J and DBA/2J mice (Fig. 3.2.4A). Similar to the patterns observed with F4/80 and CD11b, the iris of C57BL/6J mice showed very little immunoreactivity, while the iris of DBA/2J mice exhibited a strong, globular staining pattern (Fig. 3.2.4A). In the ciliary body, CD68 signal was sparse in C57BL/6J mice but appeared more prominent and widespread in DBA/2J mice (Fig. 3.2.4A).

Quantification of CD68 expression revealed no detectable differences between strains in the corneal epithelium (Fig. 3.2.4B; $p = 0.8243$), stroma (Fig. 3.2.4C; $p = 0.4937$), or endothelium (Fig. 3.2.4D; $p = 0.4937$). In contrast, the iris of DBA/2J mice showed a clear increase of in CD68 signal of around ten-fold compared to C57BL/6J controls (Fig. 3.2.4E; $p = 0.0472$). In the ciliary body, the mean CD68 signal was approximately two-fold higher in DBA/2J mice, although there was high degree of variation in the DBA/2J group and this change was not significant (Fig. 3.2.4F; $p = 0.0673$).

Taken together, immunostaining for F4/80, CD11b, and CD68 indicated increased levels of myeloid-lineage cells, likely activated macrophages, in the iris, and to a lesser extent the ciliary body, of DBA/2J mice compared to C57BL/6J controls.

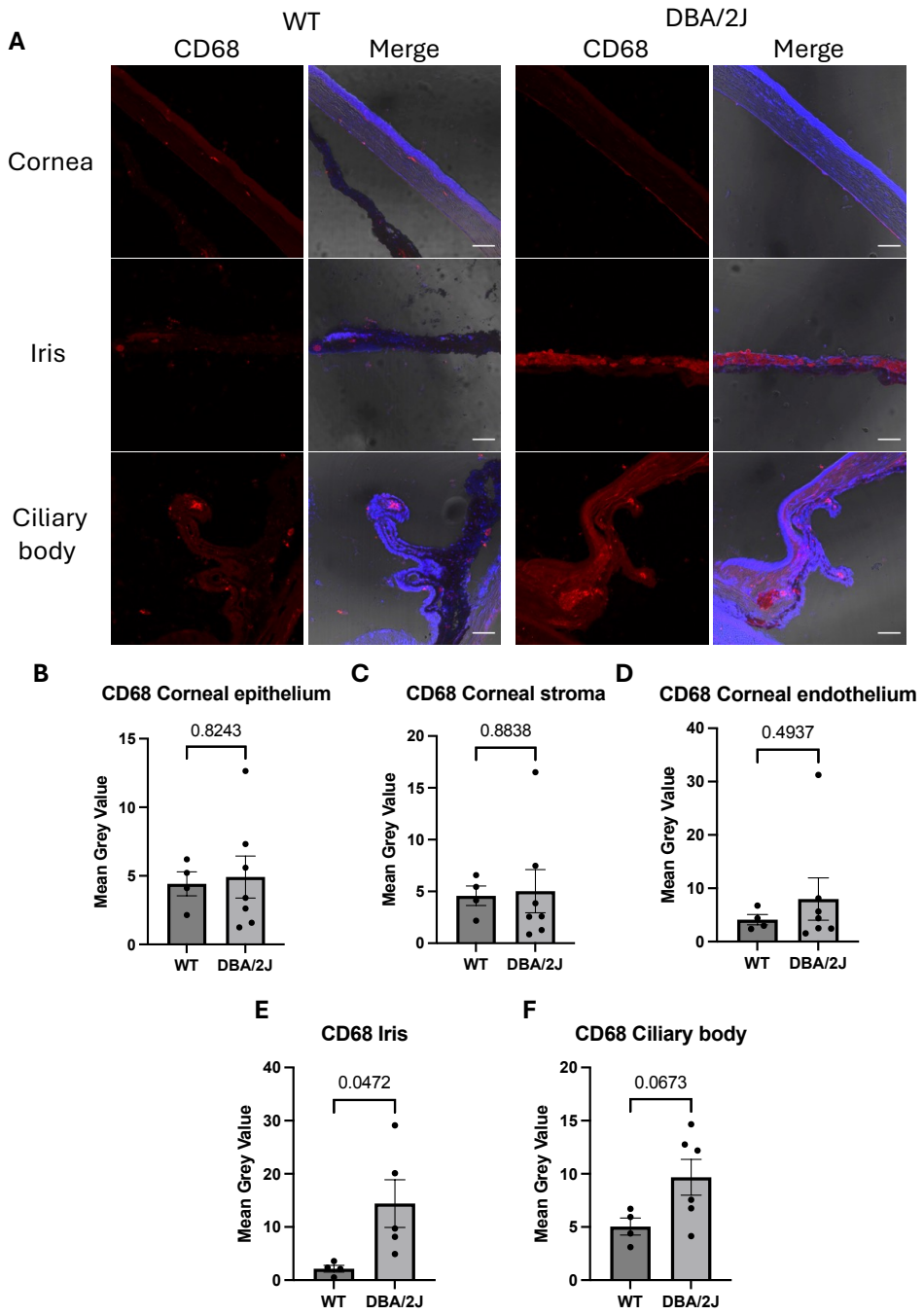



**Figure 3.2.4| CD68 immunostaining in DBA/2J anterior segments**

***(A)*** *Representative images showing CD68 immunostaining (red) in the cornea, iris, and ciliary body, with merged images with brightfield and DAPI (grey/blue). Scale bar = 50 µm.* ***(B-F)*** *Quantification of CD68 signal intensity in the corneal epithelium, corneal stroma, corneal endothelium, iris, and ciliary body. Mean grey values were measured and compared between groups using an unpaired Student's t-test. n = 4 WT; 7 DBA/2J (Cornea), n = 4 WT; 5 DBA/2J (Iris), n = 4 WT; 6 DBA/2J (Ciliary Body).*

Given the apparent increase in activated myeloid-lineage cells in the anterior segment of DBA/2J mice, immunostaining was performed for the inflammasome components NLRP3, AIM2, NLRP1, and NLRC4 to investigate whether inflammasome activation may contribute to a pro inflammatory environment in the anterior chamber.

NLRP3 is the most well-characterised inflammasome receptor in age-related eye disease and is known to form an active inflammasome complex in response to a wide range of stimuli, including extracellular ATP, mitochondrial dysfunction signals, and particulate matter (Mugisho & Green, 2022; Swanson et al., 2019). This leads to the downstream cleavage and maturation of the pro-inflammatory cytokines IL-1β and IL-18. Immunostaining for NLRP3 revealed low levels of diffuse signal throughout the cornea in both C57BL/6J and DBA/2J mice. In the iris, signal was minimal in C57BL/6J mice but appeared more pronounced in DBA/2J mice, displaying a globular pattern. In the ciliary body, NLRP3 immunoreactivity was observed in both strains; however, the signal in DBA/2J mice appeared more ubiquitous compared to controls (Fig. 3.2.5A).

Quantitative analysis of NLRP3 expression revealed no significant differences between strains in the corneal epithelium ($p = 0.2175$; Fig. 3.2.5B), stroma ($p = 0.2521$; Fig. 3.2.5C), or endothelium ($p = 0.3607$; Fig. 3.2.5D), although DBA/2J mice showed a slight, non-appreciable increase in all three layers. In contrast, NLRP3 expression was markedly elevated in the iris (Fig. 3.2.5E; $p = 0.0266$) and ciliary body (Fig. 3.2.5F; $p = 0.0176$) of DBA/2J mice, suggesting increased NLRP3 inflammasome activity in these regions.

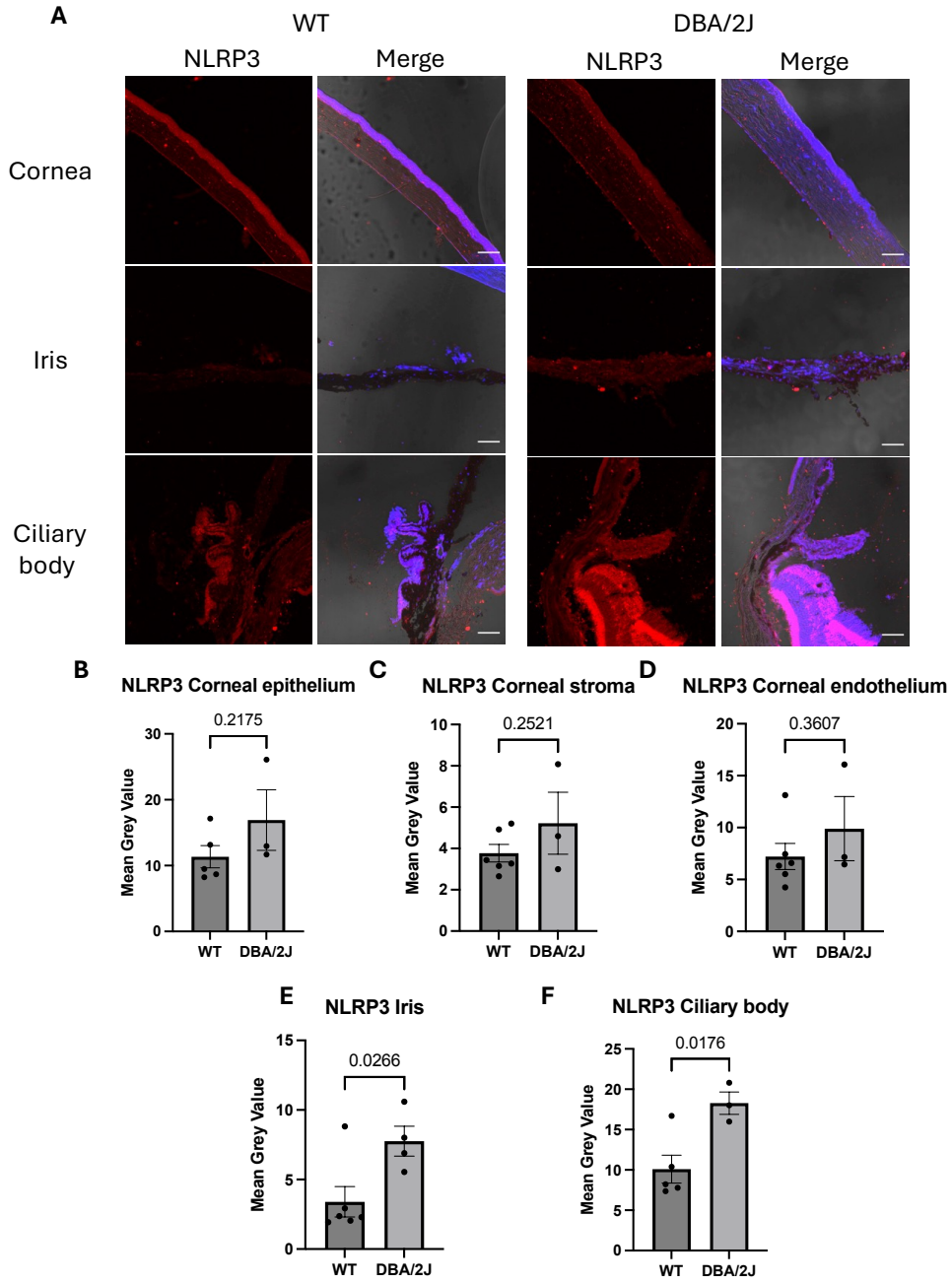



**Figure 3.2.5| NLRP3 immunostaining in DBA/2J anterior segments**

***(A)*** *Representative images showing NLRP3 immunostaining (red) in the cornea, iris, and ciliary body, with merged images with brightfield and DAPI (grey/blue). Scale bar = 50 µm.* ***(B-F)*** *Quantification of NLRP3 signal intensity in the corneal epithelium, corneal stroma, corneal endothelium, iris, and ciliary body. Mean grey values were measured and compared between groups using an unpaired Student's t-test. n = 5 WT; 3 DBA/2J (Corneal Epithelium), n = 6 WT; 3 DBA/2J (Corneal Stroma and Endothelium), n = 6 WT; 4 DBA/2J (Iris), n = 5 WT; 3 DBA/2J (Ciliary Body).*

AIM2 is an inflammasome sensor that is activated by the direct binding of cytosolic double-stranded DNA. In the context of sterile inflammation, AIM2 can be activated by host-derived nuclear or mitochondrial DNA (Kumari et al., 2020). It was thus hypothesised that AIM2 activation may occur in the anterior chamber in response to oxidative damage or cellular stress in TM cells.

Upon immunostaining for AIM2, low-level expression was observed throughout the cornea in both C57BL/6J and DBA/2J mice. In the iris, as with NLRP3, sparse regions of immunoreactivity were detected in C57BL/6J mice, while DBA/2J mice exhibited a more prominent AIM2 signal. In the ciliary body, AIM2 expression was present in both strains (Fig. 3.2.6A).

Quantification of AIM2 expression revealed no differences between groups in the corneal epithelium (Fig. 3.2.6B; $p = 0.5727$) or stroma (Fig. 3.2.6C; $p = 0.9888$). A slight decrease in expression was observed in the corneal endothelium of DBA/2J mice; however, there was high variability in the C57BL/6J group (Fig. 3.2.6D; $p = 0.3641$). In the iris, a trend toward increased AIM2 expression was observed in DBA/2J mice, though this did not meet the threshold for significance (Fig. 3.2.6E; $p = 0.0690$). No difference in expression between the groups was detected in the ciliary body (Fig. 3.2.6F; $p = 0.6358$).

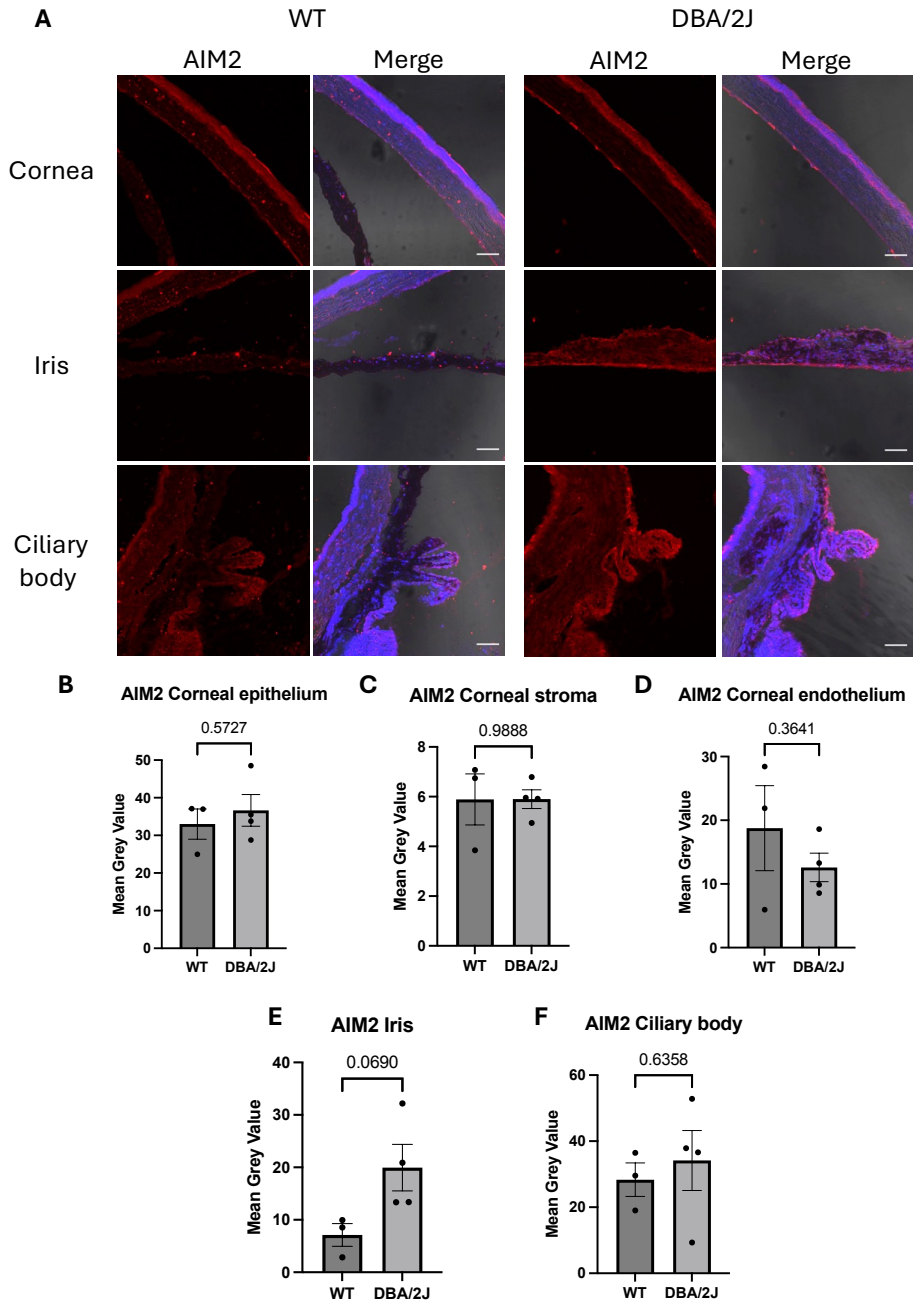



**Figure 3.2.6| AIM2 immunostaining in DBA/2J anterior segments**

***(A)*** *Representative images showing AIM2 immunostaining (red) in the cornea, iris, and ciliary body, with merged images with brightfield and DAPI (grey/blue). Scale bar = 50 µm.* ***(B-F)*** *Quantification of AIM2 signal intensity in the corneal epithelium, corneal stroma, corneal endothelium, iris, and ciliary body. Mean grey values were measured and compared between groups using an unpaired Student's t-test. n = 3 WT; 4 DBA/2J for all comparisons.*

Although less commonly associated with DAMP-mediated activation, both NLRP1 and NLRP4 have been shown to participate in sterile inflammatory responses in the CNS (de Rivero Vaccari et al., 2016; Freeman et al., 2017). Sterile danger signals that activate NLRP1 include oxidative stress, and protein folding stress (Ball et al., 2022; Liao & Mogridge, 2013; Orth-He et al., 2023), while NLRC4 activation has been reported in response to lysophosphatidylcholine, a lipid-derived DAMP (Freeman et al., 2017). On this basis, it was hypothesised that NLRP1 and NLRC4 may be activated by ER stress and lipid dysregulation, respectively, in the outflow tissues.

Immunostaining for NLRP1 revealed low expression throughout the anterior segment in both C57BL/6J and DBA/2J mice, with slightly more prominent staining in the ciliary body of C57BL/6J mice (Fig. 3.2.7A). Quantification showed no differences in the corneal epithelium (Fig. 3.2.7B; $p = 0.7866$), corneal stroma (Fig. 3.2.7C; $p = 0.3388$), or iris (Fig. 3.2.7E; $p = 0.4312$). However, expression was reduced in DBA/2J mice relative to controls in both the corneal endothelium (Fig. 3.2.7D; $p = 0.0329$) and ciliary body (Fig. 3.2.7F; $p = 0.0431$).

In contrast, NLRC4 staining showed low expression across all examined tissues in both strains, with no apparent differences between groups. Quantification confirmed no significant differences in the corneal epithelium (Fig. 3.2.8B; $p = 0.5592$), stroma (Fig. 3.2.8C; $p = 0.1775$), endothelium (Fig. 3.2.8D; $p = 0.1180$), iris (Fig. 3.2.8E; $p = 0.6755$), or ciliary body (Fig. 3.2.8F; $p = 0.8093$).

Taken together, findings from immunostaining for NLRP3**,** AIM2**,** NLRP1, and NLRC4 suggest increased canonical inflammasome activation in the iris, and to a lesser extent the ciliary body, of DBA/2J mice. This appeared to be mediated by inflammasome sensors NLRP3 and AIM2.

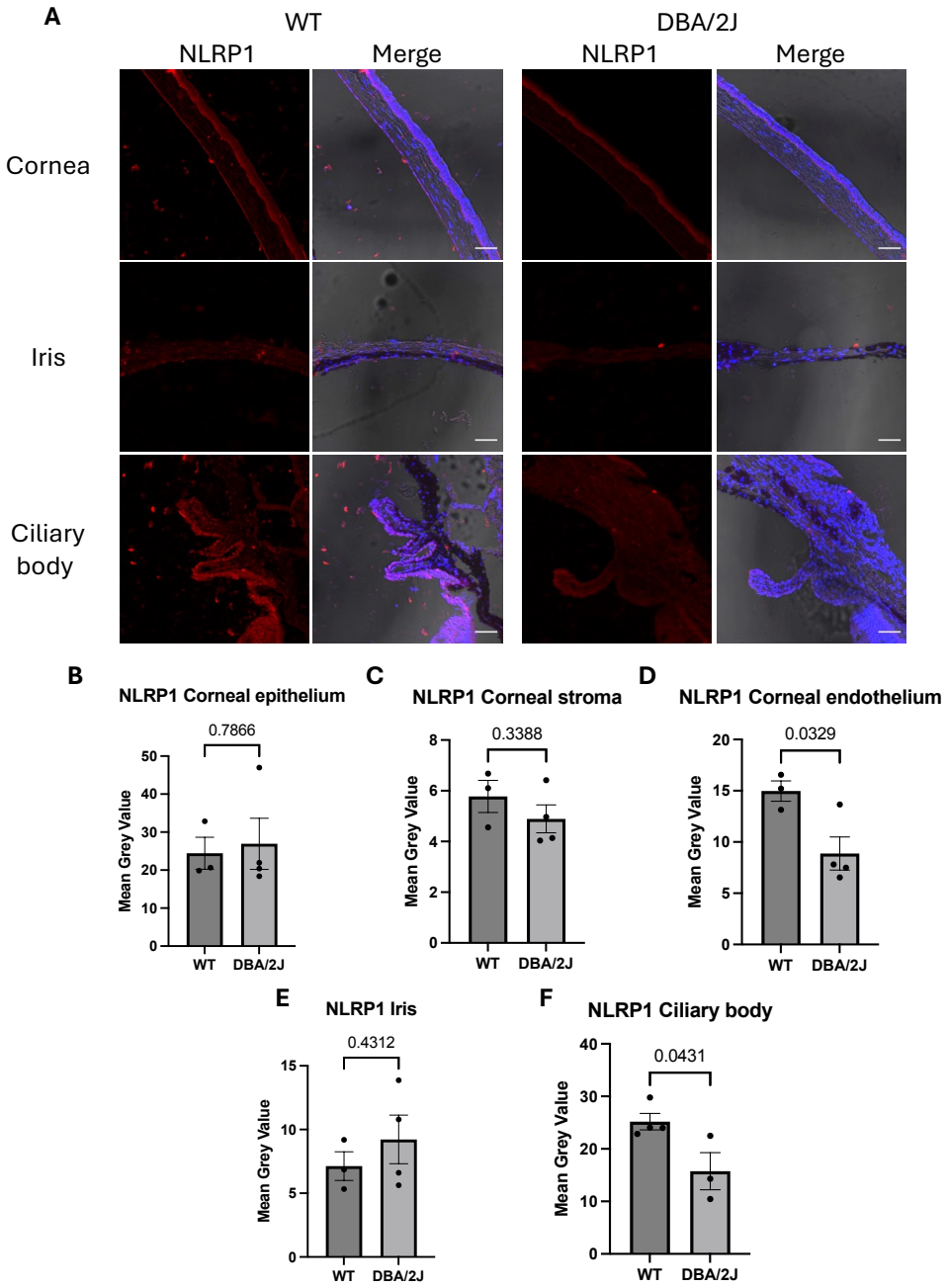



**Figure 3.2.7| NLRP1 immunostaining in DBA/2J anterior segments**

***(A)*** *Representative images showing NLRP1 immunostaining (red) in the cornea, iris, and ciliary body, with merged images with brightfield and DAPI (grey/blue). Scale bar = 50 µm.* ***(B-F)*** *Quantification of NLRP1 signal intensity in the corneal epithelium, corneal stroma, corneal endothelium, iris, and ciliary body. Mean grey values were measured and compared between groups using an unpaired Student's t-test. n = 3 WT; 4 DBA/2J (Corneal epithelium), n = 3 WT; 4 DBA/2J (Corneal Stroma, Corneal Endothelium, Iris), n = 4 WT; 3 DBA/2J (Ciliary Body).*

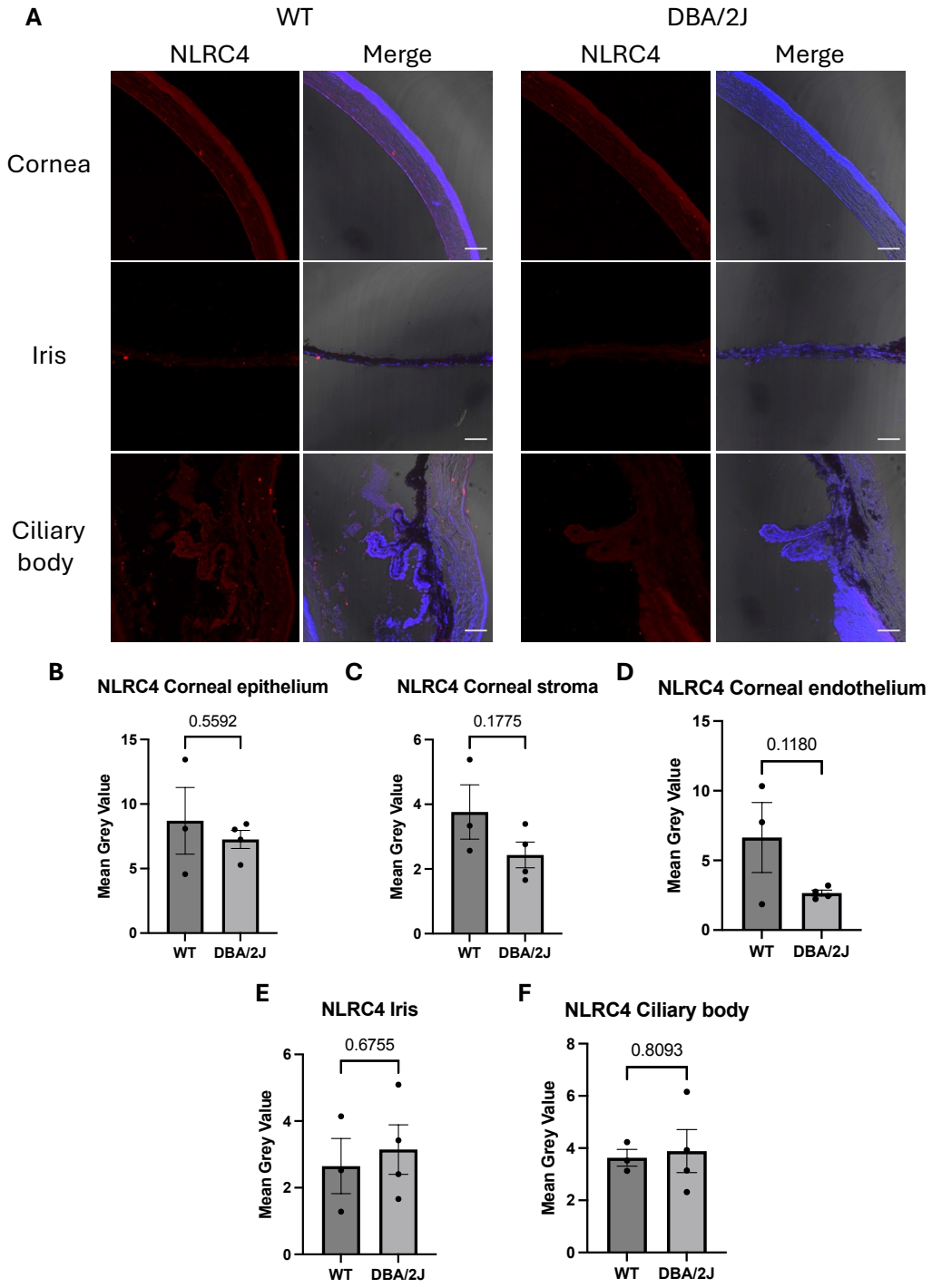



**Figure 3.2.8| NLRC4 immunostaining in DBA/2J anterior segments**

***(A)*** *Representative images showing NLRC4 immunostaining (red) in the cornea, iris, and ciliary body, with merged images with brightfield and DAPI (grey/blue). Scale bar = 50 µm.* ***(B-F)*** *Quantification of NLRC4 signal intensity in the corneal epithelium, corneal stroma, corneal endothelium, iris, and ciliary body. Mean grey values were measured and compared between groups using an unpaired Student's t-test. n = 3 WT; 4 DBA/2J for all comparisons*

As key pro-inflammatory cytokines processed downstream of inflammasome activation, IL-1β and IL-18 expression were next examined to assess whether increased inflammasome activity in DBA/2J mice was associated with elevated cytokine production in the anterior segment.

IL-1β showed diffuse immunoreactivity across the cornea and ciliary body in both C57BL/6J and DBA/2J mice. In the iris, staining was observed in both groups but appeared visibly more prominent in DBA/2J mice (Fig. 3.2.9A). Quantification revealed a trend toward reduced IL-1β expression in the corneal epithelium (Fig. 3.2.9B; $p = 0.0750$) and corneal endothelium (Fig. 3.2.9D; $p = 0.0713$) of DBA/2J mice, although this reduction was not evident on visual inspection. No difference was observed in the corneal stroma (Fig. 3.2.9C; $p = 0.4617$). In the iris, IL-1β expression was significantly increased in DBA/2J mice, with approximately a twofold elevation relative to controls (Fig. 3.2.9E; $p = 0.0097$). No difference between groups was detected in the ciliary body (Fig. 3.2.9F; $p = 0.2415$).

A diffuse IL-18 expression was observed in the cornea and ciliary body of both strains. In the iris, signal was minimal in C57BL/6J mice and visibly brighter in DBA/2J mice (Fig. 3.2.10A). Quantitative analysis showed no differences in IL-18 expression between groups in the corneal epithelium (Fig. 3.2.10B; $p = 0.7700$), stroma (Fig. 3.2.10C; $p = 0.8274$), or endothelium (Fig. 3.2.10D; $p = 0.7702$). In the iris, IL-18 expression was approximately twofold higher in DBA/2J mice compared to C57BL/6J controls (Fig. 3.2.10E; $p = 0.0145$). No significant difference was observed in the ciliary body (Fig. 3.2.10F; $p = 0.2833$).

Together, these findings indicate that increased inflammasome activity in the iris of DBA/2J mice is accompanied by elevated expression of downstream cytokines IL-1β and IL-18 in the iris, supporting the presence of a local pro-inflammatory environment in the anterior segment of DBA/2J mice.

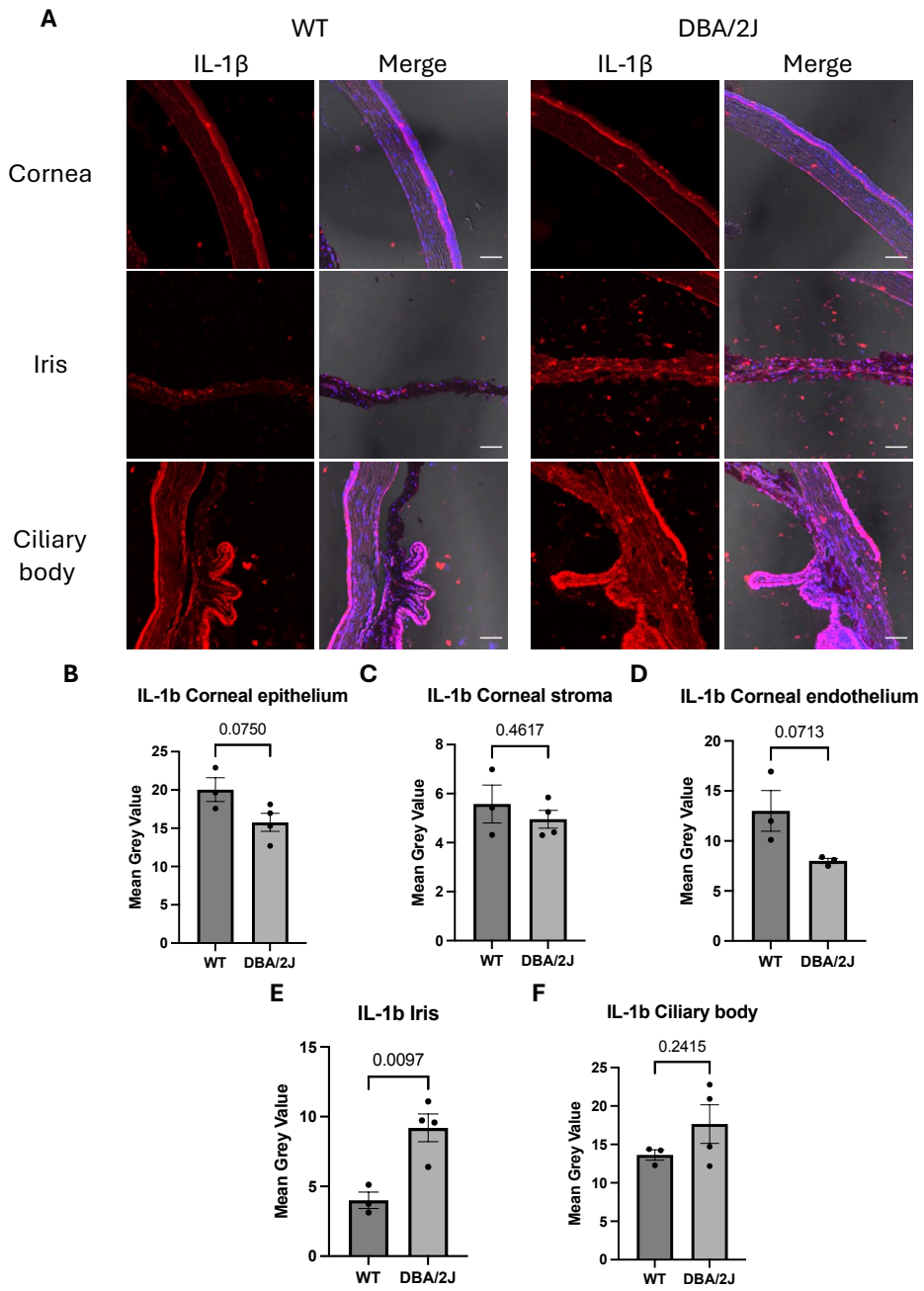



**Figure 3.2.9| IL-1β immunostaining in DBA/2J anterior segments**

***(A)*** *Representative images showing IL-1β immunostaining (red) in the cornea, iris, and ciliary body, with merged images with brightfield and DAPI (grey/blue). Scale bar = 50 µm.* ***(B-F)*** *Quantification of IL-1β signal intensity in the corneal epithelium, corneal stroma, corneal endothelium, iris, and ciliary body. Mean grey values were measured and compared between groups using an unpaired Student's t-test. n = 3 WT; 4 DBA/2J (Corneal epithelium, Corneal Stroma, Iris, Ciliary Body), n = 3 WT; 3 DBA/2J (Corneal endothelium).*

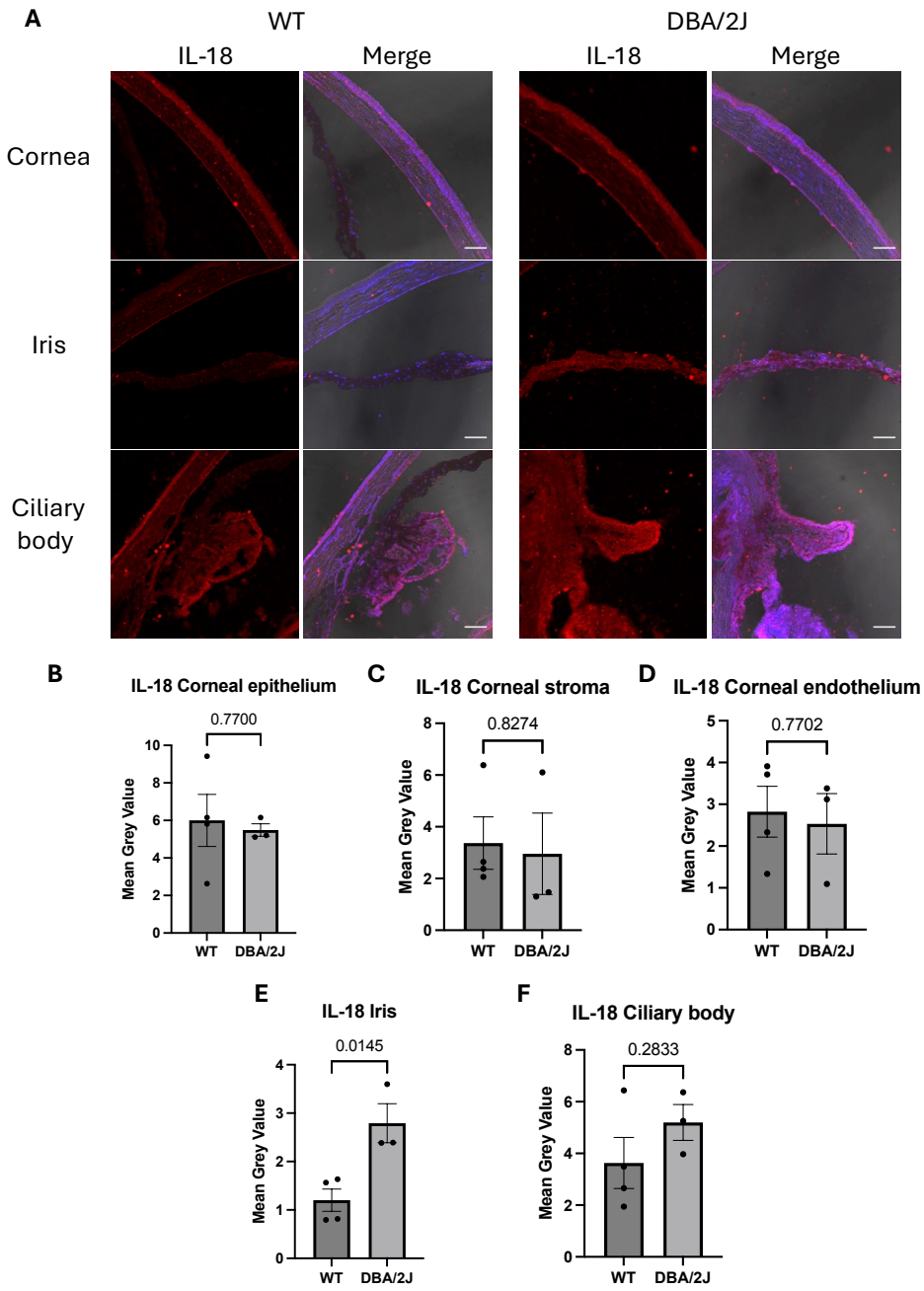



**Figure 3.2.10| IL-18 immunostaining in DBA/2J anterior segments**

***(A)*** *Representative images showing IL-18 immunostaining (red) in the cornea, iris, and ciliary body, with merged images with brightfield and DAPI (grey/blue). Scale bar = 50 um.* ***(B-F)*** *Quantification of IL-18 signal intensity in the corneal epithelium, corneal stroma, corneal endothelium, iris, and ciliary body. Mean grey values were measured and compared between groups using an unpaired Student's t-test. n = 4 WT; 3 DBA/2J for all comparisons.*

### 3.2.2 Dissecting canonical and non-canonical inflammasome signalling in AH outflow regulation

Given the pro-inflammatory profile detected in the anterior chamber of DBA/2J mice, this section aimed to dissect the roles of canonical and non-canonical inflammasome pathways in regulating AH outflow. The effects of canonical inflammasome activation were examined by measuring outflow facility in mice treated with, or deficient in, downstream effectors of canonical inflammasome signalling, while the contribution of non-canonical inflammasome activity was investigated by determining how caspase-11 deficiency influences the progression of dexamethasone-induced OHT. These approaches allowed for the contribution of each inflammatory signalling pathway to outflow resistance in glaucoma to be assessed, in addition to the possibility of using inflammatory modulation as a therapeutic strategy.

To investigate the downstream effects of canonical inflammasome activation on AH outflow, recombinant IL-18 and IL-1β, the effector cytokines generated following activation of caspase-1, were administered to C57BL/6J mice via intracameral injection and allowed to circulate for 48 and 72 hours, respectively. Following this, eyes were enucleated and for ex vivo measurement of outflow facility using the iPerfusion system (Sherwood et al., 2016). Intracameral injection of 50 ng/mL recombinant IL-18 resulted in a 34% (CI 10, 52%) reduction in outflow facility relative to PBS-injected eyes ($p = 0.016$; n = 10) (Fig. 3.2.11), indicating that IL-18 negatively regulates AH drainage. In contrast, intracameral injection of 133 ng/mL recombinant IL-1β produced a 49% (CI 6, 110%) increase in outflow facility relative to PBS injected eyes $p = 0.0265$; $n = 9$ in both groups) (Fig. 3.2.12). Together, these findings indicated that the downstream effectors of canonical inflammasome activation exert opposing effects on AH outflow.

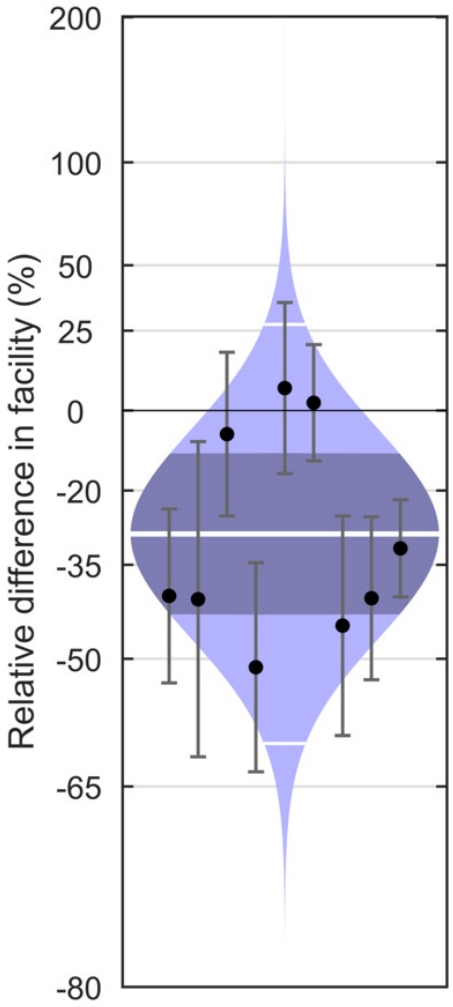



**Figure 3.2.11| Outflow facility following intracameral injection of IL-18**

*Mice were intracamerally injected with 1.5µL of 50 ng/mL IL-18 in one eye, and sterile PBS in the contralateral eye. After 48 hours, outflow facility was measured using the iPerfusion system (Sherwood et al., 2016). Each data point represents a pair of eyes, plotted as the % difference between the IL-18-injected eye and the PBS-injected eye. Error bars for each data point represent one and two standard deviations. Middle white line represents the mean difference between control and experimental eyes. Outer white lines represent two standard deviations from the mean. Dark shading represents the 95% confidence interval of the mean. Outer shading represents the predicted log normal distribution of the data. Data was analysed using a paired weighted t-test. Eyes injected with IL-18 had a 34% (CI 10, 52%) lower outflow facility than those injected with PBS (p = 0.016; n = 10).*

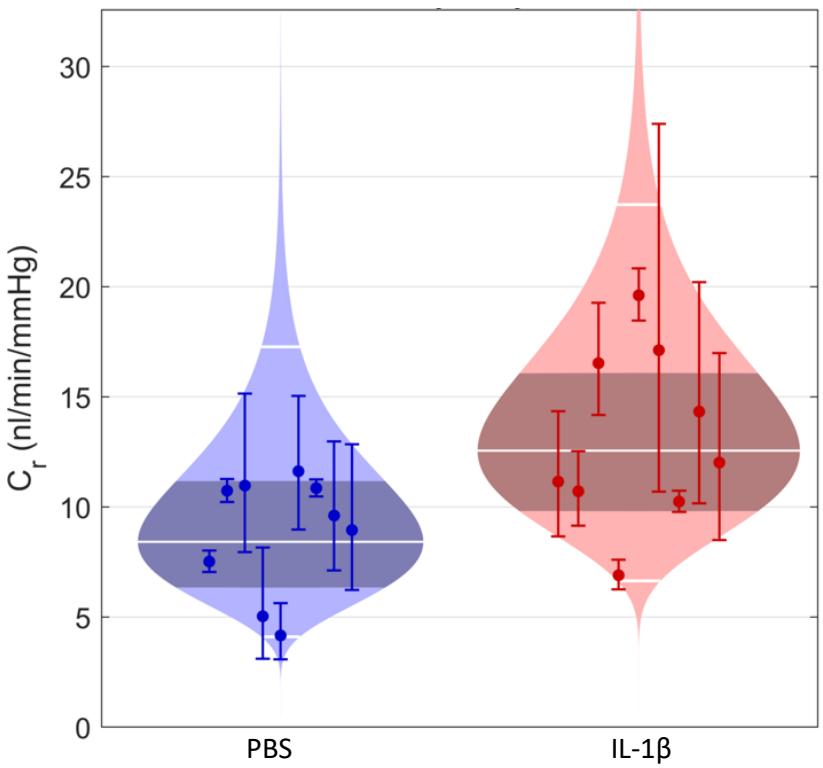



**Figure 3.2.12| Outflow facility following intracameral injection of IL-1β**

*Mice were injected intracamerally with 1.5µL of 133ng/mL of IL-1β, and sterile PBS in the contralateral eye. After 72 hours, outflow facility was measured using the iPerfusion system (Sherwood et al., 2016). Each data point represents an individual eye. Error bars represent the 95% confidence interval of each data point. Middle white line represents the weighted arithmetic mean. Outer white lines represent 2 standard deviations from the mean. Dark shading represents the 95% confidence interval of the mean. Outer shading represents the predicted log normal distribution of the data. Data was analysed using an unpaired weighted t-test. Eyes injected with IL-1β had a 49% (CI 6, 110%) higher outflow facility than those injected with PBS (p = 0.0265; n = 9 in both groups).*

To clarify the overall impact of canonical inflammasome signalling on outflow facility, mice deficient in key canonical pathway components were examined. Outflow facility was measured in mice deficient in IL-18 and in mice lacking ASC, the adaptor protein required for inflammasome assembly and caspase-1 activation. Compared to wild-type controls, *Il18*$^{-/-}$exhibited a 40% (CI 5, 86%) increase in outflow facility ($p$ = 0.0215; $n$ = 14 (WT), 16 (*Il18*$^{-/-}$)) (Fig. 3.2.13), concordant with the anti-outflow effect observed following injection of recombinant IL-18. Similarly, *Asc*$^{-/-}$ mice displayed a 40% increase in outflow facility relative to wild-type controls ($p$ = 0.0148); $n$ = 14 (WT), 11 (*Asc*$^{-/-}$)) (Fig. 3.2.14). As ASC deficiency prevents maturation of both IL-18 and Il-1β, the concordance between *Il18*$^{-/-}$ and *Asc*$^{-/-}$ mice indicated that canonical inflammasome activation acts overall to decrease outflow facility, with the anti-outflow effects of IL-18 outweighing the outflow-enhancing effects of Il-1β under physiological conditions.

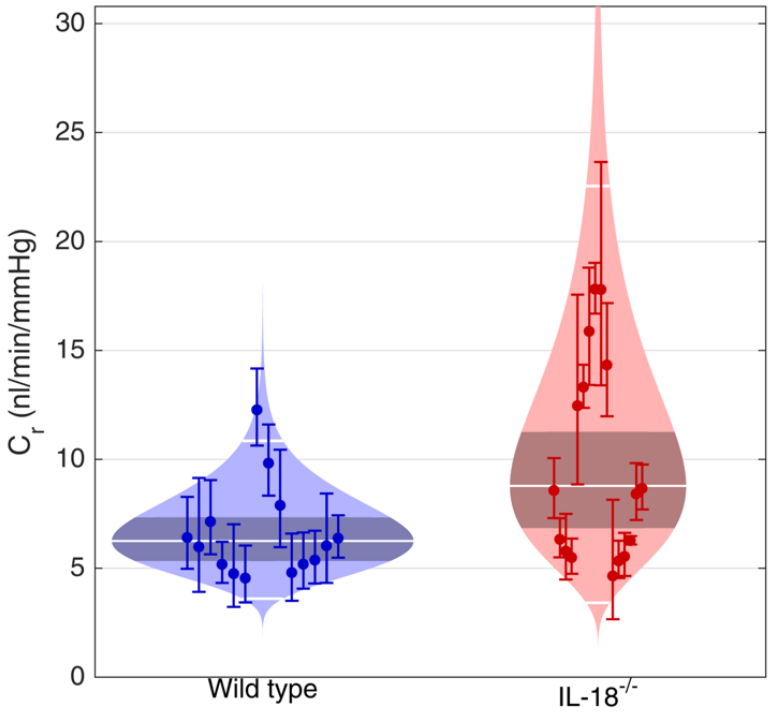



**Figure 3.2.13| Outflow facility in *Il18* $^{-/-}$ mice**

*Outflow facility was measured using the iPerfusion system (Sherwood et al., 2016). Each data point represents an individual eye. Error bars represent the 95% confidence interval of each data point. Middle white line represents the weighted arithmetic mean. Outer white lines represent 2 standard deviations from the mean. Dark shading represents the 95% confidence interval of the mean. Outer shading represents the predicted log normal distribution of the data. Data was analysed using an unpaired weighted t-test. Outflow facility was 40% (CI 5, 86%) higher in IL-18$^{-/-}$ mice, relative to WT controls (p = 0.0215; n = 14 (WT), 16 (IL-18$^{-/-}$)).*

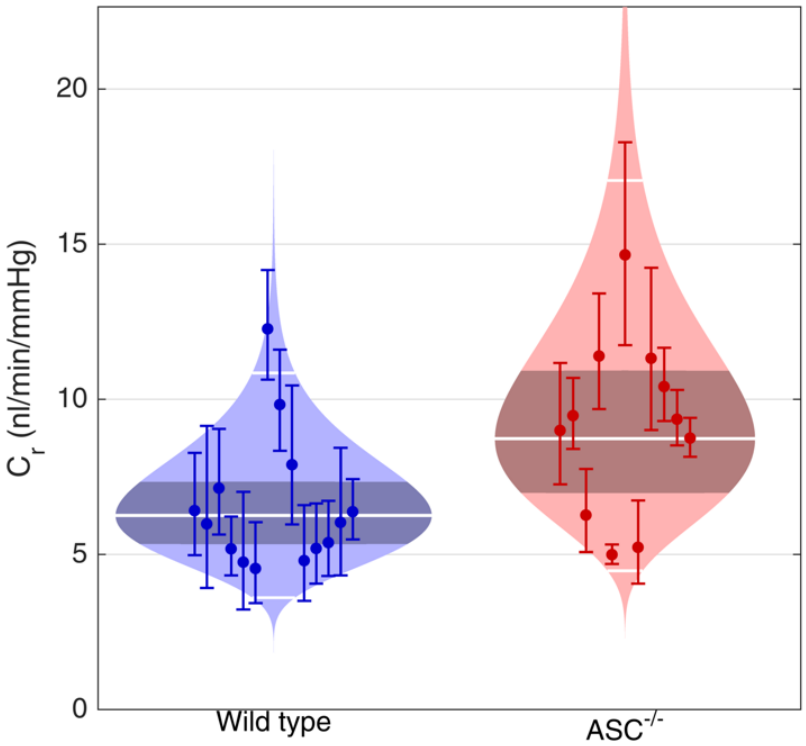



**Figure 3.2.14| Outflow facility in *Asc*$^{-/-}$ mice**

*Outflow facility was measured using the iPerfusion system (Sherwood et al., 2016). Each data point represents an individual eye. Error bars represent the 95% confidence interval of each data point. Middle white line represents the weighted arithmetic mean. Outer white lines represent 2 standard deviations from the mean. Dark shading represents the 95% confidence interval of the mean. Outer shading represents the predicted log normal distribution of the data. Data was analysed using an unpaired weighted t-test. Outflow facility was 40% (CI 8,86%) higher in Asc*$^{-/-}$ *mice, relative to WT controls (p = 0.0148; n = 14 (WT), 11 (Asc*$^{-/-}$*)).*

Next, it was investigated whether the progression of steroid-induced OHT is altered in the absence of non-canonical inflammasome signalling. Caspase-11, a component of the non-canonical inflammasome pathway, can initiate pyroptosis independently of canonical inflammasome activation. However, its contribution to inflammatory signalling in the anterior chamber is not known. ER stress in TM cells is known to contribute to outflow resistance in steroid-induced glaucoma (Zode et al., 2014) and has been shown to lead to caspase-11 activation in astrocytes following ischemia-reperfusion injury (Fradejas et al., 2010; Wan et al., 2024). Thus, it was hypothesised that caspase-11 deficiency could alter the progression of steroid-induced OHT.

Wild-type and *Casp11*$^{-/-}$ mice were subcutaneously implanted with osmotic minipumps secreting dexamethasone at a rate of 2 mg/kg/day to induce OHT. IOP was measured by rebound tonometry at baseline and for three weeks following implantation. Upon measuring IOP, consistent increases were observed in the *Casp11*$^{-/-}$ mice each week, culminating in a significant median IOP increase of 3.79 mmHg relative to baseline by the third week ($p$ = 0.0078) (Fig. 3.2.15A). In C57BL/6J mice, IOP increased consistently in the first two weeks, but decreased between week 2 and week 3, culminating in a non-significant median IOP increase of 1.75 mmHg relative to baseline (Fig. 3.2.15A). At the final timepoint, the median IOP of the *Casp11*$^{-/-}$ group was 1.7 mmHg higher than that of the C57BL/6J controls ($p$ = 0.037; $n$ = 12 (WT), 8 (*Casp11*$^{-/-}$) (Fig. 3.2.15B).

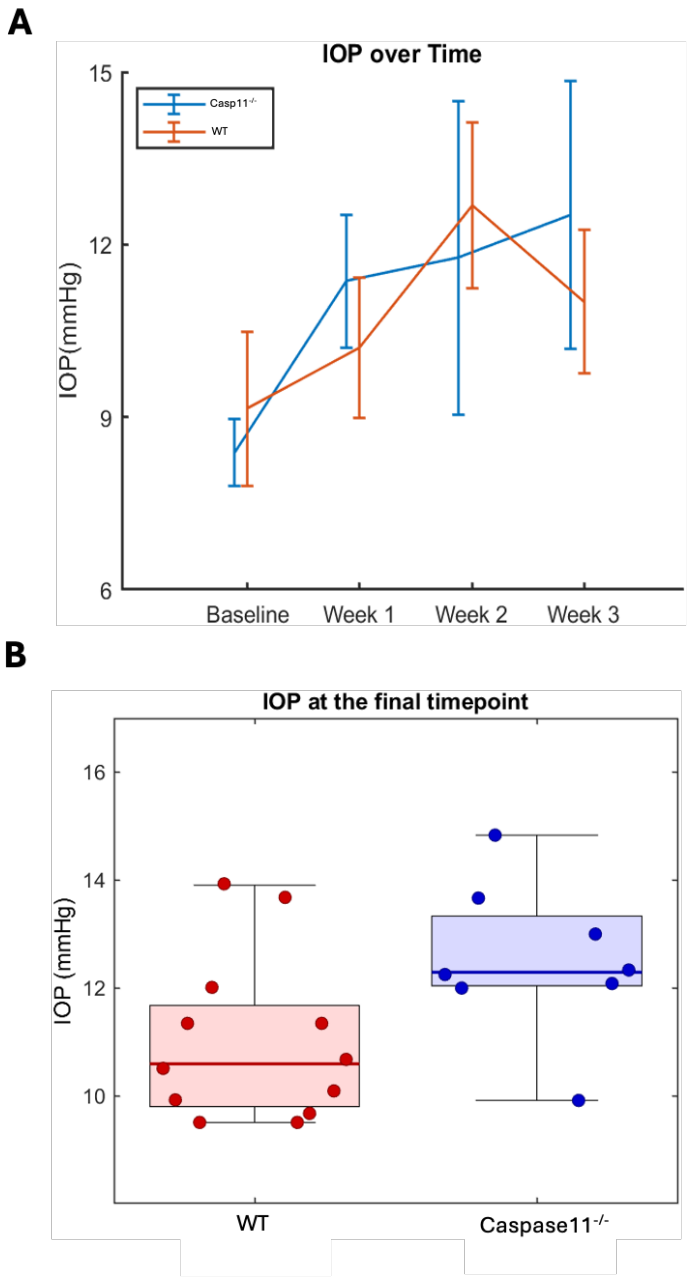



**Figure 3.2.15| IOP in *Casp11*$^{-/-}$ mice following dexamethasone treatment**

***(A)*** *IOP was measured at baseline and for three weeks thereafter in C57BL/6J (WT) (red) and Casp11*$^{-/-}$ *(blue) mice following induction of dexamethasone-induced OHT. Points represent median IOP per timepoint and group. Error bars represent 95% confidence intervals; n = 12 (WT), 8 (Casp11*$^{-/-}$*).* ***(B)*** *Boxplots comparing the final time point. IOP was 1.7 mmHg higher in the Casp11*$^{-/-}$ *mice, relative to WT controls (p = 0.037). Lines represent the median. Shaded boxes represent the interquartile range. Whiskers represent the 5*$^{th}$ *and 95*$^{th}$ *percentiles.*

To assess whether the observed elevation in IOP in *Casp11*$^{-/-}$ mice was associated with reduced AH outflow, mice were sacrificed four weeks after dexamethasone implantation, and eyes were enucleated for ex vivo measurement of outflow facility. Due to technical issues with the perfusion setup, outflow facility could only be measured in a subset of eyes, resulting in a reduced sample size in both experimental groups. Despite this limitation, the *Casp11*$^{-/-}$ mice exhibited a 33% reduction in outflow facility compared to wild-type controls (CI -66, +31%). Although this trend was consistent with the IOP findings, the difference did not reach statistical significance ($p = 0.2059$; n = 5 WT, 7 *Casp11*$^{-/-}$ ). Taken together, these results suggest a potential protective role for caspase-11 in the development of steroid-induced OHT (Fig. 3.2.12).

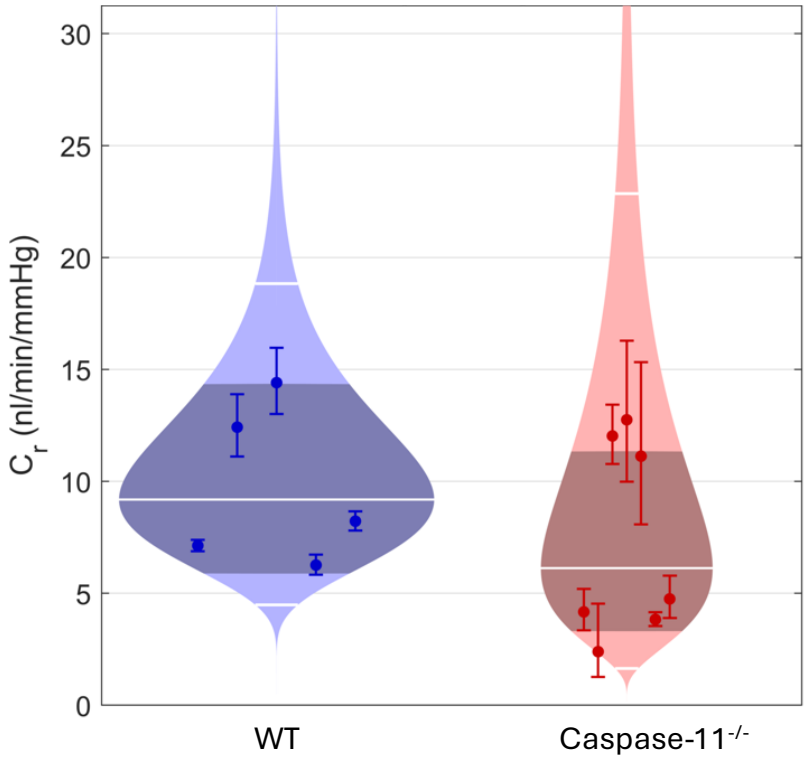



**Figure 3.2.16| Outflow facility in *Casp11*$^{-/-}$ mice following dexamethasone treatment**

*Outflow facility was measured using the iPerfusion system (Sherwood et al., 2016) in C57BL/6J (WT) and Casp11*$^{-/-}$ *mice following treatment with dexamethasone for 3 weeks. Each data point represents an individual eye. Error bars represent the 95% confidence interval of each data point. Middle white line represents the weighted arithmetic mean. Outer white lines represent 2 standard deviations from the mean. Dark shading represents the 95% confidence interval of the mean. Outer shading represents the predicted log normal distribution of the data. Data was analysed using an unpaired weighted t-test. Outflow facility was 33% (CI 66, -31%) lower in the Casp11*$^{-/-}$ *mice, relative to WT controls. This was not significant (p = 0.2059); n = 5 (WT), 7 (Casp11*$^{-/-}$*).*

## 3.3 Discussion

The overarching objective of this chapter was to evaluate whether manipulation of inflammatory pathways represents a viable strategy for reducing IOP in glaucoma. To achieve this, three lines of investigation were pursued. Firstly, the immune profile of the anterior segment was characterised in DBA/2J mice to determine whether it is altered in glaucoma. Secondly, the role of canonical inflammasome signalling was examined by measuring outflow facility in mice treated with, or deficient in, downstream effectors cytokines IL-1β and IL-18. Lastly, the contribution of non-canonical inflammasome signalling to AH outflow was determined by examining how caspase-11 deficiency influences the progression of dexamethasone-induced OHT. These approaches allowed for the contribution of inflammation to outflow resistance in glaucoma to be assessed, in addition to the possibility of using inflammatory modulation as a therapeutic strategy.

### 3.3.1 Pro-inflammatory profile in the anterior uvea of DBA/2J mice

A key finding of this chapter is that DBA/2J mice display a pro-inflammatory phenotype in the anterior segment. Immunostaining revealed significantly elevated F4/80, CD68, and CD11b in the iris, with CD11b also increased in the ciliary body and subsets of mice showing higher F4/80 and CD68 in this region. This pattern is consistent with an expanded population of myeloid-lineage immune cells, likely activated macrophages, in the anterior uvea. While immune cells are known to circulate in these vascularised tissues (Vendomèle et al., 2017), the marked increase in activation-associated markers such as CD68 suggests a breakdown of immune privilege in the anterior segment. Upregulation of the inflammasome receptors NLRP3 in the iris and ciliary body, and AIM2 in the iris, points to canonical inflammasome activation downstream from the loss of ocular immune privilege, while the simultaneous elevation of IL-1β and IL-18 in the iris confirms that canonical inflammasome signalling is functionally active.

These findings align with previous reports of blood-ocular barrier disruption, loss of ACAID, and leukocyte infiltration into the AH, iris, and ciliary body in DBA/2J mice (Mo et al., 2003). Increased IL-18 expression in the iris prior to pigment dispersion and infiltration of $CD59^{+}$ immune cells into the AC have also been described (Zhou et al., 2005). However, a detailed characterisation of inflammatory changes in the anterior segment of this model has been lacking. This is relevant given that the cause of elevated

IOP in DBA/2J mice remains uncertain. While pigment-laden cell accumulation in the outflow pathways has been reported (Schraermeyer et al., 2009), it is unclear whether outflow obstruction is purely mechanical or also driven by changes in the outflow tissue itself, as is the case in POAG. The current findings, showing clear evidence of canonical inflammasome activation, support the possibility that inflammatory remodelling of outflow tissues, such as ECM deposition or fibrosis, could contribute to increased resistance to AH drainage in this model.

A limitation of this portion of the study is that, given the pigment dispersion phenotype of DBA/2J mice, the pro-inflammatory changes observed in the anterior segment may be model-specific and not representative of glaucoma more broadly. Performing a similar characterisation in other models of OHT, such the dexamethasone-induced OHT model, would help to determine the generality of these findings. Nevertheless, as the primary objective of this chapter was to explore the manipulation of AH outflow through inflammation, this characterisation was sufficient to establish inflammatory changes in a model of OHT, providing a rationale for subsequent experiments involving direct modulation of outflow.

### 3.3.2 Canonical inflammasome activation decreases outflow facility

The second part of this chapter examined the effect of canonical inflammasome activation on AH outflow. Mice deficient in IL-18 were shown to have significantly higher outflow facility than a cohort of C57BL/6J mice. Correspondingly, C57BL/6J mouse eyes injected with IL-18 were found to have significantly lower outflow facility than those injected with PBS. Together, these findings suggest that IL-18 decreases outflow facility and increases IOP under physiological conditions. As IL-18 has a wide range of downstream effects, there are many possible ways that it could decrease outflow. One potential mechanism is via the downregulation of vascular endothelial growth factor (VEGF). VEGF-A is endogenously expressed in the conventional outflow pathway and is secreted by TM cells in response to mechanical stress. When injected intracamerally, VEGF increases outflow facility (Reina-Torres et al., 2017). This is likely an autoregulatory mechanism to adapt to transient increases in IOP under physiological conditions. IL-18 has been shown to suppress VEGF (Shen et al., 2014); thus, it is possible that increased levels of IL-18 would

prevent autoregulation of IOP via VEGF-A expression, leading to uncontrolled increases in IOP.

Contrastingly to IL-18, eyes injected with IL-1β displayed increased outflow facility, relative to PBS-injected eyes. This is concordant with previous findings that IL-1β increases outflow facility in porcine eyes (Birke et al., 2011) and that IL-1α increases outflow facility in rat eyes (Kee & Seo, 1997). Similarly to Il-18, IL-1β has a wide range of downstream effects that could underly this increase. Notably, IL-1β increases the expression of MMP-3 and MMP-9 (Cheng et al., 2010; Kelley et al., 2007). Increased expression of MMP-3 increases outflow facility and is being investigated by our group as a gene therapy for glaucoma (O'Callaghan, Crosbie, et al., 2017; O'Callaghan et al., 2023). Thus, this is a potential contributing mechanism and highlights Il-1β signalling as an additional target for decreasing IOP in glaucoma

Another finding of this study was that *Asc*$^{-/-}$ mice, similarly to *Il18*$^{-/-}$ mice, display an increase in outflow facility relative to C57BL/6J mice. Given that *Asc*$^{-/-}$ mice would not be expected to produce mature IL-1β or IL-18, and that these cytokines appear to have dichotomous effects on outflow facility, this suggests that the role of IL-18 predominates over IL-1β under physiological conditions and that activation of canonical inflammasome signalling would ultimately decrease outflow facility. A potential explanation for this is that pro-IL-18 is constitutively expressed in many cell types (Okamura et al., 1995; Puren et al., 1999), whereas expression of pro-IL-1β is tightly regulated and requires prior priming. This is likely to be particularly relevant in the anterior chamber, an immune-privileged environment in which much higher thresholds for priming would be expected. Under such conditions, canonical inflammasome activation would be expected to preferentially lead to the secretion of IL-18, rendering it the dominant effector cytokine.

One limitation of this study is that different protocols were used for the intracameral injection of IL-18 and IL-1β. The work on IL-18 was previously performed by Dr. Ester Reina Torres as part of another project (see statement on collaboration), treating mice with 1.5µL of 50 ng/mL IL-18 for 48 hours. Previous work by our group showed that treatment with 25 ng/mL of the molecule for 18 hours was sufficient to increase the expression of CD69 expressing NK cells by ~7-fold in mouse splenocytes, indicating that 50 ng/mL would be a sufficient dose to induce biologically observable changes (Doyle et al., 2014).

On the other hand, mice were treated with 1.5µL of 133 ng/mL IL-1β (= 50 specific units of activity) for 72 hours. This mirrored the protocol used for intracameral injection of IL-1α in rats (Kee & Seo, 1997). While both results are valid, this discrepancy does limit any direct comparison between the two datasets. This would be desirable, as it could confirm whether the apparent predominance of IL-18 over IL-1β, is due to the intrinsic properties of the cytokines or their initial bioavailability in the anterior chamber. Nevertheless, the results of these experiments demonstrate that canonical inflammasome activation decreases outflow facility, and highlight IL-1 family cytokine signalling as a potential target for therapies aiming to reduce IOP in glaucoma.

### 3.3.3 Potential protective role of caspase-11 in steroid induced glaucoma

The final finding of this chapter was that *Casp11*$^{-/-}$ mice subjected to dexamethasone treatment, displayed a significantly higher IOP at 3 weeks relative to C57BL/6J controls, accompanied by a concordant trend toward reduced outflow facility at 4 weeks. This suggests that caspase-11 may play a protective role in regulating IOP in steroid-induced glaucoma. Caspase-11 is the key mediator of the non-canonical inflammasome pathway. Although it does not directly cleave pro-IL-1β or pro-IL-18, caspase-11 cleaves GSDMD to form membrane pores that cause $K^+$ efflux and can secondarily lead to canonical inflammasome activation (Agnew et al., 2021).

While the most well understood mechanism of caspase-11 activation is via interaction with intracellular LPS, its activation has been reported in astrocytes in sterile inflammatory contexts such as ischemia-reperfusion injury (Wan et al., 2024). This sterile activation of caspase-11 is associated with ER stress, which is a known contributor to outflow resistance in dexamethasone-induced OHT (Fradejas et al., 2010; Zode et al., 2011; Zode et al., 2014). Thus, it is plausible that non-canonical inflammasome signalling could regulate AH outflow in disease contexts. The mechanism by which caspase-11 would protect against elevated IOP under stress is not entirely clear. Given the findings of this chapter that canonical inflammasome activation appears to reduce outflow facility, caspase-11 may support outflow by inducing a shift towards pyroptosis. One possibility is that caspase-11-driven pyroptosis promotes ATP release into the extracellular space (Yang et al., 2015). ATP is a potent activator of the P2X7 receptor, which in turn can induce expression and release of MMP-9 (Gu & Wiley, 2006). MMP-9 is capable of degrading ECM components within the trabecular meshwork and junctions between SCECs, thereby lowering outflow

resistance (O'Callaghan, Cassidy, et al., 2017) . Additionally, ATP release has previously been linked to IOP reduction through such MMP-mediated remodelling (Li et al., 2012). Loss of caspase-11 could therefore limit ATP-P2X7-MMP signalling and shift the balance toward a canonical inflammasome-driven response, resulting in a more severe elevation of IOP under stress.

Certain technical issues in this study warrant cautious interpretation of the results. In C57BL/6J mice, dexamethasone-induced IOP rose steadily over the first two weeks but then declined by week 3, resulting in a non-significant net increase from baseline in this group. This decrease in IOP between the second and third week was unexpected and has not been observed in previous studies of the model by our group (O'Callaghan et al., 2023). One possibility is a variation in the rate of dexamethasone delivery from the osmotic pumps. Because steroid-induced IOP elevation is reversible (Mohan & Muralidharan, 1989), and premature depletion of the dexamethasone reservoir by week 2 could lead to a subsequent fall in IOP. However, this does not explain why the effect was apparent in C57BL/6J but not *Casp11*$^{-/-}$ mice, given that both groups received pumps from the same batch. An alternative explanation is that the apparent reduction in IOP reflects a sampling artifact. IOP is known to fluctuate in response to a range of environmental and physiological factors, and the 95% confidence intervals indicate that a continued rise between weeks 2 and 3 remained plausible. A second limitation was that technical issues with the iPerfusion system reduced statistical power for detecting differences in outflow facility. Nevertheless, the observed decrease in outflow facility was consistent with the elevation in IOP, supporting a potential protective role for caspase-11 and warranting further investigation of non-canonical inflammasome activity in regulating outflow facility in glaucoma.

### 3.3.4 Conclusions

This chapter demonstrates that inflammation in the anterior segment is a feature of murine models of OHT and that sterile inflammation can modulate outflow facility in a complex, cytokine-dependent manner. In DBA/2J mice, immunostaining for inflammatory markers revealed a pro-inflammatory profile consistent with canonical inflammasome activation, which may contribute to IOP elevation in this model. Downstream effectors of canonical inflammasome activation had opposing effects on aqueous humour outflow: IL-18 reduced

outflow facility, whereas IL-1β increased it. Loss of the canonical inflammasome adaptor ASC increased outflow facility, indicating that under physiological conditions, canonical inflammasome activation likely reduces outflow. In the dexamethasone-induced OHT model caspase-11 deficiency was associated with greater IOP elevation, suggesting a potential protective role for non-canonical inflammasome signalling. Collectively, these findings provide mechanistic insight into how inflammation may influence IOP in glaucoma and highlight inhibition of canonical inflammasome activation or IL-18, as well as activation of caspase-11 or IL-1β, as potential protective strategies for lowering IOP.

# Chapter 4: Investigating iBRB integrity in mouse models of glaucoma

## 4.1 Introduction

### 4.1.1 The blood-retinal barrier

Anatomically and developmentally, the retina is considered as part of the CNS (London et al., 2013). Like the brain, the retina maintains a tightly regulated microenvironment compared to the periphery. This regulation is necessary for two reasons: firstly, because finely balanced ion concentrations are for required for neuronal transduction; and secondly, because neural tissue has limited regenerative capacity. At the same time, the retina is one of the most metabolically demanding tissues in the body (Wong-Riley, 2010). To balance these requirements, the transport of ions, molecules, and cells between the retina and the peripheral circulation is controlled by two specialised blood-retinal barriers (BRB) that lie at the interfaces between the retina and its blood supplies.

The outer BRB (oBRB) is formed by the retinal pigment epithelium (RPE), which separates the retina from the choriocapillaris, the innermost capillary bed of the choroidal circulation (O'Leary & Campbell, 2021) (Fig. 4.1.1). The RPE comprises a monolayer of polarised pigmented cells, with their apical surface facing the photoreceptor cell layer of the retina, and their basal surface interacting with Bruch's membrane and the choriocapillaris. TJs between adjacent RPE cells maintain the oBRB by preventing uncontrolled diffusion of molecules from the highly fenestrated choriocapillaris into the retina (Rizzolo, 2007). In addition to its barrier function, the RPE supports photoreceptor health and function by supplying cis-retinal and glucose required for visual transduction (Ban & Rizzolo, 2000; Redmond et al., 1998), phagocytosing shed photoreceptor outer segments as part of the visual cycle (Young & Bok, 1969), and absorbing excess light to minimise optical scattering (Schmidt & Peisch, 1986).

The inner BRB (iBRB) is formed by retinal endothelial cells (RECs) that line the vasculature of the inner retina, which originates from the central retinal artery and extends through the RNFL, IPL, and OPL (Fig. 4.1.1). Structurally and functionally analogous to the blood-brain barrier (BBB), the iBRB plays a crucial role in maintaining the neural retina's microenvironment (O'Leary & Campbell, 2021). Compared with peripheral endothelial cells, RECs are specialised by their lack of fenestrations, low rates of transcytosis, and high mitochondrial content. Barrier function is conferred by TJ proteins that limit paracellular diffusion (Fig. 4.1.2), together with selective influx and efflux

transporters that regulate transcellular transport, permitting uptake of key molecules for retinal function while excluding toxins and facilitating waste removal (Daneman & Prat, 2015; Hawkins & Davis, 2005). While iBRB properties are primarily manifested by RECs, they are not intrinsic to them (Keaney & Campbell, 2015). Barrier properties in RECs are induced by signalling from surrounding cells, such as pericytes, glial cells, and retinal neurons which together form a neurovascular unit (NVU) (Hawkins & Davis, 2005). It follows that the iBRB is a dynamic, heterogeneous structure; signals from other cells of the NVU are constantly changing in response to stimuli from the neural environment and peripheral circulation, which in turn leads to changes in the barrier properties of RECs (Keaney & Campbell, 2015).

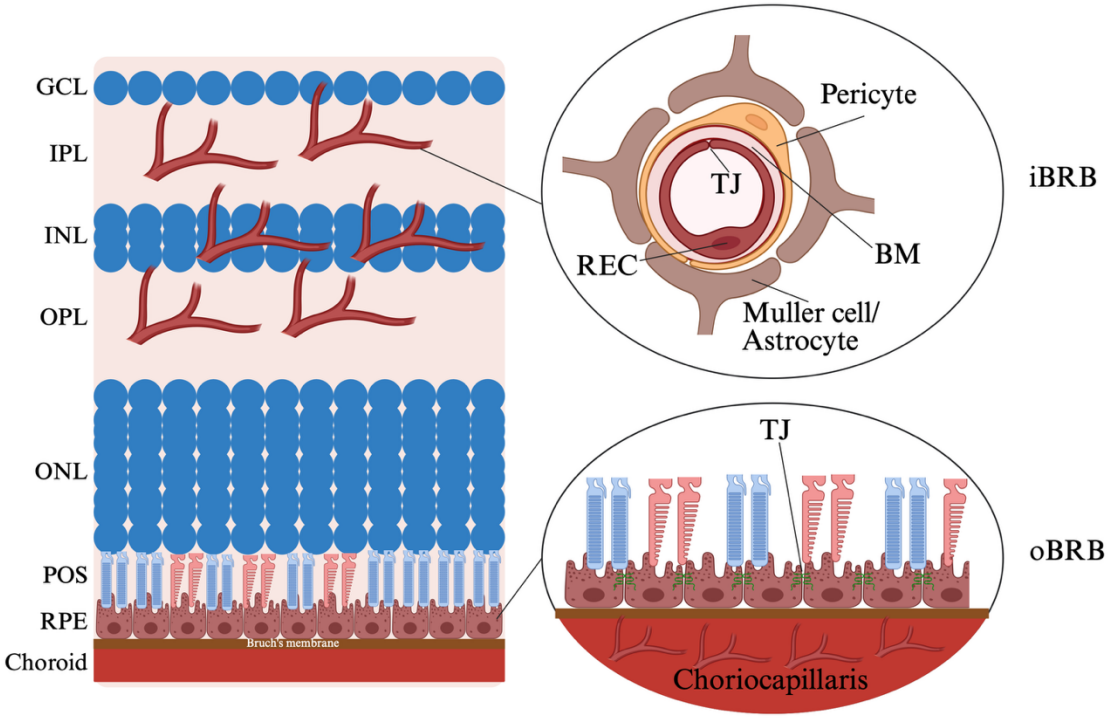



**Figure 4.1.1| Anatomical location of BRBs**

*The iBRB is formed RECs lining the vasculature of the inner retina. At the level of the capillary, the inner retinal lumen is comprised of a monolayer of endothelial cells folded upon themselves. The oBRB is formed by the RPE and regulates the exchange of material with the choroid. TJs are positioned at intercellular meeting points and regulate paracellular transport across both barriers. GCL = Ganglion cell layer, INL = inner plexiform layer, INL = inner nuclear layer, OPL = outer plexiform layer, ONL = outer nuclear layer, POS = photoreceptor outer segments. Created with BioRender. Adapted from O'Leary and Campbell (2021).*

### 4.1.2 TJs control paracellular transport

Retinal capillaries are lined by a monolayer of RECs folded upon themselves. At the apical side of inter- and intra-cellular meeting points, TJs are present, which appear on electron micrographs as fusions or "kissing points" between adjacent plasma membranes (Tsukita et al., 2001). TJs perform two complementary roles: a barrier function and a fence function. The barrier function refers to the formation of a high-resistance electrical barrier of ~1800 Ω, which tightly regulates the passage of ions, molecules, and cells between the blood and the neural retina (Butt et al., 1990). The fence function refers to their ability to restrict the lateral mobility of transport proteins and lipid rafts within the hydrophobic portion of the cell membrane, thereby preserving the apical-basal polarity of RECs (Cereijido et al., 1998). TJ complexes at the iBRB are assembled form several protein families, such as claudins, TJ-associated MARVEL proteins (TAMPs), zona occludens (ZO), and junctional adhesion molecules (JAM).

Claudins are a family of four-pass transmembrane proteins with molecular weights ranging from 20 to 34 kDa (Lal-Nag & Morin, 2009). They are both necessary and sufficient for TJ formation (Furuse, Fujita, et al., 1998; Furuse, Sasaki, et al., 1998; Kubota et al., 1999). Claudin-5 is widely accepted as the most important protein in maintaining TJs at the iBRB. It is the most highly enriched TJ component in RECs, with its mRNA levels being more than 100-fold higher than those of other claudins (He et al., 2018). Furthermore, it is the only claudin expressed in the CNS that is exclusively expressed by endothelial cells (Daneman, Zhou, Agalliu, et al., 2010; He et al., 2018; Vanlandewijck et al., 2018). In a landmark study by Nitta et al. (2003), it was shown that the BBB of *Cldn5*$^{-/-}$ mice is selectively permeable to molecules < 800 Da; however Cldn5$^{-/-}$ mice exhibit severe physiological defects and do not survive beyond early postnatal stages. Additionally targeted RNAi suppression of claudin-5 in the retina leads to increased sodium fluorescein leakage in addition to RPE atrophy when combined with a high cholesterol diet (Hudson et al., 2019).

Members of the TAMP family (occludin, tricellulin, and marvelD3) share a four-pass transmembrane structure with claudins, but their precise role in barrier integrity is less well established (Raleigh et al., 2010). Cosuppression of claudin-5 and occludin increases BBB permeability to a 3 kDa biotinylated dextran suggesting that occludin may act

synergistically with claudin-5 to regulate size-selective paracellular permeability, although loss of occludin alone does not disrupt junctional morphology (Keaney et al., 2015; Saitou et al., 2000). The ZO family of cytoplasmic scaffold proteins links transmembrane TJ proteins to the actin cytoskeleton, providing structural stability (Van Itallie et al., 2017). Of these, ZO-1 and ZO-2 are the main isoforms expressed in brain and retinal endothelium (He et al., 2018). Depletion of ZO-1 in endothelial cells reduces the recruitment of claudin-5 to TJ strands, highlighting their role in organising TJs at the iBRB (Tornavaca et al., 2015). JAMs belong to the immunoglobulin superfamily and contribute both to TJ assembly and leukocyte trafficking. In RECs, JAM-A and JAM-C are expressed, but not JAM-B (He et al., 2018). Notably, JAM-A deficiency leads to reduced claudin-5 levels, suggesting that JAMs may regulate barrier integrity indirectly through transcriptional control (Aurrand-Lions et al., 2005). Together, these TJ-associated protein families work in concert with claudin-5 to restrict paracellular transport at the iBRB.

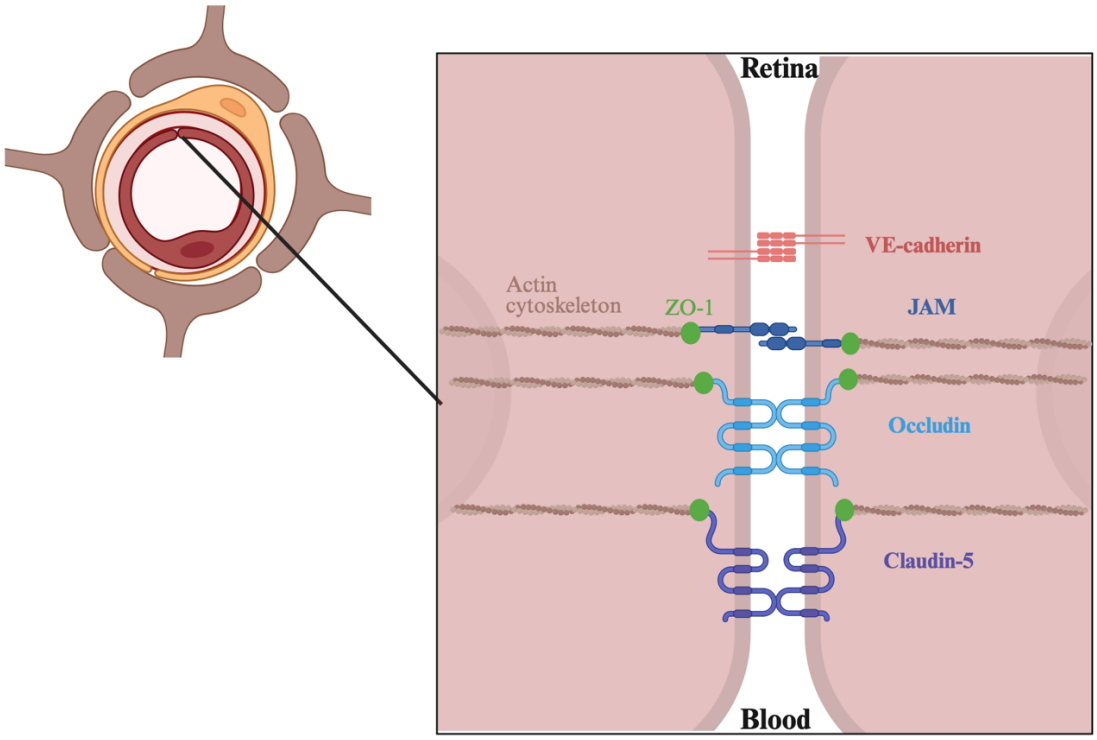



**Figure 4.1.2| Molecular structure of TJs at the iBRB**

*Schematic showing the key TJ proteins at the iBRB. Claudin-5, occludin, and JAMs are tethered to the actin cytoskeleton by ZO-1. VE-cadherin forms adherens junctions that support TJs in regulating paracellular permeability.*

### 4.1.3 Caveolin-mediated transcytosis at the iBRB

Transcytosis is a cellular transport process in which molecules are transported across the interior of cells in vesicles. Early electron microscopy experiments revealed that endothelial cells of the CNS exhibit lower rates of vesicular transport relative to those of the periphery (Reese & Karnovsky, 1967). In peripheral vessels, caveolae-mediated transport constitutes a dominant form of non-clathrin-mediated transcytosis. Caveolae are flask-shaped membrane invaginations whose formation depends on caveolin coat proteins and cavin adaptors (Bastiani & Parton, 2010).

Recent advances have highlighted the regulation of caveolae-mediated transcytosis as a crucial factor in maintaining CNS barrier integrity (Andreone et al., 2017; Ben-Zvi et al., 2014). This is mediated by Mfsd2a, a transmembrane lipid transporter specifically expressed in CNS endothelial cells that delivers docosahexaenoic acid to the inner leaflet of the plasma membrane, thereby displacing cholesterol and caveolin-1 (Cav-1), and restricting vesicular transport across the BBB/iBRB (Andreone et al., 2017). Loss of Mfsd2a in mice leads to excessive caveolae-mediated transcytosis and a leaky BBB (Ben-Zvi et al., 2014). Conversely, *Cav1* knockout in *Mfsd2a*$^{-/-}$ mice rescues barrier permeability, confirming that unrestrained caveolin-mediated transcytosis drives this phenotype (Andreone et al., 2017). Similarly, disrupted Wnt signalling at the iBRB is shown to induce retinal vascular leakage on FFA via Mdfsd2a/Cav1 signalling (Z. Wang et al., 2020). Increased caveolin mediated transport at the BBB has now been established as a feature of many CNS disorders (Knowland et al., 2014; Nag et al., 2007; Trevino et al., 2024), and ageing (Yang et al., 2020).

### 4.1.4 The vascular theory of glaucoma

While elevated IOP is a major risk factor for glaucoma, the mechanism by which it drives RGC death remain unclear. The ‘vascular theory’ of glaucoma proposes that insufficient blood supply to the retina and ONH contributes to neurodegeneration (Chan et al., 2017). This idea is supported by comorbidities with vascular disorders such as migraine, hypertension, hypotension, and diabetes (Mitchell et al., 1997; Tielsch et al., 1995; Wang et al., 1997; Wareham & Calkins, 2020), as well as imaging evidence of reduced vessel calibre, decreased blood flow, and vascular density in the retina and ONH of glaucoma patients (Flammer et al., 2002; Moghimi et al., 2018; Yabana et al., 2017; Yarmohammadi

et al., 2016). Impaired autoregulation, defined as the inability to maintain stable blood flow in response to fluctuations in perfusion pressure, has been consistently observed in the retina and ONH of glaucoma patients, and its severity correlates with visual field loss (Alarcon-Martinez et al., 2023; Kiyota et al., 2017; Kiyota et al., 2020; Prada et al., 2016). In addition, impaired neurovascular coupling, the vasodilatory response to increased neuronal activity, has been documented in glaucoma, with reduced flicker-evoked vessel dilation evident even in early disease (Feke & Pasquale, 2008; Garhöfer et al., 2004). Interestingly, NVC also declines with age, a major risk factor for glaucoma (Gugleta et al., 2013).

### 4.1.5 The iBRB in glaucoma

While most research on the retinal vasculature in glaucoma has focussed on blood flow and its regulation, growing evidence suggests that compromised iBRB integrity may also contribute to RGC degeneration. Changes in TJ protein expression have been reported in organotypic cultures of mouse retinas subjected to elevated pressure and in rats with reduced CSF pressure, mimicking the translaminar pressure differential observed in OHT (Brockhaus et al., 2020; Cheng et al., 2023). Additionally, increased fluorescein leakage around the optic disc is reported in FFA studies on non-human primates with induced OHT (Radius & Anderson, 1980) and human glaucoma patients (Arend et al., 2005; Plange et al., 2010; Plange et al., 2012).

A critical question is whether iBRB leakage in glaucoma is a direct result of OHT and precedes RGC loss, or if it is a secondary consequence of IOP-mediated RGC dysfunction. In glaucoma patients, the extent of fluorescein leakage correlates with IOP but not with other clinical markers such as visual field loss, vertical cup-to-disc ratio, disc size, arterial blood pressure, or ocular perfusion pressure, supporting the former hypothesis (Plange et al., 2012). Additionally, two recent preprints have reported iBRB dysfunction preceding extensive RGC loss in mouse models of OHT (Cueva-Vargas et al., 2024; Zhang et al., 2024). Using an ex vivo Hoescht tracer assay, Zhang et al. (2024) observed iBRB leakage in DBA/2J mice, Lmx1b$^{V265D}$ mice, and a hyaluronic acid gel-induced OHT model, while Cueva-Vargas et al. (2024) observed fluorescein leakage in a microbead OHT model. The groups propose distinct mechanisms underlying iBRB dysfunction, with Zhang et al. (2024) implicating reduced Mfsd2a expression and increased transcytosis, while Cueva-

Vargas et al. (2024) suggest mitochondrial dysfunction and reduced claudin-5 expression as contributing factors.

### 4.1.6 Chapter aims

The purpose of this chapter was to investigate the relationship between IOP elevation, iBRB integrity, and RGC degeneration in mouse models of OHT and glaucoma. To this end, there were three primary aims: (A) to determine whether retinal vascular leakage occurs in mouse models of glaucoma, (B) to establish the timing of retinal vascular leakage in relation to IOP elevation and RGC death, and (C) to identify the mechanism by which any iBRB leakage arises. To address these aims, DBA/2J mice and mice with dexamethasone-induced OHT were subjected to in vivo monitoring of IOP, retinal vascular integrity by FFA , and retinal structure by OCT, followed by immunohistochemical analysis of key iBRB components in the inner retina. While retinal vascular leakage has previously been reported in DBA/2J mice (Zhang et al., 2024), the present study assessed iBRB integrity using both in vivo and ex vivo tracer approaches, allowing methodological alignment with the work of Cueva-Vargas et al. (2024). In addition, inclusion of the dexamethasone-induced OHT model added a novel dimension by expanding the range of paradigms in which OHT-associated retinal vascular leakage has been investigated.

## 4.2 Results

### 4.2.1 Early subretinal fluid accumulation and BRB dysfunction in DBA/2J mice

To investigate the relationship between IOP elevation, retinal structure, and iBRB integrity in glaucoma, rebound tonometry, OCT and FFA were performed on cohorts of DBA/2J mice and age-matched C57BL/6J controls at 3, 6, and 9 months of age (Fig. 4.2.1).

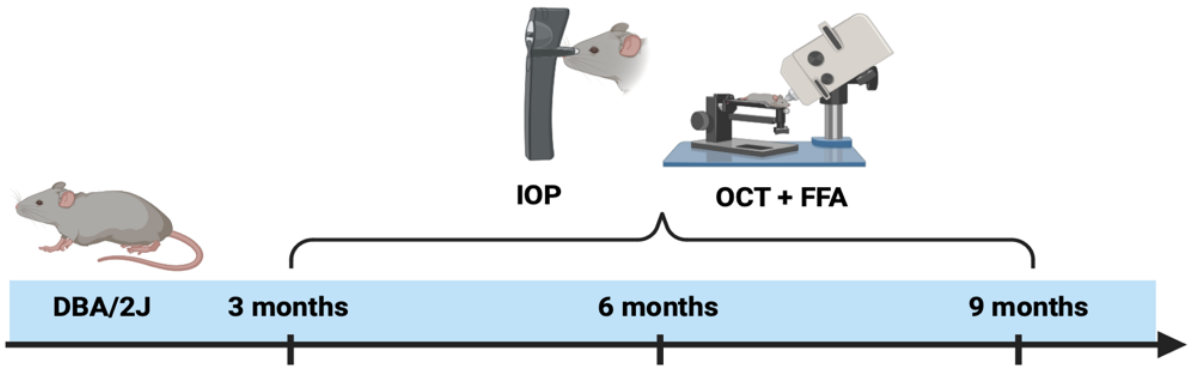



**Figure 4.2.1| Schematic of in vivo imaging protocol in DBA/2J mice**

*Rebound tonometry, OCT, and FFA were performed on cohorts of DBA/2J mice at 3, 6, and 9 months. The same protocol was also performed in age-matched C57BL/6J controls for each timepoint.*

At 3 months of age, the median IOP in DBA/2J mice was minimally higher (0.12 mmHg) than in C57BL/6J mice, with no difference observed between the groups ($p = 0.9927$; Fig. 4.2.2A). In the 6-month cohort, the median IOP in DBA/2J mice was 0.46 mmHg higher than in controls, a difference that was not significant ($p = 0.5751$; Fig. 4.2.2B). However, approximately 25 % of DBA/2J eyes exceeded 15 mmHg, indicating the emergence of OHT in a subset of animals. By 9 months, the median IOP in DBA/2J mice was 1.20 mmHg higher than in C57BL/6J mice ($p = 0.0227$; Fig. 4.2.2C). These findings indicate that while group-level IOP elevation in DBA/2J mice becomes apparent by 9 months, IOP elevation begins as early as 6 months of age.

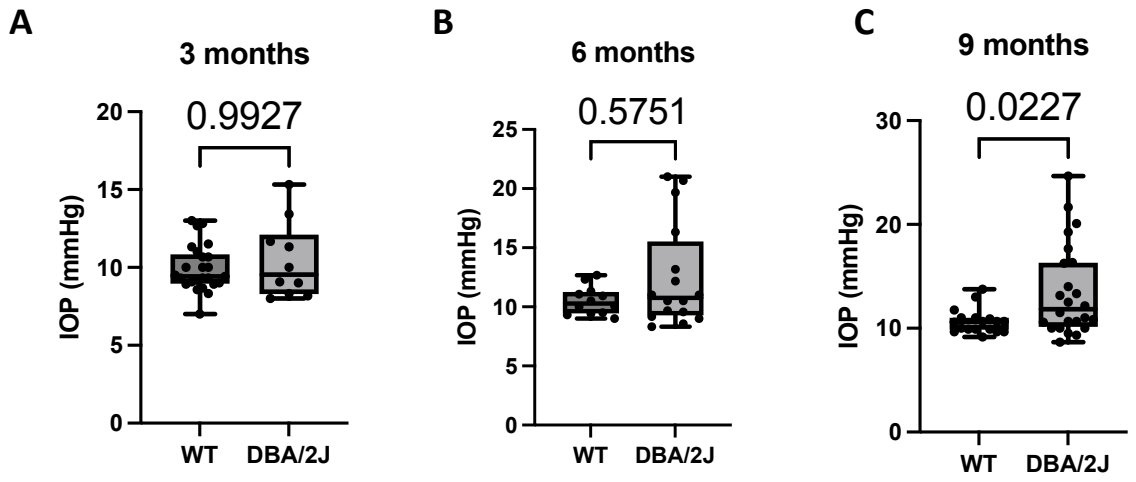



**Figure 4.2.2| IOP measurement in DBA/2J mice**

*Box and whisker plot of IOP measurements in DBA/2J and C57BL/6J mice at 3* ***(A),*** *6* ***(B)****, and 9* ***(C)*** *months of age. Boxes represent the interquartile range, whiskers represent minimum and maximum values, and horizontal lines represent the median. IOPs were compared using a Mann Whitney test.*

Upon initiation of retinal imaging, baseline fundus images were captured. These images typically display the optic disc and major retinal vessels, with the background appearing as a uniform dark green, reflecting normal pigmentation and retinal structure. However, in DBA/2J mice, fundus images were consistently brighter and exhibited a distinct yellow-tinged hue compared to age-matched C57BL/6J controls (Fig. 4.2.3). This alteration in fundus appearance was observed as early as 3 months of age. Given the pigment dispersion phenotype of DBA/2J mice, in addition to previously reported ultrastructural changes to the RPE in this model (Schraermeyer et al., 2009), it was hypothesised that these abnormalities may reflect altered melanosome structure and density, or alternatively, an accumulation of subretinal fluid, indicating a wider oBRB dysfunction. Additionally, at 9 months of age, it was observed that fundus images of all DBA/2J mice had become obscured by shadowing, which prevented further in vivo retinal imaging of these animals. This can likely be attributed to a combination of corneal calcification and poor pupil dilation, which have previously been reported as pitfalls of using the DBA/2J model (Turner et al., 2016).

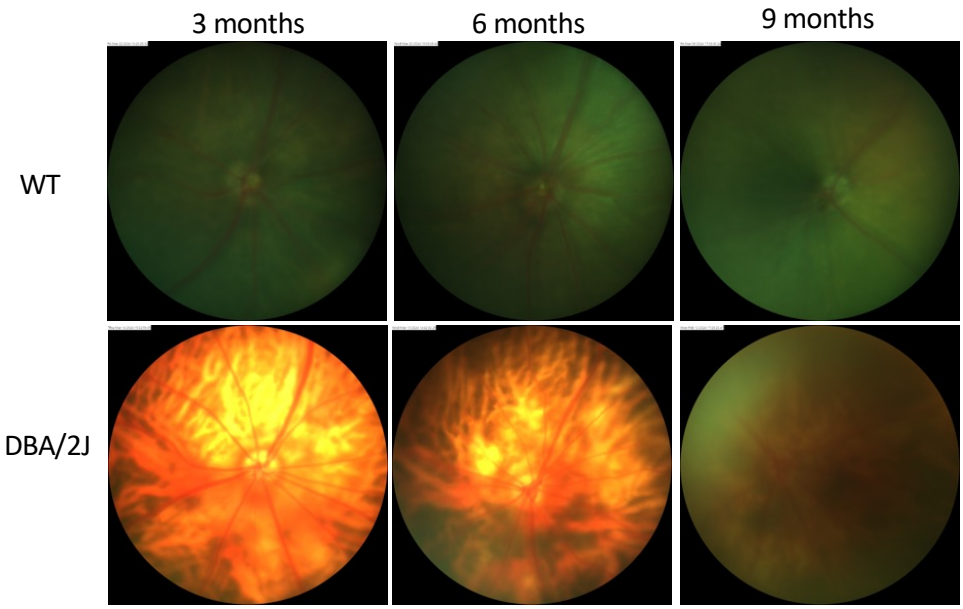



**Figure 4.2.3| Fundus images of DBA/2J mice**

*Representative fundus images of C57BL/6J (WT) eyes (top) and DBA/2J eyes (bottom) at 3, 6, and 9 months of age.*

Retinal structure at the early disease stage was evaluated using OCT scans from 3-month-old DBA/2J mice and age-matched C57BL/6J controls (Fig. 4.2.4A). Combined retinal nerve fibre layer and inner plexiform layer (RNFL + IPL) thickness was measured to assess the integrity of the RGC layer, as the RNFL alone is comparatively thin and therefore susceptible to segmentation inaccuracies and measurement variability. At this timepoint, the mean RNFL + IPL thickness was similar between groups, with no significant difference observed ($p = 0.8436$; Fig. 4.2.4B). These findings suggest that RGC degeneration had not yet occurred at this stage.

Despite the lack of difference in inner retinal thickness, differences in outer retinal morphology were observed. In C57BL/6J mice, the RPE layer appeared continuous and well defined. In contrast, DBA/2J mice exhibited discontinuity of the RPE layer, along with large hyporeflective spaces within the choroid (Fig. 4.2.4A). Choroidal thickness, measured from the RPE layer to the bottom of the globe on OCT scans, was significantly higher in DBA/2J mice compared to controls ($p = 0.0002$; Fig. 4.2.4C). Together, these findings indicate that while DBA/2J mice do not exhibit RGC loss at 3 months, they display structural abnormalities in the outer retina, suggestive of subretinal fluid accumulation and early oBRB dysfunction.

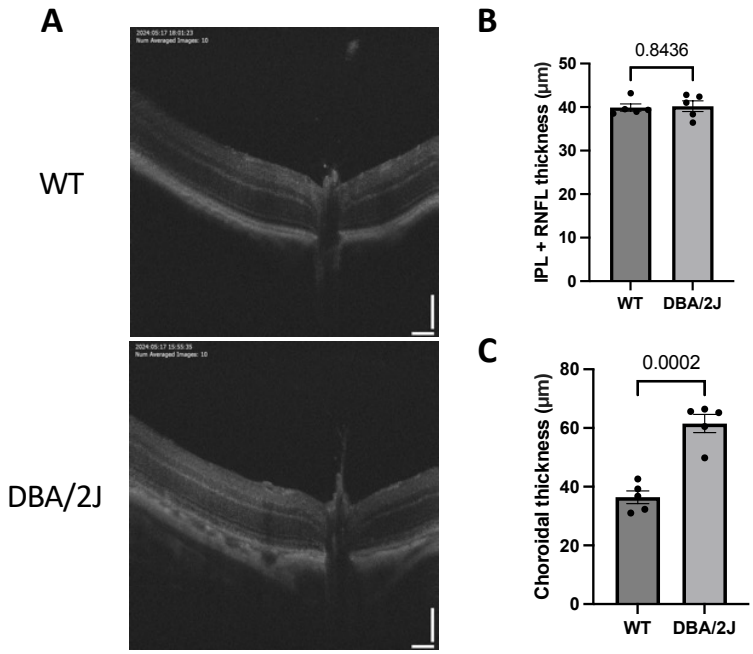



**Figure 4.2.4| OCT scans in 3-month old DBA/2J mice**

***(A)*** *Representative OCT scans of C57BL/6J (WT) (top) and DBA/2J mice (bottom).* ***(B)*** *Comparison of combined IPL + RNFL thickness and* ***(C)*** *choroidal thickness. Mean thickness was compared using an unpaired t-test. Error bars represent SEM; n = 5 in both groups.*

At 6 months of age, RNFL + IPL thickness in DBA/2J mice was significantly reduced compared to C57BL/6J mice ($p = 0.0311$; Fig. 4.2.5B), indicating that RGC loss had begun at this timepoint. Structural abnormalities in the outer retina of DBA/2J mice had also become more pronounced, with more extensive RPE disruption and larger, continuous hyporeflective spaces within the choroid. Choroidal thickness was approximately double that of controls ($p < 0.0001$; Fig. 4.2.5C).

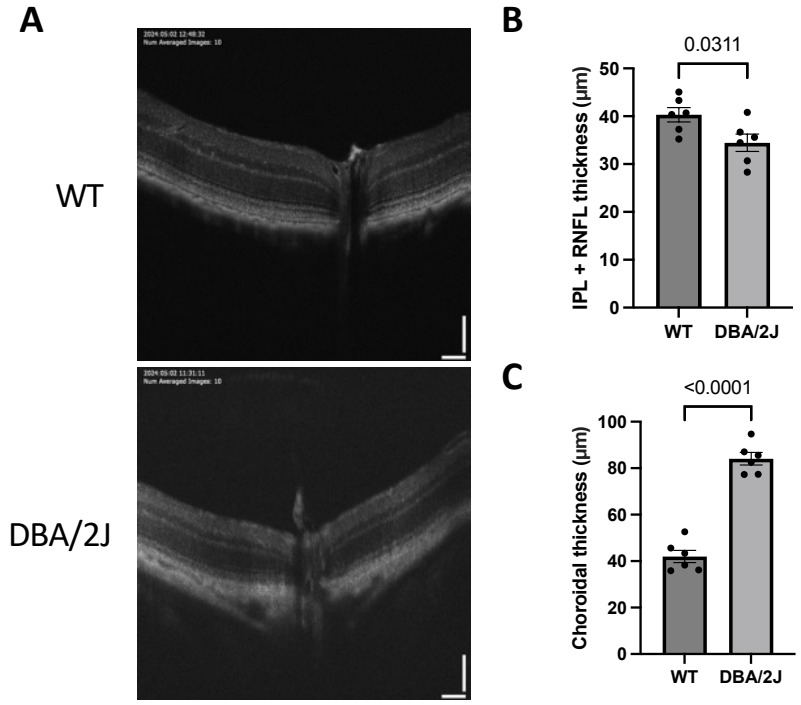



**Figure 4.2.5| OCT scans in 6-month old DBA/2J mice**

***(A)*** *Representative OCT scans of C57BL/6J (WT) (top) and DBA/2J mice (bottom).* ***(B)*** *Comparison of combined IPL + RNFL thickness and* ***(C)*** *choroidal thickness. Mean thickness was compared using an unpaired t-test. Error bars represent SEM; n = 6 in both groups.*

Retinal vascular integrity in the 3-month-old cohort was assessed by FFA. Sodium fluorescein was injected intraperitoneally and fundal images were taken at 30-second intervals over 10 minutes (Fig. 4.2.6A). The resulting images were analysed using FOVAS, a software for quantifying fluorescein leakage on FFA scans (Methods section 2.10). After masking of the major retinal vessels, the cumulative intensity was calculated for each mouse, which is the sum of signal intensity outside of the mask at each timepoint, including only those timepoints that were available across all eyes. At this timepoint, the cumulative intensity in the C57BL/6J cohort was compared to that in the DBA/2J cohort, with no significant difference in retinal vascular integrity between groups ($p = 0.5116$; Fig. 4.2.6B).

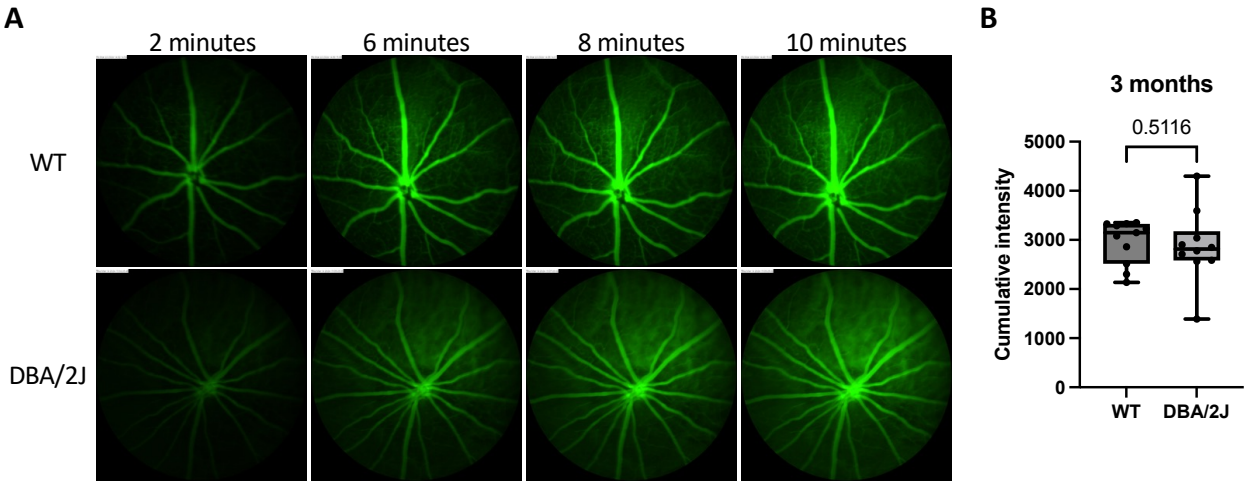



**Figure 4.2.6| FFA in 3-month old DBA/2J mice**

***(A)*** *Representative FFA images of C57BL/6J (WT) (top) and DBA/2J (bottom) eyes at 2-, 6-, 8-, and 10-minutes post fluorescein administration.* ***(B)*** *Box and whisker plot comparing cumulative fluorescein intensity (the sum of intensities across all applicable image frames) in WT and DBA/2J mice. Boxes represent the interquartile range, whiskers represent minimum and maximum values, and horizontal lines represent the median. Intensities were compared using a Mann Whitney test. n = 11 WT; n = 10 DBA/2J.*

FFA performed in the 6-month cohort revealed hazy images in DBA/2J eyes, characterised by diffuse fluorescein accumulation that obscured the fine details of the retinal microvasculature (Fig. 4.2.7A). This observation was supported by quantitative analysis, with DBA/2J mice having an approximately 2-fold higher cumulative intensity than C57BL/6J mice ($p = 0.0140$; Fig. 4.2.7B). These findings indicate that DBA/2J mice exhibit early retinal vascular leakage by 6 months of age, coinciding with RNFL + IPL thinning observed on OCT.

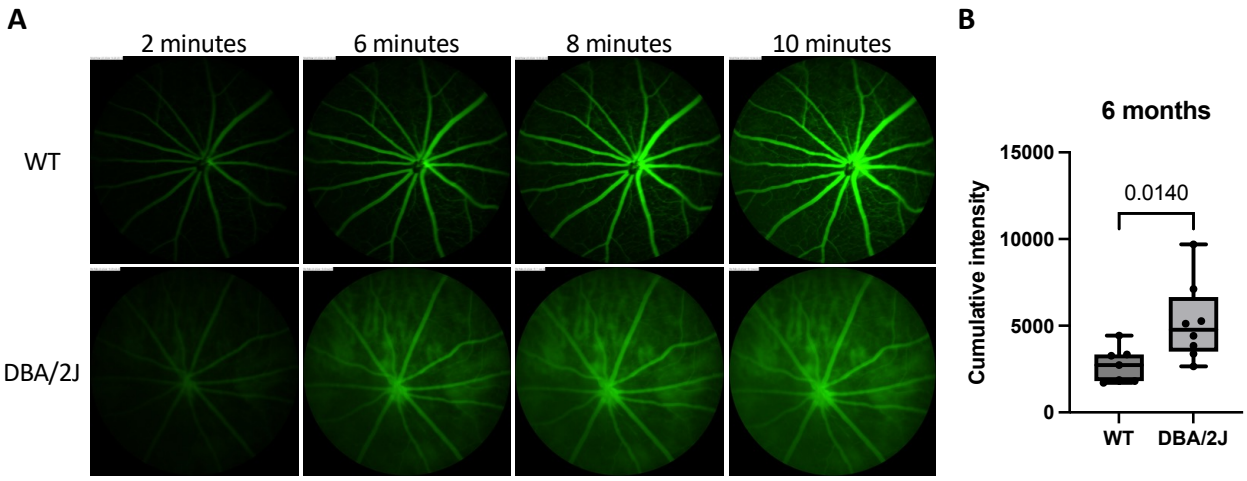



**Figure 4.2.7| FFA in 6-month old DBA/2J mice**

***(A)*** *Representative FFA images of C57BL/6J (WT) (top) and DBA/2J (bottom) eyes at 2-, 6-, 8-, and 10-minutes post fluorescein administration* ***(B)*** *Box and whisker plot comparing cumulative fluorescein intensity (the sum of intensities across all applicable image frames in WT and DBA/2J mice. Boxes represent the interquartile range, whiskers represent minimum and maximum values, and horizontal lines represent the median. Intensities were compared using a Mann Whitney test. n = 11 WT; n = 10 DBA/2J.*

The relationship between IOP and retinal vascular leakage in the 6-month DBA/2J cohort was examined by plotting IOP against cumulative fluorescein intensity for animals with both FFA and IOP measurements, followed by correlation analysis (Fig. 4.2.8). No evidence of an association was found (Spearman's $r = -0.179$, $p = 0.713$, $n = 7$).

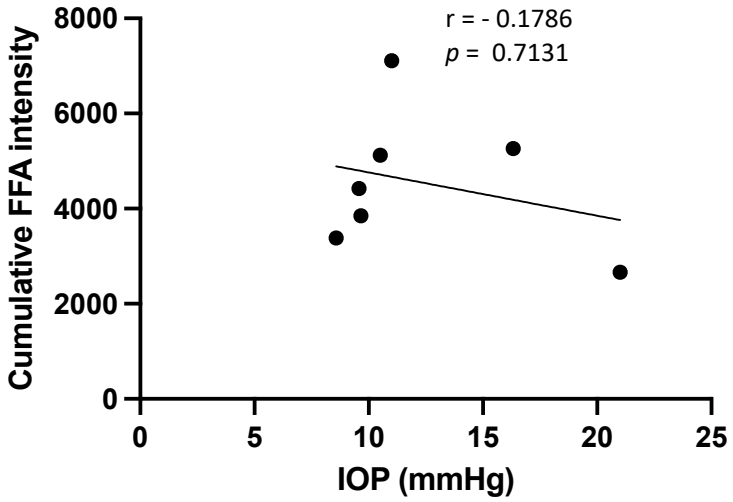



**Figure 4.2.8| Correlation between IOP and cumulative FFA intensity in 6 month old DBA/2J mice**

*Scatter plot of IOP versus cumulative FFA intensity for DBA/2J mice at 6 months of age. Spearman's rank correlation coefficient (r) and corresponding p-value are shown above the graph (n = 7).*

To determine whether retinal vascular leakage could be detected in 9-month-old DBA/2J mice, despite the inability to perform in vivo imaging due to corneal calcification and impaired pupil dilation, leakage was measured ex vivo using an intravenously injected biotinylated tracer (Sulfo-NHS-biotin; 600 Da). Immunostaining revealed that in C57BL/6J mice, the tracer remained confined within vessels, displaying a continuous vascular pattern. In contrast, DBA/2J mice exhibited a more discontinuous vascular structure, indicating tracer leakage (Fig. 4.2.9A). Quantification of leakage was performed by calculating the ratio of tracer fluorescence intensity outside the vessels to that inside the vessels across the retina. C57BL/6J mice showed a normalised fluorescence ratio of 0.70, whereas DBA/2J mice exhibited a significantly higher ratio of 0.805 ($p$ = 0.0297; Fig. 4.2.8B), confirming increased vascular permeability in the latter.

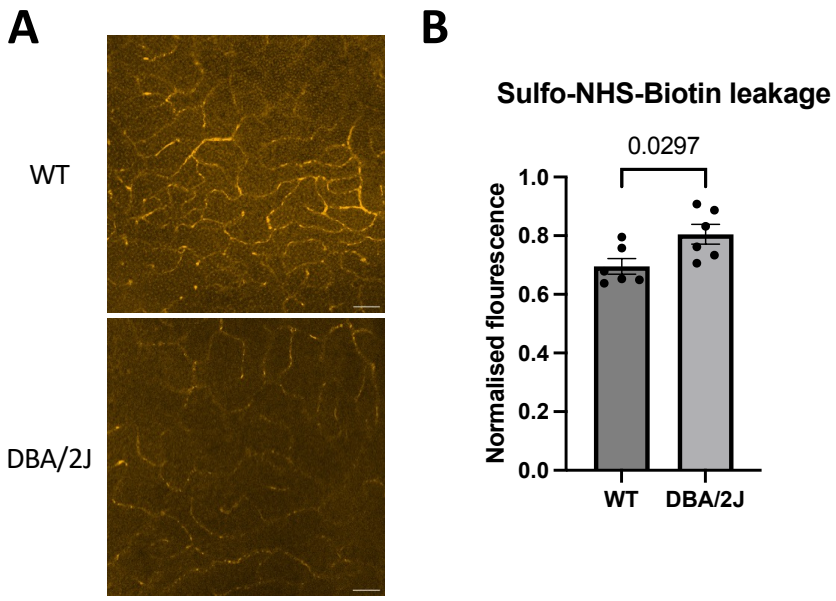



**Figure 4.2.9| Ex vivo biotin extravasation in 9-month old DBA/2J mice**

***(A)*** *Representative images of immunostaining for Sulfo-NHS-Biotin in retinal wholemounts from C57BL/6J (top) and DBA/2J (bottom) mice.* ***(B)*** *Comparison of Sulfo-NHS-Biotin extravasation. Normalised fluorescence (signal outside vessels normalised by signal inside vessels) was compared using an unpaired t-test. Error bars represent SEM; n = 6.*

### 4.2.2 iBRB leakage precedes structural RGC loss in mice with dexamethasone-induced OHT

To determine whether early loss of retinal vascular integrity is a common feature in murine models of OHT, in vivo imaging was performed in C57BL/6J mice both prior to and 4 weeks after induction of dexamethasone-induced OHT. This longitudinal approach allowed us to track changes within the same animals, correlating rising IOP with potential retinal vascular leakage and structural alterations in the retina (Fig. 4.2.10). Although weekly retinal imaging was initially planned alongside IOP monitoring, this was discontinued after a preliminary cohort revealed that repeated ketamine anaesthesia led to unexpected mortality in mice implanted with dexamethasone minipumps.

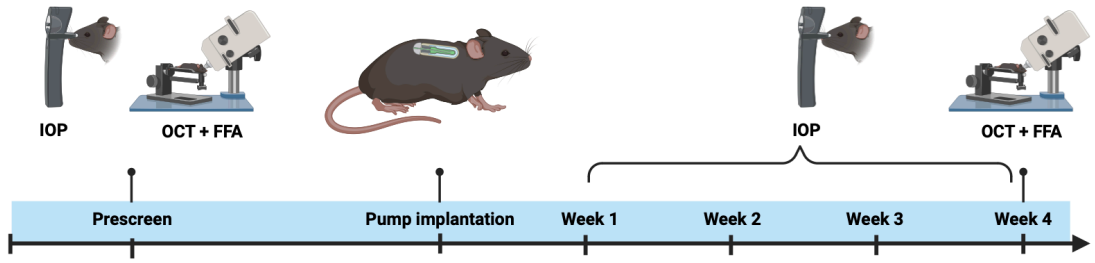



**Figure 4.2.10| In vivo imaging protocol in mice with dexamethasone-induced OHT**
*C57BL/6J mice were prescreened for IOP using rebound tonometry, retinal structure by OCT, and retinal vascular integrity by FFA. To induce OHT, mice were implanted with osmotic minipumps delivering dexamethasone at a rate of 2 mg/kg/day. IOP was monitored weekly for 4 weeks, and at the final timepoint, OCT and FFA were repeated to assess changes in retinal structure and vascular integrity.*

At baseline, the median IOP of the C57BL/6J cohort was recorded. One week after dexamethasone implant, IOP had increased by 2.09 mmHg, though this change was not statistically significant ($p$ = 0.1944). By week 2, a significant increase of 2.17 mmHg was observed ($p$ = 0.0342), which further increased to 3.05 mmHg at week 3 ($p$ = 0.0165). By the final time point, median IOP was 3.67 mmHg higher than baseline ($p$ = 0.0004; Fig. 4.2.11).

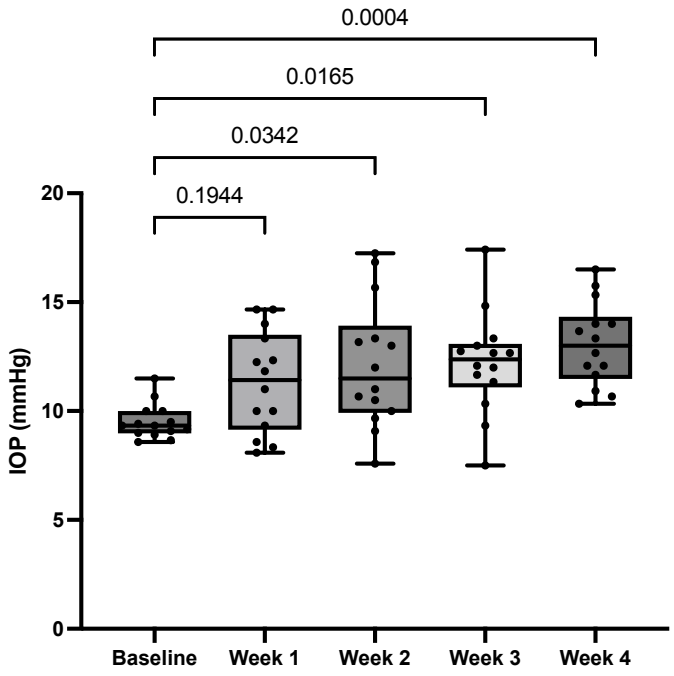



**Figure 4.2.11| IOP progression in mice with dexamethasone-induced OHT**

*Box and whisker plots showing IOP measurements in C57BL/6J mice at baseline and for 4 weeks post induction of dexamethasone-induced OHT. Boxes represent the interquartile range, whiskers represent minimum and maximum values, and horizontal lines represent the median. IOPs for weeks 1-4 were compared to baseline using a Friedman test with Dunn's correction for multiple comparisons. n = 14 eyes; 7 mice per group.*

Examination of OCT scans from mice before and after dexamethasone treatment revealed increased hyperfluorescence in the RNFL around the optic nerve following treatment, potentially indicating RGC dysfunction (Fig. 4.2.12A). Despite this, there was no significant change in RNFL+IPL thickness ($p = 0.2278$; Fig. 4.2.12B), suggesting that overt RGC loss had not yet occurred. In contrast to DBA/2J mice, dexamethasone-treated C57BL/6J mice maintained an intact and continuous RPE layer. While occasional pockets of choroidal hypofluorescence were observed, these were infrequent and did not lead to a significant difference in choroidal thickness ($p = 0.2688$; Fig. 4.2.12B). Together, these findings indicate that after 4 weeks of dexamethasone-induced OHT, there were no gross structural changes in the retina.

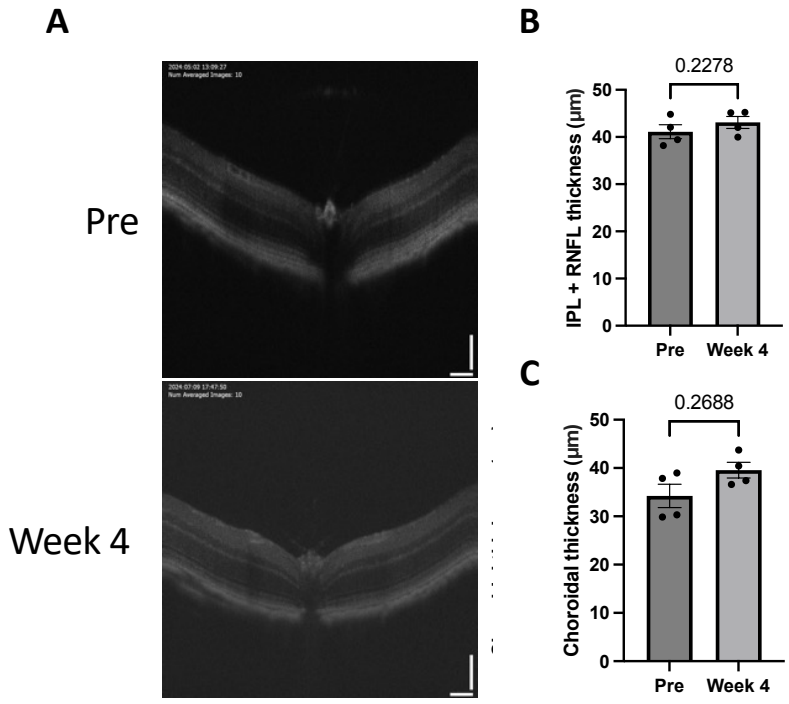



**Figure 4.2.12| OCT scans of mice with dexamethasone-induced OHT**

***(A)*** *Representative OCT scans of the same C57BL/6J eye pre (top) and 4 weeks-post (bottom) induction of dexamethasone-induced OHT.* ***(B)*** *Comparison of combined IPL + RNFL thickness and* ***(C)*** *choroidal thickness. Mean thickness was compared using a paired t-test. Error bars represent SEM; n = 4.*

FFA performed on mice before and after dexamethasone treatment revealed that treated eyes exhibited noticeably brighter images. These images showed increased fluorescence around the optic nerve head and a hazy appearance around the microvasculature, suggesting subtle, diffuse leakage. In one case, a distinct focal leakage from a major retinal vessel was also observed (Fig. 4.2.13A). Quantitative analysis using FOVAS demonstrated that the cumulative fluorescence intensity outside of the major vessels was significantly elevated in the dexamethasone-treated group, representing an approximate 30 % increase compared to baseline ($p$ = 0.0312; Fig. 4.2.13B).

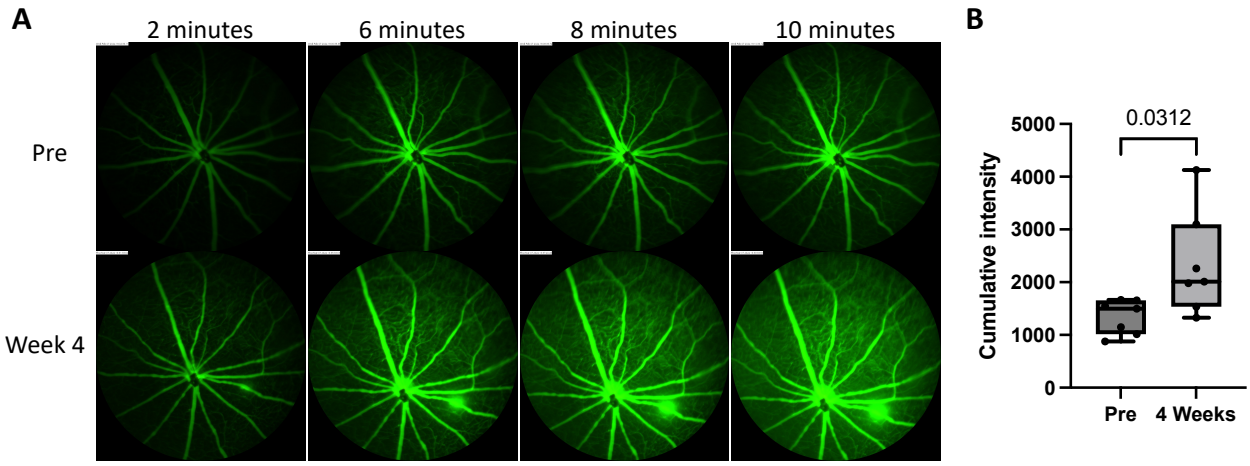



**Figure 4.2.13| FFA in dexamethasone-treated mice**

***(A)*** *Representative FFA images of the same C57BL/6J eye pre (top) and 4 weeks-post (bottom) induction of dexamethasone-induced OHT at 2-, 6-, 8-, and 10-minutes post fluorescein administration.* ***(B)*** *Box and whisker plot comparing cumulative fluorescein intensity (the sum of intensities across all applicable image frames pre and post treatment. Boxes represent the interquartile range, whiskers represent minimum and maximum values, and horizontal lines represent the median. Intensities were compared using a Wilcoxon matched pairs signed rank test. n = 7.*

To evaluate the relationship between IOP elevation and retinal vascular leakage in this model, absolute IOP and cumulative fluorescein intensity at the final time point were plotted against one another and a correlation analysis was performed (Fig. 4.2.14A). This analysis indicated a weak positive, non-significant association between these parameters (Spearman's $r = 0.324$, $p = 0.482$). To determine whether the change in IOP, rather than its absolute value, showed a stronger relationship to iBRB leakage, the change in IOP from baseline was plotted against cumulative fluorescein intensity at the final time point (Fig. 4.2.14B). This yielded a moderate positive correlation (Spearman's $r = 0.607$), although this was still not significant ($p = 0.167$, $n = 7$). While neither relationship was statistically significant, the higher correlation coefficient for IOP change suggested that variation in IOP over time may be more closely associated with iBRB leakage than absolute IOP in OHT models.

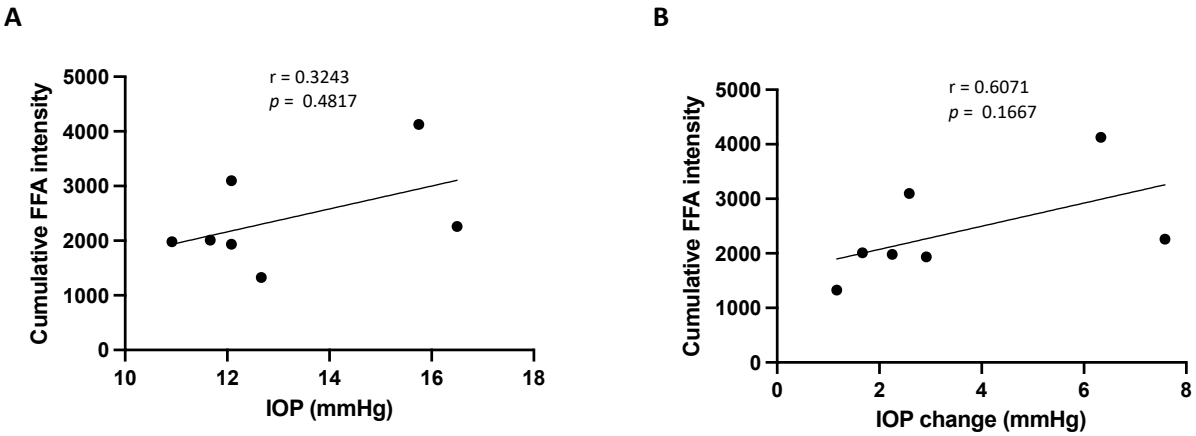



**Figure 4.2.14| Correlation between IOP elevation and final FFA intensity in dexamethasone-induced OHT**

*Scatter plots showing **(A)** absolute IOP at 4 weeks and **(B)** change in IOP from baseline versus cumulative FFA intensity at 4 weeks post-dexamethasone treatment. Spearman's rank correlation coefficient (r) and corresponding p-value are shown above each graph.*

### 4.2.3 Immunostaining for iBRB components in OHT models

To investigate the mechanism of iBRB leakage in DBA/2J and dexamethasone-induced OHT models, immunostaining was performed on retinal cryosections from these mice and compared to age-matched C57BL/6J controls to examine the levels of key iBRB molecules in the inner retina. Immunostaining for the TJ protein claudin-5 showed typical junctional staining in both models, with continuous claudin-5 strands visible in the inner retinal vasculature (Figs. 4.2.15A, C). Claudin-5 % area was quantified by normalising the percentage area of claudin-5 staining to that of the pan-vascular marker isolectin-IB4. In the DBA/2J model, claudin-5 expression was marginally higher compared to C57BL/6J controls, but this difference was not significant ($p = 0.2276$; Fig. 4.2.15B). Similarly, in the dexamethasone-induced OHT model, claudin-5 expression in treated mice was comparable to C57BL/6J controls, with no significant difference observed ($p = 0.9119$; Fig. 4.2.15D). These findings suggest that claudin-5-mediated TJ disruption was not responsible for retinal vascular leakage in either model.

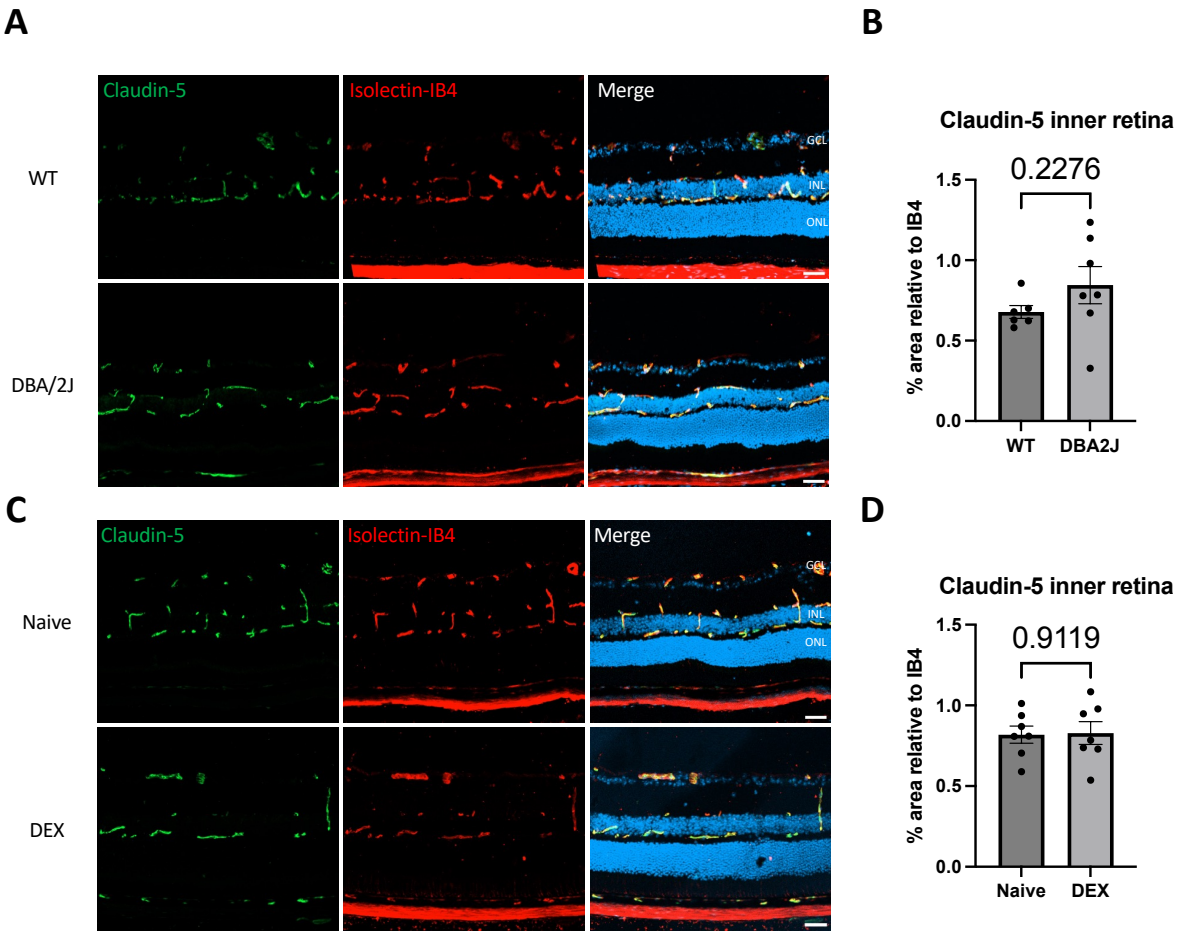



**Figure 4.2.15 | Claudin-5 immunostaining in OHT models**

*Representative images show staining for claudin-5 (green), isolectin-IB4 (red), and both channels merged with DAPI (blue) in DBA/2J* ***(A)*** *and DEX* ***(C)*** *mice and age-matched C57BL/6J controls (WT/Naïve). Quantification of claudin-5 % area in the inner retina, normalised to isolectin-IB4 area, is shown in panels* ***B*** *(DBA/2J vs WT; n = 6 WT, n = 7 DBA/2J) and* ***D*** *(DEX vs Naïve; n = 7 per group). Unpaired t-tests were used for both comparisons. Error bars represent SEM.*

The expression of VE-cadherin, a key molecule involved in forming endothelial adherens junctions, was also examined. In the DBA/2J model, VE-cadherin expression was dramatically reduced compared to age-matched controls ($p$ = 0.0002; Fig. 4.2.16B). In contrast, dexamethasone-treated mice exhibited normal VE-cadherin expression relative to their age-matched controls ($p$ = 0.4848; Fig. 4.2.16D). These findings suggest that VE-cadherin downregulation contributes to barrier disruption in DBA/2J mice but not in the dexamethasone-induced OHT model.

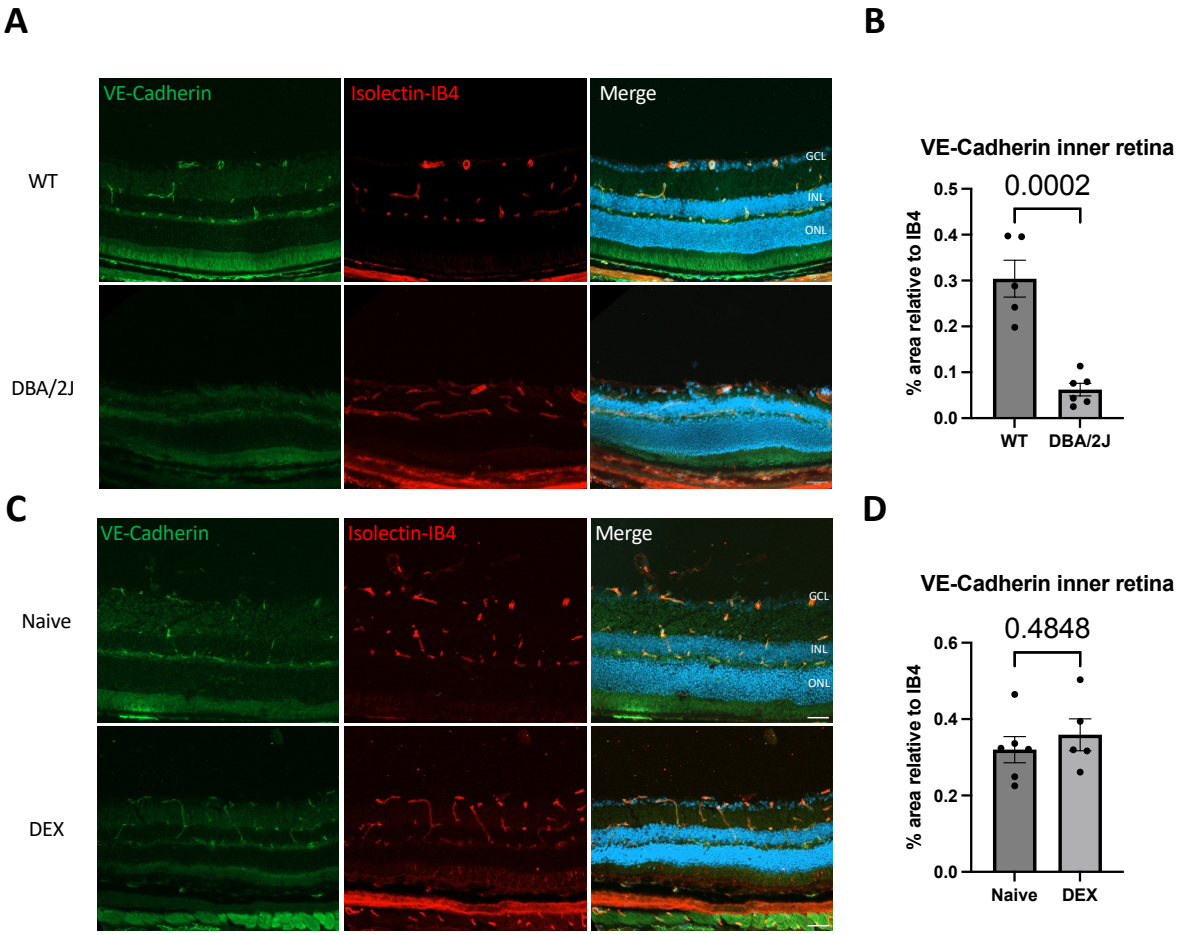



**Figure 4.2.16 | VE-Cadherin immunostaining in OHT models**

*Representative images show staining for VE-Cadherin (green), isolectin-IB4 (red), and both channels merged with DAPI (blue) in DBA/2J* ***(A)*** *and DEX* ***(C)*** *mice and age-matched C57BL/6J controls (WT/Naïve). Quantification of VE-Cadherin % area in the inner retina, normalised to isolectin-IB4 area, is shown in panels* ***B*** *(DBA/2J vs WT; n = 5 WT, n = 6 DBA/2J) and* ***D*** *(Dex vs Naïve; (n = 5 DEX, n = 6 Naïve)).*

To examine whether altered levels of transcytosis may contribute to retinal vascular leakage in these models, the expression of the negative transcytosis regulator Mfsd2a was assessed. Aged DBA/2J mice exhibited a significant reduction in Mfsd2a expression compared to wild-type controls ($p$ = 0.0008; Fig. 4.2.17B). Similarly, dexamethasone-treated mice showed significantly reduced Mfsd2a levels relative to their untreated counterparts ($p$ = 0.0130; Fig. 4.2.17D). These findings suggest that increased transcytosis, resulting from Mfsd2a downregulation, may represent a shared mechanism of iBRB dysfunction across both models.

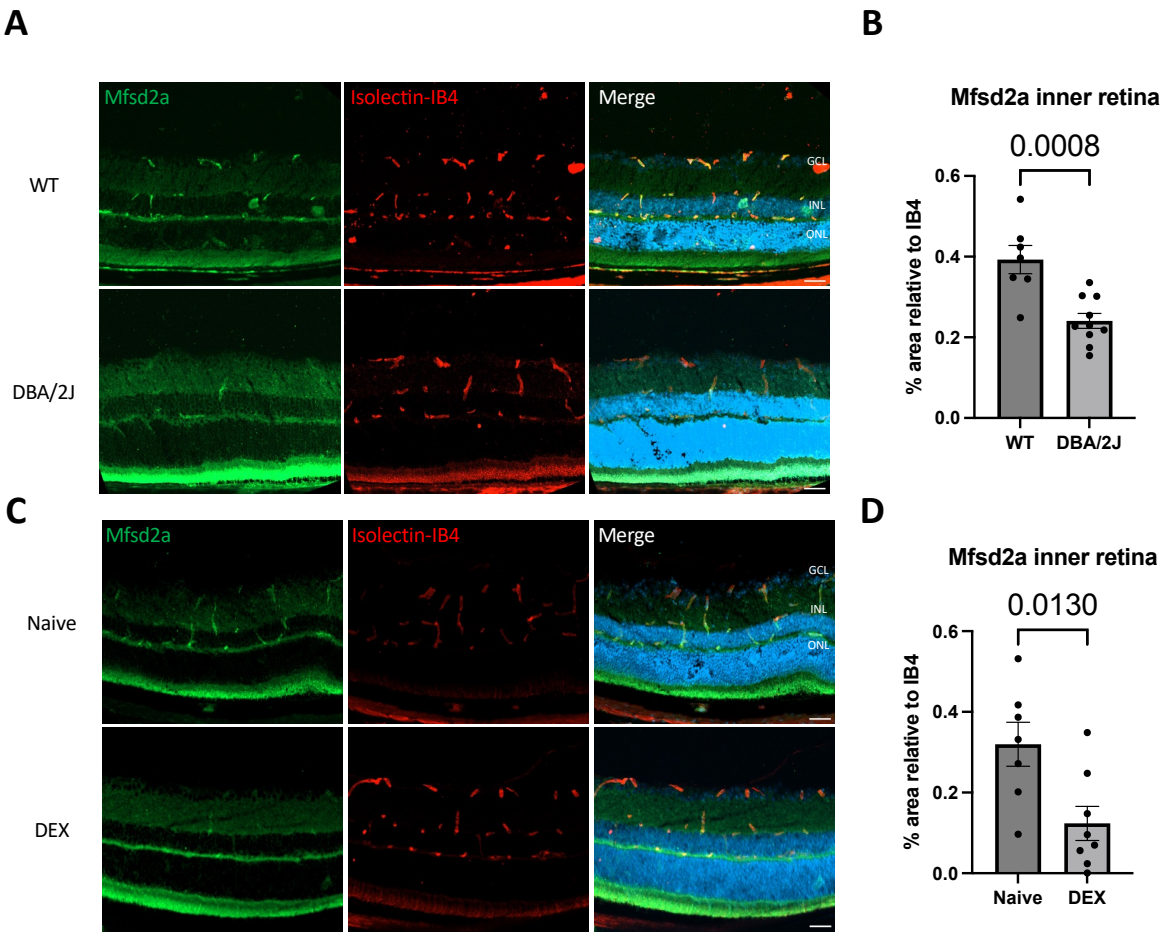



**Figure 4.2.17 | Mfsd2a immunostaining in OHT models**

*Representative images show staining for Mfsd2a (green), isolectin-IB4 (red), and both channels merged with DAPI (blue) in DBA/2J* ***(A)*** *and DEX* ***(C)*** *mice and age-matched C57BL/6J controls (WT/Naïve). Quantification of Mfsd2a % area in the inner retina, normalised to isolectin-IB4 area, is shown in panels* ***B*** *(DBA/2J vs WT; n = 7 WT, n = 10 DBA/2J) and* ***D*** *(Dex vs Naïve; (n = 8 DEX, n = 7 Naïve)).*

## 4.3 Discussion

The aims of this chapter were to determine whether iBRB dysfunction occurs in mouse models of OHT, to define its temporal relationship to RGC loss, and to investigate potential mechanisms. Previous work has shown that iBRB leakage can precede RGC degeneration in OHT models, but with differences in the reported mechanisms and detection methods. For example, Zhang et al. (2024) observed leakage in DBA/2J, Lmx1b$^{V265D}$, and hydrogel-induced OHT models, whereas Cueva-Vargas et al. (2024) reported similar findings in microbead-induced OHT. However, the groups proposed distinct mechanisms: Zhang et al. (2024) found no change in TJ expression but detected reduced Mfsd2a expression in the retinal vasculature, consistent with a transcytosis-mediated pathway, while Cueva-Vargas et al. (2024) implicated mitochondrial dysfunction in endothelial cells leading to claudin-5 disruption and paracellular leakage. Their approaches to assessing iBRB integrity also differed: Zhang et al. (2024) employed an ex vivo Hoechst tracer assay, whereas Cueva-Vargas et al. (2024) combined in vivo FFA with ex vivo sulfo-NHS-biotin labelling. This study utilised in vivo measurements, using FFA to evaluate retinal vascular integrity and OCT to assess retinal structure, thereby providing a bridge between the findings in DBA/2J mice of Zhang et al. (2024) and those of Cueva-Vargas et al. (2024) in their microbead OHT model. In addition, the inclusion of the dexamethasone-induced hypertension model, previously unreported in this context, expanded the range of OHT models in which iBRB leakage has been demonstrated, adding a novel dimension to the investigation.

### 4.3.1 Existence of iBRB leakage in OHT models

With regard to whether retinal vascular leakage is a feature of murine OHT models, the findings of this chapter align with those of Zhang et al. (2024) and Cueva-Vargas et al. (2024), confirming its presence, with FFA revealing leakage in DBA/2J mice from 6 months of age and in C57BL/6J mice following four weeks of treatment with dexamethasone to induce OHT. In terms of anatomical distribution, Zhang et al. (2024) reported that leakage in their models originated exclusively from veins and was confined to the RGC layer, whereas Cueva-Vargas et al. (2024) observed leakage throughout the retina. Although FFA alone cannot reliably differentiate venous from arterial leakage or localise leakage to specific vascular plexuses, sulfo-NHS-biotin labelling performed here in 9-month-old DBA/2J mice suggested that leakage occurred across all retinal vascular

plexuses and not in a venous specific manner. These findings emphasise the need for further studies to define the precise anatomical pattern of leakage in murine OHT models.

There were also differences in the pattern of FFA leakage detected here relative to previous studies in non-human primates with OHT and in human glaucoma patients, which report that leakage on FFAs is localised to the optic disc (Arend et al., 2005; Plange et al., 2010; Plange et al., 2012). Both DBA/2J and mice with dexamethasone-induced OHT in this study exhibited optic disc leakage alongside widespread, diffuse retinal leakage, a pattern also observed in the microbead model examined by Cueva-Vargas et al. (2024). This may reflect fundamental differences in the retinal vascular response to elevated IOP between rodents and primates, the latter possessing a more complex retinal architecture that includes a macula. Such differences are important to consider when evaluating the translational potential of BRB-targeted therapies for glaucoma, and they underscore the need to investigate this phenomenon further in intermediate models that more closely recapitulate human retinal structure.

### 4.3.2 Temporal relationship between IOP elevation, retinal vascular leakage, and RGC loss

With regard to the temporal relationship between iBRB leakage and RGC loss, fluorescein leakage was increased in DBA/2J mice at 6 months of age, coinciding with visible thinning of the RNFL/IPL on retinal OCT scans. Additionally, in mice with dexamethasone-induced OHT, vascular leakage preceded visible thinning of the RNFL/IPL on OCT. Together, these findings indicate that retinal vascular leakage at least coincides with RGC loss in murine models of OHT, and can precede it.

Of note, there were differences in the timing of key events in this study of DBA/2J mice and that of Zhang et al. (2024). In this study, retinal vascular leakage was detected at 6 months of age, at which time no group-level elevation in IOP was observed relative to C57BL/6J controls. However, a subset of animals exhibited IOP values greater than 15 mmHg at this timepoint. The lack of group level IOP difference may thus reflect the relatively small sample size examined, which could have limited the ability to detect a modest but biologically relevant group-level increase in IOP. Such elevations at this age have been reported in large-scale characterisations of the DBA/2J phenotype (Libby et al.,

2005). Zhang et al. (2024) reported elevated IOP in DBA/2J mice from 6 months of age, but observed retinal vascular leakage only from 7.5 months and RGC loss from 8 months. While the timing of IOP elevation in this study may be similar, the earlier detection of leakage and RGC loss may be explained by methodological differences. The Hoechst tracer assay (~562 Da) used by Zhang et al., in which leakage is inferred from the number of tracer-positive neurons, requires dye to cross the vascular barrier, diffuse into the retinal parenchyma, and enter neuronal nuclei before producing a detectable signal. This multi-step process is likely less sensitive to subtle or early barrier dysfunction than fluorescein angiography (~376 Da), which detects leakage directly from the extravasation of a smaller fluorophore. Similarly, counting RGCs in retinal flatmounts, as performed by Zhang et al. (2024), may be less sensitive to early neurodegenerative changes than the detection of RNFL/IPL thinning by OCT. Inter-strain variation could also contribute to these differences, as the DBA/2J mice examined in this work have been bred in TCD for several generations.

While this study was not designed or powered to perform a definitive correlation analysis between IOP and iBRB leakage, trends in the data provide some insight into the nature of this relationship. In the 6-month DBA/2J cohort, no appreciable association was detected between absolute IOP and fluorescein leakage. Similarly, in mice treated with dexamethasone for 4 weeks, the relationship between absolute IOP and leakage was only weakly positive. In contrast, a stronger association was observed when the change in IOP from baseline, rather than its absolute value, was compared with fluorescein leakage in the dexamethasone model. This pattern suggests that variation in IOP over time may be more closely related to the extent of retinal vascular leakage than the absolute IOP level. Such a dependence on IOP change rather than absolute IOP would be consistent with current understanding of the relationship between IOP and RGC death in glaucoma. IOP varies widely between individuals, and many with pressures in the hypertensive range do not develop glaucoma (Weinreb et al., 2014), while others with pressures in the normal range do (Lee et al., 1998). One proposed explanation for normotensive glaucoma is that some individuals may be more sensitive to relatively small IOP increases that remain within the normal range. Although time constraints prevented a longitudinal characterisation of IOP change in DBA/2J mice, it would be valuable to determine whether a similar pattern is present in this model. This information may help guide future studies on the relationship between elevated IOP and retinal vascular leakage.

### 4.3.3 Outer retinal abnormalities in DBA/2J mice

An incidental observation in this study was the presence of outer retinal abnormalities in DBA/2J mice. Abnormal fundus appearance, in addition to the presence of a discontinuous RPE and large outer retinal hyporeflective spaces on OCT were evident from as early as 3 months of age, preceding any detectable IOP elevation. These features are likely indicative of subretinal fluid accumulation occurring independently of IOP. The pigment dispersion phenotype and associated atrophy of the iris and ciliary body are well characterised in DBA/2J mice, but relatively little work has examined the effects of this phenotype on the RPE. One ultrastructural study has reported changes to the RPE in this model, including loss of mature melanin granules and altered melanosome structure (Schraermeyer et al., 2009). The combination of subretinal fluid accumulation and disrupted RPE continuity observed here is consistent with an oBRB defect in DBA/2J mice that has not been described previously. Such a defect is important to consider in future studies of BRB function in glaucoma using this model, as oBRB dysfunction could confound interpretation of FFA findings, which cannot readily distinguish leakage arising from the inner retinal vascular plexuses versus the choroid. oBRB leakage may therefore be a contributing factor to the retinal vascular leakage detected by FFA in DBA/2J mice and could potentially account for the absence of an apparent relationship between absolute IOP and leakage in this model, in contrast to the dexamethasone model, where a weakly positive association was observed. However, oBRB leakage alone cannot account for the leakage observed on FFAs from DBA/2J mice. Inner BRB leakage is also evident, as shown by the ex vivo sulfo-NHS-biotin assay, which would not be affected by oBRB defects.

### 4.3.4 Mechanism of vascular leakage

With regard to the mechanism of iBRB leakage, the results of this chapter are consistent with those of Zhang et al. (2024), showing no change in claudin-5 levels but a reduction in Mfsd2a levels in the inner retina of both aged DBA/2J mice and mice with dexamethasone-induced OHT. This pattern suggests a mechanism driven by increased transcytosis, rather than paracellular leakage mediated by TJ disruption. These findings are in contrast with those of Cueva-Vargas et al. (2024)*.,* who reported reduced retinal claudin-5 levels in their microbead model of OHT. This discrepancy may reflect methodological differences, as Cueva-Vargas et al. (2024) quantified absolute protein concentrations, whereas this study and that of Zhang et al. (2024) assessed claudin-5 by immunostaining. For TJ proteins,

immunostaining is advantageous because these proteins are highly stable and reduced total protein levels may not necessarily indicate a loss of the protein at the junction. It is also possible that inter-model variation contributes to these differences. This is supported by the finding in this study that the levels of VE-cadherin, a key component of endothelial adherens junctions, was reduced in DBA/2J mice but not in dexamethasone-induced OHT. Interestingly, VE-cadherin is known to stabilise claudin-5 expression by extending its half-life by sequestering β-catenin at junctions (Ramirez et al., 2013). When not sequestered, cytosolic β-catenin can translocate to the nucleus and interact with FoxO1. This β-catenin/FoxO1 transcriptional complex epigenetically suppresses *Cldn5* transcription through promoter methylation (Morini et al., 2018; Taddei et al., 2008). Why VE-cadherin expression was reduced while claudin-5 expression remained unchanged is not entirely clear. However, the protein kinase Akt can inhibit the nuclear localisation of FoxO1 through phosphorylation (Taddei et al., 2008). Akt activation can occur in endothelial cells in response to stimuli such as shear stress (Dimmeler et al., 1998), suggesting that alternative signalling pathways in the DBA/2J RECs may activate Akt and preserve claudin-5 expression despite reduced VE-cadherin levels. Additionally, loss of VE-cadherin has been associated with capillary loss in the deep vascular plexus of the Rd10 mouse model of retinitis pigmentosa (Nguyen et al., 2023). While not investigated here, it is plausible that vascular remodelling may also occur in response to elevated IOP in these mouse models of glaucoma. Future studies could address this by examining vascular architecture across vascular plexuses using pan-vessel markers in retinal flatmounts.

Other TJ proteins at the iBRB, such as ZO-1 and occludin, were not assayed in this study, so TJ-mediated leakage cannot be fully excluded in either model. Nevertheless, the reduction in Mfsd2a strongly supports a role for increased transcytosis. Mfsd2a is a negative regulator of endothelial transcytosis and has been identified as a key reason why iBRB and BBB endothelial cells exhibit low rates of caveolin-mediated transport under physiological conditions (Andreone et al., 2017; Ben-Zvi et al., 2014). Increased transcytosis is now recognised as a tight-junction-independent mechanism of iBRB/BBB leakage. Experimental models with elevated caveolin-mediated transport show FFA evidence of leakage (Z. Wang et al., 2020), supporting the plausibility that this mechanism contributes to the leakage observed here.

### 4.3.5 Conclusions

This chapter shows that disruption of the BRB is an early and consistent feature of murine models of OHT. Leakage at least coincides with, and may precede RGC loss. The extent of leakage appears to relate more closely to changes in IOP over time than to the absolute pressure level. DBA/2J mice, display abnormalities affecting the outer retina and retinal pigment epithelium that are present before detectable pressure increases and may contribute to observed leakage on FFAs, although iBRB leakage is also involved. Across models, the evidence supports a role for increased transcytosis in driving barrier dysfunction, while other mechanisms may play a secondary role.

# Chapter 5: Transcriptomic profiling of the iBRB in glaucoma

## 5.1 Introduction

### 5.1.1 NVU activation contributes to loss of iBRB integrity

As introduced in Section 4.1.1, the iBRB properties of RECs are not intrinsic to them, but are induced and maintained by surrounding cells, forming a wider NVU (Hawkins & Davis, 2005; Keaney & Campbell, 2015). In addition to RECs, the retinal NVU comprises several neuronal subtypes (RGCs , bipolar cells, horizontal cells and amacrine cells), pericytes, and glial cells (Astrocytes, Muller cells, and microglia) (Nian et al., 2021). These cell types work in concert to maintain retinal homeostasis by sustaining iBRB integrity and by regulating the inflammatory milieu of the retina, which is normally an immune-privileged environment. Retinal inflammation and iBRB function are therefore closely interconnected: barrier disruption can drive activation of other NVU components, while inflammatory signalling within the NVU can compromise barrier integrity.

Pericytes are contractile, phagocytic cells closely associated with RECs and are critical for maintaining iBRB stability (Alarcon-Martinez et al., 2020). Barrier integrity correlates with pericyte coverage, with reductions in pericyte number leading to increased permeability (Daneman, Zhou, Kebede, et al., 2010). Their recruitment during vascular development depends on endothelial-derived platelet-derived growth factor B (PDGF-B) acting on PDGF receptor-β, and disruption of this pathway reduces pericyte coverage and increases iBRB permeability (Armulik et al., 2010; Bell et al., 2010; Daneman, Zhou, Kebede, et al., 2010; Ogura et al., 2017; Park et al., 2017). Beyond vascular stability, pericytes are key regulators of neurovascular coupling, and their rupture under elevated IOP has been linked to neurovascular coupling deficits in glaucoma (Alarcon-Martinez et al., 2022). They also participate directly in neuroinflammatory processes, expressing receptors for cytokines and pathogen-associated molecules such as TNF-α, IL-1β, IL-8, LPS, and α-synuclein, and producing pro-inflammatory mediators under pathological conditions (Dohgu et al., 2019; Huang et al., 2025; Matsumoto et al., 2014; Navarro et al., 2016). Notably, pericyte-derived paracrine signals can amplify microglial activation and reduce endothelial TJ expression, thereby exacerbating iBRB dysfunction (Huang et al., 2025).

Astrocytes are located predominantly in the RNFL and INL, where their endfeet extend to make direct contact with RECs. They support iBRB integrity, as shown by increased barrier resistance in endothelial-astrocyte cocultures compared with endothelial monocultures

(Nakagawa et al., 2009). Astrocytic endfeet also express potassium channels and AQP4, which regulate ion and water homeostasis and contribute to clearance of waste products via the glymphatic system (Michinaga & Koyama, 2019; X. Wang et al., 2020). Under pathological conditions, astrocytes undergo reactive changes (Liu et al., 2020), leading to secretion of VEGF-A, MMPs, and MCP-1 (Shan et al., 2019), as well as cytokines that disrupt TJ organisation at the iBRB (Takeshita et al., 2017).

Müller glia are the most abundant glial cells in the retina, with processes spanning its entire thickness and contributing to the formation of the inner and outer limiting membranes (Bringmann et al., 2006). Their endfeet interact with synapses between retinal neurons and ensheathe retinal vessels (Vecino et al., 2016). Through the release of vasoactive molecules, Müller glia regulate neurovascular coupling (Newman, 2015). However, under stress, like astrocytes, they undergo reactive gliosis, characterised by secretion of VEGF-A, MMPs, and inflammatory cytokines that increase vascular permeability and drive ECM remodelling (Wang et al., 2015).

Microglia are resident macrophage-like cells in the retina. In their physiological surveillant state, they maintain homeostasis by clearing debris and releasing regulatory factors, including low levels of IL-10 and TGF-β, which contribute to immune quiescence (Phipps et al., 2019; Yun-Jia et al., 2021). In response to stress or injury, microglia become activated, adopting an amoeboid morphology, proliferating, and acquiring antigen-presenting capacity. Activated microglia secrete a wide range of inflammatory and neurotoxic mediators, including reactive oxygen species, glutamate, cytokines, chemokines, prostaglandins, and angiogenic factors, that compromise barrier integrity and amplify retinal inflammation (Alves et al., 2020; Nakamura, 2002).

### 5.1.2 Immune cell infiltration into the CNS

Although the retina is generally regarded as an immune-privileged environment, it is increasingly recognised that CNS physiology includes surveillance by peripheral immune to detect pathogens and injury (Lampron et al., 2013). Within the retina, the iBRB plays a central role in this process by mediating contact between leukocytes and RECs, enabling transendothelial migration (TEM). In response to danger signals such as TNF-α or IL-1β, RECs become activated, releasing pro-inflammatory mediators and upregulating adhesion

molecules including ICAM-1, VCAM-1, and E-selectin (Greenwood et al., 1995). Leukocyte adhesion then occurs through interactions between these adhesion molecules and leukocyte integrins such as LFA-1, followed by TEM, which is thought to proceed primarily via paracellular routes involving actin cytoskeleton reorganisation and TJ remodelling. Importantly, barrier integrity can be preserved during this process through PECAM-1-mediated recruitment of the lateral border recycling compartment, which displaces junctional components while sealing the intercellular gap (Keaney & Campbell, 2015; Sagar et al., 2012; Winger et al., 2014). While such immune surveillance may serve a protective, homeostatic function, excessive or dysregulated leukocyte infiltration can be considered as a form of iBRB breakdown, exacerbating neuroinflammation. This is underscored by the fact that aberrant immune cell infiltration is a pathological feature of retinal diseases such as diabetic retinopathy and multiple sclerosis (Green et al., 2010; Zhao et al., 2024).

### 5.1.3 Inflammation and RGC death in glaucoma

In glaucoma, the precise relationship between IOP elevation and RGC death remains unclear. However, studies in both animal models and humans provide substantial evidence of retinal and optic nerve head inflammation, characterised by increased activation of NVU components, increased levels of pro-inflammatory cytokines, and immune-cell infiltration (Baudouin et al., 2021). A consistent finding across species is early microglial activation. In DBA/2J mice, microglial activation originates in the central inner retina and optic nerve head before extending peripherally, preceding RGC loss (Bosco et al., 2011). The extent of early microglial activation is predictive of RGC degeneration (Bosco et al., 2015), and pharmacological inhibition with minocycline confers neuroprotection (Bosco et al., 2008). Similarly, post-mortem tissue from glaucoma patients shows increased numbers of activated microglia in the optic nerve head compared with healthy controls (Yuan & Neufeld, 2001).

Astrocytic changes are also a common feature of glaucoma. In DBA/2J mice, astrocyte processes redistribute towards the edge of the optic nerve before outright degeneration occurs (Cooper et al., 2016). Additionally, increased GFAP expression, a marker of astrogliosis, has been reported in glaucomatous retinas compared to healthy controls (Tezel et al., 2003). Prolonged gliosis can lead to an extended immune response, characterised by

increased immune cell infiltration, and elevated cytokine levels (Jiang et al., 2020). Integrin overexpression in glaucomatous astrocytes suggests that these cells may play a role in promoting immune-cell adhesion and infiltration into the retina under IOP-mediated stress (Soto & Howell, 2014).

In addition to glial responses, increased infiltration of $CD163^{+}$ macrophages and elevated cytokine levels have been reported in the retina and optic nerve head of glaucoma patients (Gramlich et al., 2013; Margeta et al., 2018). These changes are accompanied by, canonical inflammasome activation, with upregulation of NLRP3 being observed in the retina of glaucoma patients (Yang et al., 2011). Together, these findings indicate that NVU activation and immune-cell infiltration are early features and likely contributors to RGC loss in glaucoma.

### 5.1.4 Chapter aims

In the previous chapter, it was shown that mouse models of glaucoma develop early retinal vascular leakage, accompanied by reduced Mfsd2a and unchanged claudin-5 levels in the inner retina. However, as outlined in the introduction, the retinal vasculature functions within the wider NVU, which is activated in glaucoma. Examining iBRB-related proteins in isolation therefore does not fully explain how elevated IOP leads to vascular leakage or how this contributes to RGC degeneration. The central aim of this chapter was to gain deeper mechanistic insight into the pathways underlying retinal vascular dysfunction in glaucoma. To address this aim, publicly available RNA-seq datasets from Keuthan et al. (2023) were analysed, generated from the retinas of mice subjected to microbead-induced IOP elevation and ONC. These datasets are particularly valuable because of their longitudinal design, allowing expression changes to be tracked across disease progression. The analysis had three objectives: **A)** to extend the number of glaucoma models examined with regard to iBRB dysfunction, **B)** to provide an unbiased characterisation of transcriptional changes in the glaucomatous retina, and **C)** to assess whether RGC degeneration itself, independent of IOP, contributes to vascular dysfunction by comparing IOP-dependent and IOP-independent models. Together, these analyses aim to provide a more comprehensive understanding of the molecular pathways driving retinal vascular dysfunction in glaucoma and how they relate to IOP elevation and RGC loss over time.

## 5.2 Results

### 5.2.1 Early vascular expression changes in mice with microbead-induced OHT

To investigate mechanisms underlying IOP-induced iBRB dysfunction, a publicly available RNA-seq dataset from Keuthan et al. (2023) was reanalysed. The dataset included $n = 2$ retinal samples from C57BL/6J mice collected at baseline (naïve) and at 3 days, 2 weeks, and 6 weeks after OHT was induced via intracameral injection of microbeads. While the original study primarily focussed on regional gene expression differences in the ONH and retina, the current analysis aimed to uncover whether OHT is associated with transcriptional changes indicative of vascular dysregulation, and to determine the temporal nature of any such changes. To enhance statistical power, the dataset was supplemented with data from an additional five age-matched naïve C57BL/6J retinal samples previously generated by the Campbell Lab (Fig. 5.2.1)

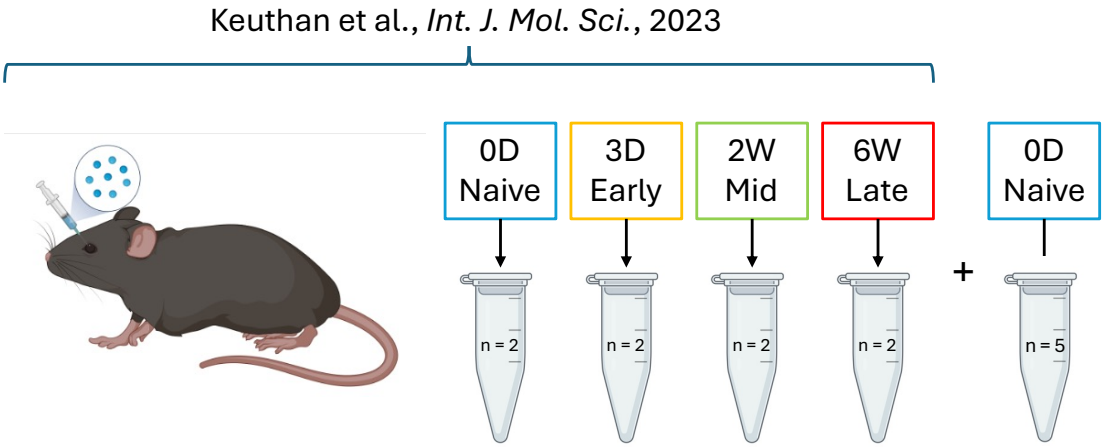



**Figure 5.2.1| Outline of groups for RNA-seq analysis of microbead-induced OHT model**

*A publicly available bulk RNA-seq dataset from Keuthan et al. (2023), derived from retinas of C57BL/6J mice at 0 days (0D, Naïve), 3 days (3D, Early), 2 weeks (2W, Mid), and 6 weeks (6W, Late) following intracameral microbead injection to induce OHT, was reanalysed with the addition of five age-matched naïve samples.*

FASTQ files from all retinal samples underwent standard quality control and were processed with DESeq2 to generate a vst count matrix. This matrix was then used for PCA, with ComBat applied to correct for technical differences between the samples from Keuthan et al. (2023) and those generated by the Campbell Lab. PCA revealed clear separation between naïve and microbead-induced OHT samples (Fig. 5.2.2). This indicated that, with batch effects accounted for, naïve samples clustered more closely with each other than with OHT samples, supporting the inclusion of the additional naïve samples for downstream expression analysis.

PCA analysis also revealed that while retinal samples from the 3-day and 6-week timepoints formed distinct clusters, one of the 2-week samples clustered more closely with the 6-week group than with the other 2-week sample (Fig. 5.2.2). This suggests the presence of individual variability in the timing of transcriptional changes induced by OHT

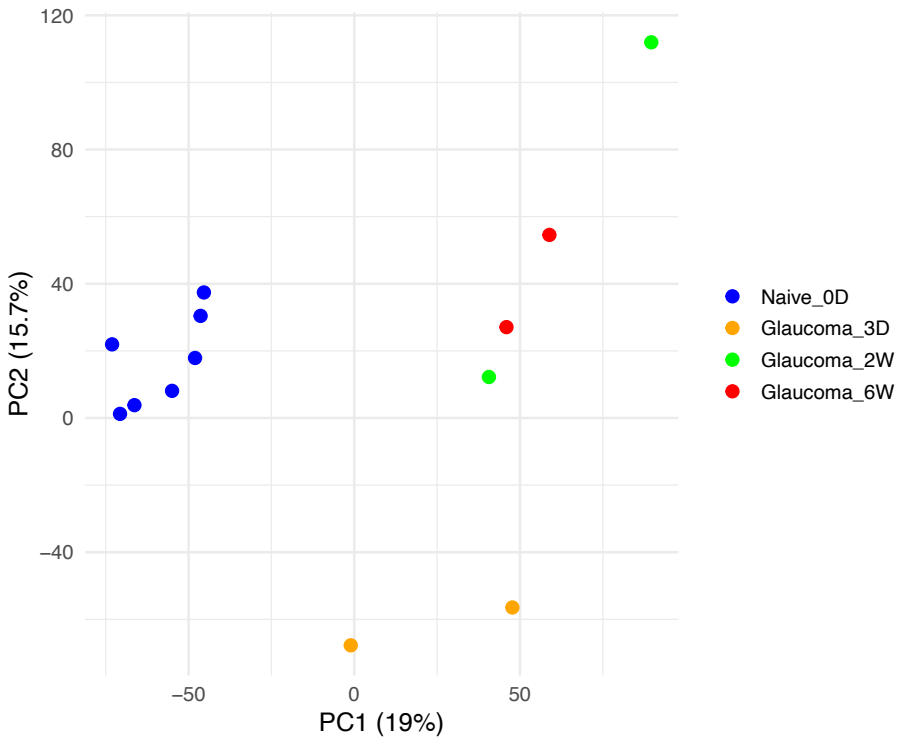



**Figure 5.2.2 | PCA of microbead-induced OHT samples**

*PCA plot showing global gene expression patterns in retinal samples from naïve mice (blue) and from mice at 3 days (orange), 2 weeks (green), and 6 weeks (red) following microbead-induced OHT. The variance explained by principal components (PC) 1 and 2 is displayed on the x- and y-axes, respectively.*

Differential gene expression analysis was performed on the samples, comparing each timepoint post OHT induction to naïve samples using a treatment + batch experimental design through DESeq2. Upon comparing the earliest 3 day timepoint to naïve samples, 103 differentially expressed genes (DEGs) were identified (Fig. 5.2.3; Appendix 1). At this timepoint, several iBRB-associated genes and endothelial activation markers were upregulated including *Cldn5*, *Vcam1*, *Cav1*, and *Vwf*. Upregulation genes that are not directly involved in maintaining the iBRB but are associated with barrier dysfunction in disease was also observed, such as *Edn2* (Alrashdi et al., 2018), *S100a6* (Tsai et al., 2019), and *Stat3* (Yun et al., 2017). Additionally, several genes associated with a pro-inflammatory retinal environment were upregulated including glial cell activation marker *Gfap*, microglial and macrophage marker *Cd68*, and complement components *C4b* and *C1qc* (Fig. 5.2.3).

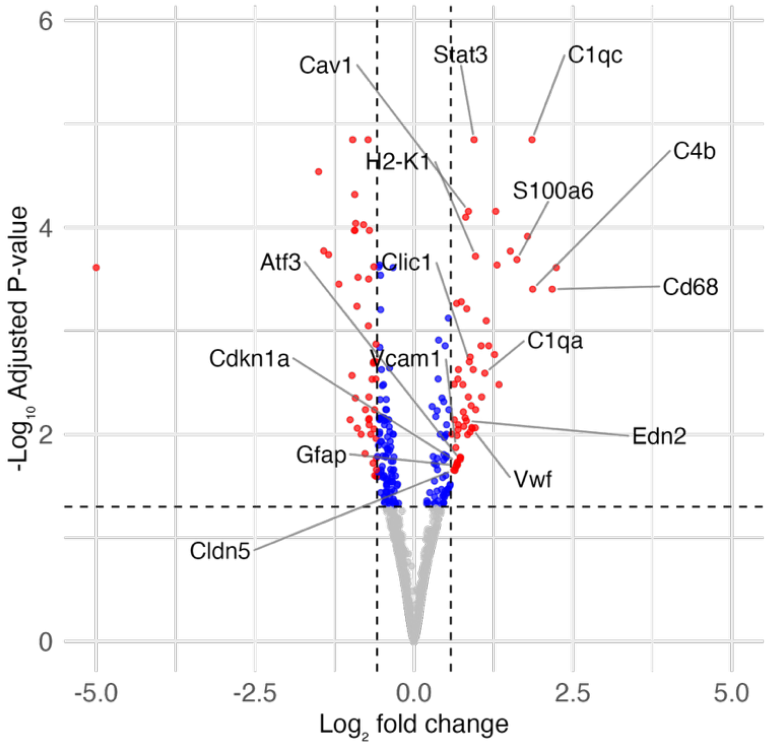



**Figure 5.2.3| Differential gene expression at 3 days post-OHT induction**

*Volcano plot comparing retinal samples 3 days after microbead-induced OHT to naïve controls. Genes meeting significance thresholds (padj < 0.05, horizontal dashed line) and with a $log_2$ fold change > 0.58 or < - 0.58 (vertical dashed lines) are highlighted in red. Genes with p < 0.05 but $log_2$ fold change between - 0.58 and 0.58 are shown in blue. Genes with a putative role in endothelial activation or retinal inflammation are highlighted. Differential expression was assessed using the Wald test, with multiple comparisons corrected using the Benjamini-Hochberg false discovery rate.*

At 2 weeks-post OHT induction, the number of DEGs identified was notably lower (30) than at the 3 day timepoint (Fig. 5.2.4; Appendix 1). *Serpina3n* was found to be upregulated at this timepoint, which has been reported to be expressed by inflamed retinal vessels during experimental autoimmune uveitis and is protective against BBB dysfunction following cerebral ischemic stroke (Li et al., 2023; Lipski et al., 2020). Of the iBRB and retinal inflammation associated hits detected at the earliest timepoint, *Stat3, Edn2* , and *C4b* remained upregulated. Notably, *Cldn5*, *Vcam1*, *Vwf*, *Cav1*, and *S100a6* were not detected as being differentially expressed at this timepoint.

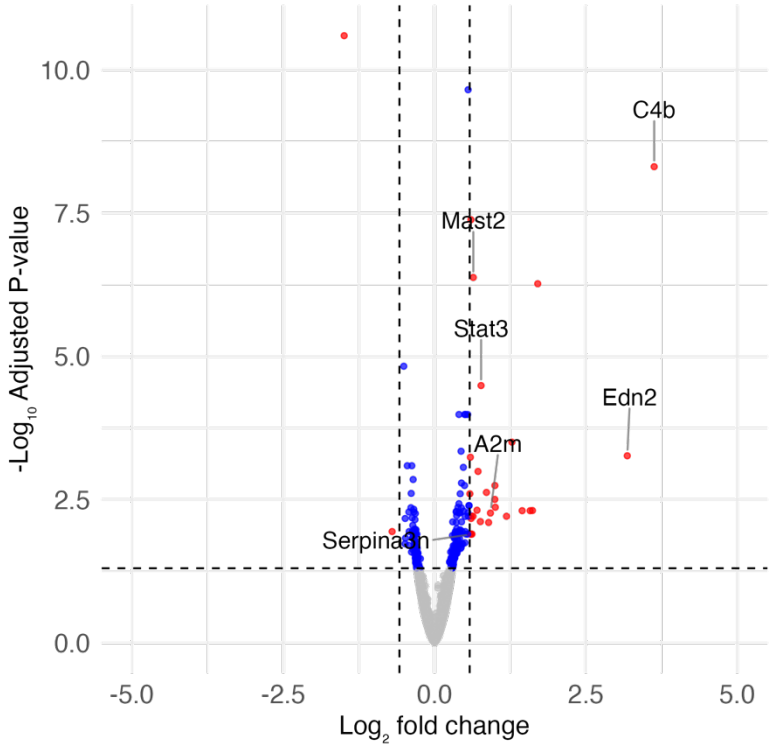



**Figure 5.2.4| Differential gene expression at 2 weeks post-OHT induction**

*Volcano plot comparing retinal samples 2 weeks after microbead-induced OHT to naïve controls. Genes meeting significance thresholds (padj < 0.05, horizontal dashed line) and with a $log_2$ fold change > 0.58 or < -0.58 (vertical dashed lines) are highlighted in red. Genes with p < 0.05 but $log_2$ fold change between -0.58 and 0.58 are shown in blue. Genes with a putative role in endothelial activation or retinal inflammation are highlighted. Differential expression was assessed using the Wald test, with multiple comparisons corrected using the Benjamini-Hochberg false discovery rate.*

At six weeks post-OHT induction, 34 DEGs were identified relative to naïve retinas (Fig. 5.2.5; Appendix 1). *Edn2* and *C4b* remained upregulated, consistent with earlier timepoints. In contrast, *Stat3* and *Serpina3n*, previously upregulated, were no longer differentially expressed. *Cd68*, upregulated at day 3 but not at two weeks, was again upregulated at six weeks. An additional complement factor, *C3*, was upregulated for the first time at this timepoint.

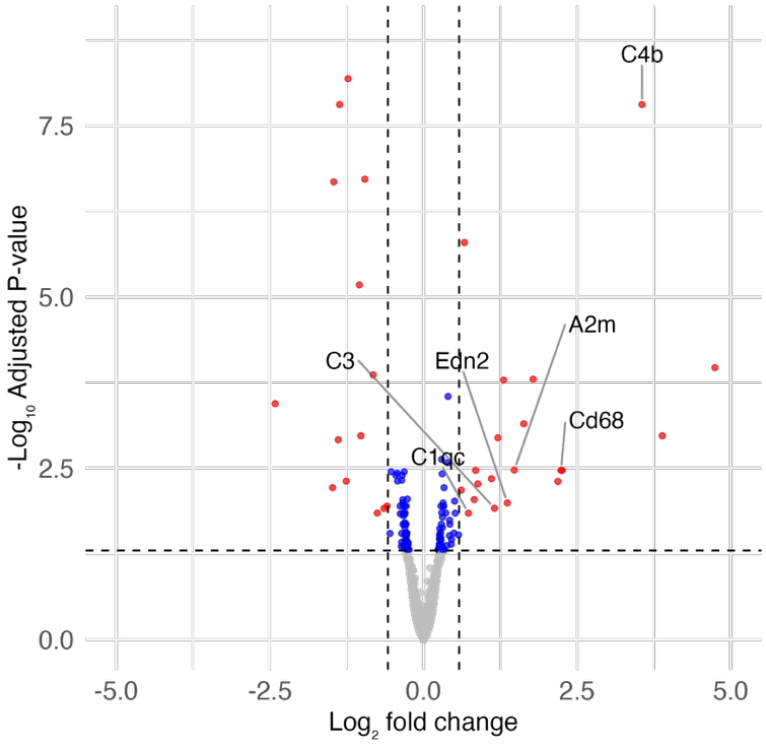



**Figure 5.2.5| Differential gene expression at 6 weeks post-OHT induction**

*Volcano plot comparing retinal samples 6 weeks after microbead-induced OHT to naïve controls. Genes meeting significance thresholds (padj < 0.05, horizontal dashed line) and with a $log_2$ fold change > 0.58 or < - 0.58 (vertical dashed lines) are highlighted in red. Genes with p < 0.05 but $log_2$ fold change between - 0.58 and 0.58 are shown in blue. Genes with a putative role in endothelial activation or retinal inflammation are highlighted. Differential expression was assessed using the Wald test, with multiple comparisons corrected using the Benjamini-Hochberg false discovery rate.*

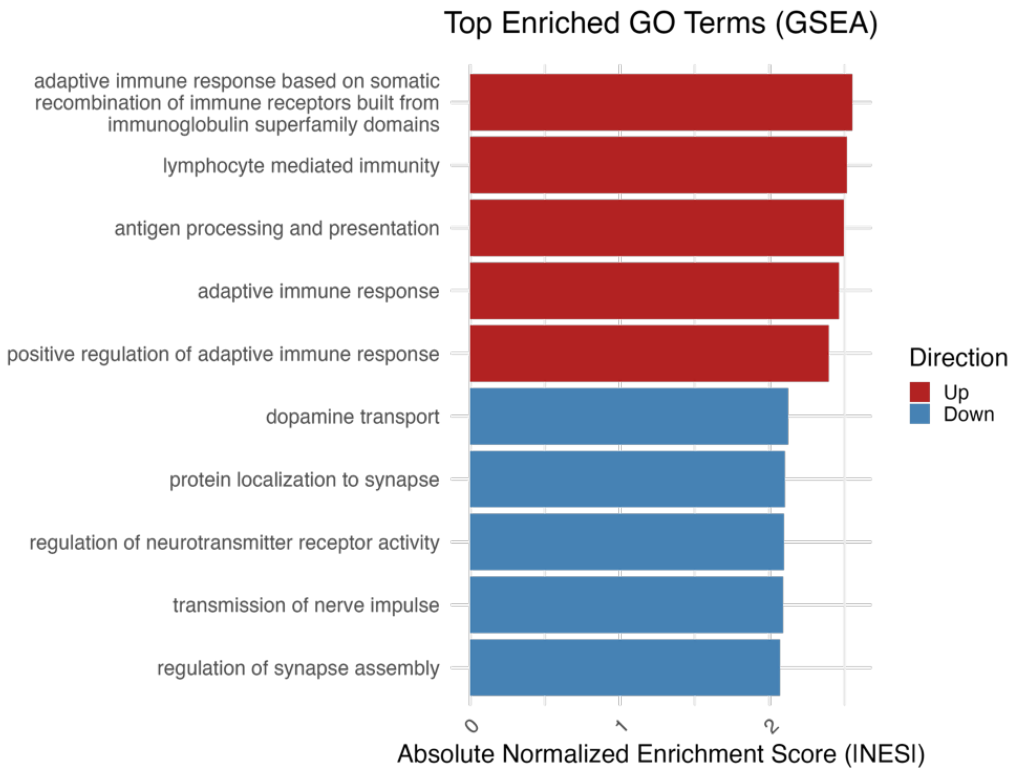
To investigate broader biological pathways underlying the observed transcriptional changes, GSEA was performed for each comparison. Genes were ranked using the product of $-\log_{10}$(p-value) and the sign of their $\log_2$ fold change. Enrichment analysis of GO Biological Process terms was then conducted using the clusterProfiler R package to determine the most positively and negatively enriched pathways. In the case of this dataset, which has relatively small sample size, and thus a relatively small number of DEGs (typically <100), this approach was preferrable to Over-Representation Analysis (ORA), which tests whether GO terms are over-represented among DEGs only.

At 3 days following microbead-induced OHT, the top five positively enriched GO terms were associated with adaptive and lymphocyte-mediated immunity, in addition to antigen presentation (Fig. 5.2.6A). The core enrichment genes underlying these terms included antigen processing and presentation machinery such as MHC class I (*H2-D1*, *H2-K1*, *B2m*, *Tap1*, *Tap2*) and MHC class II components (*Cd74*, *H2-Aa*, *H2-Ab1*). Additional contributors included immune cell adhesion/activation markers (*Icam1*, *Cd44*, *Myd88*), myeloid-associated transcripts (*Trem2*, *Fcgr3*, *Fcer1g*, *Mpeg1*, *Cd68*), and cytokine-related transcripts (*Il33*, *Il18bp*) (Appendix 2). In the sterile context of OHT, these GO terms likely reflected stress-induced activation of resident antigen-presenting cells, particularly microglia, with possible contributions from infiltrating leukocytes

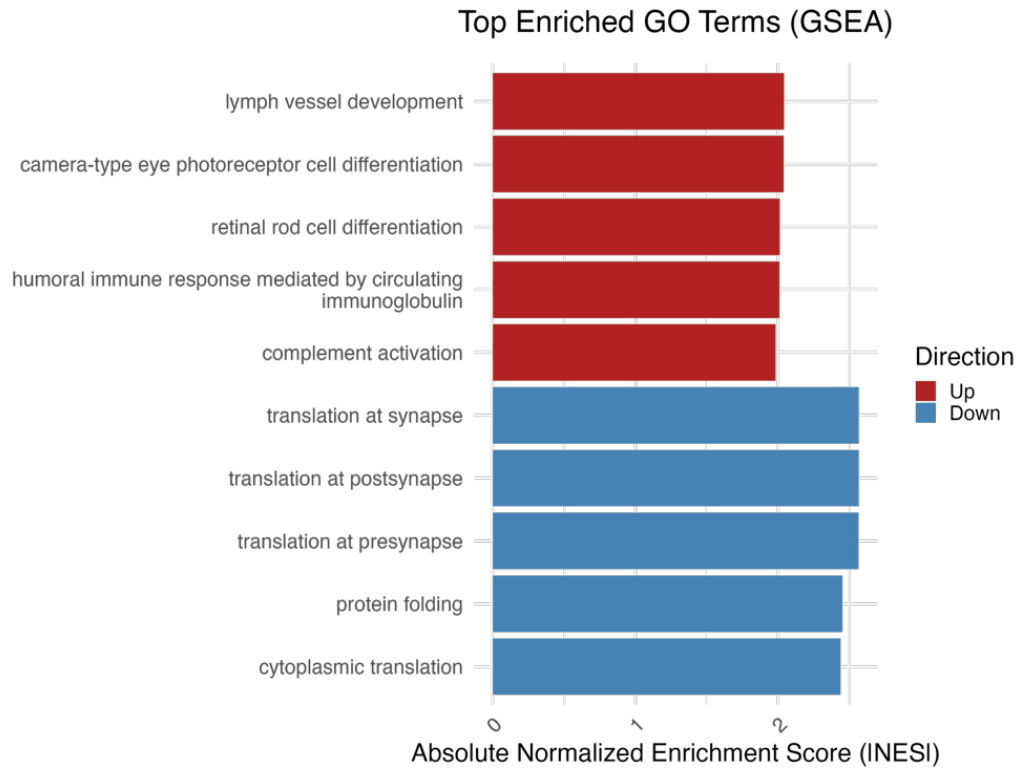
At the 2-week timepoint, the top five positively enriched terms were no longer dominated by immune-associated pathways (Fig. 5.2.6B). The three most positively enriched GO terms were “lymph vessel development,” “camera-type eye photoreceptor cell differentiation,” and “retinal rod cell differentiation.”. The core enrichment genes contributing to these pathways included VEGF signalling and vascular remodelling-associated transcripts (*Kdr*, *Flt4*, *Clec14a*, *Heg1*, *Fgf2*), in addition to markers of glial cell activation (*Stat3*, *Sox9*, *Cntf*) (Appendix 2). Immune-associated terms, including “humoral immune response mediated by circulating immunoglobulin” and “complement activation,” also appeared among the top five positively enriched terms. This suggested a transitional state in the response to OHT, characterised by vascular remodelling and glial cell activation alongside continued, but less dominant innate immune activation.

At the latest timepoint, immune-related pathways again dominated the enrichment results (Fig. 5.2.6C). The top five positively enriched terms were related to complement activation, humoral immunity, and antigen presentation. The core enrichment genes underlying these terms included components of the classical complement cascade (*C1qa, C1qb, C1qc, C1s1, C3, C4b*) and complement regulatory factors (*Serping1, Cd46, Cfh, Cfp*). Notably, there was significant overlap in the core enrichment genes with the earliest timepoint, including a reemergence off genes related to antigen presentation, including MHC class I components (*H2-D1*, *H2-K1*, *B2m*, *Tap1*) and MHC class II genes (*Cd74*, *H2-Aa*, *H2-Ab1*), as well as myeloid-associated transcripts (*Trem2*, *Fcgr3*, *Fcer1g*, *Mpeg1*) (Appendix 2). These findings suggested a biphasic pattern of inflammation in response to OHT, characterised by an early phase of myeloid cell activation, followed by a period of vascular remodelling and glial activation, and culminating in a resurgence of complement-driven innate immune signalling.

**A)**


Top Enriched GO Terms (GSEA)
adaptive immune response based on somatic recombination of immune receptors built from immunoglobulin superfamily domains
lymphocyte mediated immunity
antigen processing and presentation
adaptive immune response
positive regulation of adaptive immune response
dopamine transport
protein localization to synapse
regulation of neurotransmitter receptor activity
transmission of nerve impulse
regulation of synapse assembly
0
1
2
Absolute Normalized Enrichment Score (INESI)
Direction
Up
Down

**B)**


Top Enriched GO Terms (GSEA)
lymph vessel development
camera-type eye photoreceptor cell differentiation
retinal rod cell differentiation
humoral immune response mediated by circulating immunoglobulin
complement activation
translation at synapse
translation at postsynapse
translation at presynapse
protein folding
cytoplasmic translation
0
1
2
Absolute Normalized Enrichment Score (INESI)
Direction
Up
Down

**C)**

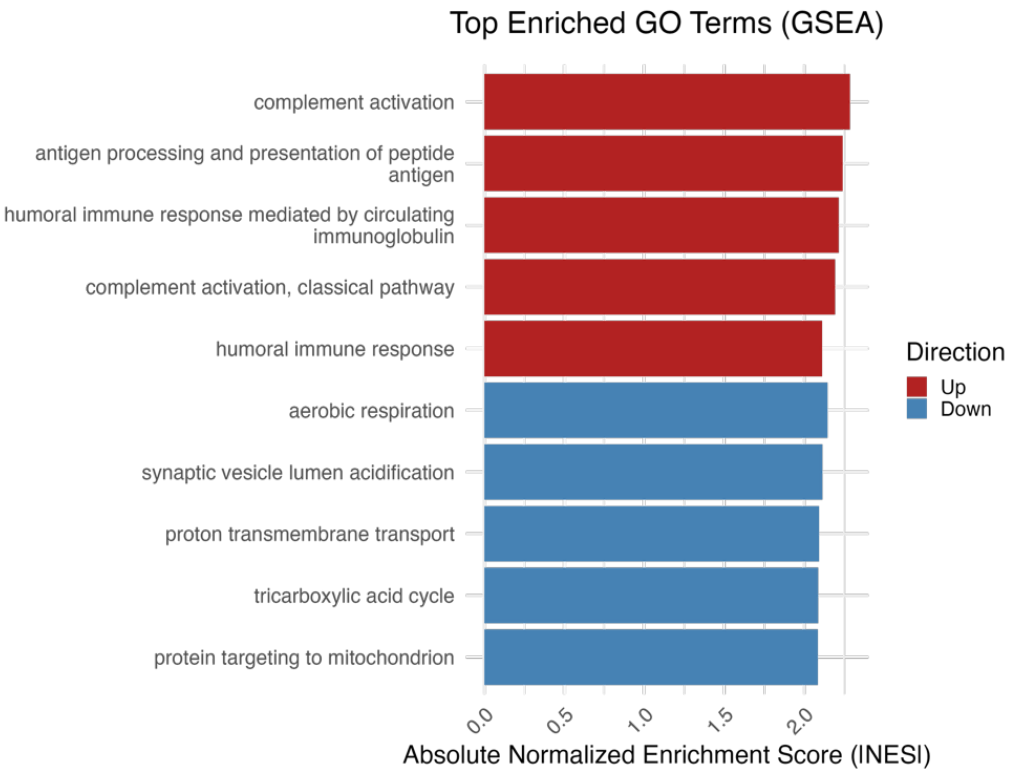



**Figure 5.2.6| GSEA plots for microbead-induced OHT model**

*Gene set enrichment analysis plots for Early vs Naïve* ***(A),*** *Mid vs Naïve* ***(B)*** *and Late vs Naïve* ***(C)*** *comparisons. Genes were ranked by the product of -log10(p-value) and the sign of their log2 fold change. The top 5 positively enriched (NES > 0) and negatively enriched (NES < 0) GO Biological Process terms are shown. Bar lengths indicate the absolute value of the normalised enrichment score (|NES|). Red bars correspond to positively enriched terms, while blue bars correspond to negatively enriched terms.*

To gain a further understanding of the temporal nature of iBRB-related gene expression changes and their relationship to RGC loss, individual gene plots were generated for iBRB-associated hits from the differential expression analysis (Fig. 5.2.7) alongside a panel of established RGC marker genes (Fig. 5.2.8). Analysis of the iBRB-associated genes confirmed a pattern of early activation. *Cldn5*, *Cav1*, and *Vwf* were significantly upregulated at 3 days post-OHT induction, returning to baseline at 2 and 6 weeks (Figs. 5.2.7A, B, D). *Vcam1*, *Stat3*, and *S100a6* (Figs. 5.2.7C, E, F) displayed a more prolonged response, remaining elevated at 2 weeks before normalising by the 6-week timepoint. These results suggest an early, transient disruption of iBRB integrity in response to OHT. Analysis of RGC-associated markers revealed that most markers, including *Rbpms1* (Fig. 5.2.8A), *Rbpms2* (Fig. 5.2.8B), *Sncg* (Fig. 5.2.8D), *Pou4f1* (Fig. 5.2.8F), *Pou4f2*, and *Pou4f3* (Fig. 5.2.8G) remained unchanged at all timepoints relative to the naïve group. The stability of these markers suggests that RGCs remain largely transcriptionally intact during the early and intermediate stages of OHT, with no evidence of widespread cell loss. *Thy1* expression was significantly downregulated at 3 days post-OHT induction (Fig. 5.2.8E), but returned to baseline levels by 2 and 6 weeks. Thy1 is a surface glycoprotein that is enriched in RGCs in the retina (Barnstable & Dräger, 1984; Laboissonniere et al., 2019). This early, transient suppression likely reflects a reversible stress response, as *Thy1* is known to be sensitive to stress and may be downregulated even in surviving RGCs (Fileta et al., 2006). In contrast, *Tubb3*, a marker of neuronal structure and cytoskeletal integrity, was significantly reduced only at the 6-week timepoint (Fig. 5.2.8C). This suggested that overt RGC degeneration, involving structural compromise or cell loss, begins only at the 6 week timepoint in this model.

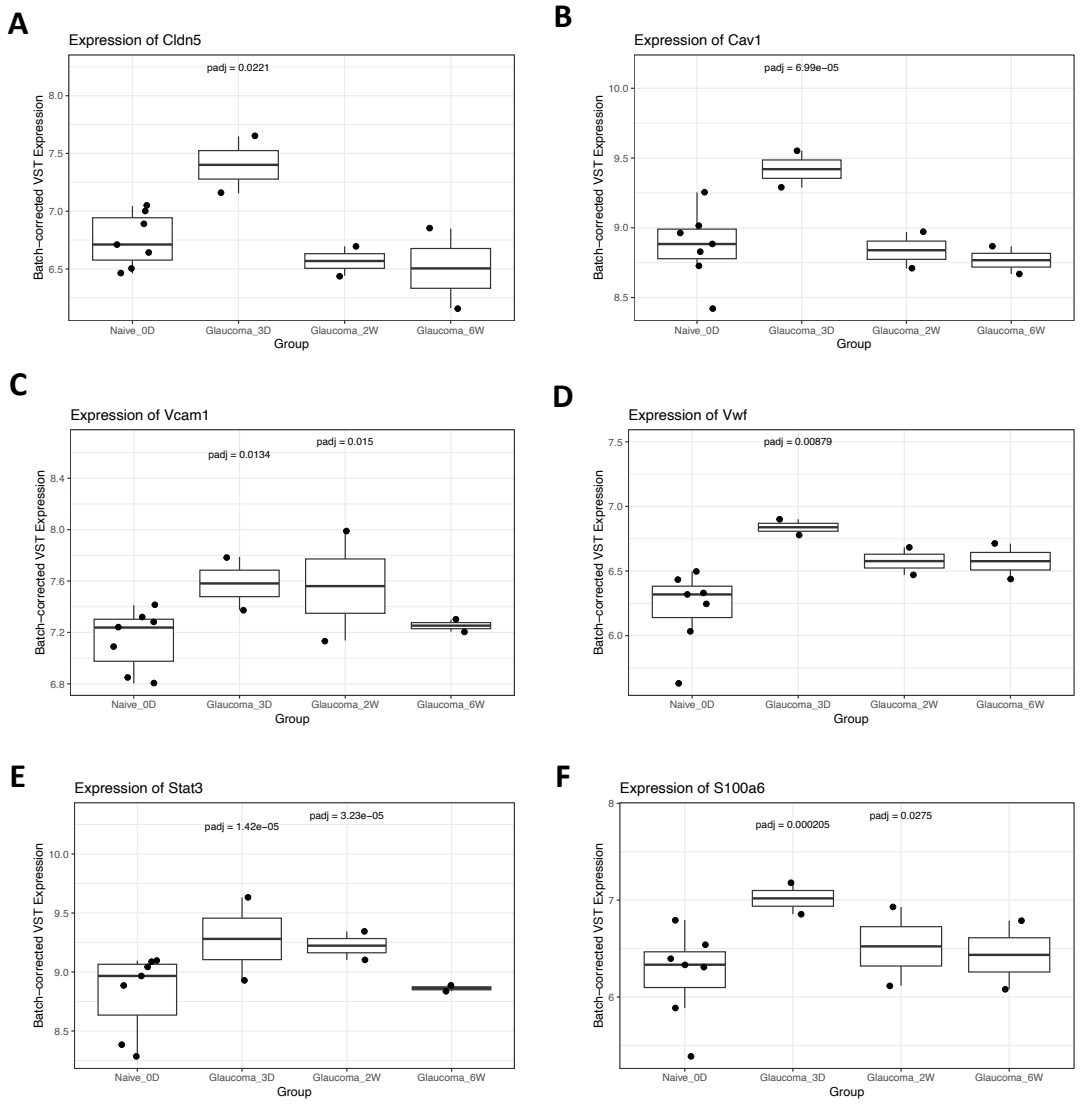



**Figure 5.2.7| Gene plots of markers of iBRB dysfunction in microbead-induced OHT model**

*Boxplots for Cldn5* ***(A)****, Cav1* ***(B)****, Vcam1* ***(C)****, Vwf* ***(D),*** *Stat3* ***(E)****, and S100a6* ***(F)*** *show variance-stabilised gene expression values for each sample. Boxes represent IQR, middle line represents the median, whiskers represent the range. Adjusted p values are shown in the case of significant differences vs Naïve group. Significance was determined via Wald tests with multiple comparisons controlled with a Benjamini-Hochberg FDR correction.*

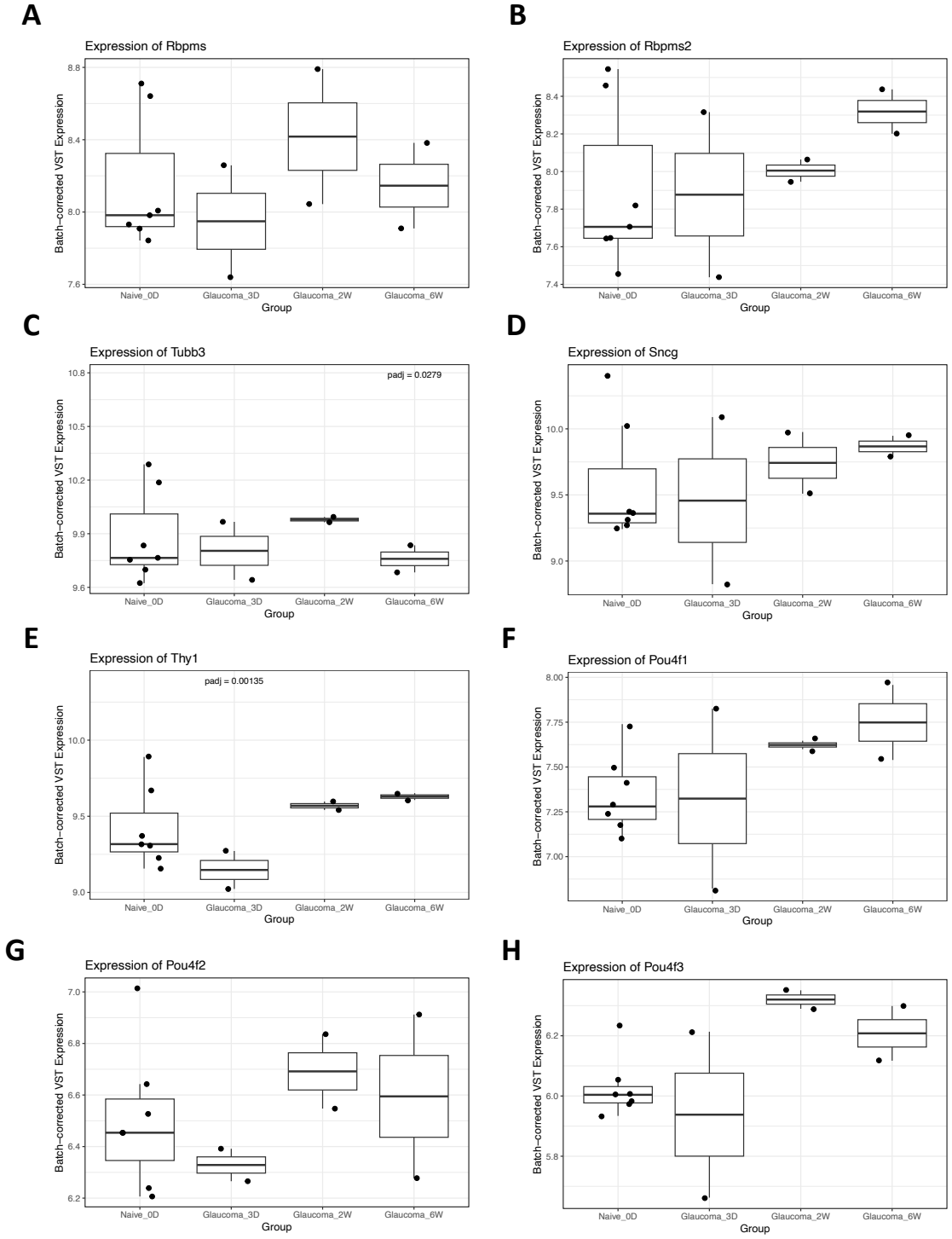



**Figure 5.2.8| Gene plots of RGC markers in microbead-induced OHT model**

*Boxplots for Rpbms* ***(A)****, Rpbms2* ***(B)****, Tubb3* ***(C)****, Sncg* ***(D),*** *Thy1* ***(E)****, Pou4f1* ***(F)****, Pou4f2* ***(G)****, and Pou4f3* ***(H)*** *show variance-stabilised gene expression values for each sample. Boxes represent IQR, middle line represents the median, whiskers represent the range. Adjusted p values are shown in the case of significant differences vs Naïve group. Significance was determined via Wald tests with multiple comparisons controlled with a Benjamini-Hochberg FDR correction.*

### 5.2 Vascular expression changes in the ONC model those mirror those in the microbead induced OHT model

Given the biphasic inflammatory response observed in the microbead-induced OHT model, it was hypothesised that a bidirectional relationship may exist between RGC damage and vascular dysfunction in glaucoma. Specifically, RGC degeneration may contribute to a secondary wave of inflammation, potentially exacerbating iBRB disruption. To investigate this possibility, a second RNA-seq dataset from Keuthan et al. (2023) was analysed, comprising retinal samples collected at 3 days and 2 weeks following ONC. As ONC is a pressure-independent model of RGC injury, it provided an opportunity to assess whether RGC loss alone is sufficient to induce iBRB-related gene expression changes. These samples were compared to the same naïve C57BL/6J control dataset used in the analysis of the microbead-induced OHT model (Fig. 5.2.9).

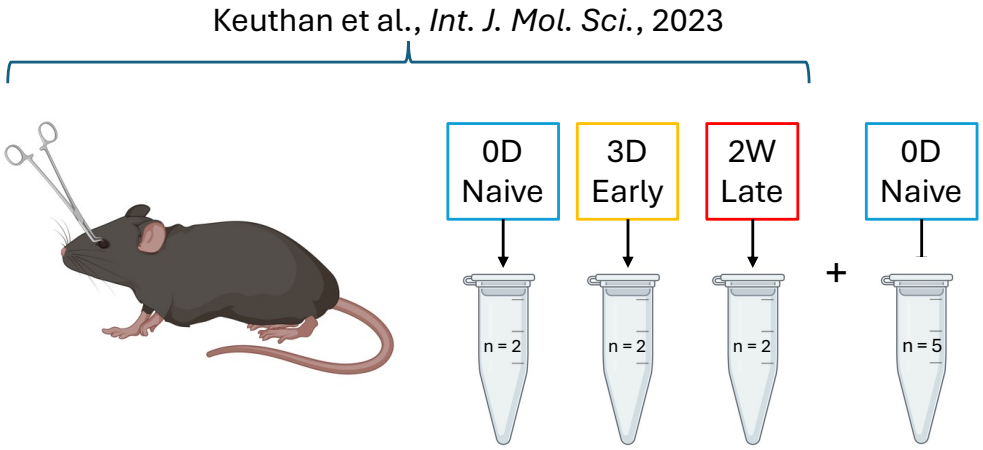



**Figure 5.2.9| Outline of groups for RNA-seq analysis of ONC model**

*A publicly available bulk RNA-seq dataset from Keuthan et al. (2023), derived from retinas of C57BL/6J mice at 0 days (0D, Naïve), 3 days (3D, Early) and 2 weeks (2W, Late) following ONC, was reanalysed with the addition of five age-matched naïve samples.*

As in the microbead model, PCA following batch correction with ComBat demonstrated clear separation between naïve and ONC retinas. All naïve samples clustered closely together and were distinct from the ONC samples, again confirming that the additional naïve retinas were appropriate for downstream analysis (Fig. 5.2.10). Consistent with the microbead data, one of the 3-day ONC samples clustered more closely with a 2-week sample than with the other 3-day replicate, indicating inter-mouse variability in the progression of the injury response (Fig. 5.2.10).

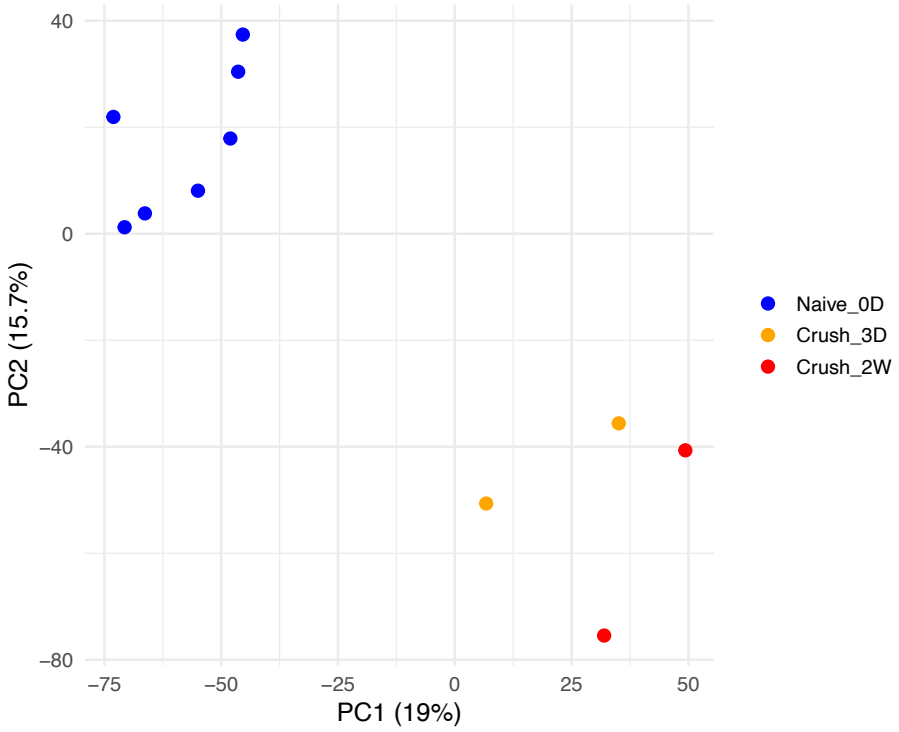



**Figure 5.2.10 | PCA of ONC samples**

*PCA plot showing global gene expression patterns in retinal samples from naïve mice (blue) and from mice at 3 days (orange) and 2 weeks (red) following ONC injury. The variance explained by principal components (PC) 1 and 2 is displayed on the x- and y-axes, respectively.*

Differential expression analysis with DESeq2 identified 52 DEGs in retinas 3 days post-crush relative to naïve controls (Fig. 5.2.11). As expected following direct optic nerve injury, several stress-response genes associated with RGC damage were upregulated, including *Atf3*, previously reported to exert protective effects in ONC (Kole et al., 2020), and *Clic1*, identified as a driver of RGC death (Tapia et al., 2024) (Fig. 5.2.11; Appendix 1). Additionally, genes associated with a pro-inflammatory retinal environment were elevated, such as *Cd68* and complement components *C4b* and *C1qc*, which were also observed to be upregulated across various timepoints in the microbead model (Fig. 5.2.11). Of the iBRB dysfunction markers identified in the microbead model, only *Stat3*, which was upregulated at early and middle timepoints in the microbead model, was elevated at the early timepoint post-crush (Fig. 5.2.11).

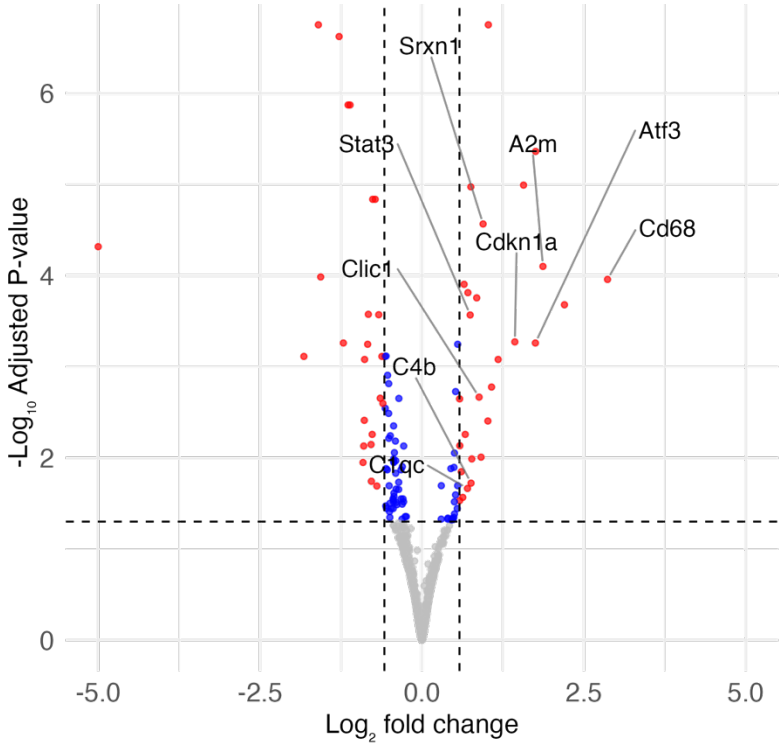



**Figure 5.2.11| Differential gene expression at 3 days post-ONC injury**

*Volcano plot comparing retinal samples 3 days after ONC to naïve controls. Genes meeting significance thresholds (padj < 0.05, horizontal dashed line) and with a $log_2$ fold change > 0.58 or < -0.58 (vertical dashed lines) are highlighted in red. Genes with p < 0.05 but $log_2$ fold change between -0.58 and 0.58 are shown in blue. Genes with a putative role in endothelial activation or retinal inflammation are highlighted. Differential expression was assessed using the Wald test, with multiple comparisons corrected using the Benjamini-Hochberg false discovery rate (FDR).*

At 2 weeks post-crush, when substantial RGC loss is expected to have occurred (Keuthan et al., 2023), a markedly higher number of 361 DEGs was detected relative to naïve retinas. At this timepoint, numerous endothelial-enriched and iBRB-associated genes were differentially expressed, with significant overlap with those identified in the microbead model, including *Cav1*, *Edn2*, and *S100a6* (Fig. 5.2.12; Appendix 1) In addition, *Mmp9*, previously associated with iBRB breakdown and diabetic retinopathy (Giebel et al., 2005), was downregulated, as was *Shh*, a key transcription factor involved in maintaining iBRB integrity (Díaz-Coránguez et al., 2017).

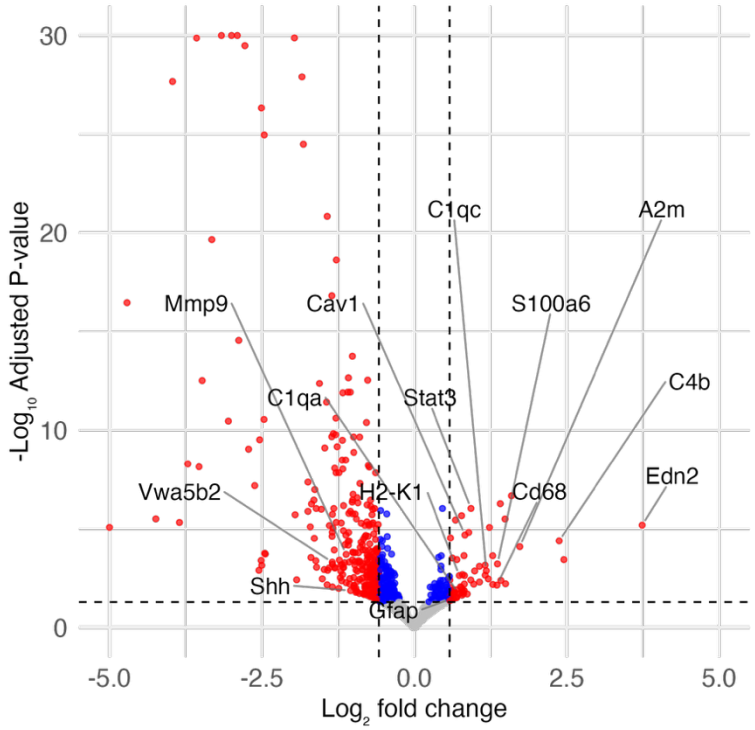
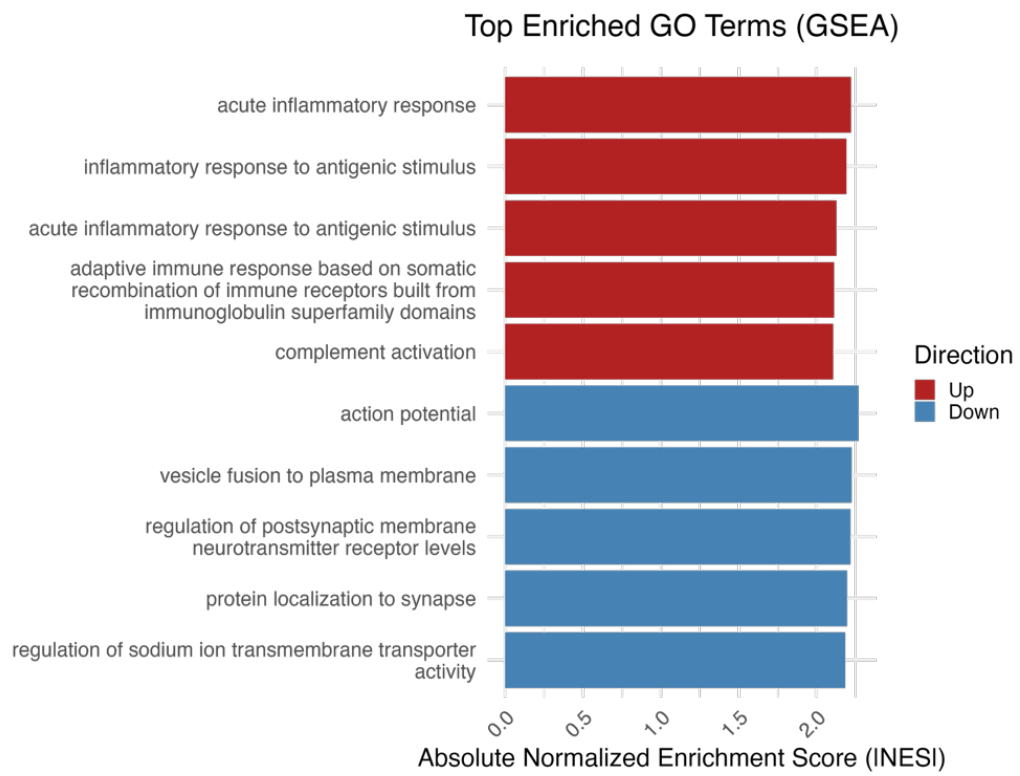



**Figure 5.2.12| Differential gene expression at 2 weeks post-ONC injury**

*Volcano plot comparing retinal samples 2 weeks after ONC to naïve controls. Genes meeting significance thresholds (padj < 0.05, horizontal dashed line) and with a $log_2$ fold change > 0.58 or < - 0.58 (vertical dashed lines) are highlighted in red. Genes with p < 0.05 but $log_2$ fold change between - 0.58 and 0.58 are shown in blue. Genes with a putative role in endothelial activation or retinal inflammation are highlighted. Differential expression was assessed using the Wald test, with multiple comparisons corrected using the Benjamini-Hochberg false discovery rate (FDR).*

GSEA revealed that at both 3 days and 2 weeks post-crush, the top five positively enriched GO terms were associated with immune activation, showing substantial overlap with those enriched at the earliest and latest stages of the microbead-induced OHT model (Fig. 5.2.13). At 3 days post-crush, enriched terms were related to acute inflammation, inflammatory response to antigens, adaptive immunity, and complement activation (Fig. 5.2.13A), whereas at 2 weeks, enriched terms were related to adaptive immunity, B-cell and immunoglobulin-mediated immunity, and inflammatory response to antigens (Fig. 5.2.13B). Among the core enrichment genes, there was substantial overlap with those observed at the earliest and latest stages of the microbead model including MHC class I and II components (*H2-D1, H2-K1, B2m, Tap1, Cd74*), immune cell adhesion and activation markers (*Icam1, Myd88*), myeloid cell-associated transcripts (*Trem2*, Fcgr3, Fcer1g, and Cd68), inflammatory cytokine-related transcripts **(***Il33*, *Il18bp***),** and complement components and regulators (*C1qa*, *C1qb*, *C1qc*, *C1s1*, *C4b*, *Serping1*) (Appendix 2). This overlap in pathways and core enrichment genes indicated that pressure-dependent and pressure independent optic nerve injury engage a shared innate immune response, despite differences in the initiating insult.

A)


Top Enriched GO Terms (GSEA)
acute inflammatory response
inflammatory response to antigenic stimulus
acute inflammatory response to antigenic stimulus
adaptive immune response based on somatic recombination of immune receptors built from immunoglobulin superfamily domains
complement activation
action potential
vesicle fusion to plasma membrane
regulation of postsynaptic membrane neurotransmitter receptor levels
protein localization to synapse
regulation of sodium ion transmembrane transporter activity
Direction
Up
Down
0.0
0.5
1.0
1.5
2.0
Absolute Normalized Enrichment Score (INESI)

B)

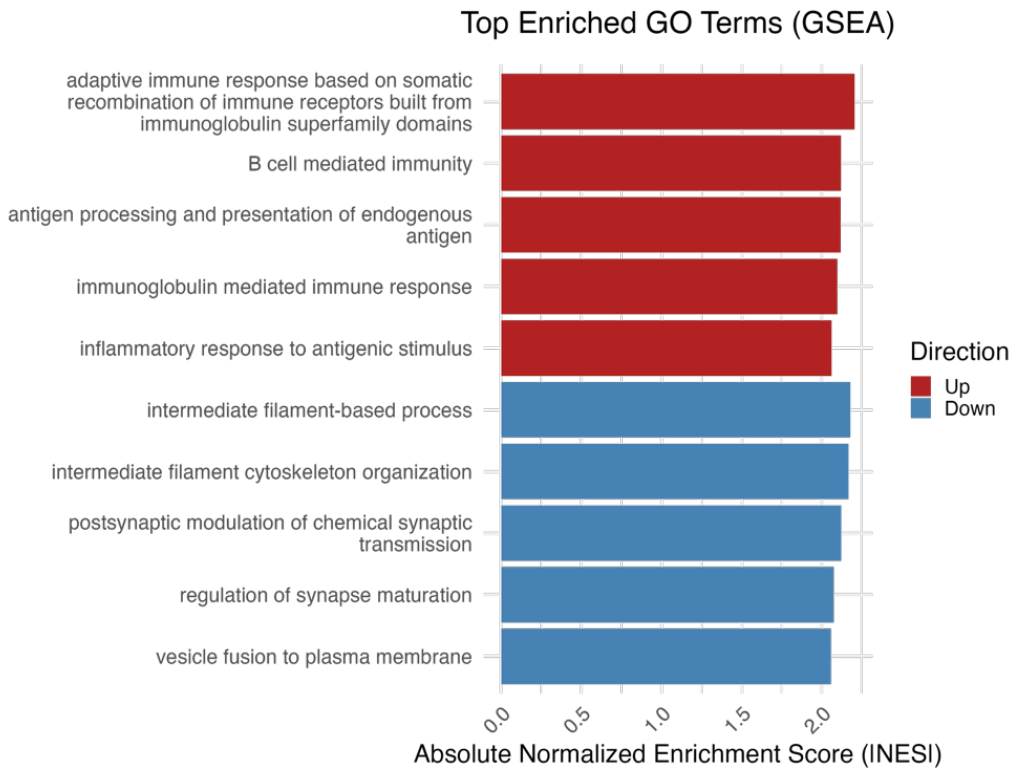

Top Enriched GO Terms (GSEA)
adaptive immune response based on somatic recombination of immune receptors built from immunoglobulin superfamily domains
B cell mediated immunity
antigen processing and presentation of endogenous antigen
immunoglobulin mediated immune response
inflammatory response to antigenic stimulus
intermediate filament-based process
intermediate filament cytoskeleton organization
postsynaptic modulation of chemical synaptic transmission
regulation of synapse maturation
vesicle fusion to plasma membrane
Direction
Up
Down
0.0
0.5
1.0
1.5
2.0
Absolute Normalized Enrichment Score (INESI)

**Figure 5.2.13| GSEA plots for ONC model**

*Gene set enrichment analysis plots for Early vs Naïve **(A)** and Late vs Naïve **(B)** comparisons. Genes were ranked by the product of -log10(p-value) and the sign of their log2 fold change. The top 5 positively enriched (NES > 0) and negatively enriched (NES < 0) GO Biological Process terms are shown. Bar lengths indicate the absolute value of the normalised enrichment score (|NES|). Red bars correspond to positively enriched terms, while blue bars correspond to negatively enriched terms.*

As in the microbead model, gene expression plots were generated for genes associated with iBRB dysfunction (Fig. 5.2.14) and for RGC marker genes (Fig. 5.2.15) to assess how iBRB-related transcriptional changes relate to RGC loss in the ONC model. Analysis of iBRB-related genes revealed a general pattern of minimal change at 3 days post-crush, followed by more pronounced alterations at 2 weeks. *Cav1* (Fig. 5.2.14A), *Edn2* (Fig. 5.2.14B), and *S100a6* (Fig. 5.2.14C) showed little change at 3 days but were significantly upregulated at 2 weeks. In contrast, *Shh* (Fig. 5.2.14D) and *Mmp9* (Fig. 5.2.14E) were downregulated at 2 weeks, after remaining stable at 3 days. *Stat3* (Fig. 5.2.14F) displayed a progressive increase, with mild upregulation at 3 days and a further increase at 2 weeks, mirroring its sustained induction in the microbead model. Overall, these patterns indicate that iBRB dysfunction is predominantly a late-stage feature in the ONC model. In contrast to the microbead model, RGC marker expression in the ONC dataset showed more widespread and consistent downregulation, as expected in a model of direct RGC injury. A subset of markers, including *Rbpms2* (Fig. 5.2.15B), *Tubb3* (Fig. 5.2.15C), and *Thy1* (Fig. 5.2.15E), were already significantly downregulated at 3 days post-crush, indicating early transcriptional changes and possible cell loss. By 2 weeks, all RGC markers examined showed significant downregulation (Fig. 5.2.15), consistent with widespread RGC dysfunction and degeneration. Taken together, these findings suggest that iBRB-related gene expression changes in the ONC model primarily emerge after the onset of RGC degeneration. This supports the idea that RGC death can contribute to iBRB dysfunction independently of IOP.

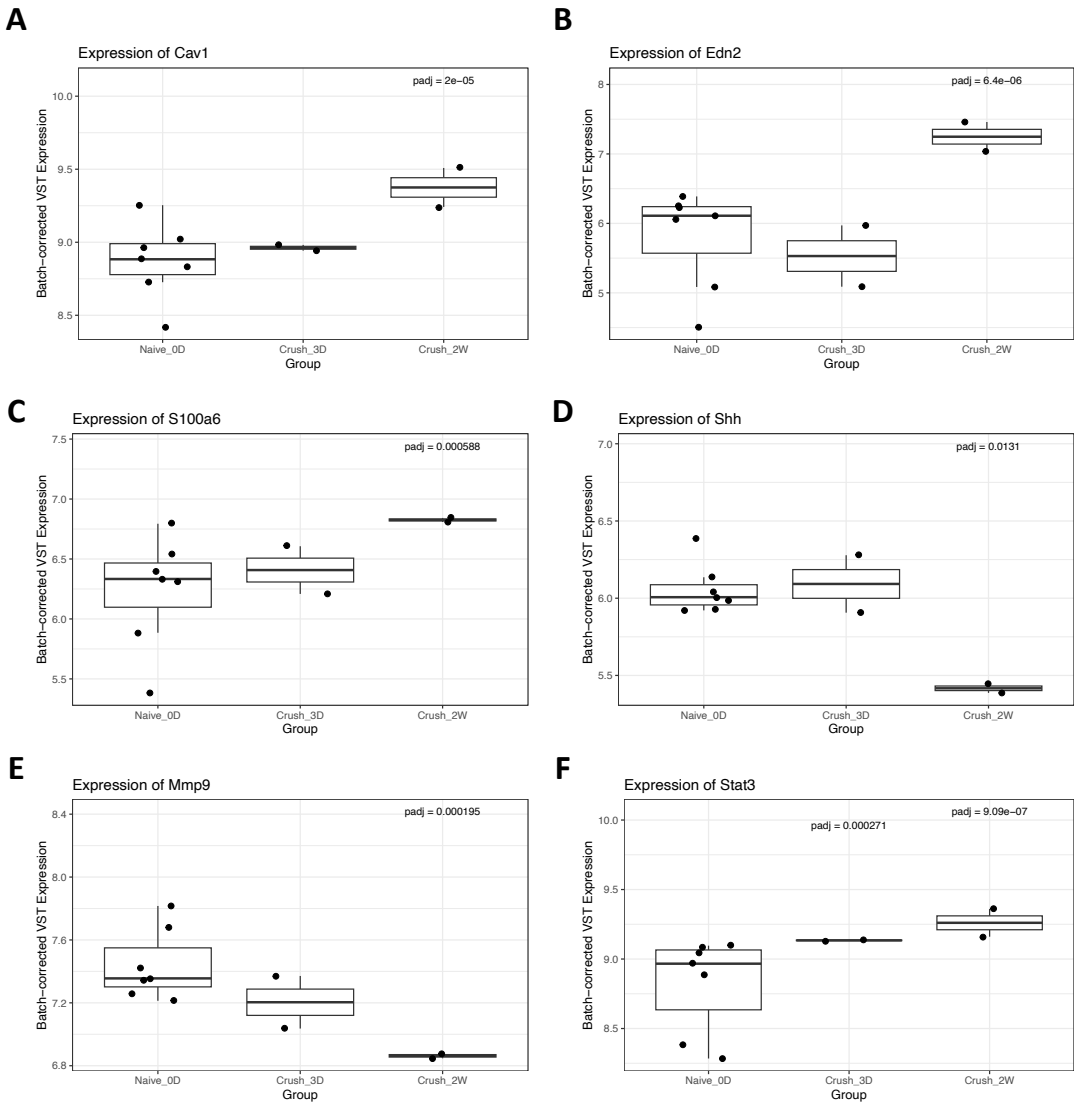



**Figure 5.2.14| Gene plots of markers of iBRB dysfunction in ONC model**

*Boxplots for Cav1* ***(A)****, Edn2* ***(B)****, S100a6* ***(C)****, Shh* ***(D),*** *Mmp9* ***(E),*** *and Stat3* ***(F)*** *show variance-stabilised gene expression values for each sample. Boxes represent IQR, middle line represents the median, whiskers represent the range. Adjusted p values are shown in the case of significant differences vs Naïve group. Significance was determined via Wald tests with multiple comparisons controlled with a Benjamini-Hochberg FDR correction.*

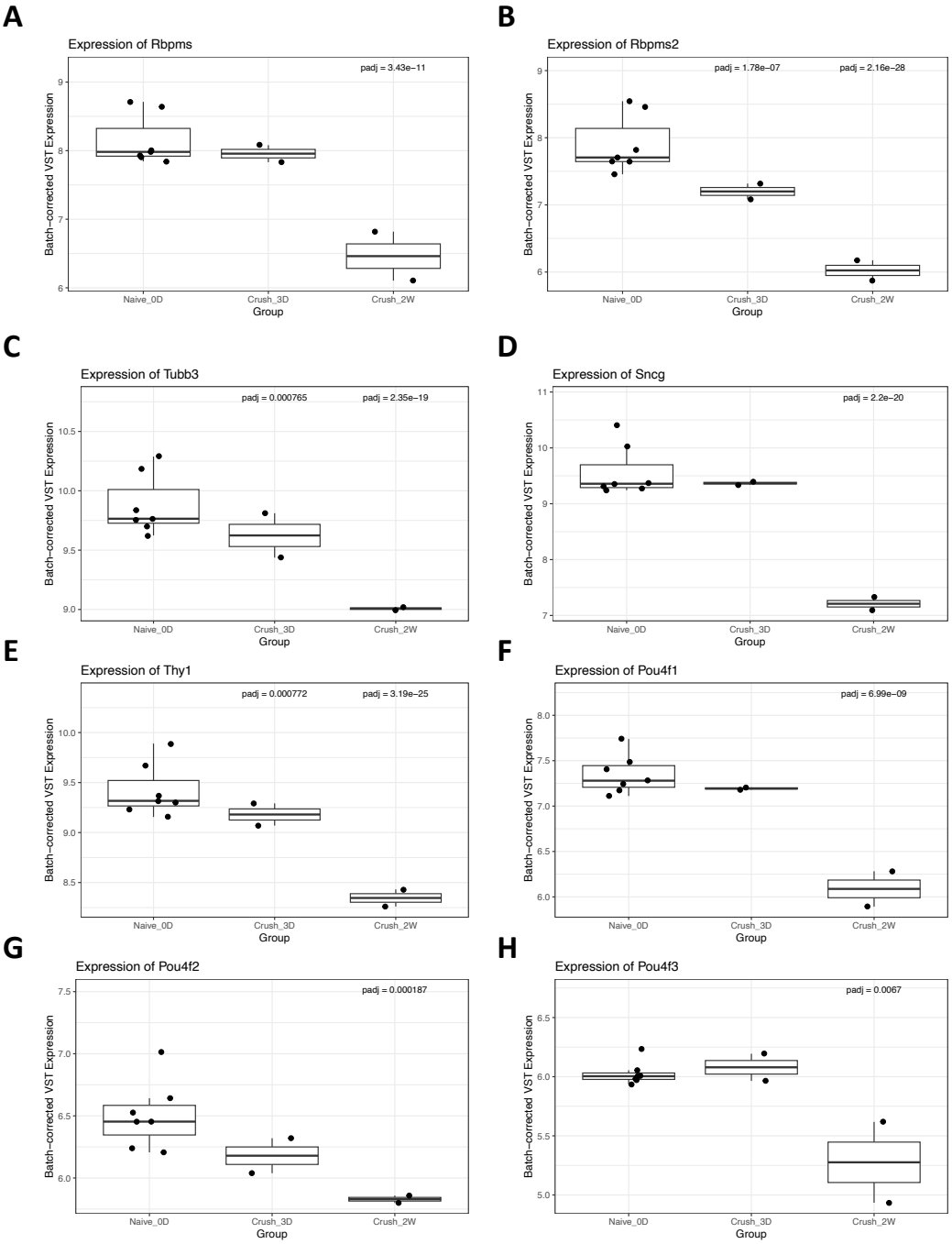



**Figure 5.2.15| Gene plots of RGC markers in ONC model**

*Boxplots for Rpbms* ***(A)****, Rpbms2* ***(B)****, Tubb3* ***(C)****, Sncg* ***(D),*** *Thy1* ***(E),*** *Pou4f1* ***(F)****, Pou4f2* ***(G),*** *and Pou4f3* ***(H)*** *show variance-stabilised gene expression values for each sample. Boxes represent IQR, middle line represents the median, whiskers represent the range. Adjusted p values are shown in the case of significant differences vs Naïve group. Significance was determined via Wald tests with multiple comparisons controlled with a Benjamini-Hochberg FDR correction.*

## 5.3 Discussion

The overarching aim of this chapter was to provide a more detailed mechanistic understanding of vascular dysfunction in glaucoma. While the findings of Chapter 4 demonstrated vascular leakage in two mouse models of OHT and implicated a transcytosis-mediated mechanism, the analysis was restricted to specific timepoints and molecular targets. By utilising the RNA-seq datasets of Keuthan et al. (2023), in which samples were collected at multiple timepoints following OHT or ONC induction, the present study built on these observations by identifying additional molecular pathways involved and characterising the temporal nature of these changes. Furthermore, these datasets expanded the range of models examined in this thesis, thereby strengthening the argument that vascular dysregulation is a common feature of glaucoma.

### 5.3.1 Upregulation of *Cav1* supports transcytosis-mediated iBRB leakage mechanism

A central finding of this chapter is the upregulation of *Cav1* at 3 days post-microbead-induced OHT and at 2 weeks post-ONC, supporting the transcytosis-driven iBRB leakage mechanism proposed in Chapter 4. *Cav1* encodes Cav-1, a structural component of caveolae that is expressed across multiple cell types. Cav-1 plays a critical role in BBB/iBRB permeability, mediating endocytosis and the transcellular transport of macromolecules and cells from the blood into the CNS (Andreone et al., 2017). Suppression of transcytosis is a defining step in iBRB maturation: while vessels entering the retina have fully formed TJs, the barrier only becomes fully established at P10, coinciding with transcytosis suppression, as demonstrated by the fact that early Cav-1 inhibition accelerates iBRB formation in young mice (Chow & Gu, 2017). Additionally, upregulation of *Cav1* has been associated with increased BBB permeability in various contexts (Chang et al., 2022; Pandit et al., 2020; Trevino et al., 2024; Yang et al., 2020). Notably, Cav1 has been reported on previously in the context of glaucoma. GWAS have identified common variants in *CAV1* as risk factors for POAG (Thorleifsson et al., 2010; Wiggs et al., 2011), while Cav-1 ablation in OHT models has shown protective effects against RGC loss (Abbasi et al., 2020), underscoring its potential as a therapeutic target.

A limitation of the bulk RNA-seq approach used here is that cell-type-specific expression changes cannot be determined. As *Cav1* is expressed by multiple cell types in the retina, its upregulation cannot be unequivocally attributed to endothelial cells. Additionally, no

changes in endothelial-specific transcytosis markers *Mfsd2a* or *Plvap* were detected here. This may indicate that Cav-1-mediated transcytosis can be upregulated through mechanisms independent of these regulators in certain injury-specific contexts. Alternatively, Cav-1 may contribute to vascular dysfunction through mechanisms outside of transcytosis, as it has been reported to play a role in facilitating immune cell infiltration into the retina (Li et al., 2014). Nonetheless, when considered alongside previous evidence of reduced Mfd2a protein levels in the inner retina of DBA/2J and dexamethasone models, this finding further supports a common transcytosis-based leakage mechanism in glaucoma.

### 5.3.2 Early endothelial activation in microbead-induced OHT

Another key finding of this chapter is that at the earliest timepoint post-microbead-induced OHT, there is upregulation of multiple markers of endothelial activation, and iBRB disruption, occurring prior to evidence of extensive RGC loss and subsiding at later timepoints. The identity and timing of these upregulated markers provide important insights into the mechanisms underlying vascular dysfunction in the context of OHT.

Among these, several endothelial-enriched genes were upregulated, providing evidence for early endothelial activation. *Cldn5*, which encodes the TJ protein claudin-5 and is expressed exclusively by endothelial cells in the retina, was elevated. While claudin-5 upregulation would typically be interpreted as a sign of enhanced barrier tightness, in the context of *Cav1* upregulation observed here and the leakage reported in Chapter 4, it may instead represent a compensatory tightening of endothelial junctions in response to increased transcytosis-mediated leakage. It should also be noted, as discussed in Chapter 4, that absolute *Cldn5* transcript or protein levels are not a reliable proxy for claudin-5 protein abundance at TJs. Nevertheless, this finding supports the view that iBRB leakage in glaucoma is not driven by reduced claudin-5 expression and argues against a paracellular leakage mechanism.

Evidence of endothelial activation was further supported by the upregulation of *Vcam1*. This gene encodes a cell adhesion molecule from the immunoglobulin superfamily that facilitates leukocyte adhesion and transmigration across the BBB/iBRB. *Vcam1* has been shown to be upregulated in RECs in various inflammatory contexts, including experimental

autoimmune uveitis (Dewispelaere et al., 2015) and oxygen-induced retinopathy (Kaur et al., 2023). In the context of OHT, *Vcam1* upregulation may promote increased recruitment of immune cells into the retina, thereby amplifying local inflammation and potentially contributing to RGC death. Indeed, a recent study demonstrated that CD4+ T-cell infiltration in a microbead model of glaucoma occurs via a Vcam-1-dependent mechanism and contributes directly to RGC loss (He et al., 2024). This highlights that the iBRB functions as a barrier to circulating immune cells as well as molecules, and that disruption of this cellular barrier may represent another important aspect of iBRB dysfunction in glaucoma.

Finally, *Vwf*, a well-established marker of endothelial activation and damage (Mannucci, 1998; Vischer, 2006), was also upregulated. It encodes von Willebrand factor (Vwf), a large circulating glycoprotein produced by endothelial cells that plays essential roles in haemostasis. Elevated plasma VWF levels have been associated with diabetic retinopathy (Kassab et al., 2023). While the role that Vwf would play in contributing to retinal vascular leakage is unclear, its upregulation nonetheless indicates an activated endothelium, strengthening the argument for vascular dysfunction in OHT.

Beyond these endothelial-enriched markers, several genes associated with iBRB dysfunction but not exclusive to endothelial cells were also upregulated. Many of these were elevated beyond the earliest timepoint, suggesting they reflect responses of other NVU components to initial endothelial activation. *S100a6* was upregulated at the earliest timepoint and has been associated with B-lymphocyte transmigration across the BBB in autoimmune encephalitis (Tsai et al., 2019), supporting the idea that immune cell infiltration across the iBRB is increased in OHT. *Edn2*, which encodes endothelin-2, a potent vasoconstrictor that regulates retinal blood flow (Ling et al., 2013) was upregulated at all timepoints following OHT induction, indicating it is a consistent marker of iBRB dysfunction in glaucoma at all disease stages. Systemic administration of Edn2 in mice induces iBRB breakdown with increased vascular leakage, macrophage infiltration, and Müller cell gliosis (Alrashdi et al., 2018), mirroring the immune cell infiltration and retinal inflammation signatures observed here. *Stat3*, a transcription factor regulating cytokine signalling (Bromberg & Darnell, 2000) was upregulated at 3 days and 2 weeks post-OHT. IL-6-mediated *Stat3* activation has been linked to increased retinal vascular permeability in mice (Yun et al., 2017), and in rat OHT models, its upregulation is associated with

microglial activation, while inhibition delays RGC death (Wang et al., 2021; Zaidi et al., 2020). *Serpina3n*, which encodes a serine protease inhibitor, was upregulated only at the 2-week timepoint. It has been reported to increase in the retina under inflammatory conditions (Lipski et al., 2020) and, in the brain, neuronal *Serpina3n* is elevated after ischemic stroke, where it attenuates BBB disruption by inhibiting granzyme B and neutrophil elastase released from T cells and neutrophils (Li et al., 2023). The timing of *Serpina3n* upregulation in the present study suggests it may act in a protective capacity in response to heightened immune cell infiltration, consistent with the observed biphasic inflammatory response (see next discussion section) and the finding that endothelial markers were elevated only at the earliest timepoint in the microbead OHT model. These observations highlight *Serpina3n* as a potential protective factor worthy of further investigation in the context of OHT.

### 5.3.3 Biphasic inflammatory response in the retina following OHT

In addition to endothelial activation and iBRB dysfunction-associated markers, several indicators of overt retinal inflammation were upregulated in response to OHT, including the immune cell activation marker *Cd68*, the gliosis marker *Gfap*, and complement components *C1qa*, *C1qc*, *C3*, and *C4b*. When these transcriptional changes are considered alongside the GSEA results, they provide important insights into how the retina responds to OHT-induced vascular dysfunction. *Cd68* was elevated at the earliest and latest timepoints, while *Gfap* was upregulated only at the earliest timepoint. In contrast, complement components were upregulated at every timepoint examined. The early upregulation of *Gfap* and *Cd68* coincided with peak endothelial marker expression, suggesting that inflammation is most pronounced and unrestrained at this stage. Consistent with this, inspection of the GSEA core enrichment genes at the earliest timepoint indicated activation of antigen-presenting and myeloid-cell associated pathways, supporting the notion that early OHT-induced iBRB disruption is accompanied by innate immune activation, likely involving resident microglia and possibly infiltrating immune cells. At the middle timepoint, only complement components were elevated, indicating a relative reduction in inflammation and endothelial activation, a shift that also coincided with the upregulation of *Serpina3n*. At this stage, the core enrichment genes in the GSEA were related to vascular remodelling and glial activation, suggesting a reparative or adaptive

response following the initial inflammatory insult. At the latest timepoint, GSEA revealed renewed enrichment of immune-related GO terms associated with antigen processing and presentation, indicating a second wave of innate immune signalling. This coincided with the downregulation of the neuronal marker *Tubb3,* suggesting that late-stage inflammation may be driven by the onset of RGC loss. Overall, these findings support a biphasic model of OHT-induced immune signalling in which early vascular dysfunction and innate immune activation gives rise to a compensatory vascular remodelling phase with reduced immune dominance, followed by a later resurgence of innate immune signalling associated with neurodegeneration. This pattern suggests that there is an early therapeutic window in which enhancing iBRB integrity and suppressing innate immune activation may be most effective in protecting RGCs.

### 5.3.4 Late iBRB-associated expression changes in ONC mirror microbead model

The final finding of this chapter was that the ONC model, which is pressure-independent, also exhibits transcriptional signatures of iBRB disruption that substantially overlap with those observed in the early stages of the microbead OHT model. This suggests that RGC death itself can contribute to vascular dysregulation, independent of IOP elevation. Both models showed upregulation of *Cav1*, *Edn2*, *S100a6*, and *Stat3*, indicating shared pathways of endothelial dysfunction. While the ONC model also displayed certain iBRB-related changes not seen in the microbead model, these nonetheless point to similar mechanisms. For example, *Shh* was downregulated which encodes a transcription factor, sonic hedgehog. In response to injury, sonic hedgehog secreted by astrocytes in the brain promotes BBB integrity by reducing endothelial expression of proinflammatory mediators and limiting leukocyte adhesion and migration (Alvarez et al., 2011; Michinaga et al., 2024). This mirrors the *Vcam1* upregulation in the microbead model and highlights immune cell infiltration as a common feature. Similarly, *Mmp9*, which encodes a matrix metalloproteinase that degrades TJs (Spampinato et al., 2017), was downregulated. This mirrors the *Cldn5* upregulation seen in the microbead model and suggests that junctional stabilisation may serve as a compensatory response to increased transcytosis, further reinforcing the idea that iBRB leakage in glaucoma is transcytosis-driven rather than paracellular. The inflammatory signatures between the two models were also closely aligned, with *Cd68*, *Gfap*, and complement components (*C1qa*, *C1qc*, *C4b*) upregulated in both. GSEA further revealed overlapping core enrichment genes relating to MHC class I and II components, immune cell adhesion and activation markers, myeloid cell-associated

transcripts, inflammatory cytokine-related transcripts, and complement components and regulators, underscoring the involvement of innate immune activation in both models. Together, these findings imply that RGC death can itself trigger a cascade of inflammation and iBRB dysfunction. This has important therapeutic implications: once RGC degeneration has begun, it may be significantly more challenging to stabilise vascular integrity and control inflammation, reinforcing the concept of an early intervention window in which targeting iBRB stability and dampening inflammation could help preserve RGCs.

### 5.3.5 Conclusions

Taken together, the findings of this chapter confirm that vascular dysfunction is a common feature of murine glaucoma models, both pressure-dependent and pressure-independent. This is characterised by transcriptional signatures of increased transcytosis, increased junctional integrity, endothelial activation, and immune cell infiltration into the retina, supporting the view that increased iBRB permeability to molecules in glaucoma is primarily mediated by transcytosis, while also highlighting immune cell infiltration as an additional facet of iBRB breakdown. The identification of a biphasic inflammatory pattern in microbead-induced OHT, together with the finding that the pressure-independent ONC model also exhibits vascular dysfunction signatures, suggests that RGC death itself can exacerbate iBRB disruption. This points to a self-reinforcing cycle of neurodegeneration and vascular compromise, emphasising that strategies to stabilise the iBRB and suppress inflammation are likely to be most effective if implemented before RGC loss has occurred.

# Chapter 6 General Discussion

Glaucoma is the leading cause of irreversible blindness worldwide, yet its pathophysiology remains poorly understood. At present, elevated IOP is the only modifiable risk factor for the disease, but the underlying cause of outflow resistance and the relationship between IOP elevation and RGC loss have yet to be fully resolved. This project contributes to addressing these knowledge gaps by investigating immune and neurovascular mechanisms involved in glaucoma across several mouse models. Chapter 3 demonstrated that inflammatory pathways can be manipulated to influence AH outflow, while Chapters 4 and 5 show that retinal vascular dysfunction is associated with OHT. By examining both the anterior segment and the retina, this work addresses the two central hallmarks of glaucoma: elevated IOP and RGC death. This final discussion will outline the key findings of the project, evaluate their implications for the pathophysiology of glaucoma, and consider the potential avenues they open for future research.

### 6.1 Inflammation as an IOP regulating mechanism

Chapter 3 of this project investigated inflammation in the anterior segment and its relationship to AH outflow. As IOP regulation is already a well-established strategy to treat glaucoma, this chapter had a more distinct therapeutic focus, as opposed to later chapters which focussed solely on understanding mechanisms of disease. Thus, the primary objective was to determine if inflammatory pathways can be manipulated to alter AH outflow. Nevertheless, this chapter does also provide mechanistic insight into how dysregulated inflammation can contribute to elevated IOP.

Chapter 3 demonstrated that in the DBA/2J model of pigmentary glaucoma, the anterior segment exhibits an immune profile consistent with loss of ocular immune privilege and sterile inflammation, characterised by increased leukocyte infiltration, elevated expression of canonical inflammasome receptors, and increased levels of IL-18 and IL-1β. In addition, canonical inflammasome activation was shown to reduce AH outflow, as $Asc^{-/-}$ and $IL\text{-}18^{-/-}$ mice displayed increased outflow facility relative to C57BL/6J controls. While it has remained unclear whether IOP elevation in the DBA/2J model results from mechanical obstruction of the outflow pathways by pigment-laden cells (Schraermeyer et al., 2009) or from molecular changes within the outflow tissues, these findings supports the latter mechanism. One possibility is that these pigment-laden cells represent activated macrophages, consistent with the immunohistochemical characterisation of the anterior

uvea in this study. Given the pro-inflammatory properties of melanin (Bora et al., 1997; Vijayasaradhi & Houghton, 1991), such macrophages would likely undergo canonical inflammasome activation and secrete IL-1β and IL-18 into the outflow tissues. Importantly, the anti-outflow effects of IL-18 appear to predominate over the pro-outflow effects of IL-1β. While the precise downstream mechanisms were not determined here, IL-18 signalling may alter the molecular environment of the TM and SC, for example by reducing VEGF-A expression (Reina-Torres et al., 2017; Shen et al., 2014). These findings highlight the DBA/2J model as a potential model of inflammatory glaucoma. It is known that the pigment dispersion phenotype in this model has a systemic origin, as demonstrated by bone marrow transplantation studies: DBA/2J mice receiving bone marrow from mice with wild-type *Gpnmb* fail to develop pigment dispersion or elevated IOP (Anderson et al., 2008; Mo et al., 2003). Thus, these findings establish a link from systemic inflammation, to pigment dispersion, to ocular immune activation, and ultimately to IOP elevation. These results also have implications for understanding pigmentary glaucoma in patients, suggesting that mechanical disruption by pigment granules is not the sole mechanism of IOP elevation, with dysregulated inflammatory responses within the outflow tissues also playing a role.

While the DBA/2J model may represent an, "inflammation-first" form of glaucoma, the outflow data of Chapter 3 has implications for hypertensive glaucoma more generally. In uveitic glaucoma, for example, inflammation in the anterior segment is a well-recognised driver of IOP elevation (Kalogeropoulos & Sung, 2018), and the present results provide a mechanistic rationale for how this occurs. Even in primary glaucoma, where there may be no outright loss of immune privilege, low-level inflammation is likely to be present. ER stress is known to play a role in mouse models of OHT, including the MYOC model and steroid-induced glaucoma (Zode et al., 2011; Zode et al., 2014), and through the unfolded protein response it can trigger sterile inflammation and inflammasome activation (Zhang & Kaufman, 2008). The finding that caspase-11 deficiency exacerbates IOP elevation in dexamethasone-induced OHT highlights this concept, suggesting that a shift towards pyroptosis may be protective in such cases, potentially by elevating MMP expression through P2X7 receptor signalling (Gu & Wiley, 2006; Li et al., 2012). Overall, the findings from Chapter 3 identify sterile inflammation as an underappreciated contributor to OHT in glaucoma and establish it as a potential therapeutic target for lowering IOP.

### 6.2 Inflammation as a therapeutic target for IOP control

As mentioned, the primary objective of Chapter 3 was to determine whether manipulation of inflammatory pathways represents a viable strategy to modulate AH outflow in glaucoma. Key evidence supporting this concept comes from the observation that IL-1β and IL-18 exert opposing effects on outflow facility, with IL-1β enhancing outflow and IL-18 reducing it. Furthermore, the finding that *Asc*$^{-/-}$ mice display increased outflow facility suggests that, under physiological conditions, the anti-outflow effects of IL-18 signalling predominate. Together, these findings identify canonical inflammasome activation and its downstream cytokine signalling as potential therapeutic targets for reducing IOP in glaucoma. However, translating such a proof of concept into a viable therapy is more complex, requiring consideration of available therapeutic agents, their safety profiles, potential off-target effects, and delivery routes.

Based on these findings, three therapeutic strategies emerge for targeting the canonical inflammasome: direct supplementation of IL-1β, suppression of IL-18, or broad inhibition of canonical inflammasome signalling. Although supplementation of IL-1β provides the most direct experimental evidence of efficacy in this study, it is unlikely to represent a viable therapeutic option. IL-1β is a strongly pro-inflammatory cytokine, and early clinical trials administering recombinant IL-1β to bone marrow transplant patients (Elkordy et al., 1997; Nemunaitis et al., 1994) reported moderate toxicities, including fever, chills, and pain around the injection site. While local intraocular administration might reduce systemic risks, increased IL-1β expression in the eye has been associated with inflammation, neovascularisation, and cell death (Da Cunha et al., 2018; Wooff et al., 2019). Thus, the potential off-target consequences of IL-1β supplementation would likely outweigh any IOP-lowering benefit in glaucoma. More generally, when modulating inflammation as a therapeutic strategy, inhibition rather than activation is preferable, as it reduces the risk of uncontrolled inflammatory responses. Thus, selective inhibition of IL-18 or inhibition of canonical inflammasome signalling appear to be more practical options.

Of these, IL-18 suppression offers the most specific approach. Unlike inflammasome-targeted therapies, it would preserve IL-1β signalling, which has been shown here to enhance outflow, potentially amplifying the overall pro-outflow effect. Moreover, IL-18 signalling is naturally regulated by IL-18 binding protein (IL-18BP), which binds IL-18

with high affinity and prevents downstream signalling (Wang, 2024). Recombinant IL-18BP has already been tested clinically, with systemic administration showing a good safety profile in a phase II trial for adult-onset Still's disease (Gabay et al., 2018). Nevertheless, studies investigating IL-18 inhibition in the eye, including IL-18BP delivery, remain scarce, making it difficult to predict its impact on intraocular physiology.

By contrast, broad inhibition of canonical inflammasome signalling has the advantage of being further developed in ophthalmic contexts. A number of NLRP3 inhibitors exist, and some have already been tested in ocular models. For example, dapansutrile (OLT1177) has demonstrated safety in human trials (Klück et al., 2020) and efficacy in suppressing neovascularisation in oxygen-induced retinopathy models (Wu et al., 2022). However, this drug is currently designed for oral administration, which may be unsuitable for IOP lowering. More relevantly, tranilast, an old anti-allergic drug now recognised as an NLRP3 inhibitor (Huang et al., 2018), has an established record of safe ophthalmic use. Notably, in glaucoma patients who received tranilast eye drops following filtering surgery, treated eyes showed greater bleb formation and sustained IOP reduction compared to controls, with no vision-threatening side effects for up to two years post-surgery (Chihara et al., 2002)

Taken together, while IL-18 inhibition represents a conceptually attractive, cytokine-specific strategy for IOP control, NLRP3 inhibition currently offers stronger translational potential. Drugs such as tranilast already have established safety profiles, ocular delivery routes, and even precedent for IOP reduction in patients. Future studies should therefore prioritise NLRP3 inhibition as the most practical route to convert the mechanistic insights from this study into a viable therapeutic strategy.

### 6.3 Retinal vascular dysfunction as a feature of glaucoma

Chapters 4 and 5 of this project focussed on the relationship between elevated IOP, retinal vascular dysfunction, and RGC loss in glaucoma. This is a critical area of investigation, as the mechanisms by which elevated IOP leads to RGC degeneration remain incompletely understood, representing a major barrier to the development of therapies that address the ultimate cause of vision loss. From these chapters, several themes emerged regarding the nature, timing, and mechanisms of retinal vascular dysfunction in glaucoma, each with important implications for understanding how IOP elevation contributes to RGC loss.

The first theme to emerge is that retinal vascular dysfunction is a common feature of glaucoma models. Across the four models examined (DBA/2J, dexamethasone-induced OHT, microbead-induced OHT, and ONC), evidence of vascular dysfunction was consistently observed. In DBA/2J and mice with dexamethasone-induced OHT, analysed in Chapter 4, retinal vascular leakage was detected by FFA, while in the microbead and ONC models, studied by RNA-seq in Chapter 5, transcriptional signatures indicated endothelial activation and BRB disruption. These findings align with previous reports of vascular leakage in DBA/2J, B6.Lmx1b$^{V265D/+}$ , hydrogel-induced OHT, and microbead-induced OHT models (Cueva-Vargas et al., 2024; Zhang et al., 2024), and in studies showing increased FFA leakage in non-human primates with OHT and in human glaucoma patients (Arend et al., 2005; Plange et al., 2010; Plange et al., 2012; Radius & Anderson, 1980). Collectively, this body of evidence supports the view that retinal vascular dysfunction is a common feature of glaucoma across models and species. Regardless of its cause or timing, BRB disruption is likely to compromise retinal health, as the barrier is critical for maintaining the tightly regulated neural microenvironment (O'Leary & Campbell, 2021). However, the retinal vasculature has remained relatively underexplored in glaucoma, with most research focusing on RGC-intrinsic mechanisms. Moreover, the vascular studies that do exist have primarily emphasised blood flow and ischemia rather than barrier integrity (Chan et al., 2017). The present findings indicate that BRB integrity is an important contributor to RGC loss in glaucoma and should be considered in future investigations.

A second theme concerns the timing of vascular dysfunction relative to neurodegeneration. In Chapter 4, retinal vascular leakage was observed in DBA/2J mice from six months of age, coinciding with detectable thinning of the RNFL and IPL on OCT. However, Zhang et al. (2024) reported that leakage precedes RGC loss in this model. In the dexamethasone-induced OHT model studied here, leakage also appeared before detectable inner retinal thinning. Similarly, in Chapter 5, endothelial activation and iBRB dysfunction markers were upregulated prior to substantial downregulation of RGC-specific transcripts in the microbead-induced OHT model. These observations are consistent with findings by Cueva-Vargas et al. (2024) in their microbead model, where vascular leakage was also shown to precede extensive RGC degeneration. Taken together, the evidence indicates that iBRB breakdown typically occurs before widespread RGC loss in murine OHT models,

suggesting that vascular dysfunction may play a direct causal role in neurodegeneration and raising the possibility that therapies targeting vascular leakage could protect RGCs.

A third theme is that similar molecular mechanisms appear to underlie vascular dysfunction across glaucoma models. In Chapter 4, reduced Mfsd2a levels were observed in the inner retina of both DBA/2J and dexamethasone-induced OHT mice, consistent with earlier findings by Zhang et al. (2024), while in Chapter 5, both microbead-induced OHT and ONC models showed upregulation of *Cav1*. Together these findings implicate dysregulated caveolin-mediated transcytosis, rather than paracellular leakage from TJ disruption, as a key driver of BRB breakdown in glaucoma. Since the discovery of Mfsd2a as an endothelial-specific negative regulator of caveolin-mediated transcytosis at the BBB/BRB is relatively recent (Andreone et al., 2017; Ben-Zvi et al., 2014), most prior studies of CNS disorders have focused on TJ-mediated barrier breakdown. The findings from Chapters 3 and 4 thus highlight that BRB leakage driven by increased transcytosis may be more relevant in glaucoma, and may be a potential therapeutic target. In addition, the findings of Chapter 5 suggest that immune-cell infiltration is a common feature of BRB dysfunction in glaucoma, with upregulation of *Vcam1*, *S100a6*, and *Cd68* being observed in the microbead model, and downregulation of *Shh* alongside increased *S100a6* and *Cd68* being detected in the ONC model. Collectively, the results indicate that dysregulated transcytosis and aberrant immune cell infiltration promote retinal inflammation in glaucoma, contributing to neurodegeneration

Finally, the results also indicate that RGC death itself can trigger vascular dysfunction. In the ONC model, most endothelial activation markers were upregulated at later stages, coinciding with widespread downregulation of RGC markers. Similarly, the biphasic inflammatory response observed in the microbead model suggests that a second wave of vascular dysfunction may follow the initiation of RGC loss. The demonstration of vascular dysfunction in a non-pressure-dependent model is particularly important, as it indicates that the relationship between vascular dysfunction and RGC degeneration is bidirectional and self-reinforcing. While vascular dysfunction appears to precede RGC death in OHT models, once degeneration has begun it can trigger further inflammation and barrier breakdown, creating a vicious cycle that is likely difficult to halt. This suggests that therapies targeting vascular leakage would be most effective if delivered before substantial RGC loss has occurred.

Taken together, these four themes allow for a timeline to be proposed for the interaction between IOP elevation, vascular dysfunction, and RGC degeneration in glaucoma. Elevated IOP may induce mechanical stress both at the optic nerve head and on endothelial cells, leading to low-level activation and the release of cytokines and pro-inflammatory mediators. As this response escalates, endothelial activation progresses to overt vascular dysfunction, with BRB breakdown characterised by immune-cell infiltration and increased caveolin-mediated transcytosis, potentially driven by reduced *Mfsd2a* expression or increased *Cav1*. Inflammation within the retina then contributes to early RGC stress and damage. Although vascular remodelling may temporarily dampen the immune response and restore barrier integrity, once RGCs pass a stress threshold they undergo degeneration. The release of DAMPs from dying RGCs triggers a second wave of inflammation and endothelial dysfunction, establishing a self-perpetuating cycle that accelerates neurodegeneration.

### 6.4 Challenges in targeting the retinal vasculature for neuroprotection

While the focus of Chapters 4 and 5 was on understanding mechanisms of disease rather than on therapeutic intervention, the ultimate rationale for such work is to lay the foundation for new treatment strategies. In this context, it is relevant to consider the current prospects for targeting the retinal vasculature as a means of neuroprotection in glaucoma. There is some precedent for this approach: Zhang et al. (2024). and Cueva-Vargas et al. (2024) demonstrated proof of concept that vascular stabilisation can delay RGC death in OHT models. Zhang et al. (2024) achieved this by transgenic expression of a stabilised form of β-catenin in DBA/2J mice, while Cueva Vargas et al. used systemic AAV9 delivery of a dominant-negative DRP1 to stabilise endothelial mitochondria in their microbead model, which was proposed to act by stabilising claudin-5 levels. Although this project did not implicate TJ disruption as a mechanism of BRB breakdown in glaucoma, mitochondrial stabilisation may still mitigate endothelial activation in a transcytosis-driven context.

Nevertheless, significant challenges remain before vascular-targeted strategies for protecting RGCs in glaucoma could realistically be advanced to the clinic. A major issue is delivery. Glaucoma is a chronic disease, meaning any intervention would need sustained expression or release. Gene therapy offers a possible solution, but vector choice and administration route are critical. Systemic AAV9 delivery, as used by Cueva-Vargas et al.

(2024), is unlikely to be acceptable in a clinical setting due to off-target risks. Intravitreal delivery of retinal-targeted vectors is hampered by the existence of a highly developed inner limiting membrane in humans and primates (Starr & Chen, 2023), while subretinal injection, although effective and used as the delivery route for Luxturna (Spark Therapeutics), the first ocular gene therapy approved by the FDA in 2017 for treating Leber's Congenital Amaurosis Type 2 (Fischer, 2017), is highly invasive, and unlikely to be suitable for common diseases such as glaucoma. Finding promotors and vectors that achieve specific transduction of endothelial cells while limiting immunogenicity would also represent a major hurdle.

Another challenge lies in timing. The findings of this study suggest that once RGC loss is initiated, it triggers a cascade of inflammation and vascular dysfunction, implying that vascular-targeted therapies would need to be given before significant neurodegeneration occurs. However, prophylactic treatment in patients who may never progress to sight-threatening disease would be difficult to justify, as the risks may outweigh the benefits. This highlights the need for biomarkers of progression. Since many patients with OHT do not develop glaucoma (Weinreb et al., 2014), detection of BRB dysfunction by FFA could provide a way to stratify patients at higher risk and identify those most likely to benefit from early intervention.

In summary, while stabilising the retinal vasculature represents an attractive therapeutic concept with encouraging early evidence, considerable obstacles remain in terms of delivery, safety, and timing of intervention. A deeper understanding of the relationship between vascular dysfunction and RGC death, coupled with advances in therapeutic delivery, will be required before such strategies can move closer to clinical translation.

### 6.5 Glaucoma as a systemic disease

A common theme of Chapters 3, 4, and 5 is the role of dysregulated inflammation as a mediator of glaucomatous pathology. It is important to place these findings in the context of ageing, the most consistent and predictable risk factor for glaucoma (Weinreb et al., 2014), as is the case for many other CNS disorders (Niccoli & Partridge, 2012) . The concept of "inflammaging" has emerged to describe the state of sterile, non-resolving, low-grade, and chronic inflammation that progressively increases with age (Feldman et al., 2015). This phenomenon is thought to arise from a variety of pathological processes

including proteostasis, mitochondrial dysfunction, altered intercellular communication and senescence (López-Otín et al., 2013). The findings of this project provide a rationale for how age-related inflammation could increase the vulnerability of both the anterior and posterior segments of the eye to glaucomatous change. In the anterior segment, heightened para-inflammation may reduce ocular immune privilege and drive stress responses in the TM, promoting canonical inflammasome activation and thereby elevating IOP. In the retina, the same background of immune activation could render endothelial cells more susceptible to IOP-induced stress, lowering the threshold of IOP required to induce overt vascular dysfunction. Once vascular integrity is compromised, an aged systemic immune system may be primed to over-react to BRB leakage, amplifying retinal inflammation and accelerating RGC loss. Taken together, these findings support the concept that glaucoma is a systemic disease that leads a loss of ocular homeostasis. Age-related inflammation may underly elevated IOP, retinal vascular dysfunction, and RGC degeneration, helping to explain why older individuals are more vulnerable to the disease and why it progresses more rapidly with age.

### 6.6 Limitations and future directions

Although this project sheds light on how inflammatory pathways and vascular dysfunction may contribute to glaucoma pathophysiology, several limitations should be acknowledged. These are outlined by for each chapter below, together with potential future experiments that could address them.

In Chapter 3, DBA/2J mice were shown to exhibit pro-inflammatory expression changes in the anterior segment, consistent with canonical inflammasome activation. However a comparable characterisation was not performed in models without systemic disease. As a result, the interpretation of these findings is limited to the DBA/2J strain, and it remains unclear how prominent canonical inflammasome activation is in POAG more generally. This gap could be addressed by performing a similar characterisation in models with less systemic inflammatory burden, such as MYOC transgenic mice or the dexamethasone-induced OHT model. Additionally, while this chapter established that IL-1β enhances and IL-18 reduces AH outflow, the downstream molecular pathways, and whether the effects are mediated directly by TM or SCECs was not established. These questions could be addressed through in vitro experiments, for example by exposing TM cells or SCECs to

cytokines in culture and measuring changes in transendothelial electrical resistance and protein expression. Single-cell RNA-seq of the anterior chamber in an OHT model, such as MYOC or dexamethasone-induced OHT, would also be valuable in order to understand cell-type-specific responses to inflammatory signalling within the outflow pathways.

In Chapter 4, retinal vascular leakage was detected in DBA/2J mice and in mice with dexamethasone-induced OHT by FFA, while changes in retinal structure were assessed by OCT. These findings could have been strengthened by including functional assessments of RGCs, for example using ERG to directly evaluate how the timing of vascular leakage and OHT relates to vision loss. Likewise, complementing OCT measurements with ex vivo RGC counts would have provided both structural and cellular evidence of neurodegeneration. The reliance on the DBA/2J model in this chapter also introduced limitations. First, corneal calcification and poor pupil dilation prevented in vivo retinal imaging beyond six months of age. Second, the presence of IOP-independent outer retinal abnormalities in DBA/2J mice may have confounded interpretation of vascular leakage observed by FFA. Future studies could overcome these issues by employing alternative genetic models of OHT, such as the MYOC model, which may allow a cleaner assessment of retinal vascular dysfunction. In addition, utilising more frequent time points would enable a clearer definition of the temporal relationship between vascular leakage and RGC loss.

A limitation of Chapter 5 was its reliance on bulk RNA-seq, which restricts the ability to resolve cell-type-specific changes. While the upregulation of genes such as *Vcam1* and *Vwf*, which are highly enriched in endothelial cells, allowed endothelial activation to be inferred, others such as *Cav1* are not strictly endothelial, making it impossible to unequivocally attribute their increased expression to endothelial cells. A further limitation is that the RNA-seq datasets from glaucoma models were obtained from a public database, preventing validation of findings by qPCR or immunostaining, since the microbead and ONC models are not currently established in our laboratory. Studies employing single-cell RNA-seq, ideally in a longitudinal design, would be valuable to provide a more precise map of the cellular responses driving vascular dysfunction in response to OHT and RGC degeneration.

Finally, there are broader limitations that span the project as a whole. All of the work was conducted in mouse models, which, while powerful for mechanistic studies, do not fully recapitulate human glaucoma. Differences in lifespan, immune context, and the lack of a macula are particularly relevant in this regard. Lastly, while this project speculates on potential therapeutic strategies, including IL-18 inhibition, NLRP3 inhibition, and vascular stabilisation, it stops short of testing them experimentally. The limitations outlined here do not diminish the findings of this project. However, they do highlight that many questions remain unresolved with regard to the contribution of inflammation and vascular dysfunction to the pathophysiology of glaucoma and point to potential avenues for future research.

### 6.7 Conclusion

In summary, this project provides evidence that dysregulated inflammation and retinal vascular dysfunction are important contributors to the pathophysiology of glaucoma. The work establishes sterile inflammation as a potential regulator of AH outflow and identifies the canonical inflammasome as a potential therapeutic target for IOP control. It also provides evidence that retinal vascular dysfunction is a common and potentially causal mediator of RGC loss across multiple models of glaucoma. By examining both the anterior segment and the retina, this thesis links elevated IOP and neurodegeneration via immune and vascular dysregulation. Although significant work remains before these findings can be applied in a therapeutic context, they point toward inflammatory and vascular pathways as promising targets in this regard. Ultimately, this work supports the view of glaucoma as a systemic disease that leads to a loss of ocular homeostasis, rather than a disease of elevated IOP or RGC loss in isolation.

# Bibliography

Abbasi, M., Gupta, V. K., Chitranshi, N., Gupta, V. B., Mirzaei, M., Dheer, Y., Garthwaite, L., Zaw, T., Parton, R. G., You, Y., & Graham, S. L. (2020). Caveolin-1 Ablation Imparts Partial Protection Against Inner Retinal Injury in Experimental Glaucoma and Reduces Apoptotic Activation. *Molecular neurobiology*, *57*(9), 3759-3784. https://doi.org/10.1007/s12035-020-01948-9

Abu-Amero, K. K., Kondkar, A. A., Mousa, A., Osman, E. A., & Al-Obeidan, S. A. (2013). Decreased total antioxidants in patients with primary open angle glaucoma. *Current Eye Research*, *38*(9), 959-964.

Abu-Hassan, D. W., Acott, T. S., & Kelley, M. J. (2014). The Trabecular Meshwork: A Basic Review of Form and Function. *J Ocul Biol*, *2*(1). https://doi.org/10.13188/2334-2838.1000017

Agnew, A., Nulty, C., & Creagh, E. M. (2021). Regulation, Activation and Function of Caspase-11 during Health and Disease. *Int J Mol Sci*, *22*(4). https://doi.org/10.3390/ijms22041506

Ahmed, I. I. K., Fea, A., Au, L., Ang, R. E., Harasymowycz, P., Jampel, H. D., Samuelson, T. W., Chang, D. F., Rhee, D. J., & Investigators, C. (2020). A prospective randomized trial comparing Hydrus and iStent microinvasive glaucoma surgery implants for standalone treatment of open-angle glaucoma: the COMPARE study. *Ophthalmology*, *127*(1), 52-61.

Aihara, M., Lindsey, J. D., & Weinreb, R. N. (2003). Aqueous humor dynamics in mice. *Invest Ophthalmol Vis Sci*, *44*(12), 5168-5173. https://doi.org/10.1167/iovs.03-0504

Alaghband, P., Baneke, A. J., Galvis, E., Madekurozwa, M., Chu, B., Stanford, M., Overby, D., & Lim, K. S. (2019). Aqueous Humor Dynamics in Uveitic Eyes. *Am J Ophthalmol*, *208*, 347-355. https://doi.org/10.1016/j.ajo.2019.08.018

Alarcon-Martinez, L., Shiga, Y., Villafranca-Baughman, D., Belforte, N., Quintero, H., Dotigny, F., Cueva Vargas, J. L., & Di Polo, A. (2022). Pericyte dysfunction and loss of interpericyte tunneling nanotubes promote neurovascular deficits in glaucoma. *Proceedings of the National Academy of Sciences*, *119*(7), e2110329119.

Alarcon-Martinez, L., Shiga, Y., Villafranca-Baughman, D., Vargas, J. L. C., Paredes, I. A. V., Quintero, H., Fortune, B., Danesh-Meyer, H., & Di Polo, A. (2023). Neurovascular dysfunction in glaucoma. *Progress in Retinal and Eye Research*, *97*, 101217.

Alarcon-Martinez, L., Villafranca-Baughman, D., Quintero, H., Kacerovsky, J. B., Dotigny, F., Murai, K. K., Prat, A., Drapeau, P., & Di Polo, A. (2020). Interpericyte tunnelling nanotubes regulate neurovascular coupling. *Nature*, *585*(7823), 91-95.

Alipanahi, B., Hormozdiari, F., Behsaz, B., Cosentino, J., McCaw, Z. R., Schorsch, E., Sculley, D., Dorfman, E. H., Foster, P. J., & Peng, L. H. (2021). Large-scale machine-learning-based phenotyping significantly improves genomic discovery for optic nerve head morphology. *The American Journal of Human Genetics*, *108*(7), 1217-1230.

Alrashdi, S. F., Deliyanti, D., Talia, D. M., & Wilkinson-Berka, J. L. (2018). Endothelin-2 Injures the Blood-Retinal Barrier and Macroglial Müller Cells: Interactions with Angiotensin II, Aldosterone, and NADPH Oxidase. *Am J Pathol*, *188*(3), 805-817. https://doi.org/10.1016/j.ajpath.2017.11.009

Alvarado, J., Alvarado, R., Yeh, R., Franse-Carman, L., Marcellino, G., & Brownstein, M. (2005). A new insight into the cellular regulation of aqueous outflow: how trabecular meshwork endothelial cells drive a mechanism that regulates the permeability of Schlemm's canal endothelial cells. *British Journal of Ophthalmology*, *89*(11), 1500-1505.

Alvarez, J. I., Dodelet-Devillers, A., Kebir, H., Ifergan, I., Fabre, P. J., Terouz, S., Sabbagh, M., Wosik, K., Bourbonniere, L., Bernard, M., van Horssen, J., de Vries, H. E., Charron, F., & Prat, A. (2011). The Hedgehog pathway promotes blood-brain barrier integrity and CNS immune quiescence. *Science*, *334*(6063), 1727-1731. https://doi.org/10.1126/science.1206936

Alves, C. H., Fernandes, R., Santiago, A. R., & Ambrosio, A. F. (2020). Microglia contribution to the regulation of the retinal and choroidal vasculature in age-related macular degeneration. *Cells*, *9*(5), 1217.

Amer, A., Franchi, L., Kanneganti, T.-D., Body-Malapel, M., Ozoren, N., Brady, G., Meshinchi, S., Jagirdar, R., Gewirtz, A., & Akira, S. (2006). Regulation of Legionella phagosome maturation and infection through flagellin and host Ipaf. *Journal of Biological Chemistry*, *281*(46), 35217-35223.

Anderson, D. R. (2003). Collaborative normal tension glaucoma study. *Curr Opin Ophthalmol*, *14*(2), 86-90. https://doi.org/10.1097/00055735-200304000-00006

Anderson, M. G., Nair, K. S., Amonoo, L. A., Mehalow, A., Trantow, C. M., Masli, S., & John, S. W. (2008). GpnmbR 150Xallele must be present in bone marrow derived cells to mediate DBA/2J glaucoma. *BMC Genetics*, *9*(1), 1-14.

Anderson, M. G., Smith, R. S., Hawes, N. L., Zabaleta, A., Chang, B., Wiggs, J. L., & John, S. W. (2002). Mutations in genes encoding melanosomal proteins cause pigmentary glaucoma in DBA/2J mice. *Nat Genet*, *30*(1), 81-85. https://doi.org/10.1038/ng794

Andreone, B. J., Chow, B. W., Tata, A., Lacoste, B., Ben-Zvi, A., Bullock, K., Deik, A. A., Ginty, D. D., Clish, C. B., & Gu, C. (2017). Blood-Brain Barrier Permeability Is Regulated by Lipid Transport-Dependent Suppression of Caveolae-Mediated Transcytosis. *Neuron*, *94*(3), 581-594.e585. https://doi.org/10.1016/j.neuron.2017.03.043

Arend, O., Remky, A., Plange, N., Kaup, M., & Schwartz, B. (2005). Fluorescein leakage of the optic disc in glaucomatous optic neuropathy. *Graefe's Archive for Clinical and Experimental Ophthalmology*, *243*, 659-664.

Armaly, M. F. (1963a). EFFECT OF CORTICOSTEROIDS ON INTRAOCULAR PRESSURE AND FLUID DYNAMICS. I. THE EFFECT OF DEXAMETHASONE IN THE NORMAL EYE. *Arch Ophthalmol*, *70*, 482-491. https://doi.org/10.1001/archopht.1963.00960050484010

Armaly, M. F. (1963b). EFFECT OF CORTICOSTEROIDS ON INTRAOCULAR PRESSURE AND FLUID DYNAMICS. II. THE EFFECT OF DEXAMETHASONE IN THE GLAUCOMATOUS EYE. *Arch Ophthalmol*, *70*, 492-499. https://doi.org/10.1001/archopht.1963.00960050494011

Armulik, A., Genove, G., Mae, M., Nisancioglu, M. H., Wallgard, E., Niaudet, C., He, L., Norlin, J., Lindblom, P., Strittmatter, K., Johansson, B. R., & Betsholtz, C. (2010). Pericytes regulate the blood-brain barrier. *Nature*, *468*(7323), 557-561. https://doi.org/10.1038/nature09522

Asano, Y., Himori, N., Kunikata, H., Yamazaki, M., Shiga, Y., Omodaka, K., Takahashi, H., & Nakazawa, T. (2017). Age-and sex-dependency of the association between systemic antioxidant potential and glaucomatous damage. *Scientific Reports*, *7*(1), 8032.

Aslam, S., & Gupta, V. (2025). Carbonic Anhydrase Inhibitors. In *StatPearls*. StatPearls Publishing

Copyright © 2025, StatPearls Publishing LLC.

Aung, T., Ozaki, M., Mizoguchi, T., Allingham, R. R., Li, Z., Haripriya, A., Nakano, S., Uebe, S., Harder, J. M., Chan, A. S., Lee, M. C., Burdon, K. P., Astakhov, Y. S., Abu-Amero, K. K., Zenteno, J. C., Nilgün, Y., Zarnowski, T., Pakravan, M., Safieh, L. A., . . . Khor, C. C. (2015). A common variant mapping to CACNA1A is associated with susceptibility to exfoliation syndrome. *Nat Genet*, *47*(4), 387-392. https://doi.org/10.1038/ng.3226

Aurrand-Lions, M., Lamagna, C., Dangerfield, J. P., Wang, S., Herrera, P., Nourshargh, S., & Imhof, B. A. (2005). Junctional adhesion molecule-C regulates the early influx of leukocytes into tissues during inflammation. *J Immunol*, *174*(10), 6406-6415. https://doi.org/10.4049/jimmunol.174.10.6406

Bahler, C. K., Howell, K. G., Hann, C. R., Fautsch, M. P., & Johnson, D. H. (2008). Prostaglandins increase trabecular meshwork outflow facility in cultured human anterior segments. *Am J Ophthalmol*, *145*(1), 114-119. https://doi.org/10.1016/j.ajo.2007.09.001

Bailey, J. N., Loomis, S. J., Kang, J. H., Allingham, R. R., Gharahkhani, P., Khor, C. C., Burdon, K. P., Aschard, H., Chasman, D. I., Igo, R. P., Jr., Hysi, P. G., Glastonbury, C. A., Ashley-Koch, A., Brilliant, M., Brown, A. A., Budenz, D. L., Buil, A., Cheng, C. Y., Choi, H., . . . Wiggs, J. L. (2016). Genome-wide association analysis identifies TXNRD2, ATXN2 and FOXC1 as susceptibility loci for primary open-angle glaucoma. *Nat Genet*, *48*(2), 189-194. https://doi.org/10.1038/ng.3482

Ball, D. P., Tsamouri, L. P., Wang, A. E., Huang, H. C., Warren, C. D., Wang, Q., Edmondson, I. H., Griswold, A. R., Rao, S. D., Johnson, D. C., & Bachovchin, D. A. (2022). Oxidized thioredoxin-1 restrains the NLRP1 inflammasome. *Sci Immunol*, *7*(77), eabm7200. https://doi.org/10.1126/sciimmunol.abm7200

Ban, Y., & Rizzolo, L. J. (2000). Regulation of glucose transporters during development of the retinal pigment epithelium. *Brain Res Dev Brain Res*, *121*(1), 89-95. https://doi.org/10.1016/s0165-3806(00)00028-6

Barnstable, C. J., & Dräger, U. C. (1984). Thy-1 antigen: A ganglion cell specific marker in rodent retina. *Neuroscience*, *11*(4), 847-855. https://doi.org/https://doi.org/10.1016/0306-4522(84)90195-7

Bastiani, M., & Parton, R. G. (2010). Caveolae at a glance. *Journal of cell science*, *123*(22), 3831-3836.

Baudouin, C., Kolko, M., Melik-Parsadaniantz, S., & Messmer, E. M. (2021). Inflammation in Glaucoma: From the back to the front of the eye, and beyond. *Progress in Retinal and Eye Research*, *83*, 100916. https://doi.org/https://doi.org/10.1016/j.preteyeres.2020.100916

Bauernfeind, F. G., Horvath, G., Stutz, A., Alnemri, E. S., MacDonald, K., Speert, D., Fernandes-Alnemri, T., Wu, J., Monks, B. G., Fitzgerald, K. A., Hornung, V., & Latz, E. (2009). Cutting edge: NF-kappaB activating pattern recognition and cytokine receptors license NLRP3 inflammasome activation by regulating NLRP3 expression. *J Immunol*, *183*(2), 787-791. https://doi.org/10.4049/jimmunol.0901363

Becker, B. (1965). Intraocular pressure response to topical corticosteroids. *Investigative Ophthalmology & Visual Science*, *4*(2), 198-205.

Bell, R. D., Winkler, E. A., Sagare, A. P., Singh, I., LaRue, B., Deane, R., & Zlokovic, B. V. (2010). Pericytes control key neurovascular functions and neuronal phenotype in the adult brain and during brain aging. *Neuron*, *68*(3), 409-427. https://doi.org/10.1016/j.neuron.2010.09.043

Ben-Zvi, A., Lacoste, B., Kur, E., Andreone, B. J., Mayshar, Y., Yan, H., & Gu, C. (2014). Mfsd2a is critical for the formation and function of the blood–brain barrier. *Nature*, *509*(7501), 507-511.

Bill, A., & Phillips, C. I. (1971). Uveoscleral drainage of aqueous humour in human eyes. *Exp Eye Res*, *12*(3), 275-281. https://doi.org/10.1016/0014-4835(71)90149-7

Birke, M. T., Birke, K., Lütjen-Drecoll, E., Schlötzer-Schrehardt, U., & Hammer, C. M. (2011). Cytokine-Dependent ELAM-1 Induction and Concomitant Intraocular Pressure Regulation in Porcine Anterior Eye Perfusion Culture. *Investigative Ophthalmology & Visual Science*, *52*(1), 468-475. https://doi.org/10.1167/iovs.10-5990

Biswas, S., & Wan, K. H. (2019). Review of rodent hypertensive glaucoma models. *Acta Ophthalmologica*, *97*(3), e331-e340. https://doi.org/https://doi.org/10.1111/aos.13983

Bollinger, K., Kim, J., Lowder, C. Y., Kaiser, P. K., & Smith, S. D. (2011). Intraocular pressure outcome of patients with fluocinolone acetonide intravitreal implant for noninfectious uveitis. *Ophthalmology*, *118*(10), 1927-1931. https://doi.org/10.1016/j.ophtha.2011.02.042

Bonnemaijer, P. W., Leeuwen, E. M. v., Iglesias, A. I., Gharahkhani, P., Vitart, V., Khawaja, A. P., Simcoe, M., Höhn, R., Cree, A. J., & Igo, R. P. (2019). Multi-trait genome-wide association study identifies new loci associated with optic disc parameters. *Communications Biology*, *2*(1), 435.

Bora, N. S., Woon, M. D., Tandhasetti, M. T., Cirrito, T. P., & Kaplan, H. J. (1997). Induction of experimental autoimmune anterior uveitis by a self-antigen: melanin complex without adjuvant. *Invest Ophthalmol Vis Sci*, *38*(10), 2171-2175.

Bosco, A., Inman, D. M., Steele, M. R., Wu, G., Soto, I., Marsh-Armstrong, N., Hubbard, W. C., Calkins, D. J., Horner, P. J., & Vetter, M. L. (2008). Reduced retina microglial activation and improved optic nerve integrity with minocycline treatment in the DBA/2J mouse model of glaucoma. *Investigative Ophthalmology & Visual Science*, *49*(4), 1437-1446.

Bosco, A., Romero, C. O., Breen, K. T., Chagovetz, A. A., Steele, M. R., Ambati, B. K., & Vetter, M. L. (2015). Neurodegeneration severity can be predicted from early microglia alterations monitored in vivo in a mouse model of chronic glaucoma. *Disease models & mechanisms*, *8*(5), 443-455.

Bosco, A., Steele, M. R., & Vetter, M. L. (2011). Early microglia activation in a mouse model of chronic glaucoma. *Journal of Comparative Neurology*, *519*(4), 599-620.

Bringmann, A., Pannicke, T., Grosche, J., Francke, M., Wiedemann, P., Skatchkov, S. N., Osborne, N. N., & Reichenbach, A. (2006). Müller cells in the healthy and diseased retina. *Progress in Retinal and Eye Research*, *25*(4), 397-424.

Brockhaus, K., Melkonyan, H., Prokosch-Willing, V., Liu, H., & Thanos, S. (2020). Alterations in Tight- and Adherens-Junction Proteins Related to Glaucoma Mimicked in the Organotypically Cultivated Mouse Retina Under Elevated Pressure. *Investigative Ophthalmology & Visual Science*, *61*(3), 46-46. https://doi.org/10.1167/iovs.61.3.46

Bromberg, J., & Darnell, J. E. (2000). The role of STATs in transcriptional control and their impact on cellular function. *Oncogene*, *19*(21), 2468-2473.

Brooks, A. M., & Gillies, W. E. (1992). Ocular beta-blockers in glaucoma management. Clinical pharmacological aspects. *Drugs Aging*, *2*(3), 208-221. https://doi.org/10.2165/00002512-199202030-00005

Broz, P., & Dixit, V. M. (2016). Inflammasomes: mechanism of assembly, regulation and signalling. *Nature Reviews Immunology*, *16*(7), 407-420. https://doi.org/10.1038/nri.2016.58

Burdon, K. P., Macgregor, S., Hewitt, A. W., Sharma, S., Chidlow, G., Mills, R. A., Danoy, P., Casson, R., Viswanathan, A. C., Liu, J. Z., Landers, J., Henders, A. K., Wood, J., Souzeau, E., Crawford, A., Leo, P., Wang, J. J., Rochtchina, E., Nyholt, D. R., . . . Craig, J. E. (2011). Genome-wide association study identifies susceptibility loci for open angle glaucoma at TMCO1 and CDKN2B-AS1. *Nat Genet*, *43*(6), 574-578. https://doi.org/10.1038/ng.824

Burgos-Blasco, B., Vidal-Villegas, B., Saenz-Frances, F., Morales-Fernandez, L., Perucho-Gonzalez, L., Garcia-Feijoo, J., & Martinez-de-la-Casa, J. M. (2020). Tear and aqueous humour cytokine profile in primary open-angle glaucoma. *Acta Ophthalmol*, *98*(6), e768-e772. https://doi.org/10.1111/aos.14374

Butt, A. M., Jones, H. C., & Abbott, N. J. (1990). Electrical resistance across the blood-brain barrier in anaesthetized rats: a developmental study. *The Journal of physiology*, *429*(1), 47-62.

Cavet, M. E., Vittitow, J. L., Impagnatiello, F., Ongini, E., & Bastia, E. (2014). Nitric oxide (NO): an emerging target for the treatment of glaucoma. *Investigative Ophthalmology & Visual Science*, *55*(8), 5005-5015.

Cereijido, M., Valdés, J., Shoshani, L., & Contreras, R. G. (1998). Role of tight junctions in establishing and maintaining cell polarity. *Annu Rev Physiol*, *60*, 161-177. https://doi.org/10.1146/annurev.physiol.60.1.161

Cesareo, M., Martucci, A., Ciuffoletti, E., Mancino, R., Cerulli, A., Sorge, R. P., Martorana, A., Sancesario, G., & Nucci, C. (2015). Association between Alzheimer's disease and glaucoma: a study based on Heidelberg retinal tomography and frequency doubling technology perimetry. *Frontiers in neuroscience*, *9*, 479.

Chan, K. K., Tang, F., Tham, C. C., Young, A. L., & Cheung, C. Y. (2017). Retinal vasculature in glaucoma: a review. *BMJ Open Ophthalmology*, *1*(1).

Chang, J.-H., Greene, C., Frudd, K., Araujo dos Santos, L., Futter, C., Nichols, B. J., Campbell, M., & Turowski, P. (2022). Methamphetamine enhances caveolar transport of therapeutic agents across the rodent blood-brain barrier. *Cell Reports Medicine*, *3*(1). https://doi.org/10.1016/j.xcrm.2021.100497

Chen, G. Y., & Nuñez, G. (2010). Sterile inflammation: sensing and reacting to damage. *Nature Reviews Immunology*, *10*(12), 826-837. https://doi.org/10.1038/nri2873

Chen, H., & Weber, A. J. (2001). BDNF enhances retinal ganglion cell survival in cats with optic nerve damage. *Invest Ophthalmol Vis Sci*, *42*(5), 966-974.

Chen, Y., Lin, Y., Vithana, E. N., Jia, L., Zuo, X., Wong, T. Y., Chen, L. J., Zhu, X., Tam, P. O., Gong, B., Qian, S., Li, Z., Liu, X., Mani, B., Luo, Q., Guzman, C., Leung, C. K., Li, X., Cao, W., . . . Yang, Z. (2014). Common variants near ABCA1 and in PMM2 are associated with primary open-angle glaucoma. *Nat Genet*, *46*(10), 1115-1119. https://doi.org/10.1038/ng.3078

Cheng, C. Y., Kuo, C. T., Lin, C. C., Hsieh, H. L., & Yang, C. M. (2010). IL-1beta induces expression of matrix metalloproteinase-9 and cell migration via a c-Src-dependent, growth factor receptor transactivation in A549 cells. *Br J Pharmacol*, *160*(7), 1595-1610. https://doi.org/10.1111/j.1476-5381.2010.00858.x

Cheng, Y., Lin, D., Wu, S., Liu, Q., Yan, X., Ren, T., Zhang, J., & Wang, N. (2023). Cerebrospinal Fluid Pressure Reduction Induces Glia-Mediated Retinal Inflammation and Leads to Retinal Ganglion Cell Injury in Rats. *Molecular neurobiology*, *60*(10), 5770-5788.

Chihara, E., Dong, J., Ochiai, H., & Hamada, S. (2002). Effects of tranilast on filtering blebs: a pilot study. *Journal of Glaucoma*, *11*(2), 127-133.

Choi, J., Kim, K. H., Jeong, J., Cho, H.-s., Lee, C. H., & Kook, M. S. (2007). Circadian fluctuation of mean ocular perfusion pressure is a consistent risk factor for normal-tension glaucoma. *Investigative Ophthalmology & Visual Science*, *48*(1), 104-111.

Choquet, H., Paylakhi, S., Kneeland, S. C., Thai, K. K., Hoffmann, T. J., Yin, J., Kvale, M. N., Banda, Y., Tolman, N. G., & Williams, P. A. (2018). A multiethnic genome-wide association study of primary open-angle glaucoma identifies novel risk loci. *Nature Communications*, *9*(1), 2278.

Chow, B. W., & Gu, C. (2017). Gradual Suppression of Transcytosis Governs Functional Blood-Retinal Barrier Formation. *Neuron*, *93*(6), 1325-1333.e1323. https://doi.org/10.1016/j.neuron.2017.02.043

Chua, J., Vania, M., Cheung, C. M., Ang, M., Chee, S. P., Yang, H., Li, J., & Wong, T. T. (2012). Expression profile of inflammatory cytokines in aqueous from glaucomatous eyes. *Mol Vis*, *18*, 431-438.

Cirulli, E. T., Lasseigne, B. N., Petrovski, S., Sapp, P. C., Dion, P. A., Leblond, C. S., Couthouis, J., Lu, Y. F., Wang, Q., Krueger, B. J., Ren, Z., Keebler, J., Han, Y., Levy, S. E., Boone, B. E., Wimbish, J. R., Waite, L. L., Jones, A. L., Carulli, J. P., . . . Goldstein, D. B. (2015). Exome sequencing in amyotrophic lateral sclerosis

identifies risk genes and pathways. *Science*, *347*(6229), 1436-1441. https://doi.org/10.1126/science.aaa3650

Claes, M., Santos, J. R. F., Masin, L., Cools, L., Davis, B. M., Arckens, L., Farrow, K., De Groef, L., & Moons, L. (2021). A Fair Assessment of Evaluation Tools for the Murine Microbead Occlusion Model of Glaucoma. *Int J Mol Sci*, *22*(11). https://doi.org/10.3390/ijms22115633

Clark, A. F., Steely, H. T., Dickerson, J. E., Jr., English-Wright, S., Stropki, K., McCartney, M. D., Jacobson, N., Shepard, A. R., Clark, J. I., Matsushima, H., Peskind, E. R., Leverenz, J. B., Wilkinson, C. W., Swiderski, R. E., Fingert, J. H., Sheffield, V. C., & Stone, E. M. (2001). Glucocorticoid induction of the glaucoma gene MYOC in human and monkey trabecular meshwork cells and tissues. *Invest Ophthalmol Vis Sci*, *42*(8), 1769-1780.

Coca-Prados, M. (2014). The Blood-Aqueous Barrier in Health and Disease. *Journal of Glaucoma*, *23*, S36-S38. https://doi.org/10.1097/ijg.0000000000000107

Cone, F. E., Gelman, S. E., Son, J. L., Pease, M. E., & Quigley, H. A. (2010). Differential susceptibility to experimental glaucoma among 3 mouse strains using bead and viscoelastic injection. *Experimental Eye Research*, *91*(3), 415-424.

Cone, F. E., Steinhart, M. R., Oglesby, E. N., Kalesnykas, G., Pease, M. E., & Quigley, H. A. (2012). The effects of anesthesia, mouse strain and age on intraocular pressure and an improved murine model of experimental glaucoma. *Exp Eye Res*, *99*(1), 27-35. https://doi.org/10.1016/j.exer.2012.04.006

Cooper, M. L., Crish, S. D., Inman, D. M., Horner, P. J., & Calkins, D. J. (2016). Early astrocyte redistribution in the optic nerve precedes axonopathy in the DBA/2J mouse model of glaucoma. *Experimental Eye Research*, *150*, 22-33.

Craig, J. E., Han, X., Qassim, A., Hassall, M., Cooke Bailey, J. N., Kinzy, T. G., Khawaja, A. P., An, J., Marshall, H., & Gharahkhani, P. (2020). Multitrait analysis of glaucoma identifies new risk loci and enables polygenic prediction of disease susceptibility and progression. *Nature genetics*, *52*(2), 160-166.

Crosson, C. E., Sloan, C. F., & Yates, P. W. (2005). Modulation of conventional outflow facility by the adenosine A1 agonist N6-cyclohexyladenosine. *Invest Ophthalmol Vis Sci*, *46*(10), 3795-3799. https://doi.org/10.1167/iovs.05-0421

Cueva-Vargas, J. L., Belforte, N., Vidal-Paredes, I. A., Dotigny, F., Vande Velde, C., Quintero, H., & Di Polo, A. (2024). Stress-induced mitochondrial fragmentation in

endothelial cells disrupts blood-retinal barrier integrity causing neurodegeneration. *bioRxiv*, 2024.2012. 2021.629919.

D'orazio, T., & Niederkorn, J. (1998). Splenic B cells are required for tolerogenic antigen presentation in the induction of anterior chamber-associated immune deviation (ACAID). *Immunology*, *95*(1), 47.

Da Cunha, A. P., Zhang, Q., Prentiss, M., Wu, X. Q., Kainz, V., Xu, Y. Y., Vrouvlianis, J., Li, H., Rangaswamy, N., Leehy, B., McGee, T. L., Bell, C. L., Bigelow, C. E., Kansara, V., Medley, Q., Huang, Q., & Wu, H. Y. (2018). The Hierarchy of Proinflammatory Cytokines in Ocular Inflammation. *Current Eye Research*, *43*(4), 553-565. https://doi.org/10.1080/02713683.2017.1410180

Daneman, R., & Prat, A. (2015). The blood-brain barrier. *Cold Spring Harb Perspect Biol*, *7*(1), a020412. https://doi.org/10.1101/cshperspect.a020412

Daneman, R., Zhou, L., Agalliu, D., Cahoy, J. D., Kaushal, A., & Barres, B. A. (2010). The mouse blood-brain barrier transcriptome: a new resource for understanding the development and function of brain endothelial cells. *PLoS One*, *5*(10), e13741. https://doi.org/10.1371/journal.pone.0013741

Daneman, R., Zhou, L., Kebede, A. A., & Barres, B. A. (2010). Pericytes are required for blood-brain barrier integrity during embryogenesis. *Nature*, *468*(7323), 562-566. https://doi.org/10.1038/nature09513

de Rivero Vaccari, J. P., Dietrich, W. D., & Keane, R. W. (2016). Therapeutics targeting the inflammasome after central nervous system injury. *Translational Research*, *167*(1), 35-45.

Dewispelaere, R., Lipski, D., Foucart, V., Bruyns, C., Frère, A., Caspers, L., & Willermain, F. (2015). ICAM-1 and VCAM-1 are differentially expressed on blood-retinal barrier cells during experimental autoimmune uveitis. *Experimental Eye Research*, *137*, 94-102.

Díaz-Coránguez, M., Ramos, C., & Antonetti, D. A. (2017). The inner blood-retinal barrier: Cellular basis and development. *Vision research*, *139*, 123-137. https://doi.org/10.1016/j.visres.2017.05.009

Dimmeler, S., Assmus, B., Hermann, C., Haendeler, J., & Zeiher, A. M. (1998). Fluid shear stress stimulates phosphorylation of Akt in human endothelial cells: involvement in suppression of apoptosis. *Circ Res*, *83*(3), 334-341. https://doi.org/10.1161/01.res.83.3.334

Dohgu, S., Takata, F., Matsumoto, J., Kimura, I., Yamauchi, A., & Kataoka, Y. (2019). Monomeric α-synuclein induces blood-brain barrier dysfunction through activated brain pericytes releasing inflammatory mediators in vitro. *Microvasc Res*, *124*, 61-66. https://doi.org/10.1016/j.mvr.2019.03.005

Downs, J. C., & Girkin, C. A. (2017). Lamina cribrosa in glaucoma. *Curr Opin Ophthalmol*, *28*(2), 113-119. https://doi.org/10.1097/icu.0000000000000354

Downs, K. P., Nguyen, H., Dorfleutner, A., & Stehlik, C. (2020). An overview of the non-canonical inflammasome. *Mol Aspects Med*, *76*, 100924. https://doi.org/10.1016/j.mam.2020.100924

Doyle, S. L., Ozaki, E., Brennan, K., Humphries, M. M., Mulfaul, K., Keaney, J., Kenna, P. F., Maminishkis, A., Kiang, A.-S., Saunders, S. P., Hams, E., Lavelle, E. C., Gardiner, C., Fallon, P. G., Adamson, P., Humphries, P., & Campbell, M. (2014). IL-18 Attenuates Experimental Choroidal Neovascularization as a Potential Therapy for Wet Age-Related Macular Degeneration. *Science Translational Medicine*, *6*(230), 230ra244-230ra244. https://doi.org/doi:10.1126/scitranslmed.3007616

Elkordy, M., Crump, M., Vredenburgh, J. J., Petros, W. P., Hussein, A., Rubin, P., Ross, M., Gilbert, C., Modlin, C., Meisenberg, B., Coniglio, D., Rabinowitz, J., Laughlin, M., Kurtzberg, J., & Peters, W. P. (1997). A phase I trial of recombinant human interleukin-1 beta (OCT-43) following high-dose chemotherapy and autologous bone marrow transplantation. *Bone Marrow Transplant*, *19*(4), 315-322. https://doi.org/10.1038/sj.bmt.1700633

Feke, G. T., & Pasquale, L. R. (2008). Retinal blood flow response to posture change in glaucoma patients compared with healthy subjects. *Ophthalmology*, *115*(2), 246-252.

Feldman, N., Rotter-Maskowitz, A., & Okun, E. (2015). DAMPs as mediators of sterile inflammation in aging-related pathologies. *Ageing Research Reviews*, *24*, 29-39. https://doi.org/https://doi.org/10.1016/j.arr.2015.01.003

Fellman, R. L., Mattox, C., Singh, K., Flowers, B., Francis, B. A., Robin, A. L., Butler, M. R., Shah, M. M., Giaconi, J. A., & Sheybani, A. (2020). American Glaucoma Society position paper: microinvasive glaucoma surgery. *Ophthalmology Glaucoma*, *3*(1), 1-6.

Fileta, J. B., Huang, W., Guo, Y., & Grosskreutz, C. L. (2006). Thy1 Downregulation in Retinal Ganglion Cells (RGC) in Experimental Glaucoma. *Investigative Ophthalmology & Visual Science*, *47*(13), 1261-1261.

Fingert, J. H., Robin, A. L., Scheetz, T. E., Kwon, Y. H., Liebmann, J. M., Ritch, R., & Alward, W. L. (2016). Tank-Binding Kinase 1 (TBK1) Gene and Open-Angle Glaucomas (An American Ophthalmological Society Thesis). *Trans Am Ophthalmol Soc*, *114*, T6.

Fingert, J. H., Robin, A. L., Stone, J. L., Roos, B. R., Davis, L. K., Scheetz, T. E., Bennett, S. R., Wassink, T. H., Kwon, Y. H., Alward, W. L., Mullins, R. F., Sheffield, V. C., & Stone, E. M. (2011). Copy number variations on chromosome 12q14 in patients with normal tension glaucoma. *Hum Mol Genet*, *20*(12), 2482-2494. https://doi.org/10.1093/hmg/ddr123

Fischer, A. (2017). FDA approves novel gene therapy to treat patients with a rare form of inherited vision loss. *FDA, FDA. gov*.

Flammer, J., Orgül, S., Costa, V. P., Orzalesi, N., Krieglstein, G. K., Serra, L. M., Renard, J.-P., & Stefánsson, E. (2002). The impact of ocular blood flow in glaucoma. *Progress in Retinal and Eye Research*, *21*(4), 359-393.

Fradejas, N., Pastor, M. D., Burgos, M., Beyaert, R., Tranque, P., & Calvo, S. (2010). Caspase-11 mediates ischemia-induced astrocyte death: involvement of endoplasmic reticulum stress and C/EBP homologous protein. *J Neurosci Res*, *88*(5), 1094-1105. https://doi.org/10.1002/jnr.22280

Freeman, L., Guo, H., David, C. N., Brickey, W. J., Jha, S., & Ting, J. P. (2017). NLR members NLRC4 and NLRP3 mediate sterile inflammasome activation in microglia and astrocytes. *J Exp Med*, *214*(5), 1351-1370. https://doi.org/10.1084/jem.20150237

Friedman, Z., & Neumann, E. (1972). Benzhexol-induced blindness in Parkinson's disease. *British Medical Journal*, *1*(5800), 605.

Fuchshofer, R., & Tamm, E. R. (2009). Modulation of extracellular matrix turnover in the trabecular meshwork. *Experimental Eye Research*, *88*(4), 683-688.

Fuchshofer, R., Welge-Lussen, U., & Lütjen-Drecoll, E. (2003). The effect of TGF-beta2 on human trabecular meshwork extracellular proteolytic system. *Exp Eye Res*, *77*(6), 757-765. https://doi.org/10.1016/s0014-4835(03)00220-3

Furuse, M., Fujita, K., Hiiragi, T., Fujimoto, K., & Tsukita, S. (1998). Claudin-1 and -2: novel integral membrane proteins localizing at tight junctions with no sequence

similarity to occludin. *J Cell Biol*, *141*(7), 1539-1550. https://doi.org/10.1083/jcb.141.7.1539

Furuse, M., Sasaki, H., Fujimoto, K., & Tsukita, S. (1998). A single gene product, claudin-1 or -2, reconstitutes tight junction strands and recruits occludin in fibroblasts. *J Cell Biol*, *143*(2), 391-401. https://doi.org/10.1083/jcb.143.2.391

Gabay, C., Fautrel, B., Rech, J., Spertini, F., Feist, E., Kötter, I., Hachulla, E., Morel, J., Schaeverbeke, T., Hamidou, M. A., Martin, T., Hellmich, B., Lamprecht, P., Schulze-Koops, H., Courvoisier, D. S., Sleight, A., & Schiffrin, E. J. (2018). Open-label, multicentre, dose-escalating phase II clinical trial on the safety and efficacy of tadekinig alfa (IL-18BP) in adult-onset Still's disease. *Ann Rheum Dis*, *77*(6), 840-847. https://doi.org/10.1136/annrheumdis-2017-212608

Garcia, G. P., Lavieri, M. S., Andrews, C., Liu, X., Van Oyen, M. P., Kass, M. A., Gordon, M. O., & Stein, J. D. (2019). Accuracy of Kalman Filtering in Forecasting Visual Field and Intraocular Pressure Trajectory in Patients With Ocular Hypertension. *JAMA Ophthalmol*, *137*(12), 1416-1423. https://doi.org/10.1001/jamaophthalmol.2019.4190

Garcia, G. P., Nitta, K., Lavieri, M. S., Andrews, C., Liu, X., Lobaza, E., Van Oyen, M. P., Sugiyama, K., & Stein, J. D. (2019). Using Kalman Filtering to Forecast Disease Trajectory for Patients With Normal Tension Glaucoma. *Am J Ophthalmol*, *199*, 111-119. https://doi.org/10.1016/j.ajo.2018.10.012

Garg, A., & Gazzard, G. (2018). Selective laser trabeculoplasty: past, present, and future. *Eye (Lond)*, *32*(5), 863-876. https://doi.org/10.1038/eye.2017.273

Garhöfer, G., Zawinka, C., Resch, H., Huemer, K. H., Schmetterer, L., & Dorner, G. T. (2004). Response of retinal vessel diameters to flicker stimulation in patients with early open angle glaucoma. *J Glaucoma*, *13*(4), 340-344. https://doi.org/10.1097/00061198-200408000-00013

Gaton, D. D., Sagara, T., Lindsey, J. D., Gabelt, B. T., Kaufman, P. L., & Weinreb, R. N. (2001). Increased matrix metalloproteinases 1, 2, and 3 in the monkey uveoscleral outflow pathway after topical prostaglandin F(2 alpha)-isopropyl ester treatment. *Arch Ophthalmol*, *119*(8), 1165-1170. https://doi.org/10.1001/archopht.119.8.1165

Gazzard, G., Konstantakopoulou, E., Garway-Heath, D., Garg, A., Vickerstaff, V., Hunter, R., Ambler, G., Bunce, C., Wormald, R., Nathwani, N., Barton, K., Rubin, G., & Buszewicz, M. (2019). Selective laser trabeculoplasty versus eye drops for first-line treatment of ocular hypertension and glaucoma (LiGHT): a multicentre

randomised controlled trial. *Lancet*, *393*(10180), 1505-1516. https://doi.org/10.1016/s0140-6736(18)32213-x

Gedde, S. J., Herndon, L. W., Brandt, J. D., Budenz, D. L., Feuer, W. J., Schiffman, J. C., & Group, T. V. T. S. (2012). Postoperative complications in the Tube Versus Trabeculectomy (TVT) study during five years of follow-up. *American Journal of Ophthalmology*, *153*(5), 804-814. e801.

Gedde, S. J., Heuer, D. K., Parrish, R. K., & Group, T. V. T. S. (2010). Review of results from the tube versus trabeculectomy study. *Current Opinion in Ophthalmology*, *21*(2), 123-128.

Gedde, S. J., Vinod, K., Wright, M. M., Muir, K. W., Lind, J. T., Chen, P. P., Li, T., & Mansberger, S. L. (2021). Primary Open-Angle Glaucoma Preferred Practice Pattern®. *Ophthalmology*, *128*(1), P71-P150. https://doi.org/https://doi.org/10.1016/j.ophtha.2020.10.022

Ghaffariyeh, A., Honarpisheh, N., Shakiba, Y., Puyan, S., Chamacham, T., Zahedi, F., & Zarrineghbal, M. (2009). Brain-derived neurotrophic factor in patients with normal-tension glaucoma. *Optometry*, *80*(11), 635-638. https://doi.org/10.1016/j.optm.2008.09.014

Gharahkhani, P., Jorgenson, E., Hysi, P., Khawaja, A. P., Pendergrass, S., Han, X., Ong, J. S., Hewitt, A. W., Segrè, A. V., & Rouhana, J. M. (2021). Genome-wide meta-analysis identifies 127 open-angle glaucoma loci with consistent effect across ancestries. *Nature Communications*, *12*(1), 1258.

Giebel, S. J., Menicucci, G., McGuire, P. G., & Das, A. (2005). Matrix metalloproteinases in early diabetic retinopathy and their role in alteration of the blood–retinal barrier. *Laboratory investigation*, *85*(5), 597-607.

Goel, M., Picciani, R. G., Lee, R. K., & Bhattacharya, S. K. (2010). Aqueous humor dynamics: a review. *Open Ophthalmol J*, *4*, 52-59. https://doi.org/10.2174/1874364101004010052

Gong, H., Tripathi, R. C., & Tripathi, B. J. (1996). Morphology of the aqueous outflow pathway. *Microsc Res Tech*, *33*(4), 336-367. https://doi.org/10.1002/(sici)1097-0029(19960301)33:4<336::Aid-jemt4>3.0.Co;2-n

Gottanka, J., Chan, D., Eichhorn, M., Lütjen-Drecoll, E., & Ethier, C. R. (2004). Effects of TGF-beta2 in perfused human eyes. *Invest Ophthalmol Vis Sci*, *45*(1), 153-158. https://doi.org/10.1167/iovs.03-0796

Gould, D. B., Miceli-Libby, L., Savinova, O. V., Torrado, M., Tomarev, S. I., Smith, R. S., & John, S. W. (2004). Genetically increasing Myoc expression supports a necessary pathologic role of abnormal proteins in glaucoma. *Molecular and Cellular Biology*, *24*(20), 9019-9025.

Gramlich, O. W., Beck, S., von Thun und Hohenstein-Blaul, N., Boehm, N., Ziegler, A., Vetter, J. M., Pfeiffer, N., & Grus, F. H. (2013). Enhanced insight into the autoimmune component of glaucoma: IgG autoantibody accumulation and pro-inflammatory conditions in human glaucomatous retina. *PLoS One*, *8*(2), e57557.

Grant, W. M. (1963). Experimental aqueous perfusion in enucleated human eyes. *Arch Ophthalmol*, *69*, 783-801. https://doi.org/10.1001/archopht.1963.00960040789022

Green, A. J., McQuaid, S., Hauser, S. L., Allen, I. V., & Lyness, R. (2010). Ocular pathology in multiple sclerosis: retinal atrophy and inflammation irrespective of disease duration. *Brain*, *133*(6), 1591-1601. https://doi.org/10.1093/brain/awq080

Greenwood, J., Wang, Y., & Calder, V. L. (1995). Lymphocyte adhesion and transendothelial migration in the central nervous system: the role of LFA-1, ICAM-1, VLA-4 and VCAM-1. off. *Immunology*, *86*(3), 408-415.

Grierson, I., Lee, W. R., Abraham, S., & Howes, R. C. (1978). Associations between the cells of the walls of Schlemm's canal. *Albrecht Von Graefes Arch Klin Exp Ophthalmol*, *208*(1-3), 33-47. https://doi.org/10.1007/bf00406980

Group, C. N.-T. G. S. (1998). The effectiveness of intraocular pressure reduction in the treatment of normal-tension glaucoma. *American Journal of Ophthalmology*, *126*(4), 498-505.

Gu, B. J., & Wiley, J. S. (2006). Rapid ATP-induced release of matrix metalloproteinase 9 is mediated by the P2X7 receptor. *Blood*, *107*(12), 4946-4953. https://doi.org/10.1182/blood-2005-07-2994

Gugleta, K., Türksever, C., Polunina, A., & Orgül, S. (2013). Effect of ageing on the retinal vascular responsiveness to flicker light in glaucoma patients and in ocular hypertension. *British Journal of Ophthalmology*, *97*(7), 848-851.

Gupta, V., You, Y., Li, J., Gupta, V., Golzan, M., Klistorner, A., van den Buuse, M., & Graham, S. (2014). BDNF impairment is associated with age-related changes in the inner retina and exacerbates experimental glaucoma. *Biochim Biophys Acta*, *1842*(9), 1567-1578. https://doi.org/10.1016/j.bbadis.2014.05.026

Han, J. A., Frishman, W. H., Wu Sun, S., Palmiero, P.-M., & Petrillo, R. (2008). Cardiovascular and Respiratory Considerations With Pharmacotherapy of

Glaucoma and Ocular Hypertension. *Cardiology in Review*, *16*(2). https://journals.lww.com/cardiologyinreview/fulltext/2008/03000/cardiovascular_and_respiratory_considerations_with.6.aspx

Han, X., Gharahkhani, P., Hamel, A. R., Ong, J. S., Rentería, M. E., Mehta, P., Dong, X., Pasutto, F., Hammond, C., & Young, T. L. (2023). Large-scale multitrait genome-wide association analyses identify hundreds of glaucoma risk loci. *Nature genetics*, *55*(7), 1116-1125.

Hann, C. R., Bahler, C. K., & Johnson, D. H. (2005). Cationic ferritin and segmental flow through the trabecular meshwork. *Invest Ophthalmol Vis Sci*, *46*(1), 1-7. https://doi.org/10.1167/iovs.04-0800

Hawkins, B. T., & Davis, T. P. (2005). The blood-brain barrier/neurovascular unit in health and disease. *Pharmacol Rev*, *57*(2), 173-185. https://doi.org/10.1124/pr.57.2.4

Hayreh, S. S., Zimmerman, M. B., Podhajsky, P., & Alward, W. L. (1994). Nocturnal arterial hypotension and its role in optic nerve head and ocular ischemic disorders. *American Journal of Ophthalmology*, *117*(5), 603-624.

He, C., Peng, K., Zhu, X., Wang, Z., Xiu, W., Zhang, G., Chen, Y., Sun, C., Xiao, X., & Liu, D. (2024). Th1 cells contribute to retinal ganglion cell loss in glaucoma in a VCAM-1-dependent manner. *Journal of Neuroinflammation*, *21*(1), 43.

He, L., Vanlandewijck, M., Mäe, M. A., Andrae, J., Ando, K., Del Gaudio, F., Nahar, K., Lebouvier, T., Laviña, B., Gouveia, L., Sun, Y., Raschperger, E., Segerstolpe, Å., Liu, J., Gustafsson, S., Räsänen, M., Zarb, Y., Mochizuki, N., Keller, A., . . . Betsholtz, C. (2018). Single-cell RNA sequencing of mouse brain and lung vascular and vessel-associated cell types. *Scientific Data*, *5*(1), 180160. https://doi.org/10.1038/sdata.2018.160

He, W.-t., Wan, H., Hu, L., Chen, P., Wang, X., Huang, Z., Yang, Z.-H., Zhong, C.-Q., & Han, J. (2015). Gasdermin D is an executor of pyroptosis and required for interleukin-1β secretion. *Cell Research*, *25*(12), 1285-1298. https://doi.org/10.1038/cr.2015.139

Heijl, A., Leske, M. C., Bengtsson, B., Hyman, L., Bengtsson, B., Hussein, M., & Group, E. M. G. T. (2002). Reduction of Intraocular Pressure and Glaucoma Progression: Results From the Early Manifest Glaucoma Trial. *Archives of Ophthalmology*, *120*(10), 1268-1279. https://doi.org/10.1001/archopht.120.10.1268

Henderson, J., O'Callaghan, J., & Campbell, M. (2024). Gene therapy for glaucoma: Targeting key mechanisms. *Vision research*, *225*, 108502.

Heys, J. J., & Barocas, V. H. (2002). A boussinesq model of natural convection in the human eye and the formation of Krukenberg's spindle. *Ann Biomed Eng*, *30*(3), 392-401. https://doi.org/10.1114/1.1477447

Howell, G. R., Soto, I., Ryan, M., Graham, L. C., Smith, R. S., & John, S. W. (2013). Deficiency of complement component 5 ameliorates glaucoma in DBA/2J mice. *J Neuroinflammation*, *10*, 76. https://doi.org/10.1186/1742-2094-10-76

Huang, C., Zhang, X., Wu, M., Yang, C., Ge, X., Chen, W., Li, X., Liu, S., & Yang, S. (2025). IL-1β-induced pericyte dysfunction with a secretory phenotype exacerbates retinal microenvironment inflammation via Hes1/STAT3 signaling pathway. *International Immunopharmacology*, *144*, 113611. https://doi.org/https://doi.org/10.1016/j.intimp.2024.113611

Huang, Y., Jiang, H., Chen, Y., Wang, X., Yang, Y., Tao, J., Deng, X., Liang, G., Zhang, H., Jiang, W., & Zhou, R. (2018). Tranilast directly targets NLRP3 to treat inflammasome-driven diseases. *EMBO Mol Med*, *10*(4). https://doi.org/10.15252/emmm.201708689

Hudson, N., Celkova, L., Hopkins, A., Greene, C., Storti, F., Ozaki, E., Fahey, E., Theodoropoulou, S., Kenna, P., Humphries, M., Curtis, A., Demmons, E., Browne, A., Liddie , S., Lawrence, M., Grimm, C., Cahill, M., Humphries, P., Doyle, S., & Campbell, M. (2019). Dysregulated claudin-5 cycling in the inner retina causes retinal pigment epithelial cell atrophy. *JCI insight*, *4*(15). https://doi.org/10.1172/jci.insight.130273

Hurley, D. J., Normile, C., Irnaten, M., & O'Brien, C. (2022). The Intertwined Roles of Oxidative Stress and Endoplasmic Reticulum Stress in Glaucoma. *Antioxidants*, *11*(5), 886. https://www.mdpi.com/2076-3921/11/5/886

Inman, D. M., Sappington, R. M., Horner, P. J., & Calkins, D. J. (2006). Quantitative Correlation of Optic Nerve Pathology with Ocular Pressure and Corneal Thickness in the DBA/2 Mouse Model of Glaucoma. *Investigative Ophthalmology & Visual Science*, *47*(3), 986-996. https://doi.org/10.1167/iovs.05-0925

Jeoung, J. W., Kim, Y. W., Girard, M. J., Mari, J. M., Kim, Y. K., Park, K. H., & Kim, D. M. (2016). Prelamina and lamina cribrosa in glaucoma patients with unilateral visual field loss. *Investigative Ophthalmology & Visual Science*, *57*(4), 1662-1670.

Jia, L., Cepurna, W. O., Johnson, E. C., & Morrison, J. C. (2000). Effect of general anesthetics on IOP in rats with experimental aqueous outflow obstruction. *Invest Ophthalmol Vis Sci*, *41*(11), 3415-3419.

Jiang, S., Kametani, M., & Chen, D. F. (2020). Adaptive immunity: new aspects of pathogenesis underlying neurodegeneration in glaucoma and optic neuropathy. *Frontiers in Immunology*, *11*, 65.

Joe, M. K., Sohn, S., Hur, W., Moon, Y., Choi, Y. R., & Kee, C. (2003). Accumulation of mutant myocilins in ER leads to ER stress and potential cytotoxicity in human trabecular meshwork cells. *Biochemical and Biophysical Research Communications*, *312*(3), 592-600. https://doi.org/https://doi.org/10.1016/j.bbrc.2003.10.162

John, S. W., Smith, R. S., Savinova, O. V., Hawes, N. L., Chang, B., Turnbull, D., Davisson, M., Roderick, T. H., & Heckenlively, J. R. (1998). Essential iris atrophy, pigment dispersion, and glaucoma in DBA/2J mice. *Investigative Ophthalmology & Visual Science*, *39*(6), 951-962.

Johnson, M. (2006). 'What controls aqueous humour outflow resistance?'. *Exp Eye Res*, *82*(4), 545-557. https://doi.org/10.1016/j.exer.2005.10.011

Johnson, M., Chan, D., Read, A. T., Christensen, C., Sit, A., & Ethier, C. R. (2002). The Pore Density in the Inner Wall Endothelium of Schlemm's Canal of Glaucomatous Eyes. *Investigative Ophthalmology & Visual Science*, *43*(9), 2950-2955.

Johnson, M., McLaren, J. W., & Overby, D. R. (2017). Unconventional aqueous humor outflow: A review. *Exp Eye Res*, *158*, 94-111. https://doi.org/10.1016/j.exer.2016.01.017

Johnson, T. V., & Tomarev, S. I. (2010). Rodent models of glaucoma. *Brain Res Bull*, *81*(2-3), 349-358. https://doi.org/10.1016/j.brainresbull.2009.04.004

Jonas, J. B., & Wang, N. (2013). Cerebrospinal fluid pressure and glaucoma. *J Ophthalmic Vis Res*, *8*(3), 257-263.

Kahook, M. Y., Serle, J. B., Mah, F. S., Kim, T., Raizman, M. B., Heah, T., Ramirez-Davis, N., Kopczynski, C. C., Usner, D. W., & Novack, G. D. (2019). Long-term Safety and Ocular Hypotensive Efficacy Evaluation of Netarsudil Ophthalmic Solution: Rho Kinase Elevated IOP Treatment Trial (ROCKET-2). *Am J Ophthalmol*, *200*, 130-137. https://doi.org/10.1016/j.ajo.2019.01.003

Kalogeropoulos, D., & Sung, V. C. (2018). Pathogenesis of Uveitic Glaucoma. *J Curr Glaucoma Pract*, *12*(3), 125-138. https://doi.org/10.5005/jp-journals-10028-1257

Kaplan, H. J., & Streilein, J. W. (1977). Immune response to immunization via the anterior chamber of the eye. I. F. lymphocyte-induced immune deviation. *J Immunol*, *118*(3), 809-814.

Karali, A., Russell, P., Stefani, F. H., & Tamm, E. R. (2000). Localization of myocilin/trabecular meshwork--inducible glucocorticoid response protein in the human eye. *Invest Ophthalmol Vis Sci*, *41*(3), 729-740.

Kass, M. A., Heuer, D. K., Higginbotham, E. J., Johnson, C. A., Keltner, J. L., Miller, J. P., Parrish, R. K., 2nd, Wilson, M. R., & Gordon, M. O. (2002). The Ocular Hypertension Treatment Study: a randomized trial determines that topical ocular hypotensive medication delays or prevents the onset of primary open-angle glaucoma. *Arch Ophthalmol*, *120*(6), 701-713; discussion 829-730. https://doi.org/10.1001/archopht.120.6.701

Kassab, H. S., Morsy, E. Y., Abdirahman, A. N., & Amin, N. G. (2023). Study of the relation between plasma level of von Willebrand factor and diabetic retinopathy in type 2 diabetes. *International Journal of Diabetes in Developing Countries*, *43*(5), 785-791.

Kaur, G., Sharma, D., Bisen, S., Mukhopadhyay, C. S., Gurdziel, K., & Singh, N. K. (2023). Vascular cell-adhesion molecule 1 (VCAM-1) regulates JunB-mediated IL-8/CXCL1 expression and pathological neovascularization. *Commun Biol*, *6*(1), 516. https://doi.org/10.1038/s42003-023-04905-z

Keaney, J., & Campbell, M. (2015). The dynamic blood-brain barrier. *Febs j*, *282*(21), 4067-4079. https://doi.org/10.1111/febs.13412

Keaney, J., Walsh, D. M., O'Malley, T., Hudson, N., Crosbie, D. E., Loftus, T., Sheehan, F., McDaid, J., Humphries, M. M., Callanan, J. J., Brett, F. M., Farrell, M. A., Humphries, P., & Campbell, M. (2015). Autoregulated paracellular clearance of amyloid-β across the blood-brain barrier. *Sci Adv*, *1*(8), e1500472. https://doi.org/10.1126/sciadv.1500472

Kee, C., & Seo, K. (1997). The effect of interleukin-1alpha on outflow facility in rat eyes. *J Glaucoma*, *6*(4), 246-249.

Keller, K. E., & Acott, T. S. (2013). The Juxtacanalicular Region of Ocular Trabecular Meshwork: A Tissue with a Unique Extracellular Matrix and Specialized Function. *J Ocul Biol*, *1*(1), 3.

Kelley, M. J., Rose, A. Y., Song, K., Chen, Y., Bradley, J. M., Rookhuizen, D., & Acott, T. S. (2007). Synergism of TNF and IL-1 in the induction of matrix

metalloproteinase-3 in trabecular meshwork. *Investigative Ophthalmology & Visual Science*, *48*(6), 2634-2643.

Kels, B. D., Grzybowski, A., & Grant-Kels, J. M. (2015). Human ocular anatomy. *Clinics in Dermatology*, *33*(2), 140-146. https://doi.org/https://doi.org/10.1016/j.clindermatol.2014.10.006

Keuthan, C. J., Schaub, J. A., Wei, M., Fang, W., Quillen, S., Kimball, E., Johnson, T. V., Ji, H., Zack, D. J., & Quigley, H. A. (2023). Regional Gene Expression in the Retina, Optic Nerve Head, and Optic Nerve of Mice with Optic Nerve Crush and Experimental Glaucoma. *International Journal of Molecular Sciences*, *24*(18), 13719. https://www.mdpi.com/1422-0067/24/18/13719

Khaw, P. T., Shah, P., & Elkington, A. R. (2004). Glaucoma--1: diagnosis. *Bmj*, *328*(7431), 97-99. https://doi.org/10.1136/bmj.328.7431.97

Khor, C. C., Do, T., Jia, H., Nakano, M., George, R., Abu-Amero, K., Duvesh, R., Chen, L. J., Li, Z., Nongpiur, M. E., Perera, S. A., Qiao, C., Wong, H. T., Sakai, H., Barbosa de Melo, M., Lee, M. C., Chan, A. S., Azhany, Y., Dao, T. L., . . . Aung, T. (2016). Genome-wide association study identifies five new susceptibility loci for primary angle closure glaucoma. *Nat Genet*, *48*(5), 556-562. https://doi.org/10.1038/ng.3540

Kiddee, W., Trope, G. E., Sheng, L., Beltran-Agullo, L., Smith, M., Strungaru, M. H., Baath, J., & Buys, Y. M. (2013). Intraocular pressure monitoring post intravitreal steroids: a systematic review. *Survey of Ophthalmology*, *58*(4), 291-310.

Killer, H. E., Miller, N. R., Flammer, J., Meyer, P., Weinreb, R. N., Remonda, L., & Jaggi, G. P. (2012). Cerebrospinal fluid exchange in the optic nerve in normal-tension glaucoma. *British Journal of Ophthalmology*, *96*(4), 544-548.

Killer, H. E., & Pircher, A. (2018). Normal tension glaucoma: review of current understanding and mechanisms of the pathogenesis. *Eye*, *32*(5), 924-930. https://doi.org/10.1038/s41433-018-0042-2

Kim, B. S., Savinova, O. V., Reedy, M. V., Martin, J., Lun, Y., Gan, L., Smith, R. S., Tomarev, S. I., John, S. W., & Johnson, R. L. (2001). Targeted disruption of the myocilin gene (Myoc) suggests that human glaucoma-causing mutations are gain of function. *Molecular and Cellular Biology*, *21*(22), 7707-7713.

Kim, K. E., & Park, K.-H. (2016). Update on the Prevalence, Etiology, Diagnosis, and Monitoring of Normal-Tension Glaucoma. *Asia-Pacific Journal of*

*Ophthalmology*, *5*(1), 23-31. https://doi.org/https://doi.org/10.1097/APO.0000000000000177

Kiyota, N., Shiga, Y., Suzuki, S., Sato, M., Takada, N., Maekawa, S., Omodaka, K., Maruyama, K., Kunikata, H., & Nakazawa, T. (2017). The effect of systemic hyperoxia on optic nerve head blood flow in primary open-angle glaucoma patients. *Investigative Ophthalmology & Visual Science*, *58*(7), 3181-3188.

Kiyota, N., Shiga, Y., Yasuda, M., Aizawa, N., Omodaka, K., Tsuda, S., Pak, K., Kunikata, H., & Nakazawa, T. (2020). The optic nerve head vasoreactive response to systemic hyperoxia and visual field defect progression in open-angle glaucoma, a pilot study. *Acta Ophthalmologica*, *98*(6), e747-e753.

Kizhatil, K., Ryan, M., Marchant, J. K., Henrich, S., & John, S. W. (2014). Schlemm's canal is a unique vessel with a combination of blood vascular and lymphatic phenotypes that forms by a novel developmental process. *PLoS Biol*, *12*(7), e1001912. https://doi.org/10.1371/journal.pbio.1001912

Klein, B. E., Klein, R., Sponsel, W. E., Franke, T., Cantor, L. B., Martone, J., & Menage, M. J. (1992). Prevalence of glaucoma: the Beaver Dam eye study. *Ophthalmology*, *99*(10), 1499-1504.

Klück, V., Jansen, T., Janssen, M., Comarniceanu, A., Efdé, M., Tengesdal, I. W., Schraa, K., Cleophas, M. C. P., Scribner, C. L., Skouras, D. B., Marchetti, C., Dinarello, C. A., & Joosten, L. A. B. (2020). Dapansutrile, an oral selective NLRP3 inflammasome inhibitor, for treatment of gout flares: an open-label, dose-adaptive, proof-of-concept, phase 2a trial. *Lancet Rheumatol*, *2*(5), e270-e280. https://doi.org/10.1016/s2665-9913(20)30065-5

Knowland, D., Arac, A., Sekiguchi, K. J., Hsu, M., Lutz, S. E., Perrino, J., Steinberg, G. K., Barres, B. A., Nimmerjahn, A., & Agalliu, D. (2014). Stepwise recruitment of transcellular and paracellular pathways underlies blood-brain barrier breakdown in stroke. *Neuron*, *82*(3), 603-617. https://doi.org/10.1016/j.neuron.2014.03.003

Ko, M. L., Hu, D. N., Ritch, R., Sharma, S. C., & Chen, C. F. (2001). Patterns of retinal ganglion cell survival after brain-derived neurotrophic factor administration in hypertensive eyes of rats. *Neurosci Lett*, *305*(2), 139-142. https://doi.org/10.1016/s0304-3940(01)01830-4

Kole, C., Brommer, B., Nakaya, N., Sengupta, M., Bonet-Ponce, L., Zhao, T., Wang, C., Li, W., He, Z., & Tomarev, S. (2020). Activating transcription factor 3 (ATF3)

protects retinal ganglion cells and promotes functional preservation after optic nerve crush. *Investigative Ophthalmology & Visual Science*, *61*(2), 31-31.

Kubota, K., Furuse, M., Sasaki, H., Sonoda, N., Fujita, K., Nagafuchi, A., & Tsukita, S. (1999). Ca(2+)-independent cell-adhesion activity of claudins, a family of integral membrane proteins localized at tight junctions. *Curr Biol*, *9*(18), 1035-1038. https://doi.org/10.1016/s0960-9822(99)80452-7

Küchle, M., Vinores, S. A., Mahlow, J., & Green, W. R. (1996). Blood-aqueous barrier in pseudoexfoliation syndrome: evaluation by immunohistochemical staining of endogenous albumin. *Graefes Arch Clin Exp Ophthalmol*, *234*(1), 12-18. https://doi.org/10.1007/bf00186513

Kumar, R. S., Baskaran, M., Chew, P. T. K., Friedman, D. S., Handa, S., Lavanya, R., Sakata, L. M., Wong, H.-T., & Aung, T. (2008). Prevalence of Plateau Iris in Primary Angle Closure Suspects: An Ultrasound Biomicroscopy Study. *Ophthalmology*, *115*(3), 430-434. https://doi.org/https://doi.org/10.1016/j.ophtha.2007.07.026

Kumar, R. S., Tantisevi, V., Wong, M. H., Laohapojanart, K., Chansanti, O., Quek, D. T., Koh, V. T., MohanRam, L. S., Lee, K. Y., & Rojanapongpun, P. (2009). Plateau iris in Asian subjects with primary angle closure glaucoma. *Archives of Ophthalmology*, *127*(10), 1269-1272.

Kumari, P., Russo, A. J., Shivcharan, S., & Rathinam, V. A. (2020). AIM2 in health and disease: Inflammasome and beyond. *Immunological reviews*, *297*(1), 83-95.

Laboissonniere, L. A., Goetz, J. J., Martin, G. M., Bi, R., Lund, T. J. S., Ellson, L., Lynch, M. R., Mooney, B., Wickham, H., Liu, P., Schwartz, G. W., & Trimarchi, J. M. (2019). Molecular signatures of retinal ganglion cells revealed through single cell profiling. *Scientific Reports*, *9*(1), 15778. https://doi.org/10.1038/s41598-019-52215-4

Lachkar, Y., & Bouassida, W. (2007). Drug-induced acute angle closure glaucoma. *Current Opinion in Ophthalmology*, *18*(2), 129-133.

Lal-Nag, M., & Morin, P. J. (2009). The claudins. *Genome Biol*, *10*(8), 235. https://doi.org/10.1186/gb-2009-10-8-235

Lampron, A., ElAli, A., & Rivest, S. (2013). Innate immunity in the CNS: redefining the relationship between the CNS and Its environment. *Neuron*, *78*(2), 214-232.

Latina, M. A., & Park, C. (1995). Selective targeting of trabecular meshwork cells: in vitro studies of pulsed and CW laser interactions. *Exp Eye Res*, *60*(4), 359-371. https://doi.org/10.1016/s0014-4835(05)80093-4

Lee, B. L., Bathija, R., & Weinreb, R. N. (1998). The definition of normal-tension glaucoma. *J Glaucoma*, *7*(6), 366-371.

Lee, E. J., & Kim, T. W. (2015). Lamina Cribrosa Reversal after Trabeculectomy and the Rate of Progressive Retinal Nerve Fiber Layer Thinning. *Ophthalmology*, *122*(11), 2234-2242. https://doi.org/10.1016/j.ophtha.2015.07.020

Lee, G. C., Tam, C. P., Danesh-Meyer, H. V., Myers, J. S., & Katz, L. J. (2007). Bilateral angle closure glaucoma induced by sulphonamide-derived medications. *Clinical & experimental ophthalmology*, *35*(1), 55-58.

Levkovitch–Verbin, H., Harris–Cerruti, C., Groner, Y., Wheeler, L. A., Schwartz, M., & Yoles, E. (2000). RGC death in mice after optic nerve crush injury: oxidative stress and neuroprotection. *Investigative Ophthalmology & Visual Science*, *41*(13), 4169-4174.

Li, A., Leung, C. T., Peterson-Yantorno, K., Stamer, W. D., & Civan, M. M. (2011). Cytoskeletal dependence of adenosine triphosphate release by human trabecular meshwork cells. *Invest Ophthalmol Vis Sci*, *52*(11), 7996-8005. https://doi.org/10.1167/iovs.11-8170

Li, A., Leung, C. T., Peterson-Yantorno, K., Stamer, W. D., Mitchell, C. H., & Civan, M. M. (2012). Mechanisms of ATP release by human trabecular meshwork cells, the enabling step in purinergic regulation of aqueous humor outflow. *Journal of Cellular Physiology*, *227*(1), 172-182. https://doi.org/https://doi.org/10.1002/jcp.22715

Li, F., Zhang, Y., Li, R., Li, Y., Ding, S., Zhou, J., Huang, T., Chen, C., Lu, B., Yu, W., Boltze, J., Li, P., & Wan, J. (2023). Neuronal Serpina3n is an endogenous protector against blood brain barrier damage following cerebral ischemic stroke. *Journal of Cerebral Blood Flow & Metabolism*, *43*(2), 241-257. https://doi.org/10.1177/0271678x221113897

Li, L., Bian, A., Cheng, G., & Zhou, Q. (2016). Posterior displacement of the lamina cribrosa in normal-tension and high-tension glaucoma. *Acta Ophthalmol*, *94*(6), e492-500. https://doi.org/10.1111/aos.13012

Li, T., Lindsley, K., Rouse, B., Hong, H., Shi, Q., Friedman, D. S., Wormald, R., & Dickersin, K. (2016). Comparative Effectiveness of First-Line Medications for

Primary Open-Angle Glaucoma: A Systematic Review and Network Meta-analysis. *Ophthalmology*, *123*(1), 129-140. https://doi.org/10.1016/j.ophtha.2015.09.005

Li, X., Gu, X., Boyce, T. M., Zheng, M., Reagan, A. M., Qi, H., Mandal, N., Cohen, A. W., Callegan, M. C., Carr, D. J., & Elliott, M. H. (2014). Caveolin-1 increases proinflammatory chemoattractants and blood-retinal barrier breakdown but decreases leukocyte recruitment in inflammation. *Invest Ophthalmol Vis Sci*, *55*(10), 6224-6234. https://doi.org/10.1167/iovs.14-14613

Liao, K. C., & Mogridge, J. (2013). Activation of the Nlrp1b inflammasome by reduction of cytosolic ATP. *Infect Immun*, *81*(2), 570-579. https://doi.org/10.1128/iai.01003-12

Libby, R. T., Anderson, M. G., Pang, I.-h., Robinson, Z. H., Savinova, O. V., Cosma, I. M., Snow, A., Wilson, L. A., Smith, R. S., & Clark, A. F. (2005). Inherited glaucoma in DBA/2J mice: pertinent disease features for studying the neurodegeneration. *Visual neuroscience*, *22*(5), 637-648.

Lin, H.-H., Faunce, D. E., Stacey, M., Terajewicz, A., Nakamura, T., Zhang-Hoover, J., Kerley, M., Mucenski, M. L., Gordon, S., & Stein-Streilein, J. (2005). The macrophage F4/80 receptor is required for the induction of antigen-specific efferent regulatory T cells in peripheral tolerance. *The Journal of experimental medicine*, *201*(10), 1615-1625.

Lindén, C., & Alm, A. (1999). Prostaglandin analogues in the treatment of glaucoma. *Drugs Aging*, *14*(5), 387-398. https://doi.org/10.2165/00002512-199914050-00006

Lindsey, J. D., & Weinreb, R. N. (2002). Identification of the Mouse Uveoscleral Outflow Pathway Using Fluorescent Dextran. *Investigative Ophthalmology & Visual Science*, *43*(7), 2201-2205.

Ling, L., Maguire, J. J., & Davenport, A. P. (2013). Endothelin-2, the forgotten isoform: emerging role in the cardiovascular system, ovarian development, immunology and cancer. *British journal of pharmacology*, *168*(2), 283-295.

Lipski, D. A., Foucart, V., Dewispelaere, R., Caspers, L. E., Defrance, M., Bruyns, C., & Willermain, F. (2020). Retinal endothelial cell phenotypic modifications during experimental autoimmune uveitis: a transcriptomic approach. *BMC Ophthalmology*, *20*(1), 106.

Liton, P. B., Luna, C., Bodman, M., Hong, A., Epstein, D. L., & Gonzalez, P. (2005). Induction of IL-6 expression by mechanical stress in the trabecular meshwork. *Biochemical and Biophysical Research Communications*, *337*(4), 1229-1236. https://doi.org/https://doi.org/10.1016/j.bbrc.2005.09.182

Liu, M., Xu, Z., Wang, L., Zhang, L., Liu, Y., Cao, J., Fu, Q., Liu, Y., Li, H., Lou, J., Hou, W., Mi, W., & Ma, Y. (2020). Cottonseed oil alleviates ischemic stroke injury by inhibiting the inflammatory activation of microglia and astrocyte. *J Neuroinflammation*, *17*(1), 270. https://doi.org/10.1186/s12974-020-01946-7

Liu, Y., & Vollrath, D. (2004). Reversal of mutant myocilin non-secretion and cell killing: implications for glaucoma. *Hum Mol Genet*, *13*(11), 1193-1204. https://doi.org/10.1093/hmg/ddh128

London, A., Benhar, I., & Schwartz, M. (2013). The retina as a window to the brain-from eye research to CNS disorders. *Nat Rev Neurol*, *9*(1), 44-53. https://doi.org/10.1038/nrneurol.2012.227

López-Otín, C., Blasco, M. A., Partridge, L., Serrano, M., & Kroemer, G. (2013). The hallmarks of aging. *Cell*, *153*(6), 1194-1217. https://doi.org/10.1016/j.cell.2013.05.039

Lowe, R. F. (1970). Aetiology of the anatomical basis for primary angle-closure glaucoma. Biometrical comparisons between normal eyes and eyes with primary angle-closure glaucoma. *Br J Ophthalmol*, *54*(3), 161-169. https://doi.org/10.1136/bjo.54.3.161

Lu, Z., Overby, D. R., Scott, P. A., Freddo, T. F., & Gong, H. (2008). The mechanism of increasing outflow facility by rho-kinase inhibition with Y-27632 in bovine eyes. *Exp Eye Res*, *86*(2), 271-281. https://doi.org/10.1016/j.exer.2007.10.018

Luntz, M. H., & Rosenblatt, M. (1987). Malignant glaucoma. *Survey of Ophthalmology*, *32*(2), 73-93. https://doi.org/https://doi.org/10.1016/0039-6257(87)90101-9

Ma, M., Jiang, W., & Zhou, R. (2024). DAMPs and DAMP-sensing receptors in inflammation and diseases. *Immunity*, *57*(4), 752-771.

Mäepea, O., & Bill, A. (1989). The pressures in the episcleral veins, Schlemm's canal and the trabecular meshwork in monkeys: effects of changes in intraocular pressure. *Exp Eye Res*, *49*(4), 645-663. https://doi.org/10.1016/s0014-4835(89)80060-0

Mäepea, O., & Bill, A. (1992). Pressures in the juxtacanalicular tissue and Schlemm's canal in monkeys. *Exp Eye Res*, *54*(6), 879-883. https://doi.org/10.1016/0014-4835(92)90151-h

Mancino, R., Martucci, A., Cesareo, M., Giannini, C., Corasaniti, M. T., Bagetta, G., & Nucci, C. (2018). Glaucoma and Alzheimer Disease: One Age-Related Neurodegenerative Disease of the Brain. *Curr Neuropharmacol*, *16*(7), 971-977. https://doi.org/10.2174/1570159x16666171206144045

Mannucci, P. M. (1998). von Willebrand factor: a marker of endothelial damage? *Arteriosclerosis, thrombosis, and vascular biology*, *18*(9), 1359-1362.

Marchini, G., Pagliarusco, A., Toscano, A., Tosi, R., Brunelli, C., & Bonomi, L. (1998). Ultrasound biomicroscopic and conventional ultrasonographic study of ocular dimensions in primary angle-closure glaucoma11Conducted on behalf of the Regional Council of the Veneto Region, Finalized Health Research, Venice, Italy. *Ophthalmology*, *105*(11), 2091-2098. https://doi.org/https://doi.org/10.1016/S0161-6420(98)91132-0

Margeta, M. A., Lad, E. M., & Proia, A. D. (2018). CD163+ macrophages infiltrate axon bundles of postmortem optic nerves with glaucoma. *Graefe's Archive for Clinical and Experimental Ophthalmology*, *256*(12), 2449-2456.

Matsumoto, J., Takata, F., Machida, T., Takahashi, H., Soejima, Y., Funakoshi, M., Futagami, K., Yamauchi, A., Dohgu, S., & Kataoka, Y. (2014). Tumor necrosis factor-α-stimulated brain pericytes possess a unique cytokine and chemokine release profile and enhance microglial activation. *Neurosci Lett*, *578*, 133-138. https://doi.org/10.1016/j.neulet.2014.06.052

McCann, P., Hogg, R., Wright, D. M., Pose-Bazarra, S., Chakravarthy, U., Peto, T., Cruise, S., McGuinness, B., Young, I. S., Kee, F., & Azuara-Blanco, A. (2020). Glaucoma in the Northern Ireland Cohort for the Longitudinal Study of Ageing (NICOLA): cohort profile, prevalence, awareness and associations. *British Journal of Ophthalmology*, *104*(11), 1492-1499. https://doi.org/10.1136/bjophthalmol-2019-315330

McMenamin, P. G. (1997). The distribution of immune cells in the uveal tract of the normal eye. *Eye*, *11*(2), 183-193. https://doi.org/10.1038/eye.1997.49

Medawar, P. B. (1948). Immunity to homologous grafted skin; the fate of skin homografts transplanted to the brain, to subcutaneous tissue, and to the anterior chamber of the eye. *Br J Exp Pathol*, *29*(1), 58-69.

Menaa, F., Braghini, C. A., Vasconcellos, J. P., Menaa, B., Costa, V. P., Figueiredo, E. S., & Melo, M. B. (2011). Keeping an eye on myocilin: a complex molecule

associated with primary open-angle glaucoma susceptibility. *Molecules*, *16*(7), 5402-5421. https://doi.org/10.3390/molecules16075402

Meyer, J. H., Brandi-Dohrn, J., & Funk, J. (1996). Twenty four hour blood pressure monitoring in normal tension glaucoma. *British Journal of Ophthalmology*, *80*(10), 864-867. https://doi.org/10.1136/bjo.80.10.864

Michinaga, S., Hishinuma, S., & Koyama, Y. (2024). Roles of astrocytic sonic hedgehog production and its signal for regulation of the blood-brain barrier permeability. *Vitam Horm*, *126*, 97-111. https://doi.org/10.1016/bs.vh.2024.04.006

Michinaga, S., & Koyama, Y. (2019). Dual Roles of Astrocyte-Derived Factors in Regulation of Blood-Brain Barrier Function after Brain Damage. *Int J Mol Sci*, *20*(3). https://doi.org/10.3390/ijms20030571

Minegishi, Y., Iejima, D., Kobayashi, H., Chi, Z. L., Kawase, K., Yamamoto, T., Seki, T., Yuasa, S., Fukuda, K., & Iwata, T. (2013). Enhanced optineurin E50K-TBK1 interaction evokes protein insolubility and initiates familial primary open-angle glaucoma. *Hum Mol Genet*, *22*(17), 3559-3567. https://doi.org/10.1093/hmg/ddt210

Mitchell, P., Smith, W., Chey, T., & Healey, P. R. (1997). Open-angle glaucoma and diabetes: the Blue Mountains eye study, Australia. *Ophthalmology*, *104*(4), 712-718.

Mittag, T. W., Danias, J., Pohorenec, G., Yuan, H. M., Burakgazi, E., Chalmers–Redman, R., Podos, S. M., & Tatton, W. G. (2000). Retinal damage after 3 to 4 months of elevated intraocular pressure in a rat glaucoma model. *Investigative Ophthalmology & Visual Science*, *41*(11), 3451-3459.

Mo, J. S., Anderson, M. G., Gregory, M., Smith, R. S., Savinova, O. V., Serreze, D. V., Ksander, B. R., Streilein, J. W., & John, S. W. (2003). By altering ocular immune privilege, bone marrow-derived cells pathogenically contribute to DBA/2J pigmentary glaucoma. *J Exp Med*, *197*(10), 1335-1344. https://doi.org/10.1084/jem.20022041

Moghimi, S., Zangwill, L. M., Penteado, R. C., Hasenstab, K., Ghahari, E., Hou, H., Christopher, M., Yarmohammadi, A., Manalastas, P. I. C., & Shoji, T. (2018). Macular and optic nerve head vessel density and progressive retinal nerve fiber layer loss in glaucoma. *Ophthalmology*, *125*(11), 1720-1728.

Mohan, R., & Muralidharan, A. (1989). Steroid induced glaucoma and cataract. *Indian journal of ophthalmology*, *37*(1), 13-16.

Moreno, M. C., Campanelli, J., Sande, P., Sánez, D. A., Keller Sarmiento, M. I., & Rosenstein, R. E. (2004). Retinal oxidative stress induced by high intraocular pressure. *Free Radic Biol Med*, *37*(6), 803-812. https://doi.org/10.1016/j.freeradbiomed.2004.06.001

Morgan, J. E., & Tribble, J. R. (2015). Microbead models in glaucoma. *Experimental Eye Research*, *141*, 9-14. https://doi.org/https://doi.org/10.1016/j.exer.2015.06.020

Morini, M. F., Giampietro, C., Corada, M., Pisati, F., Lavarone, E., Cunha, S. I., Conze, L. L., O'Reilly, N., Joshi, D., Kjaer, S., George, R., Nye, E., Ma, A., Jin, J., Mitter, R., Lupia, M., Cavallaro, U., Pasini, D., Calado, D. P., . . . Taddei, A. (2018). VE-Cadherin-Mediated Epigenetic Regulation of Endothelial Gene Expression. *Circ Res*, *122*(2), 231-245. https://doi.org/10.1161/circresaha.117.312392

Morton, S., Hesson, L., Peggie, M., & Cohen, P. (2008). Enhanced binding of TBK1 by an optineurin mutant that causes a familial form of primary open angle glaucoma. *FEBS Lett*, *582*(6), 997-1002. https://doi.org/10.1016/j.febslet.2008.02.047

Mueller, A., Lam, I., Kishor, K., Lee, R. K., & Bhattacharya, S. (2024). Secondary glaucoma: Toward interventions based on molecular underpinnings. *WIREs Mechanisms of Disease*, *16*(1), e1628. https://doi.org/https://doi.org/10.1002/wsbm.1628

Mugisho, O. O., & Green, C. R. (2022). The NLRP3 inflammasome in age-related eye disease: Evidence-based connexin hemichannel therapeutics. *Experimental Eye Research*, *215*, 108911. https://doi.org/https://doi.org/10.1016/j.exer.2021.108911

Nag, S., Venugopalan, R., & Stewart, D. J. (2007). Increased caveolin-1 expression precedes decreased expression of occludin and claudin-5 during blood-brain barrier breakdown. *Acta Neuropathol*, *114*(5), 459-469. https://doi.org/10.1007/s00401-007-0274-x

Nakagawa, S., Deli, M. A., Kawaguchi, H., Shimizudani, T., Shimono, T., Kittel, A., Tanaka, K., & Niwa, M. (2009). A new blood-brain barrier model using primary rat brain endothelial cells, pericytes and astrocytes. *Neurochem Int*, *54*(3-4), 253-263. https://doi.org/10.1016/j.neuint.2008.12.002

Nakamura, Y. (2002). Regulating factors for microglial activation. *Biological and Pharmaceutical Bulletin*, *25*(8), 945-953.

Navarro, R., Compte, M., Álvarez-Vallina, L., & Sanz, L. (2016). Immune Regulation by Pericytes: Modulating Innate and Adaptive Immunity. *Front Immunol*, *7*, 480. https://doi.org/10.3389/fimmu.2016.00480

Nemunaitis, J., Appelbaum, F. R., Lilleby, K., Buhles, W. C., Rosenfeld, C., Zeigler, Z. R., Shadduck, R. K., Singer, J. W., Meyer, W., & Buckner, C. D. (1994). Phase I study of recombinant interleukin-1 beta in patients undergoing autologous bone marrow transplant for acute myelogenous leukemia. *Blood*, *83*(12), 3473-3479.

Neri, P., Azuara-Blanco, A., & Forrester, J. V. (2004). Incidence of glaucoma in patients with uveitis. *J Glaucoma*, *13*(6), 461-465. https://doi.org/10.1097/01.ijg.0000146391.77618.d0

Newman, E. A. (2015). Glial cell regulation of neuronal activity and blood flow in the retina by release of gliotransmitters. *Philosophical Transactions of the Royal Society B: Biological Sciences*, *370*(1672), 20140195.

Ng, W. T., & Morgan, W. (2012). Mechanisms and treatment of primary angle closure: a review. *Clinical & experimental ophthalmology*, *40*(4), e218-e228. https://doi.org/https://doi.org/10.1111/j.1442-9071.2011.02604.x

Nguyen, M., Sullivan, J., & Shen, W. (2023). Retinal vascular remodeling in photoreceptor degenerative disease. *Experimental Eye Research*, *234*, 109566. https://doi.org/https://doi.org/10.1016/j.exer.2023.109566

Nian, S., Lo, A. C. Y., Mi, Y., Ren, K., & Yang, D. (2021). Neurovascular unit in diabetic retinopathy: pathophysiological roles and potential therapeutical targets. *Eye and Vision*, *8*(1), 15. https://doi.org/10.1186/s40662-021-00239-1

Niccoli, T., & Partridge, L. (2012). Ageing as a Risk Factor for Disease. *Current Biology*, *22*(17), R741-R752. https://doi.org/https://doi.org/10.1016/j.cub.2012.07.024

Nitta, T., Hata, M., Gotoh, S., Seo, Y., Sasaki, H., Hashimoto, N., Furuse, M., & Tsukita, S. (2003). Size-selective loosening of the blood-brain barrier in claudin-5-deficient mice. *J Cell Biol*, *161*(3), 653-660. https://doi.org/10.1083/jcb.200302070

Norose, K., Yano, A., Wang, X. C., Tokushima, T., Umihira, J., Seki, A., Nohara, M., & Segawa, K. (1994). Dominance of activated T cells and interleukin-6 in aqueous humor in Vogt-Koyanagi-Harada disease. *Invest Ophthalmol Vis Sci*, *35*(1), 33-39.

Nucci, C., Di Pierro, D., Varesi, C., Ciuffoletti, E., Russo, R., Gentile, R., Cedrone, C., Pinazo Duran, M. D., Coletta, M., & Mancino, R. (2013). Increased malondialdehyde concentration and reduced total antioxidant capacity in aqueous humor and blood samples from patients with glaucoma. *Mol Vis*, *19*, 1841-1846.

O'Callaghan, J., Cassidy, P. S., & Humphries, P. (2017). Open-angle glaucoma: therapeutically targeting the extracellular matrix of the conventional outflow

pathway. *Expert Opinion on Therapeutic Targets*, *21*(11), 1037-1050. https://doi.org/10.1080/14728222.2017.1386174

O'Callaghan, J., Crosbie, D. E., Cassidy, P. S., Sherwood, J. M., Flügel-Koch, C., Lütjen-Drecoll, E., Humphries, M. M., Reina-Torres, E., Wallace, D., Kiang, A.-S., Campbell, M., Stamer, W. D., Overby, D. R., O'Brien, C., Tam, L. C. S., & Humphries, P. (2017). Therapeutic potential of AAV-mediated MMP-3 secretion from corneal endothelium in treating glaucoma. *Human Molecular Genetics*, *26*(7), 1230-1246. https://doi.org/10.1093/hmg/ddx028

O'Callaghan, J., Delaney, C., O'Connor, M., van Batenburg-Sherwood, J., Schicht, M., Lütjen-Drecoll, E., Hudson, N., Ni Dhubhghaill, S., Humphries, P., Stanley, C., Keravala, A., Chalberg, T., Lawrence, M. S., & Campbell, M. (2023). Matrix metalloproteinase-3 (MMP-3)–mediated gene therapy for glaucoma. *Science Advances*, *9*(16), eadf6537. https://doi.org/doi:10.1126/sciadv.adf6537

O'Leary, F., & Campbell, M. (2021). The blood-retina barrier in health and disease. *Febs j*. https://doi.org/10.1111/febs.16330

Oddone, F., Roberti, G., Micera, A., Busanello, A., Bonini, S., Quaranta, L., Agnifili, L., & Manni, G. (2017). Exploring Serum Levels of Brain Derived Neurotrophic Factor and Nerve Growth Factor Across Glaucoma Stages. *PLoS One*, *12*(1), e0168565. https://doi.org/10.1371/journal.pone.0168565

Ogura, S., Kurata, K., Hattori, Y., Takase, H., Ishiguro-Oonuma, T., Hwang, Y., Ahn, S., Park, I., Ikeda, W., Kusuhara, S., Fukushima, Y., Nara, H., Sakai, H., Fujiwara, T., Matsushita, J., Ema, M., Hirashima, M., Minami, T., Shibuya, M., . . . Uemura, A. (2017). Sustained inflammation after pericyte depletion induces irreversible blood-retina barrier breakdown. *JCI insight*, *2*(3), e90905. https://doi.org/10.1172/jci.insight.90905

Ohta, K., Wiggert, B., Yamagami, S., Taylor, A. W., & Streilein, J. W. (2000). Analysis of immunomodulatory activities of aqueous humor from eyes of mice with experimental autoimmune uveitis. *The Journal of Immunology*, *164*(3), 1185-1192.

Ohta, K., Yamagami, S., Taylor, A. W., & Streilein, J. W. (2000). IL-6 antagonizes TGF-beta and abolishes immune privilege in eyes with endotoxin-induced uveitis. *Invest Ophthalmol Vis Sci*, *41*(9), 2591-2599.

Okamura, H., Tsutsi, H., Komatsu, T., Yutsudo, M., Hakura, A., Tanimoto, T., Torigoe, K., Okura, T., Nukada, Y., Hattori, K., & et al. (1995). Cloning of a new cytokine that

induces IFN-gamma production by T cells. *Nature*, *378*(6552), 88-91. https://doi.org/10.1038/378088a0

Orth-He, E. L., Huang, H. C., Rao, S. D., Wang, Q., Chen, Q., O'Mara, C. M., Chui, A. J., Saoi, M., Griswold, A. R., Bhattacharjee, A., Ball, D. P., Cross, J. R., & Bachovchin, D. A. (2023). Protein folding stress potentiates NLRP1 and CARD8 inflammasome activation. *Cell Rep*, *42*(1), 111965. https://doi.org/10.1016/j.celrep.2022.111965

Overby, D., Gong, H., Qiu, G., Freddo, T. F., & Johnson, M. (2002). The mechanism of increasing outflow facility during washout in the bovine eye. *Invest Ophthalmol Vis Sci*, *43*(11), 3455-3464.

Overby, D. R., Bertrand, J., Schicht, M., Paulsen, F., Stamer, W. D., & Lütjen-Drecoll, E. (2014). The structure of the trabecular meshwork, its connections to the ciliary muscle, and the effect of pilocarpine on outflow facility in mice. *Invest Ophthalmol Vis Sci*, *55*(6), 3727-3736. https://doi.org/10.1167/iovs.13-13699

Overby, D. R., Bertrand, J., Tektas, O.-Y., Boussommier-Calleja, A., Schicht, M., Ethier, C. R., Woodward, D. F., Stamer, W. D., & Lütjen-Drecoll, E. (2014). Ultrastructural Changes Associated With Dexamethasone-Induced Ocular Hypertension in Mice. *Investigative Ophthalmology & Visual Science*, *55*(8), 4922-4933. https://doi.org/10.1167/iovs.14-14429

Overby, D. R., & Clark, A. F. (2015). Animal models of glucocorticoid-induced glaucoma. *Exp Eye Res*, *141*, 15-22. https://doi.org/10.1016/j.exer.2015.06.002

Overby, D. R., Stamer, W. D., & Johnson, M. (2009). The changing paradigm of outflow resistance generation: towards synergistic models of the JCT and inner wall endothelium. *Exp Eye Res*, *88*(4), 656-670. https://doi.org/10.1016/j.exer.2008.11.033

Ozdemir, G., Tolun, F. I., Gul, M., & Imrek, S. (2009). Retinal oxidative stress induced by intraocular hypertension in rats may be ameliorated by brimonidine treatment and N-acetyl cysteine supplementation. *J Glaucoma*, *18*(9), 662-665. https://doi.org/10.1097/IJG.0b013e31819c46b1

Pandit, R., Koh, W. K., Sullivan, R. K. P., Palliyaguru, T., Parton, R. G., & Götz, J. (2020). Role for caveolin-mediated transcytosis in facilitating transport of large cargoes into the brain via ultrasound. *Journal of Controlled Release*, *327*, 667-675. https://doi.org/https://doi.org/10.1016/j.jconrel.2020.09.015

Pang, C. P., Leung, Y. F., Fan, B., Baum, L., Tong, W. C., Lee, W. S., Chua, J. K. H., Fan, D. S. P., Liu, Y., & Lam, D. S. C. (2002). TIGR/MYOC Gene Sequence Alterations in Individuals with and without Primary Open-Angle Glaucoma. *Investigative Ophthalmology & Visual Science*, *43*(10), 3231-3235.

Park, D. Y., Lee, J., Kim, J., Kim, K., Hong, S., Han, S., Kubota, Y., Augustin, H. G., Ding, L., & Kim, J. W. (2017). Plastic roles of pericytes in the blood–retinal barrier. *Nature Communications*, *8*(1), 15296.

Patel, G., Fury, W., Yang, H., Gomez-Caraballo, M., Bai, Y., Yang, T., Adler, C., Wei, Y., Ni, M., & Schmitt, H. (2020). Molecular taxonomy of human ocular outflow tissues defined by single-cell transcriptomics. *Proceedings of the National Academy of Sciences*, *117*(23), 12856-12867.

Patel, G. C., Liu, Y., Millar, J. C., & Clark, A. F. (2018). Glucocorticoid receptor GRβ regulates glucocorticoid-induced ocular hypertension in mice. *Scientific Reports*, *8*(1), 1-13.

Pease, M. E., McKinnon, S. J., Quigley, H. A., Kerrigan–Baumrind, L. A., & Zack, D. J. (2000). Obstructed axonal transport of BDNF and its receptor TrkB in experimental glaucoma. *Investigative Ophthalmology & Visual Science*, *41*(3), 764-774.

Pedrigi, R. M., Simon, D., Reed, A., Stamer, W. D., & Overby, D. R. (2011). A model of giant vacuole dynamics in human Schlemm's canal endothelial cells. *Exp Eye Res*, *92*(1), 57-66. https://doi.org/10.1016/j.exer.2010.11.003

Pereira, I. C., van de Wijdeven, R., Wyss, H. M., Beckers, H. J., & den Toonder, J. M. (2021). Conventional glaucoma implants and the new MIGS devices: a comprehensive review of current options and future directions. *Eye*, *35*(12), 3202-3221.

Phipps, J. A., Dixon, M. A., Jobling, A. I., Wang, A. Y., Greferath, U., Vessey, K. A., & Fletcher, E. L. (2019). The renin-angiotensin system and the retinal neurovascular unit: A role in vascular regulation and disease. *Exp Eye Res*, *187*, 107753. https://doi.org/10.1016/j.exer.2019.107753

Pircher, A., Montali, M., Berberat, J., Remonda, L., & Killer, H. E. (2017). The optic canal: a bottleneck for cerebrospinal fluid dynamics in normal-tension glaucoma? *Frontiers in neurology*, *8*, 47.

Plange, N., Bienert, M., Remky, A., & Arend, K. O. (2012). Optic disc fluorescein leakage and intraocular pressure in primary open-angle glaucoma. *Current Eye Research*, *37*(6), 508-512.

Plange, N., Kaup, M., Doehmen, B., Remky, A., & Arend, K. O. (2010). Fluorescein leakage of the optic disc: time course in primary open-angle glaucoma. *Ophthalmic and Physiological Optics*, *30*(3), 315-320.

Polansky, J., Friedman, Z., Fauss, D., Kurtz, R., & Alvarado, J. (1989). Effects of betaxolol/timolol on epinephrine stimulated cyclic-AMP levels in human trabecular meshwork cells. *International Ophthalmology*, *13*(1), 95-97.

Prada, D., Harris, A., Guidoboni, G., Siesky, B., Huang, A. M., & Arciero, J. (2016). Autoregulation and neurovascular coupling in the optic nerve head. *Survey of Ophthalmology*, *61*(2), 164-186.

Puren, A. J., Fantuzzi, G., & Dinarello, C. A. (1999). Gene expression, synthesis, and secretion of interleukin 18 and interleukin 1β are differentially regulated in human blood mononuclear cells and mouse spleen cells. *Proceedings of the National Academy of Sciences*, *96*(5), 2256-2261. https://doi.org/doi:10.1073/pnas.96.5.2256

Quigley, H. A., & Addicks, E. M. (1980). Chronic experimental glaucoma in primates. I. Production of elevated intraocular pressure by anterior chamber injection of autologous ghost red blood cells. *Investigative Ophthalmology & Visual Science*, *19*(2), 126-136.

Quigley, H. A., Addicks, E. M., Green, W. R., & Maumenee, A. E. (1981). Optic nerve damage in human glaucoma. II. The site of injury and susceptibility to damage. *Arch Ophthalmol*, *99*(4), 635-649. https://doi.org/10.1001/archopht.1981.03930010635009

Quigley, H. A., & Broman, A. T. (2006). The number of people with glaucoma worldwide in 2010 and 2020. *Br J Ophthalmol*, *90*(3), 262-267. https://doi.org/10.1136/bjo.2005.081224

Quigley, H. A., Friedman, D. S., & Congdon, N. G. (2003). Possible mechanisms of primary angle-closure and malignant glaucoma. *Journal of Glaucoma*, *12*(2), 167-180.

Quigley, H. A., McKinnon, S. J., Zack, D. J., Pease, M. E., Kerrigan-Baumrind, L. A., Kerrigan, D. F., & Mitchell, R. S. (2000). Retrograde axonal transport of BDNF in

retinal ganglion cells is blocked by acute IOP elevation in rats. *Invest Ophthalmol Vis Sci*, *41*(11), 3460-3466.

Radius, R. L., & Anderson, D. R. (1980). Breakdown of the normal optic nerve head blood-brain barrier following acute elevation of intraocular pressure in experimental animals. *Investigative Ophthalmology & Visual Science*, *19*(3), 244-255.

Raleigh, D. R., Marchiando, A. M., Zhang, Y., Shen, L., Sasaki, H., Wang, Y., Long, M., & Turner, J. R. (2010). Tight junction-associated MARVEL proteins marveld3, tricellulin, and occludin have distinct but overlapping functions. *Mol Biol Cell*, *21*(7), 1200-1213. https://doi.org/10.1091/mbc.e09-08-0734

Ramirez, M. L. G., Poreba, M., Snipas, S. J., Groborz, K., Drag, M., & Salvesen, G. S. (2018). Extensive peptide and natural protein substrate screens reveal that mouse caspase-11 has much narrower substrate specificity than caspase-1. *J Biol Chem*, *293*(18), 7058-7067. https://doi.org/10.1074/jbc.RA117.001329

Ramirez, S. H., Fan, S., Dykstra, H., Rom, S., Mercer, A., Reichenbach, N. L., Gofman, L., & Persidsky, Y. (2013). Inhibition of glycogen synthase kinase 3β promotes tight junction stability in brain endothelial cells by half-life extension of occludin and claudin-5. *PLoS One*, *8*(2), e55972. https://doi.org/10.1371/journal.pone.0055972

Ramulu, P. Y., Hochberg, C., Maul, E. A., Chan, E. S., Ferrucci, L., & Friedman, D. S. (2014). Glaucomatous visual field loss associated with less travel from home. *Optom Vis Sci*, *91*(2), 187-193. https://doi.org/10.1097/opx.0000000000000139

Ramulu, P. Y., Swenor, B. K., Jefferys, J. L., Friedman, D. S., & Rubin, G. S. (2013). Difficulty with Out-Loud and Silent Reading in Glaucoma. *Investigative Ophthalmology & Visual Science*, *54*(1), 666-672. https://doi.org/10.1167/iovs.12-10618

Razeghinejad, M. R., Myers, J. S., & Katz, L. J. (2011). Iatrogenic Glaucoma Secondary to Medications. *The American Journal of Medicine*, *124*(1), 20-25. https://doi.org/https://doi.org/10.1016/j.amjmed.2010.08.011

Redmond, T. M., Yu, S., Lee, E., Bok, D., Hamasaki, D., Chen, N., Goletz, P., Ma, J. X., Crouch, R. K., & Pfeifer, K. (1998). Rpe65 is necessary for production of 11-cis-vitamin A in the retinal visual cycle. *Nat Genet*, *20*(4), 344-351. https://doi.org/10.1038/3813

Reese, T. S., & Karnovsky, M. J. (1967). Fine structural localization of a blood-brain barrier to exogenous peroxidase. *J Cell Biol*, *34*(1), 207-217. https://doi.org/10.1083/jcb.34.1.207

Reina-Torres, E., Wen, J. C., Liu, K. C., Li, G., Sherwood, J. M., Chang, J. Y. H., Challa, P., Flügel-Koch, C. M., Stamer, W. D., Allingham, R. R., & Overby, D. R. (2017). VEGF as a Paracrine Regulator of Conventional Outflow Facility. *Investigative Ophthalmology & Visual Science*, *58*(3), 1899-1908. https://doi.org/10.1167/iovs.16-20779

Rezaie, T., Child, A., Hitchings, R., Brice, G., Miller, L., Coca-Prados, M., Héon, E., Krupin, T., Ritch, R., Kreutzer, D., Crick, R. P., & Sarfarazi, M. (2002). Adult-onset primary open-angle glaucoma caused by mutations in optineurin. *Science*, *295*(5557), 1077-1079. https://doi.org/10.1126/science.1066901

Rezaie, T., & Sarfarazi, M. (2005). Molecular cloning, genomic structure, and protein characterization of mouse optineurin. *Genomics*, *85*(1), 131-138. https://doi.org/10.1016/j.ygeno.2004.10.011

Richa, S., & Yazbek, J.-C. (2010). Ocular adverse effects of common psychotropic agents: a review. *CNS drugs*, *24*, 501-526.

Richter, B., Sliter, D. A., Herhaus, L., Stolz, A., Wang, C., Beli, P., Zaffagnini, G., Wild, P., Martens, S., & Wagner, S. A. (2016). Phosphorylation of OPTN by TBK1 enhances its binding to Ub chains and promotes selective autophagy of damaged mitochondria. *Proceedings of the National Academy of Sciences*, *113*(15), 4039-4044.

Ritch, R., Krupin, T., Henry, C., & Kurata, F. (1994). Oral imipramine and acute angle closure glaucoma. *Archives of Ophthalmology*, *112*(1), 67-68.

Ritch, R., & Schlötzer-Schrehardt, U. (2001). Exfoliation syndrome. *Surv Ophthalmol*, *45*(4), 265-315. https://doi.org/10.1016/s0039-6257(00)00196-x

Rizzolo, L. J. (2007). Development and Role of Tight Junctions in the Retinal Pigment Epithelium. In *International Review of Cytology* (Vol. 258, pp. 195-234). Academic Press. https://doi.org/https://doi.org/10.1016/S0074-7696(07)58004-6

Robin, A. L., & Muir, K. W. (2019). Medication adherence in patients with ocular hypertension or glaucoma. *Expert Review of Ophthalmology*, *14*(4-5), 199-210.

Rock, K. L., Latz, E., Ontiveros, F., & Kono, H. (2010). The sterile inflammatory response. *Annu Rev Immunol*, *28*, 321-342. https://doi.org/10.1146/annurev-immunol-030409-101311

Rognon, G. T., Liao, A. Y., Pasteurin, R. P., Soundararajan, A., & Pattabiraman, P. P. (2025). Lipids and lipid regulators in intraocular pressure homeostasis. *Curr Opin Pharmacol*, *82*, 102523. https://doi.org/10.1016/j.coph.2025.102523

Rosdahl, J. A., & Gupta, D. (2020). Prospective studies of minimally invasive glaucoma surgeries: systematic review and quality assessment. *Clinical Ophthalmology*, 231-243.

Rühl, S., & Broz, P. (2015). Caspase-11 activates a canonical NLRP3 inflammasome by promoting K(+) efflux. *Eur J Immunol*, *45*(10), 2927-2936. https://doi.org/10.1002/eji.201545772

Sagar, D., Lamontagne, A., Foss, C. A., Khan, Z. K., Pomper, M. G., & Jain, P. (2012). Dendritic cell CNS recruitment correlates with disease severity in EAE via CCL2 chemotaxis at the blood–brain barrier through paracellular transmigration and ERK activation. *Journal of Neuroinflammation*, *9*(1), 245.

Saitou, M., Furuse, M., Sasaki, H., Schulzke, J. D., Fromm, M., Takano, H., Noda, T., & Tsukita, S. (2000). Complex phenotype of mice lacking occludin, a component of tight junction strands. *Mol Biol Cell*, *11*(12), 4131-4142. https://doi.org/10.1091/mbc.11.12.4131

Salvetat, M. L., Pellegrini, F., Spadea, L., Salati, C., & Zeppieri, M. (2023). Pharmaceutical Approaches to Normal Tension Glaucoma. *Pharmaceuticals*, *16*(8), 1172. https://www.mdpi.com/1424-8247/16/8/1172

Samuelson, T. W., Chang, D. F., Marquis, R., Flowers, B., Lim, K. S., Ahmed, I. I. K., Jampel, H. D., Aung, T., Crandall, A. S., & Singh, K. (2019). A Schlemm canal microstent for intraocular pressure reduction in primary open-angle glaucoma and cataract: the HORIZON study. *Ophthalmology*, *126*(1), 29-37.

Savinova, O. V., Sugiyama, F., Martin, J. E., Tomarev, S. I., Paigen, B. J., Smith, R. S., & John, S. W. (2001). Intraocular pressure in genetically distinct mice: an update and strain survey. *BMC Genet*, *2*, 12. https://doi.org/10.1186/1471-2156-2-12

Schmidt, S. Y., & Peisch, R. D. (1986). Melanin concentration in normal human retinal pigment epithelium. Regional variation and age-related reduction. *Invest Ophthalmol Vis Sci*, *27*(7), 1063-1067.

Schmier, J. K., Hulme-Lowe, C. K., & Covert, D. W. (2014). Adjunctive therapy patterns in glaucoma patients using prostaglandin analogs. *Clinical Ophthalmology*, 1097-1104.

Scholz, M., Buder, T., Seeber, S., Adamek, E., Becker, C.-M., & Lutjen-Drecoll, E. (2008). Dependency of intraocular pressure elevation and glaucomatous changes in DBA/2J and DBA/2J-Rj mice. *Investigative Ophthalmology & Visual Science*, *49*(2), 613-621.

Schraermeyer, M., Schnichels, S., Julien, S., Heiduschka, P., Bartz-Schmidt, K. U., & Schraermeyer, U. (2009). Ultrastructural analysis of the pigment dispersion syndrome in DBA/2J mice. *Graefes Arch Clin Exp Ophthalmol*, *247*(11), 1493-1504. https://doi.org/10.1007/s00417-009-1146-y

Schroder, K., & Tschopp, J. (2010). The inflammasomes. *Cell*, *140*(6), 821-832. https://doi.org/10.1016/j.cell.2010.01.040

Schwartz, G. F., & Quigley, H. A. (2008). Adherence and persistence with glaucoma therapy. *Surv Ophthalmol*, *53 Suppl1*, S57-68. https://doi.org/10.1016/j.survophthal.2008.08.002

Scuderi, G., Contestabile, M. T., Scuderi, L., Librando, A., Fenicia, V., & Rahimi, S. (2019). Pigment dispersion syndrome and pigmentary glaucoma: a review and update. *International Ophthalmology*, *39*, 1651-1662.

Serle, J. B., Katz, L. J., McLaurin, E., Heah, T., Ramirez-Davis, N., Usner, D. W., Novack, G. D., & Kopczynski, C. C. (2018). Two Phase 3 Clinical Trials Comparing the Safety and Efficacy of Netarsudil to Timolol in Patients With Elevated Intraocular Pressure: Rho Kinase Elevated IOP Treatment Trial 1 and 2 (ROCKET-1 and ROCKET-2). *Am J Ophthalmol*, *186*, 116-127. https://doi.org/10.1016/j.ajo.2017.11.019

Shabana, N., Aquino, M. C., See, J., Ce, Z., Tan, A. M., Nolan, W. P., Hitchings, R., Young, S. M., Loon, S. C., & Sng, C. C. (2012). Quantitative evaluation of anterior chamber parameters using anterior segment optical coherence tomography in primary angle closure mechanisms. *Clinical & experimental ophthalmology*, *40*(8), 792-801.

Shan, Y., Tan, S., Lin, Y., Liao, S., Zhang, B., Chen, X., Wang, J., Deng, Z., Zeng, Q., Zhang, L., Wang, Y., Hu, X., Qiu, W., Peng, L., & Lu, Z. (2019). The glucagon-like peptide-1 receptor agonist reduces inflammation and blood-brain barrier breakdown in an astrocyte-dependent manner in experimental stroke. *J Neuroinflammation*, *16*(1), 242. https://doi.org/10.1186/s12974-019-1638-6

Shen, J., Choy, D. F., Yoshida, T., Iwase, T., Hafiz, G., Xie, B., Hackett, S. F., Arron, J. R., & Campochiaro, P. A. (2014). Interleukin-18 Has Antipermeablity and

Antiangiogenic Activities in the Eye: Reciprocal Suppression With VEGF. *Journal of Cellular Physiology*, *229*(8), 974-983. https://doi.org/https://doi.org/10.1002/jcp.24575

Sherwood, J. M., Reina-Torres, E., Bertrand, J. A., Rowe, B., & Overby, D. R. (2016). Measurement of Outflow Facility Using iPerfusion. *PLoS One*, *11*(3), e0150694. https://doi.org/10.1371/journal.pone.0150694

Sijssens, K. M., Rijkers, G. T., Rothova, A., Stilma, J. S., Schellekens, P. A., & de Boer, J. H. (2007). Cytokines, chemokines and soluble adhesion molecules in aqueous humor of children with uveitis. *Exp Eye Res*, *85*(4), 443-449. https://doi.org/10.1016/j.exer.2007.06.011

Simon, M. J., & Iliff, J. J. (2016). Regulation of cerebrospinal fluid (CSF) flow in neurodegenerative, neurovascular and neuroinflammatory disease. *Biochim Biophys Acta*, *1862*(3), 442-451. https://doi.org/10.1016/j.bbadis.2015.10.014

Singh, N., Kizhatil, K., Duraikannu, D., Choquet, H., & Saidas Nair, K. (2025). Structural framework to address variant-gene relationship in primary open-angle glaucoma. *Vision research*, *226*, 108505. https://doi.org/https://doi.org/10.1016/j.visres.2024.108505

Sommer, A., Tielsch, J. M., Katz, J., Quigley, H. A., Gottsch, J. D., Javitt, J., & Singh, K. (1991). Relationship between intraocular pressure and primary open angle glaucoma among white and black Americans: the Baltimore Eye Survey. *Archives of Ophthalmology*, *109*(8), 1090-1095.

Sonoda, K.-H., & Stein-Streilein, J. (2002). Ocular immune privilege and CD1d-reactive natural killer T cells. *Cornea*, *21*, S33-S38.

Soto, I., & Howell, G. R. (2014). The complex role of neuroinflammation in glaucoma. *Cold Spring Harbor perspectives in medicine*, *4*(8), a017269.

Spampinato, S. F., Merlo, S., Sano, Y., Kanda, T., & Sortino, M. A. (2017). Astrocytes contribute to Aβ-induced blood–brain barrier damage through activation of endothelial MMP 9. *Journal of Neurochemistry*, *142*(3), 464-477.

Stamer, W. D., & Acott, T. S. (2012). Current understanding of conventional outflow dysfunction in glaucoma. *Current Opinion in Ophthalmology*, *23*(2), 135-143. https://doi.org/10.1097/ICU.0b013e32834ff23e

Stamer, W. D., & Clark, A. F. (2017). The many faces of the trabecular meshwork cell. *Exp Eye Res*, *158*, 112-123. https://doi.org/10.1016/j.exer.2016.07.009

Stamer, W. D., Piwnica, D., Jolas, T., Carling, R. W., Cornell, C. L., Fliri, H., Martos, J., Pettit, S. N., Wang, J. W., & Woodward, D. F. (2010). Cellular basis for bimatoprost effects on human conventional outflow. *Invest Ophthalmol Vis Sci*, *51*(10), 5176-5181. https://doi.org/10.1167/iovs.09-4955

Starr, C., & Chen, B. (2023). Adeno-associated virus mediated gene therapy for neuroprotection of retinal ganglion cells in glaucoma. *Vision research*, *206*, 108196. https://doi.org/https://doi.org/10.1016/j.visres.2023.108196

Stein, J. D., Khawaja, A. P., & Weizer, J. S. (2021). Glaucoma in Adults—Screening, Diagnosis, and Management: A Review. *JAMA*, *325*(2), 164-174. https://doi.org/10.1001/jama.2020.21899

Stein, J. D., Kim, D. D., Peck, W. W., Giannetti, S. M., & Hutton, D. W. (2012). Cost-effectiveness of Medications Compared With Laser Trabeculoplasty in Patients With Newly Diagnosed Open-Angle Glaucoma. *Archives of Ophthalmology*, *130*(4), 497-505. https://doi.org/10.1001/archophthalmol.2011.2727

Stone, E. M., Fingert, J. H., Alward, W. L. M., Nguyen, T. D., Polansky, J. R., Sunden, S. L. F., Nishimura, D., Clark, A. F., Nystuen, A., Nichols, B. E., Mackey, D. A., Ritch, R., Kalenak, J. W., Craven, E. R., & Sheffield, V. C. (1997). Identification of a Gene That Causes Primary Open Angle Glaucoma. *Science*, *275*(5300), 668-670. https://doi.org/doi:10.1126/science.275.5300.668

Streeten, B. W., Bookman, L., Ritch, R., Prince, A. M., & Dark, A. J. (1987). Pseudoexfoliative fibrillopathy in the conjunctiva. A relation to elastic fibers and elastosis. *Ophthalmology*, *94*(11), 1439-1449. https://doi.org/10.1016/s0161-6420(87)33268-3

Streilein, J. W. (1996). Ocular immune privilege and the Faustian dilemma. The Proctor lecture. *Invest Ophthalmol Vis Sci*, *37*(10), 1940-1950.

Su, W., Li, Z., Jia, Y., & Zhuo, Y. (2014). Rapamycin is neuroprotective in a rat chronic hypertensive glaucoma model. *PLoS One*, *9*(6), e99719.

Sudhakar, C., Nagabhushana, A., Jain, N., & Swarup, G. (2009). NF-kappaB mediates tumor necrosis factor alpha-induced expression of optineurin, a negative regulator of NF-kappaB. *PLoS One*, *4*(4), e5114. https://doi.org/10.1371/journal.pone.0005114

Sun, X., Dai, Y., Chen, Y., Yu, D.-Y., Cringle, S. J., Chen, J., Kong, X., Wang, X., & Jiang, C. (2017). Primary angle closure glaucoma: What we know and what we

don’t know. *Progress in Retinal and Eye Research*, *57*, 26-45. https://doi.org/https://doi.org/10.1016/j.preteyeres.2016.12.003

Suzuki, T., Franchi, L., Toma, C., Ashida, H., Ogawa, M., Yoshikawa, Y., Mimuro, H., Inohara, N., Sasakawa, C., & Nuñez, G. (2007). Differential regulation of caspase-1 activation, pyroptosis, and autophagy via Ipaf and ASC in Shigella-infected macrophages. *PLoS pathogens*, *3*(8), e111.

Swanson, K. V., Deng, M., & Ting, J. P. Y. (2019). The NLRP3 inflammasome: molecular activation and regulation to therapeutics. *Nature Reviews Immunology*, *19*(8), 477-489. https://doi.org/10.1038/s41577-019-0165-0

Taddei, A., Giampietro, C., Conti, A., Orsenigo, F., Breviario, F., Pirazzoli, V., Potente, M., Daly, C., Dimmeler, S., & Dejana, E. (2008). Endothelial adherens junctions control tight junctions by VE-cadherin-mediated upregulation of claudin-5. *Nature Cell Biology*, *10*(8), 923-934. https://doi.org/10.1038/ncb1752

Takahashi, H., Noda, S., Imamura, Y., Nagasawa, A., Kubota, R., Mashima, Y., Kudoh, J., Oguchi, Y., & Shimizu, N. (1998). Mouse Myocilin (Myoc) Gene Expression in Ocular Tissues1. *Biochemical and Biophysical Research Communications*, *248*(1), 104-109.

Takai, Y., Tanito, M., & Ohira, A. (2012). Multiplex cytokine analysis of aqueous humor in eyes with primary open-angle glaucoma, exfoliation glaucoma, and cataract. *Invest Ophthalmol Vis Sci*, *53*(1), 241-247. https://doi.org/10.1167/iovs.11-8434

Takeshita, Y., Obermeier, B., Cotleur, A. C., Spampinato, S. F., Shimizu, F., Yamamoto, E., Sano, Y., Kryzer, T. J., Lennon, V. A., Kanda, T., & Ransohoff, R. M. (2017). Effects of neuromyelitis optica-IgG at the blood-brain barrier in vitro. *Neurol Neuroimmunol Neuroinflamm*, *4*(1), e311. https://doi.org/10.1212/nxi.0000000000000311

Tam, L. C., Reina-Torres, E., Sherwood, J. M., Cassidy, P. S., Crosbie, D. E., Lütjen-Drecoll, E., Flügel-Koch, C., Perkumas, K., Humphries, M. M., Kiang, A. S., O'Callaghan, J., Callanan, J. J., Read, A. T., Ethier, C. R., O'Brien, C., Lawrence, M., Campbell, M., Stamer, W. D., Overby, D. R., & Humphries, P. (2017). Enhancement of Outflow Facility in the Murine Eye by Targeting Selected Tight-Junctions of Schlemm's Canal Endothelia. *Sci Rep*, *7*, 40717. https://doi.org/10.1038/srep40717

Tamm, E. R. (2009). The trabecular meshwork outflow pathways: structural and functional aspects. *Exp Eye Res*, *88*(4), 648-655. https://doi.org/10.1016/j.exer.2009.02.007

Tang, Z., Zhang, S., Lee, C., Kumar, A., Arjunan, P., Li, Y., Zhang, F., & Li, X. (2011). An optic nerve crush injury murine model to study retinal ganglion cell survival. *J Vis Exp*(50). https://doi.org/10.3791/2685

Tanito, M., Kaidzu, S., Takai, Y., & Ohira, A. (2016). Association between systemic oxidative stress and visual field damage in open-angle glaucoma. *Scientific Reports*, *6*(1), 25792.

Tanna, A. P., & Johnson, M. (2018). Rho Kinase Inhibitors as a Novel Treatment for Glaucoma and Ocular Hypertension. *Ophthalmology*, *125*(11), 1741-1756. https://doi.org/10.1016/j.ophtha.2018.04.040

Tapia, M., Levay, K., Tsoulfas, P., & Park, K. K. (2024). Retrograde AAV-mediated gene modulation reveals chloride intracellular channel proteins as potent regulators of retinal ganglion cell death. *Experimental Neurology*, *377*, 114810.

Tarasoff-Conway, J. M., Carare, R. O., Osorio, R. S., Glodzik, L., Butler, T., Fieremans, E., Axel, L., Rusinek, H., Nicholson, C., Zlokovic, B. V., Frangione, B., Blennow, K., Ménard, J., Zetterberg, H., Wisniewski, T., & de Leon, M. J. (2015). Clearance systems in the brain—implications for Alzheimer disease. *Nature Reviews Neurology*, *11*(8), 457-470. https://doi.org/10.1038/nrneurol.2015.119

Tarongoy, P., Ho, C. L., & Walton, D. S. (2009). Angle-closure Glaucoma: The Role of the Lens in the Pathogenesis, Prevention, and Treatment. *Survey of Ophthalmology*, *54*(2), 211-225. https://doi.org/https://doi.org/10.1016/j.survophthal.2008.12.002

Taurone, S., Ripandelli, G., Pacella, E., Bianchi, E., Plateroti, A. M., De Vito, S., Plateroti, P., Grippaudo, F. R., Cavallotti, C., & Artico, M. (2015). Potential regulatory molecules in the human trabecular meshwork of patients with glaucoma: immunohistochemical profile of a number of inflammatory cytokines. *Mol Med Rep*, *11*(2), 1384-1390. https://doi.org/10.3892/mmr.2014.2772

Taylor, A. W. (2005). The immunomodulating neuropeptide alpha-melanocyte-stimulating hormone (α-MSH) suppresses LPS-stimulated TLR4 with IRAK-M in macrophages. *Journal of Neuroimmunology*, *162*(1), 43-50. https://doi.org/10.1016/j.jneuroim.2005.01.008

Taylor, A. W., Yee, D. G., & Streilein, J. W. (1998). Suppression of nitric oxide generated by inflammatory macrophages by calcitonin gene-related peptide in aqueous humor. *Invest Ophthalmol Vis Sci*, *39*(8), 1372-1378.

Tezel, G. l. n., Chauhan, B. C., LeBlanc, R. P., & Wax, M. B. (2003). Immunohistochemical Assessment of the Glial Mitogen-Activated Protein Kinase Activation in Glaucoma. *Investigative Ophthalmology & Visual Science*, *44*(7), 3025-3033. https://doi.org/10.1167/iovs.02-1136

Tham, Y. C., Li, X., Wong, T. Y., Quigley, H. A., Aung, T., & Cheng, C. Y. (2014). Global prevalence of glaucoma and projections of glaucoma burden through 2040: a systematic review and meta-analysis. *Ophthalmology*, *121*(11), 2081-2090. https://doi.org/10.1016/j.ophtha.2014.05.013

Thorleifsson, G., Magnusson, K. P., Sulem, P., Walters, G. B., Gudbjartsson, D. F., Stefansson, H., Jonsson, T., Jonasdottir, A., Jonasdottir, A., Stefansdottir, G., Masson, G., Hardarson, G. A., Petursson, H., Arnarsson, A., Motallebipour, M., Wallerman, O., Wadelius, C., Gulcher, J. R., Thorsteinsdottir, U., . . . Stefansson, K. (2007). Common sequence variants in the LOXL1 gene confer susceptibility to exfoliation glaucoma. *Science*, *317*(5843), 1397-1400. https://doi.org/10.1126/science.1146554

Thorleifsson, G., Walters, G. B., Hewitt, A. W., Masson, G., Helgason, A., DeWan, A., Sigurdsson, A., Jonasdottir, A., Gudjonsson, S. A., Magnusson, K. P., Stefansson, H., Lam, D. S., Tam, P. O., Gudmundsdottir, G. J., Southgate, L., Burdon, K. P., Gottfredsdottir, M. S., Aldred, M. A., Mitchell, P., . . . Stefansson, K. (2010). Common variants near CAV1 and CAV2 are associated with primary open-angle glaucoma. *Nat Genet*, *42*(10), 906-909. https://doi.org/10.1038/ng.661

Tielsch, J. M., Katz, J., Sommer, A., Quigley, H. A., & Javitt, J. C. (1995). Hypertension, perfusion pressure, and primary open-angle glaucoma. A population-based assessment. *Arch Ophthalmol*, *113*(2), 216-221. https://doi.org/10.1001/archopht.1995.01100020100038

To, C. H., Kong, C. W., Chan, C. Y., Shahidullah, M., & Do, C. W. (2002). The mechanism of aqueous humour formation. *Clin Exp Optom*, *85*(6), 335-349.

Toris, C. B., Yablonski, M. E., Wang, Y. L., & Camras, C. B. (1999). Aqueous humor dynamics in the aging human eye. *Am J Ophthalmol*, *127*(4), 407-412. https://doi.org/10.1016/s0002-9394(98)00436-x

Tornavaca, O., Chia, M., Dufton, N., Almagro, L. O., Conway, D. E., Randi, A. M., Schwartz, M. A., Matter, K., & Balda, M. S. (2015). ZO-1 controls endothelial adherens junctions, cell–cell tension, angiogenesis, and barrier formation. *Journal of Cell Biology*, *208*(6), 821-838.

Trevino, T. N., Almousawi, A. A., Robinson, K. F., Fogel, A. B., Class, J., Minshall, R. D., Tai, L. M., Richner, J. M., & Lutz, S. E. (2024). Caveolin-1 mediates blood-brain barrier permeability, neuroinflammation, and cognitive impairment in SARS-CoV-2 infection. *Journal of Neuroimmunology*, *388*, 578309. https://doi.org/https://doi.org/10.1016/j.jneuroim.2024.578309

Tripathi, R. C., Li, J., Chan, W. F., & Tripathi, B. J. (1994). Aqueous humor in glaucomatous eyes contains an increased level of TGF-beta 2. *Exp Eye Res*, *59*(6), 723-727. https://doi.org/10.1006/exer.1994.1158

Tripathi, R. C., Parapuram, S. K., Tripathi, B. J., Zhong, Y., & Chalam, K. (1999). Corticosteroids and glaucoma risk. *Drugs & aging*, *15*, 439-450.

Tsai, M. H., Lin, C. H., Tsai, K. W., Lin, M. H., Ho, C. J., Lu, Y. T., Weng, K. P., Lin, Y., Lin, P. H., & Li, S. C. (2019). S100A6 Promotes B Lymphocyte Penetration Through the Blood-Brain Barrier in Autoimmune Encephalitis. *Front Genet*, *10*, 1188. https://doi.org/10.3389/fgene.2019.01188

Tsukita, S., Furuse, M., & Itoh, M. (2001). Multifunctional strands in tight junctions. *Nature Reviews Molecular Cell Biology*, *2*(4), 285-293. https://doi.org/10.1038/35067088

Turner, A. J., Vander Wall, R., Gupta, V., Klistorner, A., & Graham, S. L. (2017). DBA/2J mouse model for experimental glaucoma: pitfalls and problems. *Clinical & experimental ophthalmology*, *45*(9), 911-922. https://doi.org/https://doi.org/10.1111/ceo.12992

Turner, A. J., Vanderwall, R., Gupta, V., Klistorner, A., & Graham, S. L. (2016). DBA 2J mouse model for experimental glaucoma – pitfalls and problems. *Investigative Ophthalmology & Visual Science*, *57*(12), 5143-5143.

Underwood, J. L., Murphy, C. G., Chen, J., Franse-Carman, L., Wood, I., Epstein, D. L., & Alvarado, J. A. (1999). Glucocorticoids regulate transendothelial fluid flow resistance and formation of intercellular junctions. *Am J Physiol*, *277*(2), C330-342. https://doi.org/10.1152/ajpcell.1999.277.2.C330

Van Itallie, C. M., Tietgens, A. J., & Anderson, J. M. (2017). Visualizing the dynamic coupling of claudin strands to the actin cytoskeleton through ZO-1. *Molecular Biology of the Cell*, *28*(4), 524-534.

Vanlandewijck, M., He, L., Mäe, M. A., Andrae, J., Ando, K., Gaudio, F. D., Nahar, K., Lebouvier, T., Laviña, B., Gouveia, L., Sun, Y., Raschperger, E., Räsänen, M., Zarb, Y., Mochizuki, N., Keller, A., Lendahl, U., & Betsholtz, C. (2018). A molecular atlas of cell types and zonation in the brain vasculature [OriginalPaper]. *Nature*, *554*(7693), 475-480. https://doi.org/doi:10.1038/nature25739

Vecino, E., Rodriguez, F. D., Ruzafa, N., Pereiro, X., & Sharma, S. C. (2016). Glia–neuron interactions in the mammalian retina. *Progress in Retinal and Eye Research*, *51*, 1-40. https://doi.org/https://doi.org/10.1016/j.preteyeres.2015.06.003

Vendomèle, J., Khebizi, Q., & Fisson, S. (2017). Cellular and Molecular Mechanisms of Anterior Chamber-Associated Immune Deviation (ACAID): What We Have Learned from Knockout Mice. *Front Immunol*, *8*, 1686. https://doi.org/10.3389/fimmu.2017.01686

Verma, M. J., Lloyd, A., Rager, H., Strieter, R., Kunkel, S., Taub, D., & Wakefield, D. (1997). Chemokines in acute anterior uveitis. *Curr Eye Res*, *16*(12), 1202-1208. https://doi.org/10.1076/ceyr.16.12.1202.5034

Vijayasaradhi, S., & Houghton, A. N. (1991). Purification of an autoantigenic 75-kDa human melanosomal glycoprotein. *Int J Cancer*, *47*(2), 298-303. https://doi.org/10.1002/ijc.2910470221

Vinod, K., Gedde, S. J., Feuer, W. J., Panarelli, J. F., Chang, T. C., Chen, P. P., & Parrish, R. K., 2nd. (2017). Practice Preferences for Glaucoma Surgery: A Survey of the American Glaucoma Society. *J Glaucoma*, *26*(8), 687-693. https://doi.org/10.1097/ijg.0000000000000720

Vischer, U. (2006). von Willebrand factor, endothelial dysfunction, and cardiovascular disease. *Journal of thrombosis and haemostasis*, *4*(6), 1186-1193.

Vithana, E. N., Khor, C. C., Qiao, C., Nongpiur, M. E., George, R., Chen, L. J., Do, T., Abu-Amero, K., Huang, C. K., Low, S., Tajudin, L. A., Perera, S. A., Cheng, C. Y., Xu, L., Jia, H., Ho, C. L., Sim, K. S., Wu, R. Y., Tham, C. C. Y., . . . Aung, T. (2012). Genome-wide association analyses identify three new susceptibility loci for primary angle closure glaucoma. *Nat Genet*, *44*(10), 1142-1146. https://doi.org/10.1038/ng.2390

Wagner, I. V., Stewart, M. W., & Dorairaj, S. K. (2022). Updates on the Diagnosis and Management of Glaucoma. *Mayo Clin Proc Innov Qual Outcomes*, *6*(6), 618-635. https://doi.org/10.1016/j.mayocpiqo.2022.09.007

Wan, Y., Li, J., Pu, J., Yang, J., Pei, C., & Qi, Y. (2024). Role of caspase-11 non-canonical inflammasomes in retinal ischemia/reperfusion injury. *Molecular Medicine*, *30*(1), 159. https://doi.org/10.1186/s10020-024-00938-0

Wang, D., Huang, W., Li, Y., Zheng, Y., Foster, P. J., Congdon, N., & He, M. (2011). Intraocular pressure, central corneal thickness, and glaucoma in chinese adults: the liwan eye study. *American Journal of Ophthalmology*, *152*(3), 454-462. e451.

Wang, F. (2024). Interleukin-18 binding protein: Biological properties and roles in human and animal immune regulation (Review). *Biomed Rep*, *20*(6), 87. https://doi.org/10.3892/br.2024.1775

Wang, J., & Dong, Y. (2016). Characterization of intraocular pressure pattern and changes of retinal ganglion cells in DBA2J glaucoma mice. *Int J Ophthalmol*, *9*(2), 211-217. https://doi.org/10.18240/ijo.2016.02.05

Wang, J. J., Mitchell, P., & Smith, W. (1997). Is There an Association between Migraine Headache and Open-angle Glaucoma?: Findings from the Blue Mountains Eye Study. *Ophthalmology*, *104*(10), 1714-1719. https://doi.org/https://doi.org/10.1016/S0161-6420(97)30075-X

Wang, J. J., Zhu, M., & Le, Y. Z. (2015). Functions of Müller cell-derived vascular endothelial growth factor in diabetic retinopathy. *World J Diabetes*, *6*(5), 726-733. https://doi.org/10.4239/wjd.v6.i5.726

Wang, X., Lou, N., Eberhardt, A., Yang, Y., Kusk, P., Xu, Q., Förstera, B., Peng, S., Shi, M., Ladrón-de-Guevara, A., Delle, C., Sigurdsson, B., Xavier, A. L. R., Ertürk, A., Libby, R. T., Chen, L., Thrane, A. S., & Nedergaard, M. (2020). An ocular glymphatic clearance system removes β-amyloid from the rodent eye. *Science Translational Medicine*, *12*(536), eaaw3210. https://doi.org/doi:10.1126/scitranslmed.aaw3210

Wang, Y., Chen, S., Wang, J., Liu, Y., Chen, Y., Wen, T., Fang, X., Vidal-Sanz, M., Jonas, J. B., & Zhang, X. (2021). MicroRNA-93/STAT3 signalling pathway mediates retinal microglial activation and protects retinal ganglion cells in an acute ocular hypertension model. *Cell Death & Disease*, *12*(1), 41. https://doi.org/10.1038/s41419-020-03337-5

Wang, Z., Liu, C. H., Huang, S., Fu, Z., Tomita, Y., Britton, W. R., Cho, S. S., Chen, C. T., Sun, Y., Ma, J. X., He, X., & Chen, J. (2020). Wnt signaling activates MFSD2A to suppress vascular endothelial transcytosis and maintain blood-retinal barrier. *Sci Adv*, *6*(35), eaba7457. https://doi.org/10.1126/sciadv.aba7457

Wareham, L. K., & Calkins, D. J. (2020). The Neurovascular Unit in Glaucomatous Neurodegeneration. *Front Cell Dev Biol*, *8*, 452. https://doi.org/10.3389/fcell.2020.00452

Weinreb, R. N., Aung, T., & Medeiros, F. A. (2014). The Pathophysiology and Treatment of Glaucoma: A Review. *JAMA*, *311*(18), 1901-1911. https://doi.org/10.1001/jama.2014.3192

Weinreb, R. N., Scassellati Sforzolini, B., Vittitow, J., & Liebmann, J. (2016). Latanoprostene Bunod 0.024% versus Timolol Maleate 0.5% in Subjects with Open-Angle Glaucoma or Ocular Hypertension: The APOLLO Study. *Ophthalmology*, *123*(5), 965-973. https://doi.org/10.1016/j.ophtha.2016.01.019

Wetsel, R. A., Fleischer, D. T., & Haviland, D. L. (1990). Deficiency of the murine fifth complement component (C5). A 2-base pair gene deletion in a 5'-exon. *Journal of Biological Chemistry*, *265*(5), 2435-2440. https://doi.org/https://doi.org/10.1016/S0021-9258(19)39817-5

Whitlock, N. A., McKnight, B., Corcoran, K. N., Rodriguez, L. A., & Rice, D. S. (2010). Increased intraocular pressure in mice treated with dexamethasone. *Invest Ophthalmol Vis Sci*, *51*(12), 6496-6503. https://doi.org/10.1167/iovs.10-5430

Wiggs, J. L. (2015). Glaucoma Genes and Mechanisms. *Prog Mol Biol Transl Sci*, *134*, 315-342. https://doi.org/10.1016/bs.pmbts.2015.04.008

Wiggs, J. L., Kang, J. H., Yaspan, B. L., Mirel, D. B., Laurie, C., Crenshaw, A., Brodeur, W., Gogarten, S., Olson, L. M., Abdrabou, W., DelBono, E., Loomis, S., Haines, J. L., & Pasquale, L. R. (2011). Common variants near CAV1 and CAV2 are associated with primary open-angle glaucoma in Caucasians from the USA. *Hum Mol Genet*, *20*(23), 4707-4713. https://doi.org/10.1093/hmg/ddr382

Wiggs, J. L., & Pasquale, L. R. (2017). Genetics of glaucoma. *Hum Mol Genet*, *26*(R1), R21-r27. https://doi.org/10.1093/hmg/ddx184

Wiggs, J. L., Yaspan, B. L., Hauser, M. A., Kang, J. H., Allingham, R. R., Olson, L. M., Abdrabou, W., Fan, B. J., Wang, D. Y., Brodeur, W., Budenz, D. L., Caprioli, J., Crenshaw, A., Crooks, K., Delbono, E., Doheny, K. F., Friedman, D. S., Gaasterland, D., Gaasterland, T., . . . Haines, J. L. (2012). Common variants at

9p21 and 8q22 are associated with increased susceptibility to optic nerve degeneration in glaucoma. *PLoS Genet*, *8*(4), e1002654. https://doi.org/10.1371/journal.pgen.1002654

Wilbanks, G. A., & Wayne Streilein, J. (1992). Fluids from immune privileged sites endow macrophages with the capacity to induce antigen-specific immune deviation via a mechanism involving transforming growth factor-β. *European Journal of Immunology*, *22*(4), 1031-1036. https://doi.org/https://doi.org/10.1002/eji.1830220423

Wild, P., Farhan, H., McEwan, D. G., Wagner, S., Rogov, V. V., Brady, N. R., Richter, B., Korac, J., Waidmann, O., Choudhary, C., Dötsch, V., Bumann, D., & Dikic, I. (2011). Phosphorylation of the autophagy receptor optineurin restricts Salmonella growth. *Science*, *333*(6039), 228-233. https://doi.org/10.1126/science.1205405

Winger, R. C., Koblinski, J. E., Kanda, T., Ransohoff, R. M., & Muller, W. A. (2014). Rapid remodeling of tight junctions during paracellular diapedesis in a human model of the blood-brain barrier. *J Immunol*, *193*(5), 2427-2437. https://doi.org/10.4049/jimmunol.1400700

Winkler, N. S., & Fautsch, M. P. (2013). Effects of Prostaglandin Analogues on Aqueous Humor Outflow Pathways. *Journal of Ocular pharmacology and therapeutics*, *30*(2-3), 102-109. https://doi.org/10.1089/jop.2013.0179

Wong-Riley, M. T. (2010). Energy metabolism of the visual system. *Eye Brain*, *2*, 99-116. https://doi.org/10.2147/eb.S9078

Wooff, Y., Man, S. M., Aggio-Bruce, R., Natoli, R., & Fernando, N. (2019). IL-1 Family Members Mediate Cell Death, Inflammation and Angiogenesis in Retinal Degenerative Diseases. *Front Immunol*, *10*, 1618. https://doi.org/10.3389/fimmu.2019.01618

Wu, P., Tang, X., Cui, K., Wu, P., & Liang, X. (2022). OLT1177 (Dapansutrile) Attenuates Retinal Neovascularization by Inhibiting NLRP3 Inflammasome Activation. *Investigative Ophthalmology & Visual Science*, *63*(7), 1759 – F0219-1759 – F0219.

Yabana, T., Shiga, Y., Kawasaki, R., Omodaka, K., Takahashi, H., Kimura, K., Togashi, K., Horii, T., Sasaki, K., & Yuasa, T. (2017). Evaluating retinal vessel diameter with optical coherence tomography in normal-tension glaucoma patients. *Japanese Journal of Ophthalmology*, *61*, 378-387.

Yam, G. H.-F., Gaplovska-Kysela, K., Zuber, C., & Roth, J. (2007). Aggregated Myocilin Induces Russell Bodies and Causes Apoptosis: Implications for the Pathogenesis of Myocilin-Caused Primary Open-Angle Glaucoma. *The American Journal of Pathology*, *170*(1), 100-109. https://doi.org/https://doi.org/10.2353/ajpath.2007.060806

Yamaguchi, Y., Watanabe, T., Hirakata, A., & Hida, T. (2006). Localization and ontogeny of aquaporin-1 and -4 expression in iris and ciliary epithelial cells in rats. *Cell Tissue Res*, *325*(1), 101-109. https://doi.org/10.1007/s00441-005-0122-z

Yang, A. C., Stevens, M. Y., Chen, M. B., Lee, D. P., Stähli, D., Gate, D., Contrepois, K., Chen, W., Iram, T., Zhang, L., Vest, R. T., Chaney, A., Lehallier, B., Olsson, N., du Bois, H., Hsieh, R., Cropper, H. C., Berdnik, D., Li, L., . . . Wyss-Coray, T. (2020). Physiological blood–brain transport is impaired with age by a shift in transcytosis. *Nature*, *583*(7816), 425-430. https://doi.org/10.1038/s41586-020-2453-z

Yang, D., He, Y., Muñoz-Planillo, R., Liu, Q., & Núñez, G. (2015). Caspase-11 Requires the Pannexin-1 Channel and the Purinergic P2X7 Pore to Mediate Pyroptosis and Endotoxic Shock. *Immunity*, *43*(5), 923-932. https://doi.org/10.1016/j.immuni.2015.10.009

Yang, X., Luo, C., Cai, J., Powell, D. W., Yu, D., Kuehn, M. H., & Tezel, G. (2011). Neurodegenerative and inflammatory pathway components linked to TNF-α/TNFR1 signaling in the glaucomatous human retina. *Investigative Ophthalmology & Visual Science*, *52*(11), 8442-8454.

Yarmohammadi, A., Zangwill, L. M., Diniz-Filho, A., Suh, M. H., Manalastas, P. I., Fatehee, N., Yousefi, S., Belghith, A., Saunders, L. J., & Medeiros, F. A. (2016). Optical coherence tomography angiography vessel density in healthy, glaucoma suspect, and glaucoma eyes. *Investigative Ophthalmology & Visual Science*, *57*(9), OCT451-OCT459.

Young, R. W., & Bok, D. (1969). Participation of the retinal pigment epithelium in the rod outer segment renewal process. *J Cell Biol*, *42*(2), 392-403. https://doi.org/10.1083/jcb.42.2.392

Yuan, L., & Neufeld, A. H. (2001). Activated microglia in the human glaucomatous optic nerve head. *Journal of neuroscience research*, *64*(5), 523-532.

Yun, J. H., Park, S. W., Kim, K. J., Bae, J. S., Lee, E. H., Paek, S. H., Kim, S. U., Ye, S., Kim, J. H., & Cho, C. H. (2017). Endothelial STAT3 activation increases vascular

leakage through downregulating tight junction proteins: implications for diabetic retinopathy. *Journal of Cellular Physiology*, *232*(5), 1123-1134.

Yun-Jia, L., Xi, C., Jie-Qiong, Z., Jing-Yi, Z., Sen, L., & Jian, Y. (2021). Semaphorin3A increases M1-like microglia and retinal ganglion cell apoptosis after optic nerve injury. *Cell & Bioscience*, *11*(1), 97. https://doi.org/10.1186/s13578-021-00603-7

Zaidi, S., Singh, S., Guzman, W., & Husain, S. (2020). Regulation of acetylation and phosphorylation of STAT-3 by delta-opioid receptor (DOR) activation in glaucoma. *Investigative Ophthalmology & Visual Science*, *61*(7), 4955-4955.

Zhang, C., Simón, M., Lim, H., Tolman, N. G., Horbal, L., Juarez, F. A., Bhandari, A., Montgomery, C., & John, S. W. M. (2024). IOP-induced blood-retinal barrier compromise contributes to RGC death in glaucoma (Preprint). *bioRxiv*, 2024.2010.2015.618539. https://doi.org/10.1101/2024.10.15.618539

Zhang, J. L., Song, X. Y., Chen, Y. Y., Nguyen, T. H. A., Zhang, J. Y., Bao, S. S., & Zhang, Y. Y. (2019). Novel inflammatory cytokines (IL-36, 37, 38) in the aqueous humor from patients with chronic primary angle closure glaucoma. *Int Immunopharmacol*, *71*, 164-168. https://doi.org/10.1016/j.intimp.2019.03.016

Zhang, K., & Kaufman, R. J. (2008). From endoplasmic-reticulum stress to the inflammatory response. *Nature*, *454*(7203), 455-462. https://doi.org/10.1038/nature07203

Zhang, X., Clark, A. F., & Yorio, T. (2005). Regulation of glucocorticoid responsiveness in glaucomatous trabecular meshwork cells by glucocorticoid receptor-beta. *Invest Ophthalmol Vis Sci*, *46*(12), 4607-4616. https://doi.org/10.1167/iovs.05-0571

Zhao, B., Zhao, Y., & Sun, X. (2024). Mechanism and therapeutic targets of circulating immune cells in diabetic retinopathy. *Pharmacological Research*, *210*, 107505. https://doi.org/https://doi.org/10.1016/j.phrs.2024.107505

Zhao, J., Solano, M. M., Oldenburg, C. E., Liu, T., Wang, Y., Wang, N., & Lin, S. C. (2019). Prevalence of normal-tension glaucoma in the Chinese population: a systematic review and meta-analysis. *American Journal of Ophthalmology*, *199*, 101-110.

Zhavoronkov, A., Izumchenko, E., Kanherkar, R. R., Teka, M., Cantor, C., Manaye, K., Sidransky, D., West, M. D., Makarev, E., & Csoka, A. B. (2016). Pro-fibrotic pathway activation in trabecular meshwork and lamina cribrosa is the main driving force of glaucoma. *Cell Cycle*, *15*(12), 1643-1652.

Zhou, X., Li, F., Kong, L., Tomita, H., Li, C., & Cao, W. (2005). Involvement of inflammation, degradation, and apoptosis in a mouse model of glaucoma. *J Biol Chem*, *280*(35), 31240-31248. https://doi.org/10.1074/jbc.M502641200

Zode, G. S., Kuehn, M. H., Nishimura, D. Y., Searby, C. C., Mohan, K., Grozdanic, S. D., Bugge, K., Anderson, M. G., Clark, A. F., Stone, E. M., & Sheffield, V. C. (2011). Reduction of ER stress via a chemical chaperone prevents disease phenotypes in a mouse model of primary open angle glaucoma. *J Clin Invest*, *121*(9), 3542-3553. https://doi.org/10.1172/jci58183

Zode, G. S., Sharma, A. B., Lin, X., Searby, C. C., Bugge, K., Kim, G. H., Clark, A. F., & Sheffield, V. C. (2014). Ocular-specific ER stress reduction rescues glaucoma in murine glucocorticoid-induced glaucoma. *J Clin Invest*, *124*(5), 1956-1965. https://doi.org/10.1172/jci69774

# Appendix 1: DEG list for RNA-seq analysis

Glaucoma_early_vs_Naive.deseq2.results_significant_DEGs

| gene_id | baseMean | log2FoldChange | lfcSE | pvalue | padj | SYMBOL |
|---|---|---|---|---|---|---|
| ENSMUSG00000059498.14_Fcgr3 | 27.32238 | 2.238796 | 0.88083098 | 4.761393E-07 | 0.0002442594 | Fcgr3 |
| ENSMUSG00000018774.14_Cd68 | 28.43354 | 2.173894 | 1.03424067 | 9.30708E-07 | 0.0003954662 | Cd68 |
| ENSMUSG00000073418.5_C4b | 125.2086 | 1.866973 | 0.65107875 | 9.421981E-07 | 0.0003954662 | C4b |
| ENSMUSG00000036896.6_C1qc | 99.02991 | 1.856838 | 0.37945711 | 3.224544E-09 | 1.420384E-05 | C1qc |
| ENSMUSG00000022146.13_Osmr | 60.41351 | 1.785234 | 0.45968941 | 1.322632E-07 | 0.0001221319 | Osmr |
| ENSMUSG00000001025.9_S100a6 | 80.87384 | 1.619505 | 0.4428412 | 2.95536E-07 | 0.0002046735 | S100a6 |
| ENSMUSG00000005087.18_Cd44 | 87.94049 | 1.515576 | 0.39820422 | 2.081137E-07 | 0.0001695637 | Cd44 |
| ENSMUSG00000073409.13_H2-Q6 | 24.60088 | 1.336001 | 0.8966724 | 1.566018E-05 | 0.003306241 | H2-Q6 |
| ENSMUSG00000028128.14_F3 | 75.41666 | 1.305819 | 0.35309089 | 3.669339E-07 | 0.0002310183 | F3 |
| ENSMUSG00000029338.14_Antxr2 | 110.7853 | 1.285746 | 0.29600034 | 3.671469E-08 | 6.98922E-05 | Antxr2 |
| ENSMUSG00000026547.16_Tagln2 | 55.58847 | 1.267533 | 0.48962154 | 5.864892E-06 | 0.001692388 | Tagln2 |
| ENSMUSG00000024338.16_Psmb8 | 57.05762 | 1.177258 | 0.4190592 | 4.606597E-06 | 0.001394743 | Psmb8 |
| ENSMUSG00000002325.16_Irf9 | 108.0072 | 1.135954 | 0.36038965 | 2.304457E-06 | 0.0007979758 | Irf9 |
| ENSMUSG00000036887.6_C1qa | 53.76387 | 1.114076 | 0.4537025 | 1.072975E-05 | 0.002562374 | C1qa |
| ENSMUSG00000027078.15_Ube2l6 | 54.29837 | 1.065713 | 0.50570918 | 2.205236E-05 | 0.004350902 | Ube2l6 |
| ENSMUSG00000087168.2_Gm15983 | 130.1613 | 1.056794 | 0.35793729 | 4.453852E-06 | 0.001394743 | Gm15983 |
| ENSMUSG00000021360.17_Gcnt2 | 43.9593 | 0.9709469 | 0.48147217 | 3.348172E-05 | 0.005771627 | Gcnt2 |
| ENSMUSG00000061232.17_H2-K1 | 315.0114 | 0.9683316 | 0.24190177 | 2.607228E-07 | 0.0001900669 | H2-K1 |
| ENSMUSG00000046805.11_Mpeg1 | 26.05173 | 0.9648722 | 0.7429971 | 6.867542E-05 | 0.008647484 | Mpeg1 |
| ENSMUSG00000004040.17_Stat3 | 546.6797 | 0.9461746 | 0.1817361 | 1.425999E-09 | 1.420384E-05 | Stat3 |
| ENSMUSG00000022912.9_Pros1 | 90.54399 | 0.9314399 | 0.33886138 | 9.717881E-06 | 0.002361445 | Pros1 |
| ENSMUSG00000001930.18_Vwf | 51.06012 | 0.9171441 | 0.58195061 | 7.108354E-05 | 0.008790876 | Vwf |
| ENSMUSG00000031762.8_Mt2 | 174.0734 | 0.9092336 | 0.55110538 | 6.748542E-05 | 0.008575601 | Mt2 |
| ENSMUSG00000024206.16_Rfx2 | 77.95385 | 0.900365 | 0.40419204 | 2.940521E-05 | 0.0052895 | Rfx2 |
| ENSMUSG00000002602.17_Axl | 113.8235 | 0.8840303 | 0.29522235 | 6.317912E-06 | 0.001785906 | Axl |
| ENSMUSG00000001123.16_Lgals9 | 39.50677 | 0.8811931 | 0.55745871 | 8.046939E-05 | 0.009526337 | Lgals9 |
| ENSMUSG00000007041.10_Clic1 | 159.9321 | 0.8717788 | 0.29665856 | 7.460877E-06 | 0.001987319 | Clic1 |
| ENSMUSG00000007655.17_Cav1 | 428.0948 | 0.8579373 | 0.18972809 | 4.036803E-08 | 6.98922E-05 | Cav1 |
| ENSMUSG00000032359.15_Ctsh | 160.7727 | 0.8564698 | 0.34937123 | 2.226614E-05 | 0.004350902 | Ctsh |
| ENSMUSG00000060802.9_B2m | 264.9985 | 0.84471 | 0.533042 | 9.159456E-05 | 0.01006886 | B2m |
| ENSMUSG00000031207.17_Msn | 175.703 | 0.8296934 | 0.23447794 | 1.629665E-06 | 0.0006100673 | Msn |
| ENSMUSG00000028635.8_Edn2 | 70.41897 | 0.8241677 | 0.98182904 | 5.403179E-05 | 0.007391326 | Edn2 |
| ENSMUSG00000073411.13_H2-D1 | 995.1638 | 0.8126555 | 0.18149098 | 5.176763E-08 | 7.967038E-05 | H2-D1 |
| ENSMUSG00000031765.9_Mt1 | 1038.378 | 0.8044146 | 0.37390265 | 4.597973E-05 | 0.006922448 | Mt1 |
| ENSMUSG00000067212.9_H2-T23 | 72.92002 | 0.7830147 | 0.39274829 | 6.474678E-05 | 0.00838138 | H2-T23 |
| ENSMUSG00000033880.12_Lgals3bp | 124.1623 | 0.7767133 | 0.33604913 | 3.770674E-05 | 0.006072978 | Lgals3bp |
| ENSMUSG00000028583.15_Pdpn | 248.02 | 0.7692812 | 0.28129125 | 1.599294E-05 | 0.003306241 | Pdpn |
| ENSMUSG00000016918.16_Sulf1 | 297.6971 | 0.7444908 | 0.20291628 | 1.282914E-06 | 0.0005226366 | Sulf1 |
| ENSMUSG00000052160.8_Pld4 | 21.83193 | 0.7350718 | 0.66657222 | 0.0001864672 | 0.01677115 | Pld4 |
| ENSMUSG00000026628.14_Atf3 | 159.2188 | 0.7252147 | 0.63168346 | 0.000198856 | 0.01754366 | Atf3 |
| ENSMUSG00000060550.17_H2-Q7 | 24.27928 | 0.7245009 | 0.71377389 | 0.0001814408 | 0.01657262 | H2-Q7 |
| ENSMUSG00000020467.16_Efemp1 | 365.1446 | 0.6985995 | 0.23056113 | 9.5536E-06 | 0.002361445 | Efemp1 |
| ENSMUSG00000038068.16_Rnf144b | 151.0344 | 0.6962819 | 0.3150028 | 6.05136E-05 | 0.00808263 | Rnf144b |
| ENSMUSG00000030560.18_Ctsc | 112.9115 | 0.6929825 | 0.32855837 | 7.391752E-05 | 0.008980979 | Ctsc |

| | | | | | | |
|---|---|---|---|---|---|---|
| **ENSMUSG00000053279.9_Aldh1a1** | 270.7315 | 0.6904882 | 0.23671843 | 1.30809E-05 | 0.002922316 | Aldh1a1 |
| **ENSMUSG00000027907.5_S100a11** | 41.65606 | 0.6852224 | 0.65026757 | 0.0002350106 | 0.01972807 | S100a11 |
| **ENSMUSG00000023067.15_Cdkn1a** | 75.99805 | 0.6808872 | 0.48485001 | 0.0002155381 | 0.01854297 | Cdkn1a |
| **ENSMUSG00000073421.7_H2-Ab1** | 40.12326 | 0.6787699 | 0.68997024 | 0.0002258627 | 0.01915631 | H2-Ab1 |
| **ENSMUSG00000031239.6_Itm2a** | 99.03616 | 0.6768536 | 0.33741455 | 9.448268E-05 | 0.01025593 | Itm2a |
| **ENSMUSG00000026728.10_Vim** | 696.9822 | 0.6705152 | 0.18127362 | 1.372002E-06 | 0.00054296 | Vim |
| **ENSMUSG00000020932.15_Gfap** | 208.6542 | 0.6633926 | 0.4844486 | 0.0002410769 | 0.01999495 | Gfap |
| **ENSMUSG00000027962.15_Vcam1** | 122.1723 | 0.6582704 | 0.3569908 | 0.0001336298 | 0.01341236 | Vcam1 |
| **ENSMUSG00000029622.17_Arpc1b** | 57.30986 | 0.6572157 | 0.49124163 | 0.0002547982 | 0.0208829 | Arpc1b |
| **ENSMUSG00000071637.6_Cebpd** | 155.2881 | 0.6459822 | 0.6325253 | 0.000284969 | 0.02230003 | Cebpd |
| **ENSMUSG00000118504.2_Gm53012** | 132.6905 | 0.6356644 | 0.26541842 | 5.225494E-05 | 0.007237832 | Gm53012 |
| **ENSMUSG00000120606.1_ENSMUSG00** | 246.1406 | 0.6333791 | 0.216219 | 1.5139E-05 | 0.003276411 | ENSMUSG0 |
| **ENSMUSG00000041378.3_Cldn5** | 81.80455 | 0.6258139 | 0.44622079 | 0.0002793872 | 0.0221131 | Cldn5 |
| **ENSMUSG00000111755.2_Gm47160** | 178.817 | 0.5943627 | 0.26667222 | 8.631794E-05 | 0.009963249 | Gm47160 |
| **ENSMUSG00000054793.9_Cadm4** | 182.2208 | -0.5923235 | 0.3792487 | 0.0002724054 | 0.02193656 | Cadm4 |
| **ENSMUSG00000038740.10_Mvb12b** | 226.4341 | -0.5932813 | 0.33032597 | 0.0001913187 | 0.0169869 | Mvb12b |
| **ENSMUSG00000032988.5_Slc16a8** | 31.22625 | -0.5938545 | 0.64809653 | 0.0003427296 | 0.02549642 | Slc16a8 |
| **ENSMUSG00000034684.13_Sema3f** | 591.3333 | -0.5959774 | 0.18362777 | 7.161355E-06 | 0.001983839 | Sema3f |
| **ENSMUSG00000020723.4_Cacng4** | 246.4573 | -0.5964663 | 0.27990182 | 0.000103757 | 0.01097052 | Cacng4 |
| **ENSMUSG00000032011.6_Thy1** | 607.1082 | -0.5982428 | 0.17485944 | 4.175987E-06 | 0.001345153 | Thy1 |
| **ENSMUSG00000033768.18_Nrxn2** | 702.9043 | -0.6002646 | 0.19814774 | 1.297582E-05 | 0.002922316 | Nrxn2 |
| **ENSMUSG00000036948.18_Trappc14** | 103.3519 | -0.6170033 | 0.48983549 | 0.0003282993 | 0.02500092 | Trappc14 |
| **ENSMUSG00000007670.11_Khsrp** | 458.7083 | -0.620327 | 0.23688476 | 3.37522E-05 | 0.005771627 | Khsrp |
| **ENSMUSG00000096883.3_Shisa8** | 123.8264 | -0.6288123 | 0.27969885 | 7.243647E-05 | 0.008878916 | Shisa8 |
| **ENSMUSG00000038502.18_Ptov1** | 807.0212 | -0.6306841 | 0.15513307 | 3.985027E-07 | 0.0002399853 | Ptov1 |
| **ENSMUSG00000021536.8_Adcy2** | 303.9692 | -0.6350719 | 0.19875571 | 7.321014E-06 | 0.001987319 | Adcy2 |
| **ENSMUSG00000048142.10_Nat8l** | 295.712 | -0.6387973 | 0.20172507 | 7.849059E-06 | 0.00205127 | Nat8l |
| **ENSMUSG00000020701.13_Tmem132e** | 85.55218 | -0.6438877 | 0.42001757 | 0.0002219307 | 0.01897507 | Tmem132e |
| **ENSMUSG00000039809.11_Gabbr2** | 303.4935 | -0.660346 | 0.22421407 | 1.334284E-05 | 0.002933518 | Gabbr2 |
| **ENSMUSG00000045532.6_C1ql1** | 299.3419 | -0.6810347 | 0.33421242 | 8.792409E-05 | 0.00998352 | C1ql1 |
| **ENSMUSG00000028677.20_Rnf220** | 859.1194 | -0.7017728 | 0.16149144 | 1.080364E-07 | 0.0001068866 | Rnf220 |
| **ENSMUSG00000042388.15_Dlgap3** | 210.4433 | -0.704908 | 0.32289932 | 6.172811E-05 | 0.00808263 | Dlgap3 |
| **ENSMUSG00000040105.4_Plpp6** | 149.4898 | -0.7066528 | 0.3047784 | 4.729309E-05 | 0.007043619 | Plpp6 |
| **ENSMUSG00000028782.15_Adgrb2** | 214.0571 | -0.7088766 | 0.2655037 | 2.230265E-05 | 0.004350902 | Adgrb2 |
| **ENSMUSG00000034472.14_Rasd2** | 114.1641 | -0.7123121 | 0.31339553 | 5.06824E-05 | 0.007232204 | Rasd2 |
| **ENSMUSG00000010517.8_Faf1** | 245.234 | -0.7132782 | 0.18434977 | 6.83297E-07 | 0.0003154782 | Faf1 |
| **ENSMUSG00000039910.11_Cited2** | 579.6064 | -0.7171221 | 0.20712986 | 2.651458E-06 | 0.0008957401 | Cited2 |
| **ENSMUSG00000119584.1_Rn18s-rs5** | 16286.06 | -0.7217358 | 0.14313414 | 4.101897E-09 | 1.420384E-05 | Rn18s-rs5 |
| **ENSMUSG00000025576.18_Rbfox3** | 166.6508 | -0.7644675 | 0.3207683 | 3.417023E-05 | 0.005771799 | Rbfox3 |
| **ENSMUSG00000080058.3_Gm11175** | 34.42211 | -0.7702609 | 0.68010874 | 0.0001586621 | 0.01536803 | Gm11175 |
| **ENSMUSG00000026959.14_Grin1** | 415.3226 | -0.7933752 | 0.18040833 | 7.476343E-08 | 9.414075E-05 | Grin1 |
| **ENSMUSG00000118642.2_AY036118** | 46.33257 | -0.8320596 | 0.50655475 | 8.975582E-05 | 0.00998352 | AY036118 |
| **ENSMUSG00000020396.9_Nefh** | 386.0855 | -0.8813838 | 0.23210753 | 6.360013E-07 | 0.0003037674 | Nefh |
| **ENSMUSG00000030600.16_Lrfn1** | 73.83482 | -0.8923128 | 0.53427698 | 6.99059E-05 | 0.008723123 | Lrfn1 |
| **ENSMUSG00000028889.18_Yrdc** | 127.5 | -0.897752 | 0.25533893 | 1.501601E-06 | 0.0005777408 | Yrdc |
| **ENSMUSG00000002763.17_Pex6** | 242.5931 | -0.9168866 | 0.20908696 | 6.598898E-08 | 9.140134E-05 | Pex6 |

Glaucoma_mid_vs_Naive.deseq2.results_significant_DEGs

| gene_id | baseMean | log2FoldChange | lfcSE | pvalue | padj | SYMBOL |
|---|---|---|---|---|---|---|
| **ENSMUSG00000073418.5_C4b** | 125.2086 | 3.628925 | 0.54594297 | 1.01519E-12 | 4.888478E-09 | C4b |
| **ENSMUSG00000028635.8_Edn2** | 70.41897 | 3.184384 | 1.20629144 | 5.646318E-07 | 0.0005437781 | Edn2 |
| **ENSMUSG00000087168.2_Gm15983** | 130.1613 | 1.704966 | 0.29591216 | 2.244684E-10 | 5.404452E-07 | Gm15983 |
| **ENSMUSG00000012428.10_Steap4** | 18.92477 | 1.617709 | 1.87178755 | 1.326423E-05 | 0.004913206 | Steap4 |
| **ENSMUSG00000069516.9_Lyz2** | 215.3701 | 1.579386 | 1.84031204 | 1.403235E-05 | 0.00494418 | Lyz2 |
| **ENSMUSG00000001288.16_Rarg** | 32.09305 | 1.44778 | 1.36173323 | 1.374061E-05 | 0.00494418 | Rarg |
| **ENSMUSG00000070498.4_Tmem132b** | 84.48132 | 1.277831 | 0.41778056 | 2.830963E-07 | 0.0003145853 | Tmem132b |
| **ENSMUSG00000026822.15_Lcn2** | 241.6967 | 1.18925 | 1.72565132 | 2.441372E-05 | 0.006192397 | Lcn2 |
| **ENSMUSG00000103436.2_Gm36995** | 48.40187 | 1.003613 | 0.65408408 | 9.846673E-06 | 0.004310456 | Gm36995 |
| **ENSMUSG00000024206.16_Rfx2** | 77.95385 | 0.9971607 | 0.50630257 | 2.875726E-06 | 0.001797764 | Rfx2 |
| **ENSMUSG00000103897.2_Pcdhga8** | 60.16329 | 0.9952951 | 0.58447066 | 6.302765E-06 | 0.003139646 | Pcdhga8 |
| **ENSMUSG00000030111.10_A2m** | 59.20573 | 0.9235141 | 0.71734316 | 1.918901E-05 | 0.00543538 | A2m |
| **ENSMUSG00000041782.15_Lad1** | 26.904 | 0.8931658 | 0.9620265 | 3.675134E-05 | 0.007946152 | Lad1 |
| **ENSMUSG00000054509.8_Parp4** | 88.90314 | 0.8576727 | 0.47071604 | 4.1043E-06 | 0.002371629 | Parp4 |
| **ENSMUSG00000004040.17_Stat3** | 546.6797 | 0.768647 | 0.24799443 | 1.79117E-08 | 3.234405E-05 | Stat3 |
| **ENSMUSG00000102523.2_Gm37783** | 34.45711 | 0.7574104 | 0.64856096 | 3.343126E-05 | 0.00766584 | Gm37783 |
| **ENSMUSG00000029720.10_Gm20605** | 289.4556 | 0.7184338 | 0.34114188 | 1.412229E-06 | 0.001020053 | Gm20605 |
| **ENSMUSG00000110997.2_2610028D06Rik** | 70.85802 | 0.7015127 | 0.45941135 | 1.27683E-05 | 0.00485397 | 2610028D06Rik |
| **ENSMUSG00000003810.15_Mast2** | 811.5091 | 0.6397852 | 0.14862905 | 1.452541E-10 | 4.196682E-07 | Mast2 |
| **ENSMUSG00000089736.3_Tgfbr3l** | 78.95697 | 0.6364956 | 0.46004199 | 2.417218E-05 | 0.006192397 | Tgfbr3l |
| **ENSMUSG00000021091.9_Serpina3n** | 113.3595 | 0.6181785 | 1.19011677 | 8.660284E-05 | 0.01268545 | Serpina3n |
| **ENSMUSG00000025650.14_Col7a1** | 81.94956 | 0.6081526 | 0.42454448 | 2.293302E-05 | 0.006135009 | Col7a1 |
| **ENSMUSG00000057802.10_Gm10030** | 20.44716 | 0.6068509 | 0.70584692 | 8.790229E-05 | 0.01268545 | Gm10030 |
| **ENSMUSG00000002325.16_Irf9** | 108.0072 | 0.6039718 | 0.44182703 | 2.854702E-05 | 0.006760496 | Irf9 |
| **ENSMUSG00000050556.10_Kcnb1** | 10045.26 | 0.6013035 | 0.11932126 | 1.139787E-11 | 4.11634E-08 | Kcnb1 |
| **ENSMUSG00000037225.14_Fgf2** | 164.8499 | 0.5928878 | 0.62997793 | 8.388978E-05 | 0.01268545 | Fgf2 |
| **ENSMUSG00000034156.17_Tspoap1** | 491.7091 | 0.5917699 | 0.2349654 | 6.384641E-07 | 0.0005764533 | Tspoap1 |
| **ENSMUSG00000037355.15_Uvssa** | 138.6664 | 0.5831981 | 0.29883693 | 4.862254E-06 | 0.002508576 | Uvssa |
| **ENSMUSG00000048489.13_Depp1** | 23.45403 | -0.7011224 | 0.84292507 | 6.565494E-05 | 0.01142712 | Depp1 |
| **ENSMUSG00000064360.1_mt-Nd3** | 751.8625 | -1.493541 | 0.19422918 | 1.747984E-15 | 2.525137E-11 | mt-Nd3 |

Glaucoma_late_vs_Naive.deseq2.results_significant_DEGs

| gene_id | baseMean | log2FoldChange | lfcSE | pvalue | padj | SYMBOL |
|---|---|---|---|---|---|---|
| **ENSMUSG00000012428.10_Steap4** | 18.92477 | 4.743335 | 1.11422696 | 5.929985E-08 | 0.0001070807 | Steap4 |
| **ENSMUSG00000026822.15_Lcn2** | 241.6967 | 3.88651 | 1.71939814 | 1.172803E-06 | 0.001058895 | Lcn2 |
| **ENSMUSG00000073418.5_C4b** | 125.2086 | 3.556709 | 0.55585267 | 3.215558E-12 | 1.548398E-08 | C4b |
| **ENSMUSG00000064246.11_Chil1** | 342.1569 | 2.257658 | 1.30721486 | 5.45362E-06 | 0.00338671 | Chil1 |
| **ENSMUSG00000018774.14_Cd68** | 28.43354 | 2.236806 | 1.28113683 | 5.374343E-06 | 0.00338671 | Cd68 |
| **ENSMUSG00000069516.9_Lyz2** | 215.3701 | 2.186513 | 1.94958529 | 1.190237E-05 | 0.004912618 | Lyz2 |
| **ENSMUSG00000106994.2_Gm10829** | 40.86597 | 1.783599 | 0.41658366 | 1.095548E-07 | 0.0001582629 | Gm10829 |
| **ENSMUSG00000103436.2_Gm36995** | 48.40187 | 1.631432 | 0.47373145 | 6.861017E-07 | 0.0007079589 | Gm36995 |
| **ENSMUSG00000030111.10_A2m** | 59.20573 | 1.477818 | 0.65586653 | 4.868562E-06 | 0.003349107 | A2m |
| **ENSMUSG00000028635.8_Edn2** | 70.41897 | 1.365521 | 1.42488903 | 3.141254E-05 | 0.01013825 | Edn2 |
| **ENSMUSG00000029338.14_Antxr2** | 110.7853 | 1.302729 | 0.30614886 | 1.240161E-07 | 0.000162867 | Antxr2 |
| **ENSMUSG00000110997.2_2610028D06Rik** | 70.85802 | 1.211716 | 0.4035838 | 1.332705E-06 | 0.001132486 | 2610028D06Rik |
| **ENSMUSG00000024164.16_C3** | 53.7592 | 1.155173 | 1.77737088 | 4.599258E-05 | 0.01208016 | C3 |
| **ENSMUSG00000102653.2_Gm37079** | 49.36809 | 1.105753 | 0.56868227 | 9.635357E-06 | 0.004490076 | Gm37079 |
| **ENSMUSG00000087168.2_Gm15983** | 130.1613 | 0.8844513 | 0.50277545 | 1.330452E-05 | 0.005338807 | Gm15983 |
| **ENSMUSG00000023191.10_P3h3** | 104.3689 | 0.8470777 | 0.41477561 | 5.626543E-06 | 0.00338671 | P3h3 |
| **ENSMUSG00000055320.19_Tead1** | 105.978 | 0.8238698 | 0.54713986 | 2.565672E-05 | 0.009039926 | Tead1 |
| **ENSMUSG00000036896.6_C1qc** | 99.02991 | 0.7307306 | 0.61537781 | 6.211226E-05 | 0.01428852 | C1qc |
| **ENSMUSG00000002028.14_Kmt2a** | 1337.375 | 0.6649741 | 0.16800578 | 6.634124E-10 | 1.597276E-06 | Kmt2a |
| **ENSMUSG00000059434.10_Gckr** | 231.7532 | 0.6138226 | 0.38595052 | 1.779997E-05 | 0.006593293 | Gckr |
| **ENSMUSG00000074064.7_Mlycd** | 186.1111 | -0.5936 | 0.43813017 | 4.196961E-05 | 0.01124997 | Mlycd |
| **ENSMUSG00000055493.5_Epm2a** | 181.1125 | -0.6425539 | 0.49004175 | 4.703964E-05 | 0.01213455 | Epm2a |
| **ENSMUSG00000044982.8_Sft2d3** | 209.2811 | -0.7527634 | 0.62740569 | 5.875095E-05 | 0.01418975 | Sft2d3 |
| **ENSMUSG00000024750.12_Zfand5** | 711.196 | -0.8202813 | 0.24706969 | 8.480167E-08 | 0.0001361161 | Zfand5 |
| **ENSMUSG00000028677.20_Rnf220** | 859.1194 | -0.9556138 | 0.16103225 | 5.270801E-11 | 1.90355E-07 | Rnf220 |
| **ENSMUSG00000040105.4_Plpp6** | 149.4898 | -1.019659 | 0.35716489 | 1.137201E-06 | 0.001058895 | Plpp6 |
| **ENSMUSG00000039910.11_Cited2** | 579.6064 | -1.045241 | 0.20352188 | 3.218816E-09 | 6.642717E-06 | Cited2 |
| **ENSMUSG00000010517.8_Faf1** | 245.234 | -1.227795 | 0.17459339 | 4.494358E-13 | 6.492549E-09 | Faf1 |
| **ENSMUSG00000044795.13_Cyb5d1** | 59.09886 | -1.259366 | 0.69398158 | 1.142555E-05 | 0.004854515 | Cyb5d1 |
| **ENSMUSG00000044502.17_Bod1** | 408.011 | -1.365082 | 0.20324586 | 3.00108E-12 | 1.548398E-08 | Bod1 |
| **ENSMUSG00000040331.17_Nsmce4a** | 374.6564 | -1.388648 | 0.46126383 | 1.506964E-06 | 0.001209422 | Nsmce4a |
| **ENSMUSG00000028889.18_Yrdc** | 127.5 | -1.462243 | 0.23671189 | 7.193132E-11 | 2.07824E-07 | Yrdc |
| **ENSMUSG00000071076.9_Jund** | 363.2943 | -1.480549 | 1.03602043 | 1.553681E-05 | 0.006051521 | Jund |
| **ENSMUSG00000080058.3_Gm11175** | 34.42211 | -2.414743 | 0.69558539 | 3.243071E-07 | 0.00036038 | Gm11175 |

Crush_early_vs_Naive.deseq2.results_significant_DEGs

| gene_id | baseMean | log2FoldChange | lfcSE | pvalue | padj | SYMBOL |
|---|---|---|---|---|---|---|
| ENSMUSG00000018774.14_Cd68 | 28.43354 | 2.866369 | 1.02125666 | 1.196891E-07 | 0.0001105209 | Cd68 |
| ENSMUSG00000063632.7_Sox11 | 36.20163 | 2.201169 | 0.69826526 | 2.871994E-07 | 0.0002093683 | Sox11 |
| ENSMUSG00000030111.10_A2m | 59.20573 | 1.868945 | 0.44064985 | 7.466257E-08 | 7.95501E-05 | A2m |
| ENSMUSG00000087006.4_Gm13889 | 88.42172 | 1.756227 | 0.3350285 | 1.888433E-09 | 4.359447E-06 | Gm13889 |
| ENSMUSG00000026628.14_Atf3 | 159.2188 | 1.752424 | 0.56211166 | 9.928948E-07 | 0.0005501035 | Atf3 |
| ENSMUSG00000005667.9_Mthfd2 | 108.8285 | 1.569446 | 0.31332202 | 5.159737E-09 | 1.020965E-05 | Mthfd2 |
| ENSMUSG00000023067.15_Cdkn1a | 75.99805 | 1.434881 | 0.41839819 | 8.873915E-07 | 0.0005344026 | Cdkn1a |
| ENSMUSG00000041313.15_Slc7a1 | 144.7745 | 1.177533 | 0.37459977 | 1.98509E-06 | 0.0008331963 | Slc7a1 |
| ENSMUSG00000037447.17_Arid5a | 73.81704 | 1.075198 | 0.3794952 | 4.346784E-06 | 0.001672425 | Arid5a |
| ENSMUSG00000010755.18_Cars | 353.5304 | 1.025857 | 0.17633864 | 1.709869E-11 | 1.78259E-07 | Cars |
| ENSMUSG00000053398.12_Phgdh | 104.8708 | 1.018561 | 0.44383581 | 1.308795E-05 | 0.003940896 | Phgdh |
| ENSMUSG00000032802.9_Srxn1 | 560.6782 | 0.9443786 | 0.20903215 | 2.1634E-08 | 2.724114E-05 | Srxn1 |
| ENSMUSG00000029552.20_Tes | 65.01271 | 0.9135371 | 0.54196375 | 4.18414E-05 | 0.0098228 | Tes |
| ENSMUSG00000007041.10_Clic1 | 159.9321 | 0.8828332 | 0.30892893 | 5.921394E-06 | 0.002158348 | Clic1 |
| ENSMUSG00000040354.15_Mars1 | 619.8831 | 0.8459447 | 0.2091412 | 2.286087E-07 | 0.0001759144 | Mars1 |
| ENSMUSG00000037428.15_Vgf | 127.701 | 0.7700054 | 0.40529862 | 4.516836E-05 | 0.01026626 | Vgf |
| ENSMUSG00000073418.5_C4b | 125.2086 | 0.758592 | 0.78929912 | 0.000103784 | 0.01891464 | C4b |
| ENSMUSG00000037851.14_Iars | 432.4963 | 0.755164 | 0.15107951 | 6.158792E-09 | 1.066318E-05 | Iars |
| ENSMUSG00000004040.17_Stat3 | 546.6797 | 0.7450524 | 0.18569596 | 4.306021E-07 | 0.0002711032 | Stat3 |
| ENSMUSG00000028811.13_Yars | 631.1348 | 0.710086 | 0.16535012 | 1.894132E-07 | 0.0001543272 | Yars |
| ENSMUSG00000036896.6_C1qc | 99.02991 | 0.7036572 | 0.55670059 | 0.0001265607 | 0.02164188 | C1qc |
| ENSMUSG00000031207.17_Msn | 175.703 | 0.6685071 | 0.25536328 | 1.955401E-05 | 0.005527401 | Msn |
| ENSMUSG00000029777.11_Gars | 785.0407 | 0.6511224 | 0.14615494 | 1.443207E-07 | 0.0001249366 | Gars |
| ENSMUSG00000022098.11_Bmp1 | 89.81959 | 0.630652 | 0.51197846 | 0.0001703649 | 0.02712326 | Bmp1 |
| ENSMUSG00000030272.16_Camk1 | 233.4755 | 0.6087189 | 0.31036577 | 7.369959E-05 | 0.01417796 | Camk1 |
| ENSMUSG00000120606.1_ENSMUSG00000120606 | 246.1406 | 0.5848772 | 0.22575619 | 2.866934E-05 | 0.007353686 | ENSMUSG00000120606 |
| ENSMUSG00000024206.16_Rfx2 | 77.95385 | 0.5820371 | 0.45004501 | 0.0001953608 | 0.02941242 | Rfx2 |
| ENSMUSG00000022241.7_Tars | 399.7727 | 0.5817641 | 0.17636169 | 6.672292E-06 | 0.002254096 | Tars |
| ENSMUSG00000034926.4_Dhcr24 | 461.2995 | -0.6031889 | 0.18810734 | 7.66619E-06 | 0.0025282 | Dhcr24 |
| ENSMUSG00000032011.6_Thy1 | 607.1082 | -0.61847 | 0.16337884 | 1.641672E-06 | 0.0007720669 | Thy1 |
| ENSMUSG00000021728.9_Emb | 223.6713 | -0.6441661 | 0.19962614 | 6.245281E-06 | 0.002218036 | Emb |
| ENSMUSG00000042182.17_Bend6 | 333.2499 | -0.6671356 | 0.16068572 | 4.084199E-07 | 0.0002693821 | Bend6 |
| ENSMUSG00000074968.12_Ano3 | 72.36011 | -0.6964591 | 0.51099161 | 0.0001174647 | 0.02033755 | Ano3 |
| ENSMUSG00000022055.8_Nefl | 3135.109 | -0.7219768 | 0.1461059 | 1.054789E-08 | 1.460989E-05 | Nefl |
| ENSMUSG00000028926.16_Cdk14 | 687.8001 | -0.7604479 | 0.15550305 | 1.005285E-08 | 1.460989E-05 | Cdk14 |
| ENSMUSG00000050822.12_Slc29a4 | 122.238 | -0.7683019 | 0.31711966 | 1.926386E-05 | 0.005527401 | Slc29a4 |
| ENSMUSG00000067242.12_Lgi1 | 49.21831 | -0.7807632 | 0.61170113 | 9.646441E-05 | 0.01805579 | Lgi1 |
| ENSMUSG00000034648.10_Lrrn1 | 97.65444 | -0.7855585 | 0.35915826 | 2.730419E-05 | 0.007135666 | Lrrn1 |
| ENSMUSG00000064360.1_mt-Nd3 | 751.8625 | -0.8276269 | 0.21095595 | 3.850467E-07 | 0.0002666641 | mt-Nd3 |
| ENSMUSG00000038530.12_Rgs4 | 359.8645 | -0.8383289 | 0.2340883 | 1.10683E-06 | 0.0005678036 | Rgs4 |
| ENSMUSG00000058441.8_Panx2 | 195.8999 | -0.8856643 | 0.26683137 | 1.971456E-06 | 0.0008331963 | Panx2 |
| ENSMUSG00000026347.14_Tmem163 | 95.92404 | -0.8899047 | 0.3606988 | 1.259526E-05 | 0.003876821 | Tmem163 |
| ENSMUSG00000032564.17_Cpne4 | 68.18191 | -0.8993738 | 0.46342886 | 2.997411E-05 | 0.007413775 | Cpne4 |
| ENSMUSG00000020635.9_Fkbp1b | 40.2908 | -0.9101579 | 0.60572842 | 5.271079E-05 | 0.01123226 | Fkbp1b |
| ENSMUSG00000031492.14_Chrnb3 | 378.6815 | -1.110437 | 0.21138532 | 4.757819E-10 | 1.34976E-06 | Chrnb3 |
| ENSMUSG00000022454.18_Nell2 | 225.6444 | -1.140907 | 0.21688305 | 4.872427E-10 | 1.34976E-06 | Nell2 |
| ENSMUSG00000031491.11_Chrna6 | 571.1376 | -1.213956 | 0.35326849 | 9.529993E-07 | 0.0005499997 | Chrna6 |
| ENSMUSG00000020396.9_Nefh | 386.0855 | -1.278847 | 0.22240231 | 5.19386E-11 | 2.398005E-07 | Nefh |
| ENSMUSG00000069372.4_Ctxn3 | 58.14415 | -1.56401 | 0.37049162 | 1.048577E-07 | 0.0001037418 | Ctxn3 |
| ENSMUSG00000032387.16_Rbpms2 | 158.3184 | -1.599662 | 0.26439797 | 2.573951E-11 | 1.78259E-07 | Rbpms2 |
| ENSMUSG00000046480.7_Scn4b | 44.84776 | -1.823281 | 0.70737314 | 1.685479E-06 | 0.0007720669 | Scn4b |
| ENSMUSG00000061167.10_Rpl15-ps3 | 39.37808 | -7.386238 | 1.8389749 | 4.184689E-08 | 4.830178E-05 | Rpl15-ps3 |

Crush_late_vs_Naive.deseq2.results_significant_DEGs

| gene_id | baseMean | log2FoldChange | lfcSE | pvalue | padj | SYMBOL |
|---|---|---|---|---|---|---|
| **ENSMUSG00000028635.8_Edn2** | 70.41897 | 3.737248 | 0.79408155 | 4.21477E-08 | 6.401026E-06 | Edn2 |
| **ENSMUSG00000059498.14_Fcgr3** | 27.32238 | 2.454048 | 0.88573384 | 4.118815E-06 | 0.0003569407 | Fcgr3 |
| **ENSMUSG00000073418.5_C4b** | 125.2086 | 2.376114 | 0.64474107 | 3.314521E-07 | 3.971988E-05 | C4b |
| **ENSMUSG00000030111.10_A2m** | 59.20573 | 1.731913 | 0.49266592 | 7.027014E-07 | 7.867691E-05 | A2m |
| **ENSMUSG00000087168.2_Gm15983** | 130.1613 | 1.592081 | 0.30862598 | 7.837466E-10 | 2.072739E-07 | Gm15983 |
| **ENSMUSG00000031805.18_Jak3** | 16.71756 | 1.495389 | 1.19031719 | 0.0001275004 | 0.005944465 | Jak3 |
| **ENSMUSG00000024206.16_Rfx2** | 77.95385 | 1.487175 | 0.32174653 | 1.830141E-08 | 3.119171E-06 | Rfx2 |
| **ENSMUSG00000041782.15_Lad1** | 26.904 | 1.419034 | 0.86219986 | 8.105942E-05 | 0.004032996 | Lad1 |
| **ENSMUSG00000029338.14_Antxr2** | 110.7853 | 1.40951 | 0.27455913 | 2.212563E-09 | 5.221307E-07 | Antxr2 |
| **ENSMUSG00000001025.9_S100a6** | 80.87384 | 1.363326 | 0.45463953 | 7.595997E-06 | 0.0005881278 | S100a6 |
| **ENSMUSG00000018774.14_Cd68** | 28.43354 | 1.354925 | 1.08496109 | 0.0001577835 | 0.006954715 | Cd68 |
| **ENSMUSG00000073409.13_H2-Q6** | 24.60088 | 1.287253 | 0.90758999 | 0.0001414683 | 0.006458279 | H2-Q6 |
| **ENSMUSG00000024338.16_Psmb8** | 57.05762 | 1.2853 | 0.36337481 | 2.420643E-06 | 0.0002264039 | Psmb8 |
| **ENSMUSG00000033880.12_Lgals3bp** | 124.1623 | 1.233027 | 0.26726312 | 5.830427E-08 | 8.358217E-06 | Lgals3bp |
| **ENSMUSG00000037225.14_Fgf2** | 164.8499 | 1.213991 | 0.58520998 | 6.503243E-05 | 0.003370042 | Fgf2 |
| **ENSMUSG00000036896.6_C1qc** | 99.02991 | 1.180956 | 0.42575853 | 2.09387E-05 | 0.001310934 | C1qc |
| **ENSMUSG00000116895.2_Gm3435** | 38.22832 | 1.162843 | 0.46900378 | 3.838467E-05 | 0.002188782 | Gm3435 |
| **ENSMUSG00000089669.8_Tnfsf13** | 100.3619 | 1.161948 | 0.36591082 | 9.21616E-06 | 0.0006829308 | Tnfsf13 |
| **ENSMUSG00000052336.8_Cx3cr1** | 48.26072 | 1.069234 | 0.52031827 | 0.0001003983 | 0.004858076 | Cx3cr1 |
| **ENSMUSG00000002325.16_Irf9** | 108.0072 | 1.067975 | 0.33180896 | 1.082249E-05 | 0.0007793715 | Irf9 |
| **ENSMUSG00000074896.4_Ifit3** | 152.2712 | 0.9905447 | 0.32881319 | 2.142536E-05 | 0.00133595 | Ifit3 |
| **ENSMUSG00000106994.2_Gm10829** | 40.86597 | 0.9752153 | 0.47674872 | 0.0001351372 | 0.006206197 | Gm10829 |
| **ENSMUSG00000004040.17_Stat3** | 546.6797 | 0.929501 | 0.17569775 | 4.148118E-09 | 9.089712E-07 | Stat3 |
| **ENSMUSG00000029561.18_Oasl2** | 106.8459 | 0.926651 | 0.37487561 | 7.634958E-05 | 0.003852389 | Oasl2 |
| **ENSMUSG00000074794.11_Arrdc3** | 402.804 | 0.8930913 | 0.19332153 | 1.086855E-07 | 1.475333E-05 | Arrdc3 |
| **ENSMUSG00000047361.17_Gm973** | 14.37561 | 0.8683884 | 1.00022302 | 0.0005970754 | 0.01951833 | Gm973 |
| **ENSMUSG00000007655.17_Cav1** | 428.0948 | 0.8307848 | 0.18270097 | 1.500359E-07 | 2.001218E-05 | Cav1 |
| **ENSMUSG00000032495.9_Lrrc2** | 238.8276 | 0.8234943 | 0.28424292 | 4.034576E-05 | 0.002283629 | Lrrc2 |
| **ENSMUSG00000110997.2_2610028D06Rik** | 70.85802 | 0.8216078 | 0.35371427 | 0.0001328141 | 0.006120488 | 2610028D06Rik |
| **ENSMUSG00000027078.15_Ube2l6** | 54.29837 | 0.8196002 | 0.4767392 | 0.0003521213 | 0.01314005 | Ube2l6 |
| **ENSMUSG00000053279.9_Aldh1a1** | 270.7315 | 0.8155198 | 0.21083015 | 2.39102E-06 | 0.0002250053 | Aldh1a1 |
| **ENSMUSG00000052160.8_Pld4** | 21.83193 | 0.8083773 | 0.63673437 | 0.0005860017 | 0.0192508 | Pld4 |
| **ENSMUSG00000026547.16_Tagln2** | 55.58847 | 0.8002685 | 0.49050076 | 0.0004212849 | 0.0151337 | Tagln2 |
| **ENSMUSG00000060802.9_B2m** | 264.9985 | 0.7917258 | 0.49514206 | 0.0004518715 | 0.01589738 | B2m |
| **ENSMUSG00000028868.14_Wasf2** | 123.8555 | 0.7906269 | 0.26439046 | 3.443403E-05 | 0.002031475 | Wasf2 |
| **ENSMUSG00000005470.9_Asf1b** | 61.26583 | 0.7895134 | 0.41551159 | 0.0002985754 | 0.01165356 | Asf1b |
| **ENSMUSG00000051435.12_Fhad1** | 18.87207 | 0.7830411 | 0.74352286 | 0.0007242776 | 0.02248926 | Fhad1 |
| **ENSMUSG00000075254.13_Heg1** | 593.3746 | 0.7759982 | 0.15317938 | 1.198374E-08 | 2.112857E-06 | Heg1 |
| **ENSMUSG00000070498.4_Tmem132b** | 84.48132 | 0.772034 | 0.36935778 | 0.0002300374 | 0.009359531 | Tmem132b |
| **ENSMUSG00000079470.9_Utp14b** | 149.3397 | 0.75713 | 0.34546435 | 0.000200203 | 0.008459819 | Utp14b |
| **ENSMUSG00000024087.5_Cyp1b1** | 59.91282 | 0.7410649 | 0.47829094 | 0.0005747258 | 0.0190358 | Cyp1b1 |
| **ENSMUSG00000061232.17_H2-K1** | 315.0114 | 0.7387007 | 0.24884868 | 4.011737E-05 | 0.002279113 | H2-K1 |
| **ENSMUSG00000036887.6_C1qa** | 53.76387 | 0.7261473 | 0.44760933 | 0.0005511207 | 0.01853869 | C1qa |
| **ENSMUSG00000051439.8_Cd14** | 19.08507 | 0.6989846 | 0.73708258 | 0.00101783 | 0.02912779 | Cd14 |
| **ENSMUSG00000042613.10_Pbxip1** | 370.2178 | 0.698673 | 0.1861561 | 4.09486E-06 | 0.000356881 | Pbxip1 |
| **ENSMUSG00000025885.19_Myo5b** | 90.83003 | 0.6891911 | 0.33677542 | 0.0003132115 | 0.01204098 | Myo5b |
| **ENSMUSG00000059555.7_Tor4a** | 19.95052 | 0.688986 | 0.71431219 | 0.001057826 | 0.02993726 | Tor4a |
| **ENSMUSG00000079415.3_Cntf** | 38.83226 | 0.6868385 | 0.56267243 | 0.0009775166 | 0.0282908 | Cntf |

| | | | | | | |
|---|---|---|---|---|---|---|
| **ENSMUSG00000023439.12_Gnb3** | 3584.13 | 0.676379 | 0.13628526 | 2.09151E-08 | 3.525459E-06 | Gnb3 |
| **ENSMUSG00000082361.7_Btc** | 131.1439 | 0.6609236 | 0.34471856 | 0.0004267517 | 0.01525861 | Btc |
| **ENSMUSG00000027907.5_S100a11** | 41.65606 | 0.6444781 | 0.60096069 | 0.001260923 | 0.03429308 | S100a11 |
| **ENSMUSG00000002602.17_Axl** | 113.8235 | 0.6396907 | 0.30353841 | 0.0003212163 | 0.01222615 | Axl |
| **ENSMUSG00000032554.16_Trf** | 1248.292 | 0.6382875 | 0.32681131 | 0.000428045 | 0.01526926 | Trf |
| **ENSMUSG00000067212.9_H2-T23** | 72.92002 | 0.6325118 | 0.37648242 | 0.0006928278 | 0.02174901 | H2-T23 |
| **ENSMUSG00000022146.13_Osmr** | 60.41351 | 0.6277738 | 0.52512402 | 0.001283109 | 0.03465072 | Osmr |
| **ENSMUSG00000051444.10_Bbs12** | 262.5425 | 0.6265859 | 0.16294978 | 3.381619E-06 | 0.0002981072 | Bbs12 |
| **ENSMUSG00000113670.2_Gm49686** | 19.43485 | 0.620031 | 0.72356257 | 0.001404977 | 0.03702912 | Gm49686 |
| **ENSMUSG00000069633.13_Pex11g** | 47.30496 | 0.6154998 | 0.42656617 | 0.001043545 | 0.02964247 | Pex11g |
| **ENSMUSG00000026896.15_Ifih1** | 24.50662 | 0.6129405 | 0.59408789 | 0.001472383 | 0.0382147 | Ifih1 |
| **ENSMUSG00000020932.15_Gfap** | 208.6542 | 0.6029868 | 0.45528135 | 0.001268152 | 0.03436782 | Gfap |
| **ENSMUSG00000059336.15_Slc14a1** | 100.5289 | 0.5999752 | 0.32421784 | 0.000575827 | 0.0190358 | Slc14a1 |
| **ENSMUSG00000089842.3_Pitpnm2os2** | 460.2818 | 0.594518 | 0.13167434 | 2.266825E-07 | 2.850068E-05 | Pitpnm2os2 |
| **ENSMUSG00000034121.13_Mks1** | 132.5357 | 0.5907118 | 0.25011032 | 0.0002232122 | 0.009203904 | Mks1 |
| **ENSMUSG00000108780.2_5430434F05Rik** | 18.58538 | 0.5857652 | 0.67681647 | 0.001649657 | 0.04203193 | 5430434F05Rik |
| **ENSMUSG00000016918.16_Sulf1** | 297.6971 | 0.5834762 | 0.20442471 | 7.632085E-05 | 0.003852389 | Sulf1 |
| **ENSMUSG00000054717.8_Hmgb2** | 576.7066 | 0.5832508 | 0.35863835 | 0.0008893737 | 0.02623481 | Hmgb2 |
| **ENSMUSG00000055026.14_Gabrg3** | 93.50689 | -0.5802341 | 0.34753815 | 0.0008365735 | 0.02501404 | Gabrg3 |
| **ENSMUSG00000028937.15_Acot7** | 940.7191 | -0.580343 | 0.14847448 | 3.059644E-06 | 0.0002742313 | Acot7 |
| **ENSMUSG00000032290.8_Ptpn9** | 98.44654 | -0.5804631 | 0.33808811 | 0.0007718937 | 0.02358581 | Ptpn9 |
| **ENSMUSG00000018340.14_Anxa6** | 263.7321 | -0.5818328 | 0.18147418 | 3.06527E-05 | 0.00182241 | Anxa6 |
| **ENSMUSG00000062991.10_Nrg1** | 87.47539 | -0.5835622 | 0.32509755 | 0.0006679408 | 0.02121231 | Nrg1 |
| **ENSMUSG00000063239.18_Grm4** | 50.7558 | -0.5837186 | 0.46172501 | 0.001466043 | 0.03813984 | Grm4 |
| **ENSMUSG00000067925.5_Rtl8a** | 253.9203 | -0.5845682 | 0.17778182 | 2.405003E-05 | 0.001475613 | Rtl8a |
| **ENSMUSG00000018417.15_Myo1b** | 149.9842 | -0.5847733 | 0.26623799 | 0.0003161237 | 0.01209232 | Myo1b |
| **ENSMUSG00000019843.15_Fyn** | 218.4677 | -0.5891724 | 0.22783253 | 0.0001393683 | 0.006381406 | Fyn |
| **ENSMUSG00000043388.9_Tmem130** | 748.6128 | -0.5922791 | 0.12126924 | 3.864975E-08 | 5.942262E-06 | Tmem130 |
| **ENSMUSG00000024887.11_Asah2** | 25.53414 | -0.5955193 | 0.63851272 | 0.001600389 | 0.04091395 | Asah2 |
| **ENSMUSG00000022421.22_Nptxr** | 237.705 | -0.5982577 | 0.3169206 | 0.0005418431 | 0.01834731 | Nptxr |
| **ENSMUSG00000019647.17_Sema6a** | 266.5658 | -0.5982951 | 0.17431318 | 1.496311E-05 | 0.000997909 | Sema6a |
| **ENSMUSG00000041112.18_Elmo1** | 435.2026 | -0.6024143 | 0.14421315 | 9.748361E-07 | 0.0001060497 | Elmo1 |
| **ENSMUSG00000025104.14_Hdgfl3** | 565.9444 | -0.6035509 | 0.14687196 | 1.286043E-06 | 0.0001323933 | Hdgfl3 |
| **ENSMUSG00000050908.13_Tvp23a** | 153.3643 | -0.6067539 | 0.24401946 | 0.0001646072 | 0.007152719 | Tvp23a |
| **ENSMUSG00000038331.16_Satb2** | 15.03129 | -0.6073213 | 0.94694834 | 0.001323112 | 0.03548113 | Satb2 |
| **ENSMUSG00000026959.14_Grin1** | 415.3226 | -0.6077827 | 0.17337921 | 1.155382E-05 | 0.0008242977 | Grin1 |
| **ENSMUSG00000046447.4_Camk2n1** | 825.6617 | -0.6107665 | 0.14565054 | 8.881224E-07 | 9.73065E-05 | Camk2n1 |
| **ENSMUSG00000006342.16_Susd2** | 61.0323 | -0.6121177 | 0.44574205 | 0.001155009 | 0.03209543 | Susd2 |
| **ENSMUSG00000026603.14_Smyd2** | 193.7298 | -0.6137977 | 0.2124865 | 6.455304E-05 | 0.003356539 | Smyd2 |
| **ENSMUSG00000001794.14_Capns1** | 462.8164 | -0.6144922 | 0.1507058 | 1.417618E-06 | 0.0001440056 | Capns1 |
| **ENSMUSG00000070687.12_Htr1d** | 40.25221 | -0.6152877 | 0.48229526 | 0.001267805 | 0.03436782 | Htr1d |
| **ENSMUSG00000051177.17_Plcb1** | 134.7979 | -0.6171614 | 0.29716312 | 0.000362448 | 0.01330046 | Plcb1 |
| **ENSMUSG00000042804.14_Gpr153** | 413.3948 | -0.6174183 | 0.21983817 | 7.762223E-05 | 0.003891005 | Gpr153 |
| **ENSMUSG00000038910.8_Plcl2** | 67.70088 | -0.6174645 | 0.39424626 | 0.0008696096 | 0.02575085 | Plcl2 |
| **ENSMUSG00000021719.10_Rgs7bp** | 399.7661 | -0.6184278 | 0.17870455 | 1.295398E-05 | 0.0008950499 | Rgs7bp |
| **ENSMUSG00000104148.6_Pcdha2** | 39.6855 | -0.6215751 | 0.65189635 | 0.001417742 | 0.03723759 | Pcdha2 |
| **ENSMUSG00000008140.19_Emc10** | 489.3569 | -0.6216994 | 0.15068647 | 1.140542E-06 | 0.0001194625 | Emc10 |
| **ENSMUSG00000020349.5_Ppp2ca** | 1100.101 | -0.6217019 | 0.13082546 | 6.739492E-08 | 9.484135E-06 | Ppp2ca |
| **ENSMUSG00000031738.15_Irx6** | 106.0163 | -0.6229293 | 0.27556988 | 0.0002503663 | 0.01000096 | Irx6 |
| **ENSMUSG00000024873.8_Cnih2** | 114.5461 | -0.6260521 | 0.35689398 | 0.0006267318 | 0.02023882 | Cnih2 |

| | | | | | | |
|---|---|---|---|---|---|---|
| **ENSMUSG00000031447.8_Lamp1** | 1051.511 | -0.6284095 | 0.15143934 | 1.015477E-06 | 0.000109693 | Lamp1 |
| **ENSMUSG00000028445.8_Enho** | 196.1298 | -0.6284346 | 0.21815766 | 6.340144E-05 | 0.00333053 | Enho |
| **ENSMUSG00000052957.9_Gas1** | 140.0208 | -0.6290932 | 0.33792354 | 0.0005169034 | 0.01774933 | Gas1 |
| **ENSMUSG00000020525.18_Ppm1d** | 306.143 | -0.6295365 | 0.22969861 | 8.823828E-05 | 0.004310468 | Ppm1d |
| **ENSMUSG00000035547.15_Capn5** | 110.9505 | -0.6313047 | 0.36079658 | 0.0006209632 | 0.02009484 | Capn5 |
| **ENSMUSG00000033152.14_Podxl2** | 887.6739 | -0.6330666 | 0.15368097 | 1.13703E-06 | 0.0001194625 | Podxl2 |
| **ENSMUSG00000021087.19_Rtn1** | 2260.827 | -0.6331064 | 0.10469265 | 4.834377E-11 | 1.426048E-08 | Rtn1 |
| **ENSMUSG00000017167.7_Cntnap1** | 316.8873 | -0.6332341 | 0.22620093 | 7.618039E-05 | 0.003852389 | Cntnap1 |
| **ENSMUSG00000061911.16_Myt1l** | 382.628 | -0.6355626 | 0.14306733 | 2.795625E-07 | 3.40334E-05 | Myt1l |
| **ENSMUSG00000037509.22_Arhgef4** | 268.3115 | -0.6362381 | 0.20663684 | 3.748463E-05 | 0.002161567 | Arhgef4 |
| **ENSMUSG00000011589.10_Fsd1** | 93.13496 | -0.6407541 | 0.37888963 | 0.0006626469 | 0.02108784 | Fsd1 |
| **ENSMUSG00000029207.17_Apbb2** | 338.5916 | -0.6422393 | 0.17335722 | 5.412768E-06 | 0.0004416301 | Apbb2 |
| **ENSMUSG00000052516.20_Robo2** | 330.481 | -0.6447001 | 0.17153766 | 4.448501E-06 | 0.0003784603 | Robo2 |
| **ENSMUSG00000049807.17_Arhgap23** | 231.1498 | -0.6447203 | 0.25029101 | 0.000123004 | 0.005780149 | Arhgap23 |
| **ENSMUSG00000022378.15_Cyrib** | 301.3033 | -0.6472523 | 0.17631646 | 6.020268E-06 | 0.0004796238 | Cyrib |
| **ENSMUSG00000022456.19_Septin3** | 784.5413 | -0.6500511 | 0.12335261 | 4.326111E-09 | 9.107631E-07 | Septin3 |
| **ENSMUSG00000021974.16_Fgf9** | 224.6261 | -0.6502932 | 0.19003457 | 1.353532E-05 | 0.0009227477 | Fgf9 |
| **ENSMUSG00000044982.8_Sft2d3** | 209.2811 | -0.651387 | 0.46936973 | 0.0009733629 | 0.02823114 | Sft2d3 |
| **ENSMUSG00000004328.16_Hif3a** | 23.60005 | -0.651698 | 0.64344764 | 0.001234439 | 0.03369228 | Hif3a |
| **ENSMUSG00000026335.17_Pam** | 427.3822 | -0.654398 | 0.16868423 | 2.789321E-06 | 0.000254675 | Pam |
| **ENSMUSG00000041548.5_Hspb8** | 44.53888 | -0.6552018 | 0.48893031 | 0.001009148 | 0.0289333 | Hspb8 |
| **ENSMUSG00000044117.13_Bmerb1** | 681.8821 | -0.6632709 | 0.14436634 | 1.3063E-07 | 1.757661E-05 | Bmerb1 |
| **ENSMUSG00000043866.12_Taf10** | 433.5309 | -0.6652874 | 0.20061681 | 1.804719E-05 | 0.001168042 | Taf10 |
| **ENSMUSG00000032024.11_Clmp** | 70.59343 | -0.6670719 | 0.35297969 | 0.000439415 | 0.01553038 | Clmp |
| **ENSMUSG00000000305.13_Cdh4** | 209.7103 | -0.6675943 | 0.20976923 | 2.633701E-05 | 0.001596772 | Cdh4 |
| **ENSMUSG00000063646.19_Jakmip1** | 67.00246 | -0.6687573 | 0.41806084 | 0.0006933482 | 0.02174901 | Jakmip1 |
| **ENSMUSG00000049556.6_Lingo1** | 215.5832 | -0.6694686 | 0.22403855 | 4.399064E-05 | 0.002453718 | Lingo1 |
| **ENSMUSG00000025221.17_Kcnip2** | 72.08557 | -0.6739413 | 0.35252339 | 0.0004146471 | 0.01493021 | Kcnip2 |
| **ENSMUSG00000026202.14_Tuba4a** | 759.4162 | -0.6767145 | 0.13833319 | 2.998212E-08 | 4.841008E-06 | Tuba4a |
| **ENSMUSG00000062252.10_Lhfpl5** | 43.24451 | -0.6778317 | 0.4747619 | 0.0008395941 | 0.02505551 | Lhfpl5 |
| **ENSMUSG00000028546.18_Elavl4** | 191.4378 | -0.6785638 | 0.19934938 | 1.34938E-05 | 0.0009227477 | Elavl4 |
| **ENSMUSG00000045114.11_Prrt2** | 161.3096 | -0.6806474 | 0.26978987 | 0.000126246 | 0.005903924 | Prrt2 |
| **ENSMUSG00000046709.19_Mapk10** | 521.535 | -0.6807919 | 0.1300062 | 4.937248E-09 | 9.971766E-07 | Mapk10 |
| **ENSMUSG00000058441.8_Panx2** | 195.8999 | -0.6812647 | 0.24789274 | 7.663293E-05 | 0.003854008 | Panx2 |
| **ENSMUSG00000056749.8_Nfil3** | 95.5192 | -0.6814208 | 0.31930583 | 0.0002726371 | 0.01071498 | Nfil3 |
| **ENSMUSG00000029376.9_Mthfd2l** | 82.35676 | -0.6830714 | 0.31256526 | 0.00024655 | 0.009900081 | Mthfd2l |
| **ENSMUSG00000042751.15_Nmnat2** | 220.6364 | -0.6847929 | 0.21700752 | 2.73683E-05 | 0.001639853 | Nmnat2 |
| **ENSMUSG00000031278.13_Acsl4** | 138.6054 | -0.6851776 | 0.28291664 | 0.0001540813 | 0.006830405 | Acsl4 |
| **ENSMUSG00000071547.5_Nt5dc2** | 278.413 | -0.6856396 | 0.17427994 | 2.138694E-06 | 0.0002037604 | Nt5dc2 |
| **ENSMUSG00000058975.8_Kcnc1** | 497.6541 | -0.6869886 | 0.19355664 | 8.38014E-06 | 0.0006332166 | Kcnc1 |
| **ENSMUSG00000024109.19_Nrxn1** | 273.1916 | -0.691056 | 0.17070314 | 1.356046E-06 | 0.0001386693 | Nrxn1 |
| **ENSMUSG00000037373.13_Ctbp1** | 646.8641 | -0.6911697 | 0.14259162 | 3.686976E-08 | 5.77087E-06 | Ctbp1 |
| **ENSMUSG00000040035.15_Disp2** | 621.9408 | -0.6919887 | 0.13583869 | 1.041631E-08 | 1.879715E-06 | Disp2 |
| **ENSMUSG00000044716.13_Dok7** | 32.8465 | -0.6935114 | 0.56932434 | 0.0009520611 | 0.02786959 | Dok7 |
| **ENSMUSG00000026824.12_Kcnj3** | 67.85339 | -0.6977939 | 0.40241307 | 0.0005151358 | 0.01774933 | Kcnj3 |
| **ENSMUSG00000074238.7_Ap1ar** | 242.2752 | -0.6983949 | 0.20923837 | 1.586726E-05 | 0.001049086 | Ap1ar |
| **ENSMUSG00000025889.14_Snca** | 153.2529 | -0.7034675 | 0.24080261 | 4.836776E-05 | 0.002678387 | Snca |
| **ENSMUSG00000054793.9_Cadm4** | 182.2208 | -0.7037631 | 0.32216562 | 0.0002337732 | 0.009461337 | Cadm4 |
| **ENSMUSG00000024897.10_Apba1** | 445.0916 | -0.707751 | 0.18372977 | 2.820098E-06 | 0.0002559614 | Apba1 |
| **ENSMUSG00000025318.14_Jph3** | 209.4767 | -0.7089431 | 0.20416045 | 1.032525E-05 | 0.0007541855 | Jph3 |

| | | | | | | |
|---|---|---|---|---|---|---|
| **ENSMUSG00000074968.12_Ano3** | 72.36011 | -0.7097671 | 0.41875295 | 0.0005254167 | 0.01786999 | Ano3 |
| **ENSMUSG00000034687.9_Fras1** | 36.87839 | -0.7106109 | 0.52089925 | 0.0007901837 | 0.02404887 | Fras1 |
| **ENSMUSG00000027419.10_Pcsk2** | 197.7067 | -0.7125667 | 0.22466799 | 2.482038E-05 | 0.001516812 | Pcsk2 |
| **ENSMUSG00000030302.18_Atp2b2** | 776.9294 | -0.7137849 | 0.1343329 | 3.180463E-09 | 7.070308E-07 | Atp2b2 |
| **ENSMUSG00000058153.16_Sez6l** | 190.139 | -0.7166921 | 0.30087901 | 0.0001545179 | 0.006830405 | Sez6l |
| **ENSMUSG00000022594.15_Lynx1** | 922.9769 | -0.7170593 | 0.13126289 | 1.392326E-09 | 3.44466E-07 | Lynx1 |
| **ENSMUSG00000071076.9_Jund** | 363.2943 | -0.7253669 | 0.71202397 | 0.0009071438 | 0.02660551 | Jund |
| **ENSMUSG00000025477.15_Inpp5a** | 206.0292 | -0.7254725 | 0.21387762 | 1.287937E-05 | 0.0008950499 | Inpp5a |
| **ENSMUSG00000036186.6_Dipk1b** | 171.0536 | -0.725537 | 0.23900653 | 3.473406E-05 | 0.002041325 | Dipk1b |
| **ENSMUSG00000023927.16_Satb1** | 130.3366 | -0.7259523 | 0.25428547 | 5.42165E-05 | 0.002938611 | Satb1 |
| **ENSMUSG00000018012.12_Rac3** | 55.3563 | -0.7282187 | 0.42436801 | 0.0004793051 | 0.01666774 | Rac3 |
| **ENSMUSG00000020978.11_Klhdc2** | 669.5759 | -0.7282883 | 0.2191 | 1.568908E-05 | 0.001041796 | Klhdc2 |
| **ENSMUSG00000039395.9_Mreg** | 315.8754 | -0.7302161 | 0.1705387 | 4.932693E-07 | 5.732013E-05 | Mreg |
| **ENSMUSG00000027533.11_Fabp5** | 185.0689 | -0.7321918 | 0.26772715 | 7.063916E-05 | 0.003636021 | Fabp5 |
| **ENSMUSG00000028124.16_Gclm** | 233.4268 | -0.7335104 | 0.19027708 | 2.702634E-06 | 0.0002497331 | Gclm |
| **ENSMUSG00000071234.4_Syndig1l** | 110.2691 | -0.7354956 | 0.31606144 | 0.0001642386 | 0.007152719 | Syndig1l |
| **ENSMUSG00000075318.14_Scn2a** | 234.7154 | -0.7369886 | 0.20373495 | 6.193102E-06 | 0.000487159 | Scn2a |
| **ENSMUSG00000036564.18_Ndrg4** | 3379.46 | -0.7370767 | 0.11967983 | 2.236154E-11 | 7.297951E-09 | Ndrg4 |
| **ENSMUSG00000022848.9_Slc49a4** | 182.8161 | -0.7373391 | 0.22745986 | 1.956353E-05 | 0.001240021 | Slc49a4 |
| **ENSMUSG00000042298.19_Ttc19** | 335.0067 | -0.7398865 | 0.15428179 | 4.625635E-08 | 6.822366E-06 | Ttc19 |
| **ENSMUSG00000027894.15_Slc6a17** | 549.0012 | -0.7409109 | 0.1820597 | 1.1771E-06 | 0.0001219969 | Slc6a17 |
| **ENSMUSG00000022099.18_Dmtn** | 410.7739 | -0.7437017 | 0.15392129 | 3.873957E-08 | 5.942262E-06 | Dmtn |
| **ENSMUSG00000055493.5_Epm2a** | 181.1125 | -0.7516952 | 0.32134847 | 0.0001540398 | 0.006830405 | Epm2a |
| **ENSMUSG00000018965.12_Ywhah** | 1792.839 | -0.7517915 | 0.12131693 | 1.784233E-11 | 6.081857E-09 | Ywhah |
| **ENSMUSG00000002763.17_Pex6** | 242.5931 | -0.7554304 | 0.19644326 | 2.733746E-06 | 0.0002510954 | Pex6 |
| **ENSMUSG00000010517.8_Faf1** | 245.234 | -0.7565856 | 0.16788836 | 1.804945E-07 | 2.326559E-05 | Faf1 |
| **ENSMUSG00000029875.6_Ccdc184** | 130.0186 | -0.761839 | 0.2552278 | 3.684427E-05 | 0.002132657 | Ccdc184 |
| **ENSMUSG00000026576.13_Atp1b1** | 2104.338 | -0.7632324 | 0.09879954 | 3.718886E-16 | 2.8522E-13 | Atp1b1 |
| **ENSMUSG00000022528.9_Hes1** | 64.50738 | -0.7635257 | 0.43623244 | 0.0004060891 | 0.01472577 | Hes1 |
| **ENSMUSG00000016382.16_Pls3** | 212.292 | -0.7649144 | 0.21304025 | 6.529612E-06 | 0.0005110088 | Pls3 |
| **ENSMUSG00000037348.16_Paqr7** | 172.1249 | -0.7677023 | 0.24689593 | 2.655881E-05 | 0.00159759 | Paqr7 |
| **ENSMUSG00000034898.18_Filip1** | 23.94936 | -0.7684699 | 0.67291521 | 0.0007345745 | 0.0227629 | Filip1 |
| **ENSMUSG00000021373.17_Cap2** | 216.2558 | -0.7698911 | 0.19760436 | 2.239665E-06 | 0.0002120631 | Cap2 |
| **ENSMUSG00000050822.12_Slc29a4** | 122.238 | -0.7712323 | 0.27017476 | 4.948709E-05 | 0.002720726 | Slc29a4 |
| **ENSMUSG00000029608.11_Rph3a** | 881.2728 | -0.7724914 | 0.14433705 | 2.625775E-09 | 6.011457E-07 | Rph3a |
| **ENSMUSG00000032908.10_Sgpp2** | 186.8745 | -0.7728215 | 0.20775299 | 4.192998E-06 | 0.0003613281 | Sgpp2 |
| **ENSMUSG00000042429.9_Adora1** | 395.0822 | -0.7757253 | 0.15788982 | 2.599868E-08 | 4.334714E-06 | Adora1 |
| **ENSMUSG00000029309.8_Sparcl1** | 1231.421 | -0.7830893 | 0.11167274 | 7.931624E-14 | 4.055439E-11 | Sparcl1 |
| **ENSMUSG00000004933.18_Matk** | 136.3658 | -0.7836999 | 0.2648662 | 3.767918E-05 | 0.002164648 | Matk |
| **ENSMUSG00000032034.7_Kcnj5** | 84.6985 | -0.7912652 | 0.34978458 | 0.0001607874 | 0.007049341 | Kcnj5 |
| **ENSMUSG00000040811.16_Eml2** | 171.1421 | -0.7946438 | 0.23393658 | 1.14522E-05 | 0.0008208656 | Eml2 |
| **ENSMUSG00000070304.13_Scn2b** | 326.3425 | -0.7946771 | 0.1753751 | 1.607152E-07 | 2.107018E-05 | Scn2b |
| **ENSMUSG00000036062.14_Phf24** | 267.8323 | -0.7991858 | 0.19651226 | 1.144859E-06 | 0.0001194625 | Phf24 |
| **ENSMUSG00000039579.16_Grin3a** | 54.07767 | -0.8024238 | 0.41192871 | 0.0002662883 | 0.01052731 | Grin3a |
| **ENSMUSG00000020241.14_Col6a2** | 42.36869 | -0.8064104 | 0.60647789 | 0.0005638366 | 0.01891728 | Col6a2 |
| **ENSMUSG00000022076.11_Klhl1** | 71.31566 | -0.8068604 | 0.37155997 | 0.0001812416 | 0.007765545 | Klhl1 |
| **ENSMUSG00000036745.16_Ttll7** | 443.8251 | -0.8070355 | 0.16781373 | 4.385771E-08 | 6.595426E-06 | Ttll7 |
| **ENSMUSG00000031970.18_Dbndd1** | 65.67204 | -0.8086348 | 0.39258821 | 0.000218144 | 0.009043544 | Dbndd1 |
| **ENSMUSG00000029126.8_Nsg1** | 730.2391 | -0.8092363 | 0.18031165 | 1.953407E-07 | 2.476306E-05 | Nsg1 |
| **ENSMUSG00000026765.13_Lypd6b** | 29.97437 | -0.810973 | 0.57559828 | 0.000517586 | 0.01774933 | Lypd6b |

| | | | | | | |
|---|---|---|---|---|---|---|
| **ENSMUSG00000048070.5_Pirt** | 10.06811 | -0.8190235 | 1.30502849 | 0.0005702356 | 0.01895787 | Pirt |
| **ENSMUSG00000089945.14_Pakap** | 23.66103 | -0.8217965 | 0.82616267 | 0.0006514293 | 0.0208548 | Pakap |
| **ENSMUSG00000056413.17_Adap1** | 106.1899 | -0.83117 | 0.33669365 | 9.84051E-05 | 0.004776696 | Adap1 |
| **ENSMUSG00000003352.15_Cacnb3** | 266.3806 | -0.8314028 | 0.18800029 | 2.607725E-07 | 3.225798E-05 | Cacnb3 |
| **ENSMUSG00000021534.9_1700001L19Rik** | 10.2093 | -0.8418697 | 1.32283963 | 0.0005378101 | 0.01825104 | 1700001L19Rik |
| **ENSMUSG00000050447.16_Lypd6** | 133.6613 | -0.8425089 | 0.2400657 | 7.653345E-06 | 0.0005881278 | Lypd6 |
| **ENSMUSG00000049100.16_Pcdh10** | 251.8322 | -0.8431892 | 0.20702779 | 1.092901E-06 | 0.0001164168 | Pcdh10 |
| **ENSMUSG00000032231.15_Anxa2** | 124.03 | -0.8460576 | 0.31065827 | 5.658489E-05 | 0.003045458 | Anxa2 |
| **ENSMUSG00000020953.18_Coch** | 119.0184 | -0.8482535 | 0.26166483 | 1.631612E-05 | 0.001074133 | Coch |
| **ENSMUSG00000026688.6_Mgst3** | 287.9366 | -0.8489624 | 0.19970645 | 5.36136E-07 | 6.183301E-05 | Mgst3 |
| **ENSMUSG00000049281.17_Scn3b** | 137.3299 | -0.8496862 | 0.26638906 | 1.868436E-05 | 0.001194164 | Scn3b |
| **ENSMUSG00000049044.17_Rapgef4** | 127.234 | -0.860319 | 0.25077737 | 9.442329E-06 | 0.0006963264 | Rapgef4 |
| **ENSMUSG00000024750.12_Zfand5** | 711.196 | -0.8679606 | 0.17792142 | 3.224832E-08 | 5.099557E-06 | Zfand5 |
| **ENSMUSG00000041556.9_Fbxo2** | 193.2884 | -0.8704232 | 0.20132684 | 3.949689E-07 | 4.624755E-05 | Fbxo2 |
| **ENSMUSG00000057614.7_Gnai1** | 182.6843 | -0.8841724 | 0.21267169 | 7.686028E-07 | 8.543187E-05 | Gnai1 |
| **ENSMUSG00000035653.17_Lrfn5** | 125.1246 | -0.8852804 | 0.2462211 | 5.548451E-06 | 0.0004503052 | Lrfn5 |
| **ENSMUSG00000028677.20_Rnf220** | 859.1194 | -0.8887969 | 0.15174187 | 1.73295E-10 | 4.92254E-08 | Rnf220 |
| **ENSMUSG00000025867.9_Cplx2** | 956.0543 | -0.8943029 | 0.13188726 | 5.057117E-13 | 2.216318E-10 | Cplx2 |
| **ENSMUSG00000030270.12_Cpne9** | 84.8151 | -0.8953426 | 0.34827633 | 6.8678E-05 | 0.003546976 | Cpne9 |
| **ENSMUSG00000046532.9_Ar** | 13.47462 | -0.8982345 | 1.00613945 | 0.0005467811 | 0.01843313 | Ar |
| **ENSMUSG00000040105.4_Plpp6** | 149.4898 | -0.9125608 | 0.25195302 | 4.917971E-06 | 0.0004091156 | Plpp6 |
| **ENSMUSG00000040855.16_Reps2** | 200.2655 | -0.9126357 | 0.2567073 | 6.034773E-06 | 0.0004796238 | Reps2 |
| **ENSMUSG00000032020.16_Ubash3b** | 137.562 | -0.9138004 | 0.23124531 | 1.626485E-06 | 0.0001609591 | Ubash3b |
| **ENSMUSG00000034926.4_Dhcr24** | 461.2995 | -0.9231467 | 0.17002257 | 1.976356E-09 | 4.73677E-07 | Dhcr24 |
| **ENSMUSG00000070695.5_Cntnap5a** | 73.74994 | -0.9309171 | 0.39444666 | 9.231373E-05 | 0.004495239 | Cntnap5a |
| **ENSMUSG00000026426.11_Arl8a** | 313.088 | -0.9362908 | 0.16850142 | 9.951744E-10 | 2.587285E-07 | Arl8a |
| **ENSMUSG00000027895.11_Kcnc4** | 117.1207 | -0.9363012 | 0.30750907 | 2.256514E-05 | 0.001390067 | Kcnc4 |
| **ENSMUSG00000091002.3_Tcerg1l** | 14.87193 | -0.9373602 | 1.38575106 | 0.0004313524 | 0.01535154 | Tcerg1l |
| **ENSMUSG00000075585.4_6330403L08Rik** | 28.3756 | -0.9449371 | 0.7162056 | 0.0003569376 | 0.01314416 | 6330403L08Rik |
| **ENSMUSG00000025582.5_Nptx1** | 425.0535 | -0.9493508 | 0.18980964 | 1.792704E-08 | 3.089695E-06 | Nptx1 |
| **ENSMUSG00000032193.10_Ldlr** | 103.8452 | -0.9580781 | 0.30825778 | 1.849544E-05 | 0.001187036 | Ldlr |
| **ENSMUSG00000041014.18_Nrg3** | 39.4586 | -0.9585912 | 0.56967412 | 0.0002331631 | 0.009461337 | Nrg3 |
| **ENSMUSG00000049511.6_Htr1b** | 50.05825 | -0.9590996 | 1.01838201 | 0.000458222 | 0.01608391 | Htr1b |
| **ENSMUSG00000059923.14_Grb2** | 290.5225 | -0.9681583 | 0.24565577 | 1.578968E-06 | 0.0001582993 | Grb2 |
| **ENSMUSG00000041439.16_Mfsd6** | 367.2681 | -0.9689402 | 0.18890895 | 9.470358E-09 | 1.750191E-06 | Mfsd6 |
| **ENSMUSG00000036902.12_Neto2** | 119.9927 | -0.9711282 | 0.2728892 | 5.406556E-06 | 0.0004416301 | Neto2 |
| **ENSMUSG00000074064.7_Mlycd** | 186.1111 | -0.9758557 | 0.28955707 | 9.126929E-06 | 0.0006796018 | Mlycd |
| **ENSMUSG00000063446.5_Plppr1** | 35.13694 | -0.9887612 | 0.52739987 | 0.0001655023 | 0.0071713 | Plppr1 |
| **ENSMUSG00000019785.15_Clvs2** | 25.83936 | -0.988955 | 0.60837404 | 0.0002269644 | 0.009308574 | Clvs2 |
| **ENSMUSG00000031376.16_Atp2b3** | 61.78509 | -0.989465 | 0.53732444 | 0.0001727549 | 0.007452789 | Atp2b3 |
| **ENSMUSG00000062661.7_Ncs1** | 350.5463 | -0.9925239 | 0.15267845 | 3.522993E-12 | 1.318029E-09 | Ncs1 |
| **ENSMUSG00000032946.17_Rasgrp2** | 69.47083 | -0.9930484 | 0.3852594 | 5.230949E-05 | 0.002865626 | Rasgrp2 |
| **ENSMUSG00000027581.13_Stmn3** | 1217.926 | -0.9967918 | 0.14658742 | 4.846353E-13 | 2.186418E-10 | Stmn3 |
| **ENSMUSG00000038602.8_Slc35f1** | 180.8888 | -0.9984381 | 0.25461877 | 1.612644E-06 | 0.0001606256 | Slc35f1 |
| **ENSMUSG00000032890.18_Rims3** | 432.0539 | -1.005472 | 0.17849579 | 6.475478E-10 | 1.742585E-07 | Rims3 |
| **ENSMUSG00000042388.15_Dlgap3** | 210.4433 | -1.012278 | 0.25706128 | 1.486054E-06 | 0.0001499643 | Dlgap3 |
| **ENSMUSG00000039910.11_Cited2** | 579.6064 | -1.012679 | 0.1842921 | 1.37208E-09 | 3.44466E-07 | Cited2 |
| **ENSMUSG00000054459.9_Vsnl1** | 404.6009 | -1.013542 | 0.19742031 | 8.973147E-09 | 1.699248E-06 | Vsnl1 |
| **ENSMUSG00000034336.4_Ina** | 622.2639 | -1.016984 | 0.12486077 | 2.07259E-17 | 1.766192E-14 | Ina |
| **ENSMUSG00000028444.18_Cntfr** | 187.6714 | -1.017043 | 0.28216237 | 4.306317E-06 | 0.0003690201 | Cntfr |

| | | | | | | |
|---|---|---|---|---|---|---|
| **ENSMUSG00000029223.13_Uchl1** | 700.4135 | -1.019603 | 0.18722175 | 1.774381E-09 | 4.320195E-07 | Uchl1 |
| **ENSMUSG00000002633.5_Shh** | 21.97735 | -1.045937 | 1.41490362 | 0.0003567397 | 0.01314416 | Shh |
| **ENSMUSG00000057098.15_Ebf1** | 181.8231 | -1.050042 | 0.2022651 | 6.417644E-09 | 1.262054E-06 | Ebf1 |
| **ENSMUSG00000027500.11_Stmn2** | 461.1253 | -1.052305 | 0.13894804 | 1.798509E-15 | 1.182397E-12 | Stmn2 |
| **ENSMUSG00000002900.18_Lamb1** | 58.69192 | -1.058546 | 0.4442519 | 6.146242E-05 | 0.003262187 | Lamb1 |
| **ENSMUSG00000075334.3_Rprm** | 33.89144 | -1.062876 | 0.56723285 | 0.0001324774 | 0.006120488 | Rprm |
| **ENSMUSG00000021303.15_Gng4** | 146.5667 | -1.067984 | 0.24804011 | 3.41011E-07 | 4.054859E-05 | Gng4 |
| **ENSMUSG00000062257.14_Opcml** | 83.38101 | -1.069658 | 0.31015625 | 5.935912E-06 | 0.0004767066 | Opcml |
| **ENSMUSG00000016346.18_Kcnq2** | 448.8499 | -1.074578 | 0.20953255 | 8.433421E-09 | 1.617003E-06 | Kcnq2 |
| **ENSMUSG00000048899.9_Rimkla** | 298.7159 | -1.078708 | 0.23567666 | 1.086009E-07 | 1.475333E-05 | Rimkla |
| **ENSMUSG00000026833.19_Olfm1** | 709.8666 | -1.081551 | 0.13842944 | 2.692918E-16 | 2.174035E-13 | Olfm1 |
| **ENSMUSG00000025576.18_Rbfox3** | 166.6508 | -1.08462 | 0.26100329 | 5.849852E-07 | 6.646732E-05 | Rbfox3 |
| **ENSMUSG00000031760.10_Mt3** | 144.3658 | -1.087078 | 0.25372348 | 3.552591E-07 | 4.191784E-05 | Mt3 |
| **ENSMUSG00000060240.13_Cend1** | 742.1947 | -1.091787 | 0.14442188 | 1.850025E-15 | 1.182397E-12 | Cend1 |
| **ENSMUSG00000017737.3_Mmp9** | 105.7953 | -1.118846 | 0.29671583 | 2.02047E-06 | 0.0001949182 | Mmp9 |
| **ENSMUSG00000032517.17_Mobp** | 34.5962 | -1.119014 | 0.58973273 | 0.0001091484 | 0.005248362 | Mobp |
| **ENSMUSG00000052981.7_Ube2ql1** | 183.2691 | -1.122502 | 0.25110495 | 1.53651E-07 | 2.031769E-05 | Ube2ql1 |
| **ENSMUSG00000027254.14_Map1a** | 609.9455 | -1.12666 | 0.17825681 | 9.043458E-12 | 3.225991E-09 | Map1a |
| **ENSMUSG00000034648.10_Lrrn1** | 97.65444 | -1.137625 | 0.27519816 | 5.525356E-07 | 6.324883E-05 | Lrrn1 |
| **ENSMUSG00000039556.17_Ppp1r3f** | 101.7123 | -1.142994 | 0.3431722 | 6.636085E-06 | 0.0005167051 | Ppp1r3f |
| **ENSMUSG00000051111.17_Sv2c** | 223.4752 | -1.16182 | 0.21944027 | 2.902373E-09 | 6.546985E-07 | Sv2c |
| **ENSMUSG00000040331.17_Nsmce4a** | 374.6564 | -1.162039 | 0.3840554 | 1.301421E-05 | 0.0008951794 | Nsmce4a |
| **ENSMUSG00000060371.13_Caln1** | 200.8132 | -1.163404 | 0.25414068 | 8.662194E-08 | 1.207904E-05 | Caln1 |
| **ENSMUSG00000039607.18_Rbms3** | 59.83006 | -1.164078 | 0.38474684 | 1.294008E-05 | 0.0008950499 | Rbms3 |
| **ENSMUSG00000042182.17_Bend6** | 333.2499 | -1.173252 | 0.15622757 | 2.074605E-15 | 1.272895E-12 | Bend6 |
| **ENSMUSG00000039809.11_Gabbr2** | 303.4935 | -1.174254 | 0.19230834 | 2.90792E-11 | 9.102975E-09 | Gabbr2 |
| **ENSMUSG00000074576.5_Mocs3** | 47.30909 | -1.176512 | 0.46857651 | 3.489385E-05 | 0.002042888 | Mocs3 |
| **ENSMUSG00000048142.10_Nat8l** | 295.712 | -1.180019 | 0.17686538 | 7.7652E-13 | 3.2192E-10 | Nat8l |
| **ENSMUSG00000039954.10_Stk32a** | 62.29743 | -1.181881 | 0.36985547 | 8.27618E-06 | 0.000628457 | Stk32a |
| **ENSMUSG00000029120.11_Ppp2r2c** | 334.1357 | -1.184932 | 0.18839825 | 9.023408E-12 | 3.225991E-09 | Ppp2r2c |
| **ENSMUSG00000015981.13_Stk32c** | 69.37372 | -1.192996 | 0.61776398 | 8.523131E-05 | 0.004176879 | Stk32c |
| **ENSMUSG00000034472.14_Rasd2** | 114.1641 | -1.199773 | 0.2508758 | 3.096372E-08 | 4.947421E-06 | Rasd2 |
| **ENSMUSG00000007944.9_Ttc9b** | 43.30223 | -1.20575 | 0.3847704 | 8.920411E-06 | 0.0006674643 | Ttc9b |
| **ENSMUSG00000097767.10_Miat** | 107.1686 | -1.206022 | 0.44550704 | 2.219834E-05 | 0.001372985 | Miat |
| **ENSMUSG00000047963.8_Stbd1** | 36.06247 | -1.213996 | 0.55409176 | 5.410189E-05 | 0.002938611 | Stbd1 |
| **ENSMUSG00000047604.4_Frat2** | 79.30568 | -1.229565 | 0.36362364 | 4.465826E-06 | 0.0003784603 | Frat2 |
| **ENSMUSG00000061451.14_Tmem151a** | 207.8058 | -1.236656 | 0.20664194 | 4.687498E-11 | 1.409834E-08 | Tmem151a |
| **ENSMUSG00000006711.16_D130043K22Rik** | 11.32458 | -1.239321 | 1.34713462 | 0.0002565941 | 0.01020774 | D130043K22Rik |
| **ENSMUSG00000064360.1_mt-Nd3** | 751.8625 | -1.265115 | 0.19473889 | 1.684655E-12 | 6.800245E-10 | mt-Nd3 |
| **ENSMUSG00000062380.5_Tubb3** | 780.0681 | -1.277937 | 0.13675873 | 2.145807E-22 | 2.351038E-19 | Tubb3 |
| **ENSMUSG00000036422.11_Pcdh8** | 132.046 | -1.280353 | 0.27031694 | 2.785632E-08 | 4.594496E-06 | Pcdh8 |
| **ENSMUSG00000031391.19_L1cam** | 242.5185 | -1.282799 | 0.21555089 | 4.598994E-11 | 1.409834E-08 | L1cam |
| **ENSMUSG00000021728.9_Emb** | 223.6713 | -1.285006 | 0.18298632 | 4.272794E-14 | 2.427422E-11 | Emb |
| **ENSMUSG00000036585.17_Fgf1** | 282.5077 | -1.289184 | 0.19198457 | 3.492312E-13 | 1.674018E-10 | Fgf1 |
| **ENSMUSG00000067242.12_Lgi1** | 49.21831 | -1.301937 | 0.46601647 | 1.415845E-05 | 0.0009525285 | Lgi1 |
| **ENSMUSG00000014846.13_Tppp3** | 589.2976 | -1.303471 | 0.45979008 | 1.293619E-05 | 0.0008950499 | Tppp3 |
| **ENSMUSG00000064329.14_Scn1a** | 440.319 | -1.304519 | 0.21639021 | 2.59442E-11 | 8.290793E-09 | Scn1a |
| **ENSMUSG00000009734.19_Pou6f2** | 66.61772 | -1.312907 | 0.34845852 | 1.085966E-06 | 0.0001164168 | Pou6f2 |
| **ENSMUSG00000041263.15_Rusc1** | 172.996 | -1.319694 | 0.25940262 | 4.361138E-09 | 9.107631E-07 | Rusc1 |
| **ENSMUSG00000022523.11_Fgf12** | 312.6788 | -1.327722 | 0.1979562 | 2.979454E-13 | 1.474253E-10 | Fgf12 |

| | | | | | | |
|---|---|---|---|---|---|---|
| **ENSMUSG00000079598.5_Clec2l** | 132.0925 | -1.334212 | 0.29635592 | 6.238066E-08 | 8.859786E-06 | Clec2l |
| **ENSMUSG00000049176.17_Frmpd4** | 52.82505 | -1.341531 | 0.44768068 | 8.129808E-06 | 0.0006204135 | Frmpd4 |
| **ENSMUSG00000008489.19_Elavl2** | 117.219 | -1.342896 | 0.27420023 | 9.916317E-09 | 1.81079E-06 | Elavl2 |
| **ENSMUSG00000117655.3_6720468P15Rik** | 10.84989 | -1.343574 | 1.34130501 | 0.0002057538 | 0.00862787 | 6720468P15Rik |
| **ENSMUSG00000046613.20_Vwa5b2** | 49.94042 | -1.345553 | 0.43200761 | 6.088755E-06 | 0.0004814196 | Vwa5b2 |
| **ENSMUSG00000001227.13_Sema6b** | 109.7974 | -1.346239 | 0.30820357 | 1.042004E-07 | 1.439936E-05 | Sema6b |
| **ENSMUSG00000030337.17_Vamp1** | 480.3729 | -1.348449 | 0.31868594 | 1.792767E-07 | 2.326559E-05 | Vamp1 |
| **ENSMUSG00000028926.16_Cdk14** | 687.8001 | -1.352597 | 0.15314267 | 1.479863E-20 | 1.513308E-17 | Cdk14 |
| **ENSMUSG00000044502.17_Bod1** | 408.011 | -1.353826 | 0.20445307 | 4.554442E-13 | 2.116987E-10 | Bod1 |
| **ENSMUSG00000096847.3_Tmem151b** | 118.1159 | -1.392302 | 0.30821546 | 4.515E-08 | 6.723844E-06 | Tmem151b |
| **ENSMUSG00000036815.18_Dpp10** | 61.82028 | -1.396698 | 0.5213637 | 1.389447E-05 | 0.0009430413 | Dpp10 |
| **ENSMUSG00000031872.15_Bean1** | 33.76254 | -1.421138 | 0.57432784 | 1.964664E-05 | 0.001240164 | Bean1 |
| **ENSMUSG00000018865.10_Sult4a1** | 653.7369 | -1.42831 | 0.14593049 | 1.126429E-24 | 1.439857E-21 | Sult4a1 |
| **ENSMUSG00000024497.5_Pou4f3** | 22.24274 | -1.429522 | 1.17611888 | 0.000147114 | 0.006696087 | Pou4f3 |
| **ENSMUSG00000031492.14_Chrnb3** | 378.6815 | -1.439001 | 0.20098327 | 6.370205E-15 | 3.758176E-12 | Chrnb3 |
| **ENSMUSG00000028889.18_Yrdc** | 127.5 | -1.468265 | 0.23336006 | 1.996714E-12 | 7.853229E-10 | Yrdc |
| **ENSMUSG00000023949.8_Tcte1** | 30.06508 | -1.477324 | 0.59682672 | 1.734479E-05 | 0.001136973 | Tcte1 |
| **ENSMUSG00000053310.12_Nrgn** | 34.51728 | -1.50929 | 0.88519084 | 6.418532E-05 | 0.003348771 | Nrgn |
| **ENSMUSG00000011751.17_Sptbn4** | 179.5055 | -1.524616 | 0.31367428 | 4.940702E-09 | 9.971766E-07 | Sptbn4 |
| **ENSMUSG00000029088.17_Kcnip4** | 247.2909 | -1.554956 | 0.2106962 | 6.058209E-16 | 4.223948E-13 | Kcnip4 |
| **ENSMUSG00000080058.3_Gm11175** | 34.42211 | -1.602559 | 0.63460573 | 1.234987E-05 | 0.0008689661 | Gm11175 |
| **ENSMUSG00000019194.16_Scn1b** | 133.264 | -1.608167 | 0.33408744 | 4.300676E-09 | 9.107631E-07 | Scn1b |
| **ENSMUSG00000066129.18_Kndc1** | 59.85265 | -1.614881 | 0.55307473 | 4.934245E-06 | 0.0004091156 | Kndc1 |
| **ENSMUSG00000040125.5_Gpr26** | 148.0644 | -1.632232 | 0.30996715 | 3.674221E-10 | 1.006409E-07 | Gpr26 |
| **ENSMUSG00000032452.13_Clstn2** | 94.95507 | -1.639638 | 0.42275269 | 2.379747E-07 | 2.967718E-05 | Clstn2 |
| **ENSMUSG00000029674.14_Limk1** | 139.7388 | -1.646494 | 0.32867207 | 1.357757E-09 | 3.44466E-07 | Limk1 |
| **ENSMUSG00000033595.8_Lgi3** | 134.5069 | -1.68585 | 0.34564017 | 2.309498E-09 | 5.367483E-07 | Lgi3 |
| **ENSMUSG00000036578.8_Fxyd7** | 48.41993 | -1.694534 | 0.55793013 | 3.154511E-06 | 0.0002796939 | Fxyd7 |
| **ENSMUSG00000060882.6_Kcnd2** | 68.12892 | -1.705373 | 0.40612856 | 5.357679E-08 | 7.826804E-06 | Kcnd2 |
| **ENSMUSG00000031491.11_Chrna6** | 571.1376 | -1.743353 | 0.32545412 | 1.445702E-10 | 4.184079E-08 | Chrna6 |
| **ENSMUSG00000032564.17_Cpne4** | 68.18191 | -1.743674 | 0.37651593 | 6.573082E-09 | 1.27626E-06 | Cpne4 |
| **ENSMUSG00000032011.6_Thy1** | 607.1082 | -1.818586 | 0.17488561 | 2.29101E-28 | 3.194709E-25 | Thy1 |
| **ENSMUSG00000003657.10_Calb2** | 1717.131 | -1.841651 | 0.16512481 | 5.701895E-32 | 1.249448E-28 | Calb2 |
| **ENSMUSG00000050138.9_Kcnk12** | 16.29026 | -1.928534 | 1.73038589 | 7.370928E-05 | 0.003756235 | Kcnk12 |
| **ENSMUSG00000060212.14_Pcnx2** | 81.84115 | -1.953428 | 0.43824965 | 1.067923E-08 | 1.904752E-06 | Pcnx2 |
| **ENSMUSG00000033615.10_Cplx1** | 745.6779 | -1.964958 | 0.16968345 | 3.436214E-34 | 1.317702E-30 | Cplx1 |
| **ENSMUSG00000031688.5_Pou4f2** | 38.63353 | -2.445127 | 0.78848408 | 1.909641E-06 | 0.0001865732 | Pou4f2 |
| **ENSMUSG00000020836.16_Coro6** | 31.14289 | -2.453996 | 0.78142356 | 1.733551E-06 | 0.0001704547 | Coro6 |
| **ENSMUSG00000020396.9_Nefh** | 386.0855 | -2.461462 | 0.23062526 | 7.078523E-29 | 1.085775E-25 | Nefh |
| **ENSMUSG00000020121.16_Srgap1** | 104.2682 | -2.465766 | 0.36537793 | 5.153984E-14 | 2.823463E-11 | Srgap1 |
| **ENSMUSG00000047228.10_A2ml1** | 17.89244 | -2.502325 | 1.06909434 | 9.491125E-06 | 0.0006965759 | A2ml1 |
| **ENSMUSG00000038530.12_Rgs4** | 359.8645 | -2.50759 | 0.22795822 | 2.744722E-30 | 4.677922E-27 | Rgs4 |
| **ENSMUSG00000040703.12_Cyp2s1** | 27.37233 | -2.512 | 0.92756608 | 4.678407E-06 | 0.0003942972 | Cyp2s1 |
| **ENSMUSG00000069372.4_Ctxn3** | 58.14415 | -2.535844 | 0.39661619 | 7.11738E-13 | 3.032597E-10 | Ctxn3 |
| **ENSMUSG00000021604.16_Irx4** | 26.0881 | -2.548239 | 2.10663248 | 1.951925E-05 | 0.001240021 | Irx4 |
| **ENSMUSG00000020635.9_Fkbp1b** | 40.2908 | -2.617472 | 0.47980685 | 2.271133E-10 | 6.333985E-08 | Fkbp1b |
| **ENSMUSG00000039252.12_Lgi2** | 93.19749 | -2.71781 | 0.42979206 | 2.35621E-12 | 9.035475E-10 | Lgi2 |
| **ENSMUSG00000022454.18_Nell2** | 225.6444 | -2.778274 | 0.23517635 | 1.281221E-33 | 3.275442E-30 | Nell2 |
| **ENSMUSG00000026347.14_Tmem163** | 95.92404 | -2.878999 | 0.34615827 | 3.08487E-18 | 2.78346E-15 | Tmem163 |
| **ENSMUSG00000022054.12_Nefm** | 1310.074 | -2.901864 | 0.16048344 | 4.044989E-74 | 3.102304E-70 | Nefm |

# Appendix 2: GSEA output tables

| Glaucoma Early vs Naïve: UP | | | | |
|---|---|---|---|---|
| **ID** | **Description** | **NES** | **p.adjust** | **core_enrichment_symbols** |
| **GO:0002460** | adaptive immune response based on somatic recombination of immune receptors built from immunoglobulin superfamily domains | 2.551073218646200 | 3.72558779191661E-08 | Stat3/C1qc/H2-D1/H2-K1/Fcgr3/C4b/C1qa/H2-Q6/Ctsh/C1s1/H2-T23/Ctsc/B2m/H2-Q7/Mr1/Cd74/Icam1/Il33/Serping1/C1qb/Tnfsf13/Ahr/Bcl3/C1ra/Anxa1/Unc93b1/Cd24a/Vsir/Tap2/Jak3/Trem2/Arid5a/Dusp22/Tnfrsf1b/C3/Fcer1g/Fosl2/Cfh/Zbtb1/Rab27a/Il18bp/Stard7/Lgals1/Myd88/Nfkbiz/Entpd7/Tmem98/Exosc3/Pnp/Malt1/Pla2g4a/Xrcc4/Mlh1/Ndfip1/Stx7 |
| **GO:0002449** | lymphocyte mediated immunity | 2.516210052576450 | 3.72558779191661E-08 | C1qc/H2-D1/H2-K1/Fcgr3/C4b/C1qa/H2-Q6/Ctsh/C1s1/H2-T23/Ctsc/Lgals9/B2m/H2-Q7/Mr1/Cd74/Icam1/Serping1/C1qb/Tnfsf13/Ahr/Bcl3/C1ra/Unc93b1/Cd24a/Vsir/Tap2/Trem2/Arid5a/Dusp22/Tnfrsf1b/C3/Fcer1g/Fosl2/Cfh/Zbtb1/Rab27a/Tap1/Prdx1/Stard7/Myd88/Nfkbiz/Exosc3/Pnp/Malt1/Xrcc4/Mlh1/Ndfip1/Stx7 |
| **GO:0019882** | antigen processing and presentation | 2.4947656661002300 | 3.72558779191661E-08 | H2-D1/H2-K1/Fcgr3/Cd68/Psmb8/H2-Q6/H2-T23/Mpeg1/B2m/H2-Q7/H2-Ab1/Mr1/Cd74/Icam1/Ctss/Unc93b1/Tap2/Psmb9/Trem2/H2-Aa/Fcer1g/Pycard/Pdia3/Rab8b/Rab27a/Tap1 |
| **GO:0002250** | adaptive immune response | 2.463249236318880 | 3.72558779191661E-08 | Stat3/C1qc/H2-D1/Cd44/H2-K1/Fcgr3/C4b/C1qa/H2-Q6/Ctsh/C1s1/H2-T23/Mpeg1/Ctsc/B |

| | | | | |
|---|---|---|---|---|
| | | | | 2m/H2-Q7/Mr1/Cd74/Icam1/Il33/Serping1/C1qb/Cx3cr1/Tnfsf13/Ahr/Bcl3/C1ra/Anxa1/Unc93b1/Cd24a/Vsir/Tap2/Jak3/Lyn/Trem2/Arid5a/Jchain/Dusp22/Tnfrsf1b/C3/Fcer1g/Pycard/Fosl2/Cfh/Pdia3/Zbtb1/Rab27a/Il18bp/Tap1/Stard7/Lgals1/Lat2/Myd88/Nfkbiz/Entpd7/Tmem98/Exosc3/Pnp/Malt1/Pla2g4a/Xrcc4/Mlh1/Ndfip1/Stx7 |
| **GO:0002821** | positive regulation of adaptive immune response | 2.394861314491080 | 1.10099752283782E-07 | H2-D1/Cd44/H2-K1/Fcgr3/H2-Q6/H2-T23/B2m/H2-Q7/Mr1/Cd74/Tnfsf13/Cd24a/Tap2/Trem2/Arid5a/C3/Fcer1g/Pycard/Zbtb1/Nfkbiz/Exosc3/Pnp/Malt1/Pla2g4a/Mlh1/Stx7 |

| **Glaucoma Early vs Naïve: DOWN** | | | | | | |
|---|---|---|---|---|---|---|
| **ID** | **Description** | **enrichmentScore** | **NES** | **p.adjust** | **rank** | **core_enrichment_symbols** |
| **GO:0015872** | dopamine transport | -0.7209669953982030 | -2.122948514645860 | 2.81770107786632E-04 | 1711 | Syt1/Kpna4/Syt11/Grm2/Gnat1/Sncg/Chrnb2/Kcna2/Syt7/Chrna4/Drd2/Prkcb/Snca/Pink1/Gabbr1/Myo5a/Rab3a/Chrna6/Nat8l |
| **GO:0035418** | protein localization to synapse | -0.6206834887366540 | -2.10114487897057 | 3.07164803007686E-06 | 2198 | Kif5c/Iqsec2/Rab4a/Stx3/Abhd17b/Cacng3/Arhgap44/Gphn/Klc1/Tnik/Lhfpl4/Lgi1/Gpc6/Dlg2/Homer1/Git1/Grin2a/Dlg3/Nrxn3/ |

| | | | | | | |
|---|---|---|---|---|---|---|
| | | | | | | Nsg1/Mapk8ip3/Reln/Baiap2/Hras/Map2k1/Mapk10/Epb41l1/Lrrtm1/Rapgef4/Stx1b/Zdhhc2/Cplx1/Grin2c/Clstn1/Asic2/Mapt/Nlgn2/Nptxr/Nrxn1/Nptx1/Map1a/Nrxn2/Grin1 |
| **GO:0099601** | regulation of neurotransmitter receptor activity | -0.7177005120475120 | -2.0955277778124020 | 1.70242335192036E-04 | 2263 | Cacng2/Nlgn3/Nlgn1/Prrt1/Cacng3/Ephb2/Mapk8ip2/Rasgrf1/Homer1/Rasgrf2/Lynx1/Begain/Cacng5/Slc6a9/Reln/Dapk1/Cnih2/Homer3/Shisa6/Nlgn2/Cacng4/Shisa8/Nrxn2 |
| **GO:0019226** | transmission of nerve impulse | -0.6392588212546240 | -2.0885449866910900 | 1.25542554136001E-05 | 2084 | Cacng3/Pawr/Hcn1/Kcnmb4/Cntnap1/Cntnap2/Kcnc4/Myh14/Ntrk3/Pak1/Ank3/Glra1/Atp1a3/Fgf12/Cacna1a/Scn1a/Efr3b/Cacng5/Chrnb2/Fkbp1b/Kcna2/Grik2/Scn2a/Chrna4/Kcnma1/Kcnd2/Rapgef4/Kcnq2/Scn1b/Cacna1g/Dpp6/Npr2/Cacng4/Sptbn4 |
| **GO:0051963** | regulation of synapse assembly | -0.5601963582958630 | -2.0689731194481430 | 4.342288826 1659E-07 | 2761 | Ptk2b/Nlgn3/Slit2/Srgap2/Cux2/Mdga2/Nlgn1/Mark1/Nectin3/Nckipsd/Lingo4/Srgap3/Amigo1/Adgrb3/Chd4/Iqsec2/Lrrtm3/Podxl/ |

| | | | | | | |
|---|---|---|---|---|---|---|
| | | | | | | Srpx2/Cbln1/Iqsec1/Ephb2/Slitrk1/Cbln2/Ntng2/Farp1/Lhfpl4/Elavl2/Crtac1/Carmil3/Rac3/Agrn/Ntrk3/Ptprs/Lrrc24/Lrtm1/Sipa1l1/Caskin1/Cpeb3/Nrg1/Flrt1/Ube3b/Cyfip2/Nectin1/Chrnb2/Il1rapl1/Six1/Asic1/L1cam/Flrt2/Zdhhc8/Lrfn5/Eif4g1/Lrrn1/Rac1/Elmo1/Lrrtm1/Lrtm2/Slc12a5/Adgrl1/Crmp1/Clstn2/Snca/Mycbp2/Ppp1r9b/Ube2m/Clstn1/Efnb3/Asic2/Nlgn2/Lrrc4b/Ephb1/Adgrb1/Nrxn1/Lrfn1/Adgrb2/Nrxn2/Grin1 |

| **Glaucoma Mid vs Naïve: UP** | | | | |
|---|---|---|---|---|
| **ID** | **Description** | **NES** | **p.adjust** | **core_enrichment_symbols** |
| **GO:0001945** | lymph vessel development | 2.042547807953790 | 0.001881627849599 5200 | Heg1/Fgf2/Kdr/Pkd1/Flt4/Pdpn/Acvr2b/Bmpr2/Clec14a |
| **GO:0060219** | camera-type eye photoreceptor cell differentiation | 2.039882456847140 0 | 0.001533801426970 5800 | Rpgrip1/Stat3/Rorb/Sox9/Crb2/Pde6c/Miat/Casz1/Cntf/Vax2os/Samd11/Cfh/Slc4a7 |
| **GO:0060221** | retinal rod cell differentiation | 2.011287763165640 0 | 0.003225673347900 4100 | Rpgrip1/Stat3/Rorb/Sox9/Miat/Casz1/Cntf/Samd11/Cfh |
| **GO:0002455** | humoral immune response mediated by circulating immunoglobulin | 2.009899146418130 0 | 0.003540971677985 500 | C4b/C1qc/C1ra/C3/Bcl3/Serping1/C1s1/C1qb |

| | | | | |
|---|---|---|---|---|
| **GO:0006956** | complement activation | 1.9819012773075700 | 0.0036292391440469400 | C4b/A2m/C1qc/C1ra/C3/Serping1/C1s1/C1qb |

| **Glaucoma Mid vs Naïve: DOWN** | | | | |
|---|---|---|---|---|
| **ID** | **Description** | **NES** | **p.adjust** | **core_enrichment_symbols** |
| **GO:0140241** | translation at synapse | -2.566641382846740 | 5.594E-08 | Rps27a/Rps16/Rpl36a/Rpl32/Rpl35/Rps10/Rpl13a/Uba52/Rps26/Rpl27/Rpl35a/Rpl27a/Rpl23a/Rpl9/Rpl8/Rpl7/Rplp2/Rpl26/Rpl17/Rpl5/Rps11/Rpl37/Rpl36/Rps14/Rpl37a/Rpl15/Rpl13/Rpl24/Rpl10a/Rps27/Rpl4/Rps28/Rpl29/Rpl7a/Rpl34/Rpl14/Rps5 |
| **GO:0140242** | translation at postsynapse | -2.566641382846740 | 5.594E-08 | Rps27a/Rps16/Rpl36a/Rpl32/Rpl35/Rps10/Rpl13a/Uba52/Rps26/Rpl27/Rpl35a/Rpl27a/Rpl23a/Rpl9/Rpl8/Rpl7/Rplp2/Rpl26/Rpl17/Rpl5/Rps11/Rpl37/Rpl36/Rps14/Rpl37a/Rpl15/Rpl13/Rpl24/Rpl10a/Rps27/Rpl4/Rps28/Rpl29/Rpl7a/Rpl34/Rpl14/Rps5 |
| **GO:0140236** | translation at presynapse | -2.563062869248120 | 5.594E-08 | Rps27a/Rps16/Rpl36a/Rpl32/Rpl35/Rps10/Rpl13a/Uba52/Rps26/Rpl27/Rpl35a/Rpl27a/Rpl23a/Rpl9/Rpl8/Rpl7/Rplp2/Rpl26/Rpl17/Rpl5/Rps11/Rpl37/Rpl36/Rps14/Rpl37a/Rpl15/Rpl13/Rpl24/Rpl10a/Rps27/Rpl4/Rps28/Rpl29/Rpl7a/Rpl34/Rpl14/Rps5 |
| **GO:0006457** | protein folding | -2.451695276084250 | 5.594E-08 | Fkbp2/Hspa1a/Ccdc47/Cct5/Pdcl/Hspb1/Wdr83os/Pdcd5/Ric8b/Selenof/Pfdn |

| | | | | |
|---|---|---|---|---|
| | | | | 6/Bag5/Stub1/Tor2a/Sdf2/Sdf2l1/Tbcb/Arl2/Hsp90aa1/Tcp1/Pdrg1/Pfdn2/Nudc/Trap1/Ppib/Dnajb1/Hspa2/Pfdn5/Pdia4/Tbcc/Dnajc3/Ppia/Hspa5/Ptges3/Dnajb6/Ahsa1/Cct6a/Cct8/Dnaja2/Cdc123/Fkbp4/St13/Chordc1/Cct7/Vbp1/Hsp90ab1/Pdia3/Cdc37/Hspe1/Cct4/Calr/Ppie/Hsph1/Cct2/Hspd1/Dnaja1/Cct3/Hspa8 |
| **GO:0002181** | cytoplasmic translation | -2.43860180107950 | 5.594E-08 | Rpl18/Mcts2/Cnbp/Eif3k/Drg1/Rps29/Rpl39/Rps27a/Rps16/Rps8/Rpl41/Rpl36a/Rpl32/Eif3f/Eif3b/Rpl35/Rps17/Rpl11/Rps15/Pkp1/Rps13/Rps10/Rpl13a/Mif4gd/Uba52/Rps26/Rpl27/Rpl35a/Rpl27a/Rps6/Rps3a1/Rpl23a/Rpl9/Rpl30/Ftsj1/Rpl8/Rpl7/Rplp2/Rpl26/Rwdd1/Rps9/Rps21/Ncbp2/Rps23/Rps3/Rpl17/Rplp1/Rpl5/Eif3i/Rps11/Rpl37/Rps2/Eif3e/Rpl36/Rps14/Rpl21/Rps25/Rps18/Rpl37a/Rpl15/Rps7/Rpl13/Slbp/Rpl24/Rpl10a/Zc3h15/Nck1/Rps19/Rplp0/Rpl4/Eif3m/Eif2b2/Rpl31/Rps28/Rpl18a/Rpl29/Rpl19/Rpl3/Rpl7a/Rpsa/Rpl34/Rpl14/Rps5/Eif3h/Eif4a2 |

| Glaucoma Late vs Naïve: UP | | | | |
|---|---|---|---|---|
| **ID** | **Description** | **NES** | **p.adjust** | **core_enrichment_symbols** |
| **GO:0006956** | complement activation | 2.286364919806230 | 3.51280927981265E-05 | C4b/A2m/C3/C1qc/Serping1/C1s1/C1qa/Cfh/Cfp/Trem2/C1qb/C1ra/Cd46 |
| **GO:0048002** | antigen processing and presentation of peptide antigen | 2.241256856953340 | 1.26819313416975E-04 | Fcgr3/Ctss/H2-T24/H2-K1/Mr1/H2-Ab1/B2m/H2-Q6/Pycard/Cd74/Trem2/Marchf1/Mpeg1/Fcer1g/Tap1/H2-Aa/H2-D1 |
| **GO:0002455** | humoral immune response mediated by circulating immunoglobulin | 2.21557090608998 | 1.26819313416975E-04 | C4b/C3/C1qc/Serping1/C1s1/C1qa/Trem2/C1qb/Bcl3/C1ra/Cd46 |
| **GO:0006958** | complement activation, classical pathway | 2.192916362552130 | 1.26819313416975E-04 | C4b/C3/C1qc/Serping1/C1s1/C1qa/Trem2/C1qb/C1ra/Cd46 |
| **GO:0006959** | humoral immune response | 2.11209586682557 | 1.30422473385474E-04 | C4b/A2m/C3/C1qc/Serping1/C1s1/Lgals3/C1qa/B2m/Rnase4/Cfh/Mef2c/Cfp/Trem2/C1qb/Bcl3/Trf/C1ra/Cd46 |

| Glaucoma Late vs Naïve: DOWN | | | | |
|---|---|---|---|---|
| **ID** | **Description** | **NES** | **p.adjust** | **core_enrichment_symbols** |
| **GO:0009060** | aerobic respiration | -2.145868934593670 | 5.95662528095778E-06 | Cs/Ndufa9/Fh1/Ndufs5/Coq7/Uqcrb/Ndufb4/Mfn2/Mtfr1l/1700066M21Rik/Cox4i1/Ndufa10/Ndufb6/Mtfr1/Ndufa12/Cox7c/Ogdh/Uqcrfs1/Pdhb/Arl2/Vcp/Ndufs8/Ndufb8/Sdhb/Ndufa13/Mtch2/Sdhaf2/Pdha1/Cycs/Ak4/Ndufa8/Tmem135/Sdhd/Cox6b1/Ndufs6/Uqcrc1/Coq9/Ndp/Cox7a2/Ndufv2/Ndufb9/Stoml2/Idh1/Aco1/Ndufv1/Sdha/Cyc1/Nipsnap2/Snca/Cox5a/Mdh1/Sucla2/Sucl |

| | | | | |
|---|---|---|---|---|
| | | | | g1/Ndufb5/Pink1/Aco2/Mdh2/Sdhc/Shmt2/Atp5pb/Atpsckmt/Msh2/Cox7a2l/Slc25a33/Idh3a |
| **GO:0097401** | synaptic vesicle lumen acidification | -2.1145964596109000 | 0.0030124678798911200 | Atp6v1g2/Atp6v1a/Atp6v1f/Atp6v0c/Atp6v0a1/Atp6v0d1/Atp6v1e1/Atp6v1g1/Slc9a6/Atp6v1b2/Atp6v0e2/Slc17a7/Atp6v1c1/Atp6ap1/Atp6ap2 |
| **GO:1902600** | proton transmembrane transport | -2.0927523366284200 | 2.38994471912557E-04 | Atp6v1a/Uqcrfs1/Atp6v1f/Atp6v0b/Atp6v0c/Ndufs8/Atp6v0a1/Surf1/Letm1/Atp6v0d1/Slc25a3/Slc18b1/Atp6v1e1/Slc25a4/Ndufv2/Slc25a12/Slc16a1/Ndufv1/Cyc1/Slc25a14/Atp6v1g1/Slc25a5/Taco1/Slc9a6/Atp6v1b2/Atp6v0e2/Atp5pb/Atp1b1/Coa8/Slc17a7/Atpsckmt/Ghitm/Slc17a6/Atp6v1c1/Atp6ap1/Drd4/Atp6ap2 |
| **GO:0006099** | tricarboxylic acid cycle | -2.0866224942791600 | 0.004810087344875740 | Ogdh/Pdhb/Sdhb/Sdhaf2/Pdha1/Sdhd/Ndp/Idh1/Aco1/Sdha/Mdh1/Sucla2/Suclg1/Aco2/Mdh2/Sdhc/Idh3a |
| **GO:0006626** | protein targeting to mitochondrion | -2.0851246535945110 | 5.79947466819792E-04 | Aip/Timm8a1/Bcap31/Immp2l/Lrrk2/Tomm7/Pmpca/Agk/Samm50/Timm50/Mfn2/Grpel1/Chchd4/Pmpcb/Timm22/Fis1/Ndufa13/Mtch2/Prkaa1/Ptpn5/Dnlz/Hspa4/Tomm40l/Tomm70a/Mff/Tomm22/Aifm1/Mipep/Bag4/Timm44/Pink1/Parl/Hspd1/Dusp18/Grpel2/Timm23/Timm29/Ywhaz |

| Crush Early vs Naïve: UP | | | | |
|---|---|---|---|---|
| **ID** | **Description** | **NES** | **p.adjust** | **core_enrichment_symbols** |
| **GO:0002526** | acute inflammatory response | 2.219594196346570 0 | 1.17400777152692E -04 | A2m/Stat3/Icam1/Adcyap1/Fcgr3/Serpina3n/F3/Nupr1/Vwf/Fn1/Plscr1/Fcer1g/Casp6/C3/H2-T23 |
| **GO:0002437** | inflammatory response to antigenic stimulus | 2.191282086681190 | 4.90379868371684E -04 | A2m/Cd68/Icam1/Adcyap1/Fcgr3/Mkrn2/Trem2/Hmgb2/Fcer1g/C3/H2-T23/Rbpj/Ahcy/Cd24a/Fosl2 |
| **GO:0002438** | acute inflammatory response to antigenic stimulus | 2.126722188741380 | 4.95151734689751E -04 | A2m/Icam1/Adcyap1/Fcgr3/Fcer1g/C3/H2-T23 |
| **GO:0002460** | adaptive immune response based on somatic recombination of immune receptors built from immunoglobulin superfamily domains | 2.11119565241855 | 3.06353192860248E -07 | Stat3/Arid5a/C4b/C1qc/H2-K1/Tnfsf13/H2-Q6/H2-D1/Icam1/Fcgr3/Il33/Vsir/Ctsh/B2m/Jak3/Gadd45g/Serping1/C1ra/Myd88/Stard7/Ahr/H2-T24/Ctsc/Lef1/C1qa/C1qb/Kmt5b/Dennd1b/Trem2/Aplf/Cd74/Pcyt1a/C1s1/Ercc1/H2-Q7/Bcl3/Lgals1/Fcer1g/Traf2/Map3k7/Rab27a/C3/H2-T23/Unc93b1/Tnfrsf1b/H2-M3/Brd2/Nckap1l/Entpd7/Il1r1/Ripk2/Pkn1/Inpp5d/Rorc/Mlh1/Myo1g/Il4i1/Il18bp/Irf1/Cd24a/Brd4/Il4ra/Anxa1/Fosl2/Trpm4/Clcf1/Parp3 |
| **GO:0006956** | complement activation | 2.105446143096280 0 | 0.002548228384604 550 | A2m/C4b/C1qc/Serping1/C1ra/C1qa/C1qb/Trem2/C1s1/Krt1/C3 |

| Crush Early vs Naïve: DOWN | | | | |
|---|---|---|---|---|
| **ID** | **Description** | **NES** | **p.adjust** | **core_enrichment_symbols** |
| **GO:0001508** | action potential | -2.269555111073400 | 1.1188E-07 | Nrcam/Cntnap2/Kcnc4/Kcnn2/Kcnd1/Kcnip1/Kcnj11/Grin2a/Calm3/Cacnb2/Kcnab2/Clcn1/Ank3/Grin2b/Hnrnpa1/Scn1b/Kcnip2/Kcnmb4/Chrna4/Kcna6/Calm1/Cd36/Scn2a/Rangrf/Kcnc2/Scn3a/Cacna1g/Npr2/Kcna2/Scn2b/Kcnb2/Grik2/Kcne2/Kcnb1/Calm2/Cacna2d1/Ntrk3/Kcnc1/Kcng4/Kcnd3/Dpp6/Kcnj5/Cntnap1/Atp2a2/Fgf13/Scn1a/Scn3b/Rapgef4/Kcnq2/Kcnd2/Cacnb3/Fgf12/Fkbp1b/Scn4b |
| **GO:0099500** | vesicle fusion to plasma membrane | -2.2248449191319100 | 3.09393856629305E-05 | Stx1b/Syt1/Syt2/Trarg1/Vamp1/Rab3a/Prrt2/Cplx2/Rph3a/Snap25/Cplx1 |
| **GO:0099072** | regulation of postsynaptic membrane neurotransmitter receptor levels | -2.217007566751480 | 1.1188E-07 | Vamp2/Nrg1/Ap2a1/Lhfpl4/Cacng3/Ap2m1/Pip5k1c/Git1/Susd4/Grip1/Cntnap2/Hpca/Ppfia1/Myo6/Inpp4a/Rala/Ppp3r1/Hras/Tamalin/Ap2s1/Sh3glb2/Dlg2/Rap2a/Ncdn/Zdhhc2/Gphn/Drd4/Cnih3/Ap2b1/Gpsm2/Pacsin1/Epb41l1/Nedd4/Nrxn3/Sacm1l/Stx1b/Ctnnd2/Caly/Slc12a5/Cacng4/Neto2/Clstn1/Mapk10/Synj1/Map2k1/Tfrc/Tspan7/Hsp90aa1/Nsg1/Grid1/Adam22/Nptxr/Cacng5/Syt3/Usp46/Nsg2/Rapgef4/Nptx1/Frrs1l/Lgi1/Zdhhc5/Cplx1 |
| **GO:0035418** | protein localization to synapse | -2.195529087925360 | 2.37735889192159E-06 | Camk2a/Dlg3/Neto1/Arhgap44/Rab8a/Dlgap1/Cacng2/Erbb4/Homer1/Vamp2/Lhfpl4/Cacng3/Git1/Rab27b/Grip1/Slitrk3/ |

| | | | | |
|---|---|---|---|---|
| | | | | Grin2a/Hras/Dlg2/Bsn/Nlgn3/Zdhhc2/Kif5a/Gphn/Zdhhc15/Grin2c/Cnih3/Gpsm2/Epb41l1/Nrxn3/Asic2/Rab4a/Sacm1l/Stx1b/Map1a/Neto2/Clstn1/Mapk10/Mapt/Map2k1/Lrrtm1/Baiap2/Nsg1/Nrxn2/Nlgn1/Adam22/Nptxr/Grin1/Nrxn1/Rapgef4/Nptx1/Lgi1/Cplx1 |
| **GO:2000649** | regulation of sodium ion transmembrane transporter activity | -2.1830616323424800 | 2.33616985661262E-05 | Chp1/Ank3/Scn1b/Fgf11/Drd4/Nedd4/Rangrf/Wnk3/Scn2b/Plcb1/Fgf13/Scn3b/Fgf12/Atp1b1/Scn4b |

| **Crush Late vs Naïve: UP** | | | | |
|---|---|---|---|---|
| **ID** | **Description** | **NES** | **p.adjust** | **core_enrichment_symbols** |
| **GO:0002460** | adaptive immune response based on somatic recombination of immune receptors built from immunoglobulin superfamily domains | 2.2048612180313900 | 2.1233225822029E-07 | Stat3/C4b/Fcgr3/Tnfsf13/C1qc/H2-K1/H2-D1/Jak3/H2-Q6/B2m/C1qa/H2-T23/Ctsc/Ctsh/Stard7/Mr1/Ahr/Vsir/Serping1/Myd88/Trem2/Emp2/Bcl3/Il33/C1ra/Pcyt1a/C1qb/Parp3/Il1r1/Pla2g4a/Tfrc/Lef1/Icam1/Irf1/Unc93b1/Malt1/Il18bp/Kmt5b/H2-Q7/Rab27a/Aplf/Mlh1/Dpp4/Anxa1/Traf2/Nckap1l/Tnfrsf1b/Myo1g/H2-M3/C1s1/Cd74/Irf7/Clcf1/Ufl1/Tap2/Ercc1/Ighm |
| **GO:0019724** | B cell mediated immunity | 2.1198921687752400 | 2.06587374771647E-04 | C4b/Fcgr3/Tnfsf13/C1qc/C1qa/H2-T23/Serping1/Myd88/Trem2/Bcl3/C1ra/Pcyt1a/C1qb/Parp3/Tfrc/Kmt5b/Aplf/Mlh1/H2-M3/C1s1/Cd74/Irf7/Clcf1/Ercc1/Ighm |

| | | | | |
|---|---|---|---|---|
| **GO:0019883** | antigen processing and presentation of endogenous antigen | 2.118477152386460 0 | 0.003134065309938 7300 | H2-K1/H2-D1/H2-Q6/B2m/H2-T23/Atg5/Tap1/Tapbp/H2-Q7/H2-M3/Tap2 |
| **GO:0016064** | immunoglobulin mediated immune response | 2.096614189747780 0 | 1.84681000097442E-04 | C4b/Fcgr3/Tnfsf13/C1qc/C1qa/H2-T23/Serping1/Myd88/Trem2/Bcl3/C1ra/Pcyt1a/C1qb/Parp3/Tfrc/Kmt5b/Aplf/Mlh1/C1s1/Cd74/Irf7/Clcf1/Ercc1/Ighm |
| **GO:0002437** | inflammatory response to antigenic stimulus | 2.060843923706700 0 | 0.004889104814429 140 | A2m/Fcgr3/Cd68/H2-T23/Hmgb2/Trem2/Icam1/Selenos/Mkrn2 |

| **Crush Late vs Naïve: DOWN** | | | | |
|---|---|---|---|---|
| **ID** | **Description** | **NES** | **p.adjust** | **core_enrichment_symbols** |
| **GO:0045103** | intermediate filament-based process | -2.177839121359990 0 | 1.14173238853953E-04 | Shh/Ina/Nefh/Nefm/Nefl |
| **GO:0045104** | intermediate filament cytoskeleton organization | -2.167169103048620 | 5.87144661563867E-04 | Shh/Ina/Nefh/Nefm/Nefl |
| **GO:0099170** | postsynaptic modulation of chemical synaptic transmission | -2.120702440327210 0 | 0.005405472626976 190 | Sorcs3/Prkaca/Dcc/Clmp/Plcb1/Gnao1/Fmr1/Nrgn/Fbxo2/Ina/Nefh/Nefl |
| **GO:0090128** | regulation of synapse maturation | -2.073385447448550 0 | 0.005460757184037 000 | Reln/Ywhaz/Dab2ip/Sema7a/Adgrl1/Cntnap1/Nrxn1/Nrn1/Nefl |
| **GO:0099500** | vesicle fusion to plasma membrane | -2.057331773826830 0 | 0.008000788253504 480 | Erc1/Syt7/Prrt2/Syt11/Stx1b/Rab3a/Vamp1/Snap25/Rph3a/Cplx2/Trarg1/Cplx1 |

# Appendix 3: Publications arising from this work

Vision Research 225 (2024) 108502



Contents lists available at ScienceDirect

Vision Research

journal homepage: www.elsevier.com/locate/visres





# Gene therapy for glaucoma: Targeting key mechanisms

Jeff Henderson, Jeffrey O'Callaghan, Matthew Campbell *

*Smurfit Institute of Genetics, Trinity College Dublin, Dublin 2, Ireland*

ARTICLE INFO

*Keywords:*
Gene therapy
Glaucoma
Adeno-associated virus

ABSTRACT

Glaucoma is a group of optic neuropathies characterised by progressive retinal ganglion cell (RGC) degeneration and is the leading cause of irreversible blindness worldwide. Current treatments for glaucoma focus on reducing intraocular pressure (IOP) with topical medications. However, many patients do not achieve sufficient IOP reductions with such treatments. Patient compliance to dosing schedules also poses a significant challenge, further limiting their effectiveness. While surgical options exist for resistant cases, these are invasive and carry risks of complications. Thus, there is a critical need for better strategies to prevent irreversible vision loss in glaucoma. Gene therapy holds significant promise in this regard, offering potential long-term solutions by targeting the disease's underlying causes at a molecular level. Gene therapy strategies for glaucoma primarily target the two key hallmarks of the disease: elevated IOP and RGC death. This review explores key mechanisms underlying these hallmarks and discusses the current state of gene therapies targeting them. In terms of IOP reduction, this review covers strategies aimed at enhancing extracellular matrix turnover in the conventional outflow pathway, targeting fibrosis, regulating aqueous humor production, and targeting myocilin for gene-specific therapy. Neuroprotective strategies explored include targeting neurotrophic factors and their receptors, reducing oxidative stress and mitochondrial dysfunction, and preventing Wallerian degeneration. This review also briefly highlights key research priorities for advancing gene therapies for glaucoma through the clinical pipeline, such as refining delivery vectors and improving transgene regulation. Addressing these priorities will be essential for translating advancements from preclinical models into effective clinical therapies for glaucoma.

## 1. Introduction

### 1.1. Glaucoma: An overview

Glaucoma is a group of optic neuropathies characterised by progressive optic nerve and retinal ganglion cell (RGC) degeneration. Affecting upwards of 80 million people, glaucoma is the leading cause of irreversible blindness worldwide (Tham et al., 2014). While the pathogenesis of glaucoma is not fully understood, risk factors include age, family history, and elevated intraocular pressure (IOP) (Weinreb, Aung, and Medeiros, 2014). The normal IOP range in adults is 10–21 mmHg, with IOP values exceeding 21 mmHg being classified as hypertensive (Khaw, Shah, and Elkington, 2004). Glaucoma can be broadly classed into open-angle glaucoma (OAG) and angle-closure glaucoma (ACG). These forms are distinguished based on the state of the angle between the iris and the cornea (the irideocorneal angle). This is the site of aqueous humour (AH) drainage, which, when obstructed, leads to increases in IOP. In OAG, drainage is restricted despite the irideocorneal angle remaining open. Contrastingly in ACG, elevated intraocular pressure occurs as a direct result of the iris becoming displaced and obstructing the irideocorneal angle. Glaucoma can be further broken down into primary and secondary forms. In primary glaucoma, elevations in IOP are idiopathic, while in secondary glaucoma, ocular hypertension is caused by known factors such as systemic disease, trauma, or treatment with corticosteroids (Weinreb, Aung, and Medeiros, 2014). Primary open angle glaucoma (POAG) is the most prevalent subtype of glaucoma, accounting for 74 % of all glaucoma cases (Quigley and Broman, 2006).

As it is the only modifiable risk factor for the disease, current treatments for glaucoma focus on reducing intraocular pressure (IOP) with topically administered pressure-reducing medications. However, between 25 % and 50 % of patients do not achieve sufficient IOP reductions with first-line prostaglandin analogues, and up to 10 % of patients (estimated at 6.4 million people globally) respond sub optimally to polypharmacy eye-drop treatments (Noecker et al., 2003; Scherer, 2002).

* Corresponding author.
*E-mail address:* matthew.campbell@tcd.ie (M. Campbell).

https://doi.org/10.1016/j.visres.2024.108502
Received 31 July 2024; Received in revised form 4 October 2024; Accepted 4 October 2024
Available online 18 October 2024
0042-6989/© 2024 The Authors. Published by Elsevier Ltd. This is an open access article under the CC BY license (http://creativecommons.org/licenses/by/4.0/).

Despite the effectiveness of multiple topical drops when used correctly and the development of new IOP lowering medications, such as the Rho Kinase inhibitor Netarsudil (Khouri et al., 2019), adherence to dosing schedules poses a significant challenge, resulting in poor compliance that limits the real-world effectiveness of these treatments (Newman-Casey et al., 2015; Okeke et al., 2009). While surgical options such as minimally invasive glaucoma surgery, trabeculectomy, and drainage tubes are available for resistant cases, these procedures are invasive and carry risks of complications. Additionally, a subset of patients with OAG exhibit normal tension glaucoma (NTG), characterized by IOP values that remain within the statistically normal range without treatment. Epidemiological studies indicate that NTG accounts for approximately 20–40 % of all POAG cases among Caucasians and Africans and between 47 % to 92 % in Asian populations (Salvetat et al., 2023; Klein et al., 1992; Zhao et al., 2019). While lowering of IOP is also beneficial in slowing the progression of NTG, some patients continue to experience disease progression despite IOP reduction (Anderson, 2003). Thus, there is an urgent need for better clinical tools and approaches to prevent irreversible vision loss in glaucoma patients.

### 1.2. Gene therapy for glaucoma

To date, progress towards gene therapies targeting glaucoma has been relatively limited compared to those treating inherited retinal degenerations. This disparity can be partly attributed to the multifactorial nature of glaucoma, with less than 10 % of glaucoma cases exhibiting a monogenic inheritance pattern (Weinreb, Aung, and Medeiros, 2014). Nevertheless, there has been significant progress made in this area in recent years. Gene therapy approaches in glaucoma can be broadly divided into two strategies: reducing IOP and protecting RGCs. Both strategies come with unique challenges relating to the availability of suitable animal models, target cells and pathways, and gene delivery mechanisms (Fig. 1). While neuroprotection offers a distinct advantage by targeting the ultimate cause of sight loss, the retina is a more immunogenic environment compared to the anterior chamber of the eye (Hori, 2008). Thus, in the retina immune responses to viral vectors or their expressed therapeutic proteins can pose complications, requiring careful consideration of immunomodulatory strategies. Progress towards gene therapy for glaucoma has also been limited by the incomplete understanding of its pathophysiology, which is essential for advancing effective treatments. This review will discuss a selection of mechanisms underlying the two major hallmarks of glaucoma: ocular hypertension and RGC degeneration. It will then examine the current state of gene therapies targeting these aspects, highlighting recent progress and ongoing challenges. While this review covers selected targets in detail, it is not intended to be comprehensive. For a broader overview of gene therapy targets for glaucoma, readers are directed to Sulak, Liu, and Smedowski (2024).

## 2. Gene therapies targeting ocular hypertension in glaucoma

### 2.1. Aqueous humour outflow dynamics

The flow of AH is also important for providing shape to the globe of the eye via the generation of IOP (To et al., 2002; Goel et al., 2010), while supplying surrounding structures with nutrients, removing waste metabolic products and permitting inflammatory cells and mediators to circulate the eye under pathological conditions. IOP is controlled by the dynamic balance between AH production (inflow) and the resistance to its drainage (outflow) through two key pathways at the iridocorneal angle. The first pathway, the conventional outflow pathway, involves AH passing through the trabecular meshwork (TM), crossing the inner wall of Schlemm's canal (SC) into its lumen, followed by drainage through collector channels into aqueous veins that ultimately drain into the episcleral venous circulation (Goel et al., 2010). Unconventional flow passes through the interstitial spaces between ciliary muscle fibres and into the supraciliary and suprachoroidal spaces (Fig. 2). From these spaces, AH can either be resorbed by orbital vessels (the uveoscleral

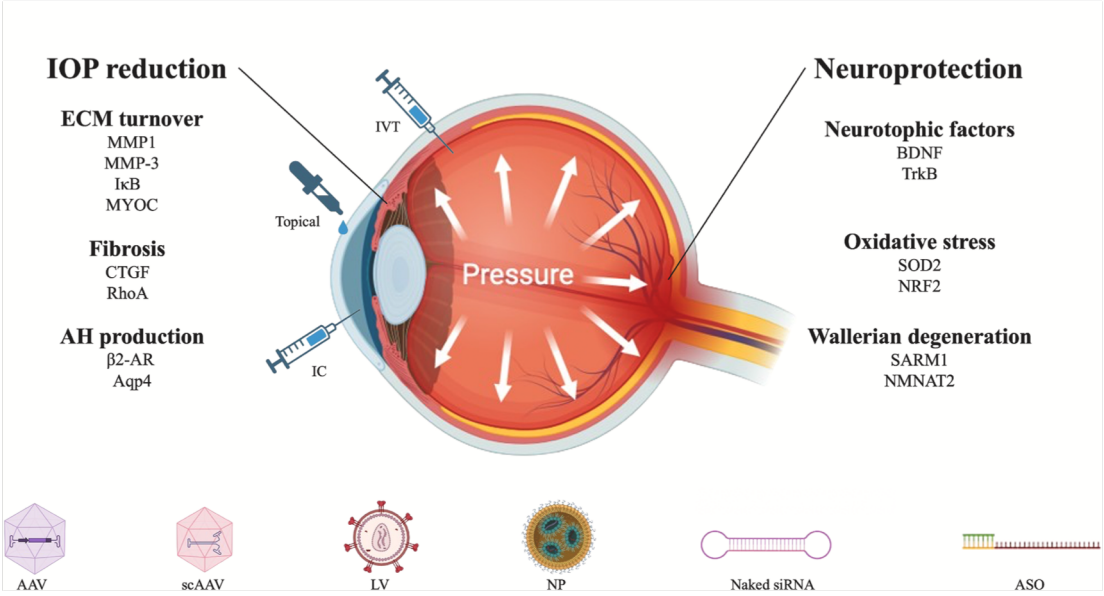



**Fig. 1.** Overview of proposed targets, delivery methods and vectors for glaucoma gene therapy. Gene therapies for glaucoma aim to reduce intraocular pressure (IOP) (left) or protect retinal ganglion cells (right). Approaches to reduce IOP include increasing extracellular matrix (ECM) turnover, reducing fibrosis and increasing aqueous humour (AH). Neuroprotective approaches include increasing levels of neurotrophic factors, reducing oxidative stress, and inhibiting Wallerian degeneration. Delivery methods include intravitreal (IVT), topical, and intracameral (IC). Vectors for gene delivery include adeno-associated viruses (AAV), self-complimentary (sc)AAVs, lentiviruses (LV), nanoparticles (NP), naked small interfering (si)RNA, and antisense aligonucleotides (ASO). Created with Biorender (www.biorender.com)
Adapted from Sulak, Liu, and Smedowski (2024)).

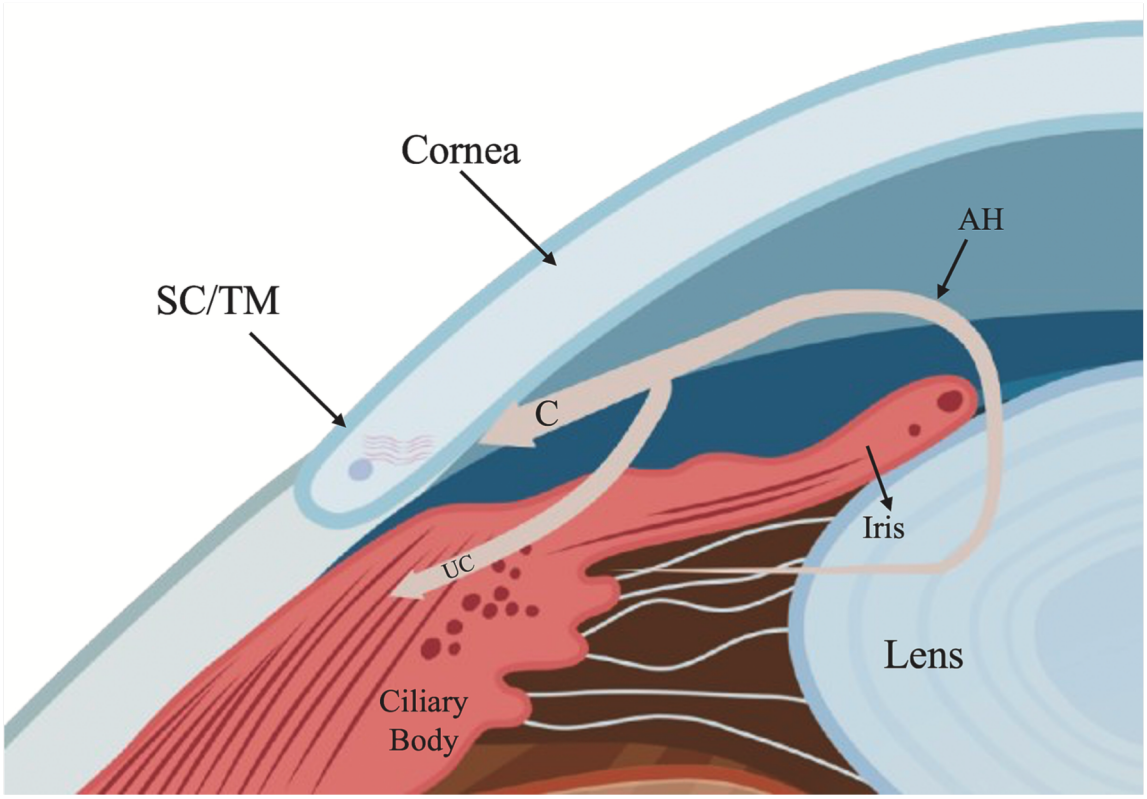



**Fig. 2.** Aqueous humour flow dynamics. Upon secretion from the ciliary body, AH moves from the posterior to the anterior chamber of the eye via the pupil. A temperature gradient causes aqueous humour (AH) to move downwards from the corneal surface, where it is drained via either the conventional outflow pathway (C) or the unconventional outflow pathway (UC). The conventional outflow pathway, involves AH passing through the trabecular meshwork (TM), crossing the inner wall of Schlemm's canal (SC) into its lumen. Unconventional flow passes through the interstitial spaces between ciliary muscle fibres into the supraciliary and suprachoroidal spaces. Created with Biorender (www.biorender.com)
Adapted from (O'Callaghan, Cassidy, and Humphries 2017).

pathway) or drained through the vortex veins via the choroid (the uveovortex pathway) (Johnson, McLaren, and Overby, 2017). The conventional outflow pathway is predominant in humans, accounting for approximately 85 % of AH outflow (Bill and Phillips, 1971), which becomes more pronounced with age (Toris et al., 1999).

### 2.2. Targets for IOP based gene therapies

#### 2.2.1. Targeting ECM turnover at the conventional outflow pathway

Homeostatic ECM turnover is crucial for regulating outflow resistance. This turnover can be triggered by factors such as the stretch or distortion of TM cells, often due to elevated IOP (Bradley et al., 2001). Juxtacanalicular (JCT) cells of the TM continuously express various ECM proteins, and these expression profiles can be altered by exposure to environmental stresses, synthetic agents, or laser trabeculoplasty surgeries (Zhao et al., 2004; Vittal et al., 2005; Lo et al., 2003; Izzotti et al., 2011). ECM turnover, driven by proteinases that target ECM components, is essential for maintaining homeostasis, as reflected by the high gene expression levels in these cells (Vittal et al., 2005). Proteinases involved in ECM turnover include zinc-dependent enzymes such as classical matrix metalloproteinases (MMPs), adamalysisns (ADAM and ADAMTS proteins), and those involved in the plasminogen activation pathway (Keller et al., 2009). MMPs are expressed constitutively throughout the TM, with their expression profiles changing in response to different stimuli (Alexander et al., 1991; Oh et al., 2006; Kelley et al., 2007). The expression of proteinases must be tightly regulated to effectively control outflow resistance. For this purpose, tissue inhibitors of metalloproteinases (TIMPs) exhibit a similar expression pattern to MMPs, with the ratio of the two groups of proteins determining the extent of ECM deposition (Tektas and Lütjen-Drecoll, 2009; Overby et al., 2014). The importance of this balance is underscored by various studies finding an imbalanced MMP:TIMP ratio in glaucoma patients relative to controls (Schlötzer-Schrehardt et al., 2003; Rönkkö et al., 2007; Fountoulakis et al., 2013). Furthermore, perfusion of ocular tissues with MMPs or MMP-activating compounds leads to increased outflow facility (Bradley et al., 1998; Pang et al., 2003; Webb et al., 2006; De Groef et al., 2013). Given its importance in regulating outflow resistance, the ECM is an appealing target for gene therapies aimed at reducing ocular hypertension in glaucoma (O'Callaghan, Cassidy, and Humphries, 2017). Several emerging therapies have emerged that exert direct or indirect effects on the ECM, a selection of which will be discussed below.

One strategy involves expressing an MMP-1 transgene within the TM under the control of a glucocorticoid-responsive promoter. Corticosteroid treatments can cause ocular hypertension in a significant number of individuals, thus steroid induced expression of MMP-1 within the TM will result in a reduction in collagen type 1, preventing an increase in IOP (Spiga and Borrás, 2010). The feasibility of this approach was initially demonstrated in sheep by intracamerally injecting an Ad vector containing the transgene, where steroid-induced expression of MMP-1 led to a decrease in IOP (Gerometta et al., 2010). The group later demonstrated the same effect upon transferring the transgene cassette to a self-complimentary (sc)AAV2 vector (Borrás, Buie, and Spiga, 2016). Another approach involves intracameral injection of an AAV9 vector

containing a plasmid expressing codon-optimised MMP-3 to transduce the corneal endothelial cells (O'Callaghan et al., 2017; O'Callaghan et al., 2023). As MMP-3 is a secretory protein, its expression in corneal endothelial cells leads to its apical secretion into the AH, where it can reach the outflow tissues via the normal flow patterns of AH. Here, MMP-3 is autoactivated with initial cleaveage by nonspecific proteases and other MMP molecules. This leads to reduced collagen and laminin levels, constriction of actin filaments and disorganisation of fibronectin networks, ultimately increasing outflow facility and reducing IOP. This approach increases outflow facility in two mouse models of glaucoma (Tg-MYOC$^{Y437H}$ myocilin model and the steroid-induced dexamethasone model), non-human primates (NHPs), and human donor eyes. Critically, ocular inflammation was not detected in NHPs following intracameral injection of AAV. Additionally, MMP-3 was detectable in the anterior segment over 200 days after injection, suggesting that this approach is both durable and clinically translatable (O'Callaghan et al., 2023).

Other approaches have aimed to target expression of upstream regulators of MMPs. For example, the secretion of MMPs is known to depend on NF-κB in macrophages and vascular smooth muscle (Bond et al., 2001; Chase et al., 2002). NF-κB-mediated upregulation of MMPs has also been shown in TM cells and human ciliary muscle cells (Lan et al., 2009; Porter, Epstein, and Liton, 2012). The IκB kinase serves to regulate the cellular response to inflammatory stimuli. NF-κB is inactive when bound to IκB in the cytoplasm, with phosphorylation of the latter leading to release of NF-κB, which then acts as a nuclear transcription factor, stimulating MMP expression in the trabecular meshwork and ciliary body (Ramkumar et al., 2011). It follows that inhibiting IκB in the outflow tissues may be a useful strategy for reducing IOP. Zeng et al. (2020) utilised hyperbranched cationic glycogen derivative vector to deliver siRNA targeting IκBα intracamerally in normotensive rats, leading to increased MMP-2 expression and a significant reduction in IOP 72 h post injection. However, the reduction in IOP was transient, with levels returning to baseline 5 days post-treatment. In a more recent study, naked IκBα-siRNA was injected intracamerally in Rhesus monkeys following laser photocoagulation to induce chronic ocular hypertension, leading a longer lasting reduction in IOP (28 days) that correlated with increased expression of MMPs-2 and −9 in the TM and ciliary body (Sun et al., 2022).

Tissue plasminogen activator (tPA) is another regulator of MMPs and has been shown to increase MMP-9 and MMP-13 expression after ocular injection. Transfection of ocular tissues using adenovirus with the transgene for tPA, encoded by the PLAT gene, was shown to increase outflow facility in wild type mice with subconjunctival injection of the corticosteroid Triamcinolone Acetonide. Interestingly, the serine protease activity of tPA is not critical for elevated outflow facility, and instead functions as a transcriptional regulator of MMPs in the anterior chamber, as shown by mRNA quantification (Gindina et al., 2021; Gindina et al., 2020).

Similar to other studies, the authors found no change in outflow facility in normotensive mice, suggesting that the intervention does not overcorrect or cause hypotony, adding to the attractiveness of ECM-modulating strategies.

Other groups have investigated the use of micro RNAs (miRNAs) to regulate ECM turnover. These are naturally occurring small non-coding RNAs that regulate biological function at the post-transcriptional level by targeting a network of molecules. Notably, the profiles of miRNAs in aqueous humour have been shown to be altered in glaucoma patients (Drewry et al., 2018; Jayaram et al., 2017). In an initial study, Tan et al. (2020) intracamerally miR-21-5p, a miRNA proposed to regulate ECM in TM cells, to the eyes of C57/BL6 mice, leading to a reduction IOP and increased outflow facility. This was accompanied by an increase in MMP-9 and a decrease in TIMP-3 expression (Tan et al., 2020). In a follow-up study, the authors packaged miR-21-5p in a polydopamine–polyethylenimine nanoparticle vector to counteract the rapid degeneration of the molecule. This was shown to enhance the stability of the genetic molecule with minimal cytotoxicity (Tan et al., 2021).

#### 2.2.2. *Targeting fibrosis pathways*

The ECM of glaucomatous tissues displays similarities to fibrotic tissue, including an excessive accumulation of ECM components such as α-SMA, progressing to a hardening or scarring of connective tissues (Mutsaers et al., 1997; Wight and Potter-Perigo, 2011). Indeed, the ECM at the JCT in glaucoma displays hallmarks of fibrosis in the form of sheath derived plaques, which are particularly evident in the ageing TM (Keller and Acott, 2013; Tektas and Lütjen-Drecoll, 2009).

Additionally, glaucomatous Schlemm's canal endothelial cells (SCECs) exhibit a fibrotic phenotype, expressing higher levels of α-SMA, collagen I-α1, and fibronectin, relative to healthy SCECs (Kelly et al., 2021). This has led to the development of various gene therapy-based approaches targeting fibrosis pathways at the conventional outflow tissue. TGF-β2 is a cytokine with an important regulatory role in this regard, inducing the expression of collagens, α-SMA, fibronectin, among others, and is known to be upregulated in glaucoma (Guo et al., 2019). TGF-β2 signalling is mediated by elastic microfibrils, specifically the fibrillin component that is responsible for the elasticity of the ECM, which is required for sequestering and activating TGF-β2 complexes (Han et al., 2011). The induction of extracellular matrix (ECM) cross-linking by TGF-β2 resembles the cross-linking observed in glaucomatous tissues and may contribute to the disease pathogenesis (Wallace et al., 2014; O'Callaghan, Cassidy, and Humphries, 2017).

Connective tissue growth factor (CTGF), is a downstream target of TGF-β2 and is proposed to be a mediator of increased outflow resistance in POAG, with overexpression in the mouse eye leading to increases in IOP and optic nerve damage, correlated with induction of TM fibronectin and α-SMA (Junglas et al., 2012; Junglas et al., 2009). In a recent study, Dillinger et al. (2018) proposed a novel therapeutic concept in which CTGF-siRNA would be delivered in layer-by-layer coated nanoparticles, with a final layer of hyaluronic acid (HA). The HA-coating is proposed to allow binding to TM and SC cells via CD44, which the authors demonstrate to be upregulated in the glaucomatous anterior chamber. While CTGF gene silencing by this method has yet to be tested in vivo, this approach is of particular interest as the gene silencing may depend on the expression profile of CTGF itself, which could provide high specificity toward tissue with pathological expression changes. Another downstream target of TGF-β cells is the RhoA/Rho-kinase (ROCK) signalling pathway. Activation of this pathway in TM cells leads to actin filament contraction and polymerisation via phosphorylation of LIM kinase-2 and myosin light chain, leading to contraction of the TM and increased outflow resistance (Sit and Manser, 2011). Upon binding of TGF-β to TGF-β receptor 1 on TM cells, a downstream signalling cascade is triggered so that RhoA-GTP and ROCK are activated. This leads to increased TM contractility, reduced AH drainage and elevated IOP (Pattabiraman, Inoue, and Rao, 2015). Inhibition of ROCK signalling has thus been investigated as a potential therapeutic avenue for ocular hypertension in glaucoma. Intracameral injection of ROCK inhibitor Y-27632 in rabbits has been shown to decrease IOP in a dose dependent manner, with a corresponding increase in outflow facility (Honjo et al., 2001). A recent study investigated the effect of siRNA-mediated knockdown of RhoA on TM fibrosis and IOP. The researchers injected TGF-β intracamerally twice a week into adult Sprague Dawley rats to induce ocular hypertension, while also injecting RhoA-siRNA in select animals. TGF-β increased TM contractile proteins and caused IOP spikes by day 7, with sustained IOP elevation and TM fibrosis being observed by day 35. siRhoA abolished the early IOP rise but not the sustained increase or RGC loss. The researchers concluded that RhoA signaling mediates the early IOP rise due to TM contractility but not the sustained elevation from fibrosis, suggesting that RhoA therapies can manage early IOP spikes but not fibrosis-related increases (Hill et al., 2018).

#### 2.2.3. Targeting aqueous humour production

Most therapeutic interventions for reducing IOP in glaucoma focus on increasing AH outflow. However, targeting AH production is also a potentially viable strategy, since IOP depends on both AH production and outflow. Currently, cycloablation of the ciliary body with cyclodiode lasers is a recognised therapeutic strategy in the management of refractory glaucoma, leading to a significant and sustained reduction in IOP. However, such procedures are associated with significant adverse events, leading to a loss of visual acuity in a subset of patients (Rotchford et al., 2010; Murphy et al., 2003). Additionally, β-blockers, which reduce IOP by reducing AH production at the ciliary body, are among most highly prescribed treatments for glaucoma (Sidjanin et al., 2008). However, these are associated with systemic adverse effects such as brachycardia, hypotension and heart failure (Han et al., 2008). Thus, gene therapy based approaches to reduce AH production may be a viable alternative to these approaches. One such example is Bamosiran, a topical eye drop solution containing siRNA targeting β-Adrenergic Receptor 2 (β2-AR). By targeting the same receptors as β-blockers, this approach held promise to reduce IOP without systemic adverse events. In preclinical studies, Bamosirsan was shown to reduce IOP in normal and hypertensive rabbit eyes, in addition to being safe and well tolerated in non-human primates (Martínez et al., 2014). It later progressed to phase 1 (Moreno-Montañés et al., 2014) and phase 2 (Gonzalez et al., 2016) clinical trials where it was shown to be safe and efficacious in humans. However, this treatment carries the same limitations related to non-compliance as conventional eye drops, as its effect on IOP is transient. Thus, despite these results, Bamosiran was ultimately discontinued as it did not offer significant advantages or better cost-benefit compared to timolol eyedrops. More recent approaches have aimed to produce longer-lasting reductions in AH production. A recent study by Wu et al. (2020) aimed to disrupt aquaporin-4 (Aqp4) expression in the ciliary body using CRISPR-Cas9 gene editing. Aquaporins water-transporting transmembrane proteins that are expressed throughout the human body (Schey et al., 2014). They play a critical role in AH production in the ciliary body, as underscored by the fact that Aqp4 null mice display reduced IOP (Zhang, Vetrivel, and Verkman, 2002). The authors utilised an AAV-Sh10 vector system to deliver two Staphylococcus aureus-derived Cas9 (SaCas9)-compatible gRNA targeting exon 1 of AQP1 intravitreally. This led to a significant decrease in IOP in C57BL/6J mice and two models of glaucoma (corticosteroid- and microbead-induced ocular hypertension), which was maintained over a 3–7 week observation period and prevented RGC loss (Wu et al., 2020; Komáromy, 2020).

#### 2.2.4. Myocillin as a gene-specific gene therapy target

As most cases of glaucoma do not follow a Mendelian inheritance pattern, the majority of gene therapies targeting ocular hypertension are gene-agnostic. However, in cases where glaucoma is caused by a well-defined genetic mutation, gene-specific therapies offer an attractive target due to their precise genetic aetiology. One such example is the gene encoding myocilin (MYOC), which was the first locus to be linked with POAG (Stone et al., 1997). MYOC mutations account for 2–4 % of overall POAG cases and 10–30 % of juvenile-onset cases (Menaa et al., 2011). *MYOC* is highly expressed in trabecular meshwork (TM) cells as well as in various ocular and non-ocular tissues (Karali et al., 2000; Takahashi et al., 1998). However, mutations in MYOC lead to a gain of function phenotype, with mutant MYOC forming detergent insoluble aggregates and accumulating in the endoplasmic reticulum (ER), resulting in ER stress (Liu and Vollrath, 2004; Yam et al., 2007; Joe et al., 2003). Chronic ER stress in TM cells results in cell death, ultimately elevating IOP (Zode et al., 2011; Joe et al., 2003), as modelled in the Tg-MYOCY437H mouse model, transgenic for the human Y437H allele (Zode et al., 2011).

Given that MYOC is not required for IOP regulation under normal conditions and that mutant MYOC leads to a gain of function phenotype, it represents an ideal target for IOP-lowering gene therapy (Kim et al., 2001; Gould et al., 2004). Two recent studies focused on using CRISPR/Cas9 gene editing to alleviate ocular hypertension in MYOC-associated glaucoma. In a proof-of-concept study, MYOC knockout was achieved by delivering a guide RNA (gRNA) targeting exon 1 of *MYOC* and Cas9 endonuclease in an Ad5 vector (Jain et al., 2017). One month post-treatment, Tg-MYOCY437H mice exhibited lower IOP, improved RGC function and reduced expression of ER stress markers. Additionally, mutant MYOC expression was reduced in a human ex vivo anterior segment perfusion culture system, supporting its potential utility in humans (Jain et al., 2017). Although an Ad5 vector was used in this study due to its strong tropism for the TM (Shepard et al., 2010), it is unsuitable for clinical use due to its pro-inflammatory nature (Millar et al., 2023). Indeed, the authors noted that inflammation was observed in the anterior chamber of mice following Ad5 injection (Jain et al., 2017). A follow-up study aimed to address this by investigating the efficacy of AAVs and lentiviral (LV) particles to target the TM (Patil et al., 2024). Of the various vectors and delivery routes assessed, it was observed that intravitreal (IVT) delivery of LV led to the most selective and efficient tropism to the TM. This approach was subsequently used to deliver Cas9 and gRNA targeting *MYOC* in Tg-MYOCY437H mice, leading to decreased accumulation of MYOC and significantly lower IOP following a single injection.

## 3. Neuroprotection based gene therapy strategies

### 3.1. Glaucomatous optic neuropathy

While ocular hypertension is the only modifiable risk factor for glaucoma, the exact mechanism by which elevated IOP leads to RGC degeneration is not fully understood. There are multiple hypothesised mechanisms of RGC death, such as mechanical damage, reduced axonal transport and oxidative stress. These factors likely interact in complex ways and may contribute to differing degrees depending on the individual and the specific subtype of glaucoma. Understanding these mechanisms and their interactions is of critical importance for the development of gene therapies targeting glaucomatous optic neuropathy. The principal site of insult to RGC cells in glaucoma is the laminar region of the optic nerve head (ONH). This can be attributed to the lamina cribrosa (LC), a fenestrated structure composed of collagen fibres that provides structural and nutritional support to RGC axons as they leave the sclera. From a biomechanical standpoint, the LC is a weak point in the posterior wall of the eye, as it is approximately one-third the thickness of the sclera and only comprises around 40 % of the total tissue volume in the laminar region of the ONH. Thus the LC must support the ONH against mechanical strain caused by IOP elevation, while also providing a pathway for RGC axons to leave the eye (Downs and Girkin, 2017). Scanning electron microscopy studies of glaucomatous ONHs show that the first structural evidence of damage is in the backward collapse of the anterior LC, followed by a prominent bowing of the whole structure (Quigley et al., 1981). Ocular hypertension may thus cause compression, deformation, and remodelling of the LC, resulting in mechanical damage to RGC axons and disrupted axonal transport (Weinreb, Aung, and Medeiros, 2014). Animal models of ocular hypertension display reduced anterograde and retrograde axonal transport of neurotrophic factors, indicating that pathological increases in IOP may lead to RGC death via trophic insufficiency (Quigley et al., 2000; Pease et al., 2000). Additionally, simultaneous IOP-induced mitochondrial dysfunction may further exacerbate RGC dysfunction (Ju et al., 2008). It must also be noted that increases in IOP are not the sole cause of glaucomatous RGC death, as evidenced by the existence of normal-tension glaucoma, in which patients develop glaucoma despite presenting with IOPs within the normal range (Lee, Bathija, and Weinreb, 1998). In such cases, an elevated pressure differential across the LC has been proposed as a contributing factor to optic nerve damage, which may occur when orbital cerebrospinal fluid (CSF) pressure is low (Jonas and Wang, 2013).

### 3.2. Targets

#### 3.2.1. Targeting neurotrophic factors and their receptors

Neurotrophins are a family of proteins that support the survival, growth, and differentiation of neurons and include nerve growth factor (NGF), brain derived neurotrophic factor (BDNF), ciliary neurotrophic factor (CNTF), and glial cell line-derived neurotrophic factor (GDNF), among others. Of the neurotrophins, BDNF and its receptor, TrkB, have emerged as potentially important mediators of glaucomatous RGC degeneration. Axonal transport of BDNF is disrupted in rodent and primate models of ocular hypertension (Quigley et al., 2000; Pease et al., 2000). Additionally, there is growing evidence of impaired BDNF signalling in human glaucoma, with reduced levels being observed in the optic nerve head, tear film, and serum of glaucoma patients, relative to controls (Gupta et al., 2014; Ghaffariyeh et al., 2009; Oddone et al., 2017).

Given the potential role of BDNF signalling in glaucoma development, its application as a neuroprotective agent has been explored. Early studies demonstrated that intravitreal injections of recombinant BDNF could delay RGC death in a rat hypertension model and an optic nerve crush model in cats (Ko et al., 2001; Chen and Weber, 2001). However, this approach has limited clinical application due to the need for multiple injections for lasting neuroprotection. Consequently, gene therapy-based strategies have been investigated for their potential to provide more durable neuroprotective effects. Two initial studies demonstrated that a prophylactic intravitreal injection of an AAV vector expressing the BDNF transgene or its receptor TrkB delayed RGC death in rat models of laser-induced ocular hypertension and optic nerve transection, respectively (Martin et al., 2003; Cheng et al., 2002). Although these studies served as proof of concept, pre-symptomatic protective measures have limited clinical relevance, as therapies would be aimed at patients after disease onset occurs. Ren et al. (2012) studied the effectiveness of BDNF expressed from an AAV2 vector in protecting RGCs in a rat model of acute IOP elevation. They found that injecting AAV2-BDNF into the vitreous 6 h post IOP elevation was ineffective at protecting RGC cells in the acute phase of retinal artery occlusion due to the slow onset of transgene expression, but did provide protection in later phases, which more closely resemble the gradual RGC loss observed from chronic IOP elevation in glaucoma. Additionally, supplementing BDNF protein once was effective in compensating for the slow onset of AAV-mediated gene expression and rescued a larger number of RGCs.

While these studies demonstrate the neuroprotective potential of BDNF expression from the retina following viral transduction, this approach comes with potential drawbacks. Firstly, binding of BDNF with its receptor, TrkB, leads to its downregulation and degradation, potentially limiting the effectiveness of sustained delivery (Sommerfeld et al., 2000; Frank et al., 1996). Secondly, overexpression of BDNF may lead to an accumulation of immature proBDNF, and its binding to p75NTR receptors, which are associated with apoptosis and may counteract neuroprotection (Teng et al., 2005). A recent study outlined a novel strategy to circumvent these issues, using an AAV2 vector to deliver a construct expressing both BDNF and TrkB from a single transgene, separated by a sequence encoding a viral 2A peptide linker. The construct contains a modified BDNF transgene lacking its pro- domain and signal peptide sequence which offers two key advantages: enabling expression of both genes within the limited 4.7 kb capacity of the AAV vector and preventing overaccumulation of proBDNF. Controlled by the constitutive cytomegalovirus enhancer/ chicken beta-actin (CAG) promoter, the construct is transcribed as a single RNA, with co-translational cleavage at the viral 2A sequence producing two separate proteins. These mature proteins are subsequently directed to their respective intracellular sites: Trk to the cell surface and BDNF to secretory vesicles for extracellular release (Osborne, Wang, et al., 2018). When injected intravitreally, AAV2 TrkB-2A-mBDNF induced high expression of both transgenes for up to 6 months in mice without causing astrogliosis or microglial activation. In a mouse optic nerve crush model, it provided greater neuroprotection than AAV2-BDNF or AAV2-TrkB alone. Additionally, AAV2 TrkB-2A-mBDNF demonstrated neuroprotective effects in a rat model of laser-induced ocular hypertension (Osborne, Khatib, et al., 2018). Another group developed an approach to generate of a constitutively active form of TrkB by farnesylation of its intracellular domain (F-iTrkB). Intravitreal injection of AAV2-iTrkB was shown to be neuroprotective in a mouse model of normotensive glaucoma (glutamate/ aspartate transporter (GLAST) KO mice), a silicon oil model of ocular hypertension, and an optic nerve crush model. Additionally, evidence of axon regeneration was observed in both in the optic nerve crush model and an optic nerve transection model, wherein the lesion was made close to the superior colliculus (Nishijima et al., 2023).

#### 3.2.2. Targeting oxidative stress and mitochondrial dysfunction

Oxidative stress is an imbalance in redox homeostasis, whereby pro-oxidative processes that generate reactive oxygen species (ROS) overcome intrinsic antioxidant defence mechanisms. This leads to DNA, protein and lipid damage in addition to mitochondrial dysfunction which further induces ROS generation. In particular, RGCs are highly susceptible to oxidative damage owing to their high metabolic demand, high lipid and glutamate content, and limited capacity for regeneration (Hurley et al., 2022). Various animal studies suggest that oxidative stress plays a major role in glaucomatous neurodegeneration (Mittag et al., 2000; Ozdemir et al., 2009; Moreno et al., 2004). Additionally, POAG patients display lower antioxidant capacity in the AH and serum relative to cataract controls and this is associated with a higher level of visual field damage, lower RGC numbers, and increased cup-to-disk ratio (Nucci et al., 2013; Tanito et al., 2016; Asano et al., 2017; Abu-Amero et al., 2013). Considering this, the potential of antioxidants as neuroprotective molecules has been explored. For example, rapamycin, a synthetic antioxidant that relieves oxidative stress by inhibiting mTor, has been shown to increase survival of RGCs in a rat chronic hypertension model (Su et al., 2014). As oxidative stress is a common mechanism in glaucomatous neurodegeneration, antioxidant enzymes are attractive gene therapy targets, as such therapies may be beneficial across a range of glaucoma subtypes.

Superoxide dismutase (SOD) is an antioxidant enzyme that catalyses the conversion of the superoxide ($O_2^-$) anion into normal molecular oxygen ($O_2$) and hydrogen peroxide ($H_2O_2$) Superoxide is produced as a by-product of oxygen metabolism and, if not regulated, causes many types of cell damage (Culotta, 2001). Jiang et al. (2016) examined the effect of chronic ocular hypertension on retinal oxidative stress and mitochondrial function in a rat laser induced ocular hypertension model. They found that RGC degeneration was associated with a decrease in SOD and catalase activity, and increased levels of malondialdehyde (MDA), the lipid peroxidation decomposition product generated by free radical damage to unsaturated fatty acids. They showed that eyes pre-treated with an intravitreal injection of recombinant AAV expressing SOD2 led to significantly lower levels of MDA accumulation and reduced RGC degeneration through a mitochondria-related pathway. However, MDA content was still higher than baseline even after administration of AAV-SOD2, indicating that the treatment did not eliminate oxidative stress and would not provide lasting RGC protection.

Nuclear factor erythroid 2-like 2 (NRF2) is a transcription factor that plays a crucial role in the response of cells against oxidative insults. NRF2 is activated by ROS, leading to the upregulation of antioxidant responsive elements- associated genes and the expression of several antioxidant proteins such as glutathione peroxidase, glutathione reductase, thioredoxin, and SODs 1, 2, and 3 (Panieri et al., 2022). Intravitreal injection of AAV2-NRF2 has been shown to be protective against RGC degeneration in a mouse optic nerve crush model (Xiong et al., 2015). In a later study, Fujita et al. (2017) aimed to optimise this strategy to only target damaged RGCs. They highlighted that many ocular gene therapy approaches, including that of Xiong et al. (2015) use constitutively active promoters to drive expression of therapeutic

transgenes. However, such promoters result in expression of the therapeutic gene in both injured and healthy cells, which could induce stress responses in healthy cells by creating a non-physiological environment. They identified the monocyte chemoattractant protein 1 (Mcp-1) promoter, which is involved in leukocyte recruitment, as being able to drive transgene expression specifically in injured RGC cells (Toney et al., 2000). They showed that Mcp-1driven NRF2 expression showed equivalent efficacy in protecting RGCs in a mouse optic nerve crush model to that driven by the CMV promoter used by Xiong et al. (2015). However, CMV mediated NRF2 expression induced cellular stress and death in healthy RGCs, which were significantly reduced by utilising the Mcp-1 promoter.

#### 3.2.3. Targeting Wallerian degeneration

Wallerian degeneration is a programmed axonal death process that occurs after a nerve fibre is cut or damaged, leading to the degeneration of the axon segment separated from the neuron's cell body. This process is closely linked to reduced levels of axonal nicotinamide adenine dinucleotide (NAD + ) (Figley and DiAntonio, 2020). Maintaining NAD + levels is essential to prevent axonal degeneration (Wang et al., 2005; Wang et al., 2015). Nicotinamide mononucleotide adenylyltransferase 2 (NMNAT2) and sterile alpha and TIR motif containing 1 (SARM1), are crucial mediators of programmed axonal death. NMNAT2 is responsible for NAD + biosynthesis; its depletion can induce Wallerian degeneration even in uninjured axons (Gilley and Coleman, 2010). Conversely, SARM1, with its intrinsic NAD + hydrolase activity, drives axonal degeneration by depleting NAD + rapidly after axonal injury. The subsequent NAD + depletion leads to decreased ATP levels and energy deficit, triggering cytoskeletal disintegration and loss of axonal membrane integrity (Conforti, Gilley, and Coleman, 2014). In glaucoma, axon degeneration is an early feature of glaucomatous optic neuropathy (Howell et al., 2007; Beirowski et al., 2008). The wallerian degeneration slow (Wlds) allele, which encodes a mutant chimeric NMNAT1 localized to axons, has shown protective effects in both the optic nerve crush model and DBA/2J mice (Howell et al., 2007; Beirowski et al., 2008). Additionally, vitamin B3 (an NAD + precursor) administration has also demonstrated protective effects against axonal degeneration in DBA/2J mice (Williams et al., 2017).

In recent years, numerous gene therapy-based strategies targeting Wallerian degeneration in glaucoma have been developed. One such strategy involves inducing the overexpression of NMNATs in retinal ganglion cells (RGCs) to maintain adequate NAD + levels and prevent axonal degeneration. For example, Williams et al. (2017) injected an AAV2.2 vector expressing murine *Nmnat1*, driven by a CMV promoter, into the vitreous of DBA/2J mice at 5.5 months of age. By 12 months, the treatment resulted in robust transgene expression, effectively preventing RGC axon and soma loss, preserving axoplasmic transport, and maintaining electrical activity in the RGCs. In another study, Fang et al. (2022) used RiboTag RNA-seq to characterise the translatome of RGCs in mice with silicone oil-induced ocular hypertension. They found that the expression of NMNAT2, but not NMNAT1 or NMNAT3, was significantly reduced relative to control eyes. Based on these findings, they designed a gene therapy approach that involved intravitreal injection of an AAV2 vector expressing a long half-life mutant NMNAT2 lacking exon 6, driven by an RGC-specific mouse γ-synuclein promoter (mSncg). This therapy provided significant neuroprotection of both RGC soma and axons, and preserved visual function in both a mouse optic nerve crush model and the silicone oil-induced ocular hypertension model.

To maintain NAD + levels and prevent axonal degeneration, another strategy is to disrupt the activity of the pro-degenerative enzyme SARM1. Liu et al. (2023) explored the effects of disrupting Sarm1 on glaucomatous neurodegeneration using two gene-based approaches: administering antisense oligonucleotides (ASO) against Sarm1 and CRISPR/Cas9-mediated knockdown of Sarm1 through co-transfection with AAV2 vectors containing Cas9 and SARM1 gRNAs under the control of an mSncg promoter. The neuroprotective capabilities of these approaches were compared to germline knockout of Sarm1 in both an optic nerve crush model and a silicone-oil induced ocular hypertension model. In the optic nerve crush model, all three methods of Sarm1 disruption preserved optic nerve axons but did not prevent RGC soma death. In the silicone-oil induced ocular hypertension model, both RGC somata and axons were preserved. However, unlike germline knockout of Sarm1, neither ASO nor CRISPR-mediated disruption improved visual acuity in either model, indicating that these methods are less effective in inhibiting SARM1 than germline deletion.

## 4. Future directions and research priorities

### 4.1. Improving viral vector efficiency

An important consideration in gene therapy is the selection of an appropriate vector for gene delivery. Vectors utilised in gene therapy can be broadly classed into viral and non-viral delivery systems. Although this review offers a brief discussion of vectors in gene therapy for glaucoma, the topic has been explored in greater depth elsewhere (Amador et al., 2022; Hakim et al., 2023). Most ocular gene therapy clinical trials to date have used viral vectors. For example, Luxturna (Spark Therapeutics), the first ocular gene therapy approved by the FDA in 2017 for treating Leber's congenital amaurosis type 2, introduces a gene encoding the retinoid isomerohydrolase enzyme using an AAV2 vector (Fischer, 2017). In glaucoma, the appropriate vector depends on the tissue being targeted. Most gene therapies aimed at reducing IOP target the TM, while neuroprotection-focussed therapies target RGCs. Thus, many studies have focussed on determining the ideal vector for delivering genetic cargo to these tissues.

The natural flow of AH directs injections of recombinant viruses in the anterior chamber to the TM, making it an ideal target for gene therapy. Adenoviruses are capable of transducing the TM in mouse, monkey and human eyes (Borrás et al., 2001; Budenz et al., 1995; Borrás et al., 1999). However, they are highly immunogenic and do not provide long lasting gene expression (Borrás, Tamm, and Zigler 1996). Single-stranded (ss) AAVs are favoured for gene therapies targeting the posterior segment due to their durable expression and low immunogenicity. However, their ability to transduce TM cells is limited. This limitation arises from the host's downregulation of DNA replication, which hinders the conversion of the ssAAV genome into double-stranded DNA (Borrás et al., 2006). To circumvent this, studies have employed self-complementary AAVs (scAAVs) that contain both the sense and antisense cDNA strands of the transgene. In particular, scAAV2 has been demonstrated to have a high transduction efficiency in the TM of rodent and primate models (Buie et al., 2010; Bogner et al., 2015). Recent efforts have been made to further characterise and optimise scAAVs as IOP lowering gene therapy vectors. For example, one study investigated whether an ocular hypertensive environment would influence the tropism of scAAVs, as previous research had only tested them under normotensive conditions. The transduction efficiencies of scAAVs 2, 5, and 8, each packaged with EGFP, were assessed in the anterior segment structures of rats with ocular hypertension induced by circumlimbal suturing. The results showed that scAAVs 2 and 5 could efficiently transduce the TM, with scAAV5 displaying higher specificity. Notably, the transduction efficiencies of these vectors increased under ocular hypertensive conditions due to the enhanced expression of their cognate receptors (Lee et al., 2019).

The efficiency and tropism of AAVs is highly species specific. Thus, findings from rodents do not necessarily translate to humans and it is important that vector efficiency is tested in the human relevant tissue. Another study investigated the transduction efficiencies of seven scAAV serotypes (1, 2, 2.5, 5, 6, 8, and 9) in primary human TM cells. Of these, scAAV2 was found to have the highest transduction efficiency, showing a 3.1x higher transgene expression than the next best serotype (scAAV2.5). It was further shown that scAAV with a tyrosine triple mutant capsid exhibited a 3.5x higher transduction efficiency than non-

mutated scAAV2, suggesting that this may be the optimal vector to deliver genes to the TM and attempt to control elevated IOP (Rodriguez-Estevez, Asokan, and Borrás, 2020).

As AAV2 is the gold standard serotype for posterior segment gene therapies and effectively targets RGCs when injected intravitreally in rodents (Han et al., 2020). However, rodent eyes are significantly different to primate and human eyes, as they lack a macula. The macula in humans, in addition to having a high photoreceptor density, can have up to 10 rows of RGCs and has a correspondingly thick nerve fibre layer, in contrast to mice which have a single RGC layer throughout the retina. In addition to this, humans have a highly developed inner limiting membrane (ILM). Thus, rodent RGCs are significantly easier to transduce (Starr and Chen, 2023). Indeed, intravitreal injection of AAV2 into the macaque eye has been shown to transduce a small population of RGCs in the fovea, but exhibits limited transduction beyond this (Yin et al., 2011).

This is a major reason that Lenadogene nolparvovec, a gene therapy for Leber's congenital optic neuropathy that utilises a recombinant AAV2/2 vector injected intravitreally to deliver a human wild-type ND4 transgene to RGCs, while generally safe, has shown only marginal benefit (Wan et al., 2016; Guy et al., 2017; Newman et al., 2022). RGC transduction efficiency has been shown to be improved in primates by performing vitrectomy or peeling back the ILM before intravitreal injection (Takahashi et al., 2017; Tshilenge et al., 2016). However, the adverse effects associated with such invasive procedures would need to be investigated before such approaches would be clinically applicable. Novel AAV capsids may provide better transduction efficiencies. For example, both AAV7m8 and AAV8BP2 have been shown to transduce RGCs in non-human primates, with AAV7m8 transducing parafoveal RGCs at high viral titres (Ramachandran et al., 2016).

An alternative strategy to circumvent the ILM involves delivering an AAV to RGCs via retrograde transport from their axon terminals. A variant of AAV2, recombinant AAV2-retro (rAAV2-retro), has been developed to increase its capacity for retrograde transport (Tervo et al., 2016). In a recent study, it was shown that when rAAV2-retro carrying fluorescent reporter genes was injected into the superior colliculus of rats, this led to widespread transduction of RGCs that lasted up to 375 days (Zheng et al., 2024). This highlights the potential utility of injecting rAAV-retro into the lateral geniculate nucleus, the primary projection site for RGCs in primates and humans, for RGC gene therapy. However the authors note that this approach comes with the disadvantage of requiring a neurosurgical procedure and would transduce both eyes simultaneously, which would make it impossible to compare a treated and control eye, a preferred comparison for clinical trials (Zheng et al., 2024).

### 4.2. Improving transgene regulation

Another crucial factor in gene therapy is the promoter that drives the expression of the therapeutic transgene. Due to the low transduction efficiency of AAV2 vectors in human RGCs, many studies have focused on improving transgene expression using RGC-specific promoters. One prominent example is the gamma synuclein (SNCG) promoter, which is specifically and ubiquitously expressed in RGCs of both rodents and humans (Surgucheva et al., 2008). A recent study demonstrated that a transgene encoding EGFP, delivered via an AAV2 vector with a mouse Sncg (mSncg) promoter, resulted in better RGC-specific gene expression in mice and human TM cells compared to the commonly used CAG promoter. Additionally, it was demonstrated that a truncated form of the mSncg promoter, while slightly less RGC specific, could be packaged into an AAV2 vector to drive expression of a CRISPR/Cas9 system to knockdown pro degenerative genes *Ddit3* and *Sarm1*, providing significant neuroprotection in an optic nerve crush model (Wang et al., 2020).

Another study has used a human *SNCG* (*hSNCG*) promoter to drive expression of channelrhodopsin in macaque RGCs (Chaffiol et al., 2017). Interestingly, Wang et al. (2020) found that m*Sncg* led to higher transgene activation than *hSNCG*, even in human RGC cells, indicating that *mSncg* may be an optimal promoter for driving transgene exporession in human gene therapy.

As AAV vectors have a small packaging capacity, further studies have aimed to short promoter elements to maximise space for delivering large cargo. One study highlighted the human synapsin (hSYN) promoter as being able to drive RGC specific transgene expression in mice. However this was not observed in post-mortem human retinal explants, which may be attributable to the low viability of neurons in post-mortem tissue and the presence of the INL (Nieuwenhuis et al., 2023). As mentioned previously, there are likely populations of both healthy and injured RGCs dispersed throughout the glaucomatous retina. RGC specific promoters, like constitutive promoters, come with the drawback of targeting both healthy and injured RGC cells, which can induce a stress response in healthy cells by creating a non-physiological environment. Fujita et al. (2017) demonstrated that transgene expression driven by the Mcp-1 promoter can target stressed RGC cells specifically and shows equivalent transgene expression to the CMV promoter, while reducing stress and death in healthy RGCs. Advancing the development of such targeted promoters could significantly enhance the efficiency of gene therapies for neuroprotection in humans.

### 4.3. Development of non-viral vectors

In recent years, non-viral vectors have come to prominence as an alternative to viral vectors. Non-viral vectors include a range of synthetic and natural systems to transport genetic cargo into cells without using viruses. These include lipids, micelles, metal atom substrates, polymers, and peptides. Non-viral vectors present a safer and more flexible alternative to viral vector mediated gene therapy, as they have a larger packaging capacity and are less immunogenic. However, they face challenges such as lower delivery efficiency and more transient gene expression compared to viral vectors (Hakim et al., 2023). While a detailed discussion of non-viral vectors is beyond the scope of this review, several of the IOP-lowering gene therapy strategies outlined here have utilised non-viral vector systems effectively. For example Dillinger et al. (2018) utilised layer-by-layer coated nanoparticles, with a hyaluronic acid (HA)-based outer layer to deliver CTGF-siRNA to the TM. In addition to circumventing the issue of immunogenicity of viral vectors, this approach has the advantage of targeting CD44, which is upregulated in the glaucomatous anterior chamber, thus providing specificity towards tissue with pathological expression changes. Additionally, Tan et al. (2021) utilised a polydopamine–polyethylenimine nanoparticle vector to deliver an ECM-regulating miRNA to TM cells, which was shown to enhance its stability while causing minimal cytotoxicity. A hyperbranched cationic glycogen derivative vector has also been used to deliver IκBα-siRNA intracamerally in normotensive rats, leading to a transient reduction in IOP (Zeng et al., 2020). Despite these positive developments, it is crucial to optimise nanoparticle vectors to prevent accumulation in the outflow pathways, which could lead to blockages or tissue damage. Developing non-viral vectors for retinal ganglion cells (RGCs) remains more challenging due to the inner limiting membrane (ILM) and the absence of a natural flow pattern towards the target tissue, unlike the flow of AH in the anterior chamber. Nonetheless, as novel non-viral delivery mechanisms continue to be developed, they may provide a superior alternative to viral vectors in the future.

## 5. Conclusion

Gene therapy holds significant promise in glaucoma treatment, offering potential long-term solutions by targeting the disease's underlying causes at a molecular level. Current treatments primarily focus on reducing intraocular pressure (IOP) through medications or surgery, often facing limitations in efficacy and patient adherence. Gene therapy strategies for glaucoma can be broadly classed into those aimed at reducing IOP and those aimed at providing neuroprotection to RGCs. As

most glaucoma is a multifactorial disease, gene therapies aim to target common pathways underlying these hallmarks of disease. In the case of reducing IOP, this can be achieved by increasing ECM turnover or reducing AH production. Neuroprotective strategies target common RGC degenerative pathways such as neurotrophic factor deprivation, oxidative stress, and Wallerian degeneration. While many positive strides have been made in these areas, particularly in rodent model systems, challenges remain in optimising delivery systems for specificity, efficacy, and safety. Continued research in non-human primates, which have eyes more anatomically similar to humans, will be crucial for translating these approaches into clinically useful therapies.

## CRediT authorship contribution statement

**Jeff Henderson:** Writing – original draft, Conceptualization. **Jeffrey O'Callaghan:** Writing – review & editing, Writing – original draft, Conceptualization. **Matthew Campbell:** Writing – review & editing, Conceptualization.

## Data availability

No data was used for the research described in the article.

## References


Abu-Amero, K. K., Kondkar, A. A., Mousa, A., Osman, E. A., & Al-Obeidan, S. A. (2013). Decreased total antioxidants in patients with primary open angle glaucoma. *Current Eye Research, 38*, 959–964.

Alexander, J. P., Samples, J. R., Van Buskirk, E. M., & Acott, T. S. (1991). Expression of matrix metalloproteinases and inhibitor by human trabecular meshwork. *Investigative Ophthalmology & Visual Science, 32*, 172–180.

Amador, C., Shah, R., Ghiam, S., Kramerov, A. A., & Ljubimov, A. V. (2022). Gene therapy in the anterior eye segment. *Current Gene Therapy, 22*, 104–131.

Anderson, D. R. (2003). Collaborative normal tension glaucoma study. *Current Opinion in Ophthalmology, 14*, 86–90.

Asano, Y., Himori, N., Kunikata, H., Yamazaki, M., Shiga, Y., Omodaka, K., Takahashi, H., & Nakazawa, T. (2017). Age-and sex-dependency of the association between systemic antioxidant potential and glaucomatous damage. *Scientific Reports, 7*, 8032.

Beirowski, B., Babetto, E., Coleman, M. P., & Martin, K. R. (2008). The WldS gene delays axonal but not somatic degeneration in a rat glaucoma model. *European Journal of Neuroscience, 28*, 1166–1179.

Bill, A., & Phillips, C. I. (1971). Uveoscleral drainage of aqueous humour in human eyes. *Experimental Eye Research, 12*, 275–281.

Bogner, B., Boye, S. L., Min, S. H., Peterson, J. J., Ruan, Q., Zhang, Z., Reitsamer, H. A., Hauswirth, W. W., & Boye, S. E. (2015). Capsid mutated adeno-associated virus delivered to the anterior chamber results in efficient transduction of trabecular meshwork in mouse and rat. *PLoS One1, 10*, e0128759.

Bond, M., Chase, A. J., Baker, A. H., & Newby, A. C. (2001). Inhibition of transcription factor NF-kappaB reduces matrix metalloproteinase-1, -3 and -9 production by vascular smooth muscle cells. *Cardiovascular Research, 50*, 556–565.

Borrás, T., Rowlette, L. L., Erzurum, S. C., & Epstein, D. L. (1999). 'Adenoviral reporter gene transfer to the human trabecular meshwork does not alter aqueous humor outflow. Relevance for potential gene therapy of glaucoma'. *Gene Therapy, 6*, 515–524.

Borrás, T., Tamm, E. R., & Zigler, J. S., Jr. (1996). Ocular adenovirus gene transfer varies in efficiency and inflammatory response. *Investigative Ophthalmology & Visual Science, 37*, 1282–1293.

Borrás, T., Buie, L. K., & Spiga, M. G. (2016). Inducible scAAV2. GRE. MMP1 lowers IOP long-term in a large animal model for steroid-induced glaucoma gene therapy. *Gene Therapy, 23*, 438–449.

Borrás, T., Gabelt, B. T., Klintworth, G. K., Peterson, J. C., & Kaufman, P. L. (2001). Non-invasive observation of repeated adenoviral GFP gene delivery to the anterior segment of the monkey eye in vivo. *The Journal of Gene Medicine: A Cross-Disciplinary Journal for Research on the Science of Gene Transfer and its Clinical Applications, 3*, 437–449.

Bradley, J. M., Vranka, J., Colvis, C. M., Conger, D. M., Preston Alexander, J., Fisk, A. S., Samples, J. R., & Acott, T. S. (1998). Effect of matrix metalloproteinases activity on outflow in perfused human organ culture. *Investigative Ophthalmology & Visual Science, 39*, 2649–2658.

Bradley, J. MB., Kelley, M. J., Zhu, XiangHong, Anderssohn, A. M., Preston Alexander, J., & Acott, T. S. (2001). Effects of mechanical stretching on trabecular matrix metalloproteinases. *Investigative Ophthalmology & Visual Science, 42*, 1505–1513.

Budenz, D. L., Bennett, J., Alonso, L., & Maguire, A. (1995). In vivo gene transfer into murine corneal endothelial and trabecular meshwork cells. *Investigative Ophthalmology & Visual Science, 36*, 2211–2225.

Buie, L. K., Rasmussen, C. A., Porterfield, E. C., Ramgolam, V. S., Choi, V. W., Markovic-Plese, S., Samulski, R. J., Kaufman, P. L., & Borrás, T. (2010). Self-complementary AAV virus (scAAV) safe and long-term gene transfer in the trabecular meshwork of living rats and monkeys. *Investigative Ophthalmology & Visual Science, 51*, 236–248.

Chaffiol, A., Caplette, R., Jaillard, C., Brazhnikova, E., Desrosiers, M., Dubus, E., Duhamel, L., Macé, E., Marre, O., Benoit, P., Hantraye, P., Bemelmans, A.-P., Bamberg, E., Duebel, J., Sahel, J.-A., Picaud, S., & Dalkara, D. (2017). A new promoter allows optogenetic vision restoration with enhanced sensitivity in macaque retina. *Molecular Therapy, 25*, 2546–2560.

Chase, A. J., Bond, M., Crook, M. F., & Newby, A. C. (2002). Role of nuclear factor-kappa B activation in metalloproteinase-1, -3, and -9 secretion by human macrophages in vitro and rabbit foam cells produced in vivo. *Arteriosclerosis, Thrombosis, and Vascular Biology, 22*, 765–771.

Chen, H., & Weber, A. J. (2001). BDNF enhances retinal ganglion cell survival in cats with optic nerve damage. *Investigative Ophthalmology & Visual Science, 42*, 966–974.

Cheng, L., Sapieha, P., Kittlerova, P., Hauswirth, W. W., & Di Polo, A. (2002). TrkB gene transfer protects retinal ganglion cells from axotomy-induced death in vivo. *The Journal of Neuroscience, 22*, 3977–3986.

Conforti, L., Gilley, J., & Coleman, M. P. (2014). Wallerian degeneration: An emerging axon death pathway linking injury and disease. *Nature Reviews Neuroscience, 15*, 394–409.

Culotta, V. C. (2001). Superoxide dismutase, oxidative stress, and cell metabolism. In E. R. Stadtman, & P. Boon Chock (Eds.), *Current Topics in.* Cellular Regulation (Academic Press).

Groef, D.e., Lies, I. V., Hove, E. D., Stalmans, I., & Moons, L. (2013). MMPs in the trabecular meshwork: Promising targets for future glaucoma therapies? *Investigative Ophthalmology & Visual Science, 54*, 7756–7763.

Dillinger, A. E., Guter, M., Froemel, F., Weber, G. R., Kristin Perkumas, W., Stamer, D., Ohlmann, A., Fuchshofer, R., & Breunig, M. (2018). Intracameral delivery of layer-by-layer coated siRNA nanoparticles for glaucoma therapy. *Small, 14*, 1803239.

Downs, J. C., & Girkin, C. A. (2017). Lamina cribrosa in glaucoma. *Current Opinion in Ophthalmology, 28*, 113–119.

Drewry, M. D., Challa, P., Kuchtey, J. G., Navarro, I., Helwa, I., Yanzhong, Hu., Hongmei, Mu., Daniel Stamer, W., Kuchtey, R. W., & Liu, Y. (2018). Differentially expressed microRNAs in the aqueous humor of patients with exfoliation glaucoma or primary open-angle glaucoma. *Human Molecular Genetics, 27*, 1263–1275.

Fang, F., Zhuang, P., Feng, X., Liu, P., Liu, D., Huang, H., Li, L., Chen, W., Liu, L., Sun, Y., Jiang, H., Ye, J., & Yang, Hu. (2022). NMNAT2 is downregulated in glaucomatous RGCs, and RGC-specific gene therapy rescues neurodegeneration and visual function. *Molecular Therapy, 30*, 1421–1431.

Figley, M. D., & DiAntonio, A. (2020). The SARM1 axon degeneration pathway: Control of the NAD(+) metabolome regulates axon survival in health and disease. *Current Opinion in Neurobiology, 63*, 59–66.

Fischer, A. 2017. 'FDA approves novel gene therapy to treat patients with a rare form of inherited vision loss', *FDA, FDA. gov*.

Fountoulakis, N., Labiris, G., Aristeidou, A., Katsanos, A., Tentes, I., Kortsaris, A., & Kozobolis, V. P. (2013). Tissue inhibitor of metalloproteinase 4 in aqueous humor of patients with primary open angle glaucoma, pseudoexfoliation syndrome and pseudoexfoliative glaucoma and its role in proteolysis imbalance. *BMC Ophthalmology, 13*, 69.

Frank, L., Ventimiglia, R., Anderson, K., Lindsay, R. M., & Rudge, J. S. (1996). BDN F down-regulates neurotrophin responsiveness, TrkB Protein and TrkB mRNA levels in cultured rat hippocampal neurons. *European Journal of Neuroscience, 8*, 1220–1230.

Fujita, K., Nishiguchi, K. M., Shiga, Y., & Nakazawa, T. (2017). Spatially and temporally regulated NRF2 gene therapy using Mcp-1 promoter in retinal ganglion cell injury. *Molecular Therapy Methods & Clinical Development, 5*, 130–141.

Gerometta, R., Spiga, M.-G., Borrás, T., & Candia, O. A. (2010). Treatment of sheep steroid–induced ocular hypertension with a glucocorticoid-inducible MMP1 gene therapy virus. *Investigative Ophthalmology & Visual Science, 51*, 3042–3308.

Ghaffariyeh, A., Honarpisheh, N., Shakiba, Y., Puyan, S., Chamacham, T., Zahedi, F., & Zarrineghbal, M. (2009). Brain-derived neurotrophic factor in patients with normal-tension glaucoma. *Optometry, 80*, 635–638.

Gilley, J., & Coleman, M. P. (2010). Endogenous Nmnat2 is an essential survival factor for maintenance of healthy axons. *PLoS Biology, 8*, e1000300.

Gindina, S., Barron, A. O., Hu, Y., Dimopoulos, A., & Danias, J. (2021). Tissue plasminogen activator rescues steroid-induced outflow facility reduction via non-enzymatic action. *Molecular Vision, 27*, 691–705.

Gindina, S., Hu, Y., Barron, A. O., Qureshi, Z., & Danias, J. (2020). Tissue plasminogen activator attenuates outflow facility reduction in mouse model of juvenile open angle glaucoma. *Experimental Eye Research, 199*, Article 108179.

Goel, M., Picciani, R. G., Lee, R. K., & Bhattacharya, S. K. (2010). Aqueous humor dynamics: A review. *Open Ophthalmol J, 4*, 52–59.

Gonzalez, V., Moreno-Montanes, J., Oll, M., Sall, K. N., Palumaa, K., Dubiner, H., Turman, K., Muñoz-Negrete, F., Ruz, V., & Jimenez, A. I. (2016). Results of Phase IIB SYLTAG clinical trial with bamosiran in patients with glaucoma. *Investigative Ophthalmology & Visual Science, 57*, 3023.

Gould, D. B., Miceli-Libby, L., Savinova, O. V., Torrado, M., Tomarev, S. I., Smith, R. S., & John, S. WM. (2004). Genetically increasing Myoc expression supports a necessary pathologic role of abnormal proteins in glaucoma. *Molecular and Cellular Biology, 24*, 9019–9025.

Guo, T., Guo, L.i., Fan, Y., Fang, L.i., Wei, J., Tan, Y.e., Chen, Y., & Fan, X. (2019). Aqueous humor levels of TGFβ2 and SFRP1 in different types of glaucoma. *BMC Ophthalmology, 19*, 170.

Gupta, V., You, Y., Li, J., Gupta, V., Golzan, M., Klistorner, A., van den Buuse, M., & Graham, S. (2014). BDNF impairment is associated with age-related changes in the inner retina and exacerbates experimental glaucoma. *Biochimica et Biophysica Acta, 1842*, 1567–1578.

Guy, J., Feuer, W. J., Davis, J. L., Porciatti, V., Gonzalez, P. J., Koilkonda, R. D., Yuan, H., Hauswirth, W. W., & Lam, B. L. (2017). Gene therapy for Leber hereditary optic neuropathy: Low-and medium-dose visual results. *Ophthalmology, 124*, 1621–1634.
Hakim, A., Guido, B., Narsineni, L., Chen, D.-W., & Foldvari, M. (2023). Gene therapy strategies for glaucoma from IOP reduction to retinal neuroprotection: Progress towards non-viral systems. *Advanced Drug Delivery Reviews, 196*, Article 114781.
Han, H., Wecker, T., Grehn, F., & Schlunck, G. (2011). Elasticity-dependent modulation of TGF-β responses in human trabecular meshwork cells. *Investigative Ophthalmology & Visual Science, 52*, 2889–2896.
Han, I. C., Cheng, J. L., Burnight, E. R., Ralston, C. L., Fick, J. L., Thomsen, G. J., Tovar, E. F., Russell, S. R., Sohn, E. H., Mullins, R. F., Stone, E. M., Tucker, B.d. A., & Wiley, L. A. (2020). Retinal tropism and transduction of adeno-associated virus varies by serotype and route of delivery (Intravitreal, Subretinal, or Suprachoroidal) in rats. *Human Gene Therapy, 31*, 1288–1299.
Han, J. A., Frishman, W. H., Sun, S. W., Palmiero, P.-M., & Petrillo, R. (2008). Cardiovascular and respiratory considerations with pharmacotherapy of glaucoma and ocular hypertension. *Cardiology in Review, 16*.
Hill, L. J., Mead, B., Thomas, C. N., Foale, S., Feinstein, E., Berry, M., Blanch, R. J., Ahmed, Z., & Logan, A. (2018). TGF-β-induced IOP elevations are mediated by RhoA in the early but not the late fibrotic phase of open angle glaucoma. *Molecular Vision, 24*, 712–726.
Honjo, M., Tanihara, H., Inatani, M., Kido, N., Sawamura, T., Yue, B. Y. J. T., Narumiya, S.u., & Honda, Y. (2001). Effects of Rho-Associated Protein Kinase Inhibitor Y-27632 on Intraocular Pressure and Outflow Facility. *Investigative Ophthalmology & Visual Science, 42*, 137–144.
Hori, J. (2008). Mechanisms of immune privilege in the anterior segment of the eye: What we learn from corneal transplantation. *Journal of Ocular Biology, Diseases, and Informatics, 1*, 94–100.
Howell, G. R., Libby, R. T., Jakobs, T. C., Smith, R. S., Campbell Phalan, F., Barter, J. W., Barbay, J. M., Marchant, J. K., Mahesh, N., & Porciatti, V. (2007). Axons of retinal ganglion cells are insulted in the optic nerve early in DBA/2J glaucoma. *The Journal of Cell Biology, 179*, 1523–1537.
Hurley, D. J., Normile, C., Irnaten, M., & O'Brien, C. (2022). The intertwined roles of oxidative stress and endoplasmic reticulum stress in glaucoma. *Antioxidants, 11*, 886.
Izzotti, A., Longobardi, M., Cartiglia, C., Rathschuler, F., & Saccà, S. C. (2011). Trabecular meshwork gene expression after selective laser trabeculoplasty. *PLoS One1, 6*, e20110.
Jain, A., Zode, G., Kasetti, R. B., Ran, F. A., Yan, W., Sharma, T. P., Bugge, K., Searby, C. C., Fingert, J. H., Zhang, F., Clark, A. F., & Sheffield, V. C. (2017). CRISPR-Cas9–based treatment of myocilin-associated glaucoma. *Proceedings of the National Academy of Sciences, 114*, 11199–11204.
Jayaram, H., Phillips, J. I., Lozano, D. C., Choe, T. E., Cepurna, W. O., Johnson, E. C., Morrison, J. C., Gattey, D. M., Saugstad, J. A., & Keller, K. E. (2017). Comparison of microRNA expression in aqueous humor of normal and primary open-angle glaucoma patients using PCR arrays: A pilot study. *Investigative Ophthalmology & Visual Science, 58*, 2884–2890.
Jiang, W., Tang, L., Zeng, J., & Chen, B. (2016). Adeno-associated virus mediated SOD gene therapy protects the retinal ganglion cells from chronic intraocular pressure elevation induced injury via attenuating oxidative stress and improving mitochondrial dysfunction in a rat model. *American Journal of Translational Research, 8*, 799–810.
Joe, M. K., Sohn, S., Hur, W., Moon, Y., Choi, Y. R., & Kee, C. (2003). Accumulation of mutant myocilins in ER leads to ER stress and potential cytotoxicity in human trabecular meshwork cells. *Biochemical and Biophysical Research Communications, 312*, 592–600.
Johnson, M., McLaren, J. W., & Overby, D. R. (2017). Unconventional aqueous humor outflow: A review. *Experimental Eye Research, 158*, 94–111.
Jonas, J. B., & Wang, N. (2013). Cerebrospinal fluid pressure and glaucoma. *J. Ophthalmic Vis. Res., 8*, 257–263.
Ju, W. K., Kim, K. Y., Lindsey, J. D., Angert, M., Duong-Polk, K. X., Scott, R. T., Kim, J. J., Kukhmazov, I., Ellisman, M. H., Perkins, G. A., & Weinreb, R. N. (2008). Intraocular pressure elevation induces mitochondrial fission and triggers OPA1 release in glaucomatous optic nerve. *Investigative Ophthalmology & Visual Science, 49*, 4903–4911.
Junglas, B., Kuespert, S., Seleem, A. A., Struller, T., Ullmann, S., Bösl, M., Bosserhoff, A., Köstler, J., Wagner, R., Tamm, E. R., & Fuchshofer, R. (2012). Connective tissue growth factor causes glaucoma by modifying the actin cytoskeleton of the trabecular meshwork. *The American Journal of Pathology, 180*, 2386–2403.
Junglas, B., Yu, A. H., Welge-Lüssen, U., Tamm, E. R., & Fuchshofer, R. (2009). Connective tissue growth factor induces extracellular matrix deposition in human trabecular meshwork cells. *Experimental Eye Research, 88*, 1065–1075.
Karali, A., Russell, P., Stefani, F. H., & Tamm, E. R. (2000). Localization of myocilin/trabecular meshwork–inducible glucocorticoid response protein in the human eye. *Investigative Ophthalmology & Visual Science, 41*, 729–740.
Keller, K. E., & Acott, T. S. (2013). The juxtacanalicular region of ocular trabecular meshwork: A tissue with a unique extracellular matrix and specialized function. *J Ocul Biol, 1*, 3.
Keller, K. E., Aga, M., Bradley, J. M., Kelley, M. J., & Acott, T. S. (2009). Extracellular matrix turnover and outflow resistance. *Experimental Eye Research, 88*, 676–682.
Kelley, M. J., Rose, A. Y., Song, K., Chen, Y., Bradley, J. M., Rookhuizen, D., & Acott, T. S. (2007). Synergism of TNF and IL-1 in the induction of matrix metalloproteinase-3 in trabecular meshwork. *Investigative Ophthalmology & Visual Science, 48*, 2634–2643.
Kelly, R. A., Perkumas, K. M., Matthew Campbell, G., Jane Farrar, W., Stamer, D., Humphries, P., O'Callaghan, J., & O'Brien, C. J. (2021). Fibrotic changes to Schlemm's canal endothelial cells in glaucoma. *International Journal of Molecular Sciences, 22*, 9446.
Khaw, P. T., Shah, P., & Elkington, A. R. (2004). Glaucoma–1: Diagnosis. *BMJ, 328*, 97–99.
Khouri, A. S., Serle, J. B., Bacharach, J., Usner, D. W., Lewis, R. A., Braswell, P., Kopczynski, C. C., & Heah, T. (2019). Once-daily netarsudil versus twice-daily timolol in patients with elevated intraocular pressure: The randomized phase 3 ROCKET-4 study. *American Journal of Ophthalmology, 204*, 97–104.
Kim, B. S., Savinova, O. V., Reedy, M. V., Martin, J., Lun, Y.i., Gan, L., Smith, R. S., Tomarev, S. I., John, S. WM., & Johnson, R. L. (2001). Targeted disruption of the myocilin gene (Myoc) suggests that human glaucoma-causing mutations are gain of function. *Molecular and Cellular Biology, 21*, 7707–7713.
Klein, B. EK., Klein, R., Sponsel, W. E., Franke, T., Cantor, L. B., Martone, J., & Menage, M. J. (1992). Prevalence of glaucoma: The Beaver Dam eye study. *Ophthalmology, 99*, 1499–1504.
Ko, M. L., Hu, D. N., Ritch, R., Sharma, S. C., & Chen, C. F. (2001). Patterns of retinal ganglion cell survival after brain-derived neurotrophic factor administration in hypertensive eyes of rats. *Neuroscience Letters, 305*, 139–142.
Komáromy, A. M. (2020). CRISPR-Cas9 disruption of aquaporin 1: An alternative to glaucoma eye drop therapy? *Molecular Therapy, 28*, 706–778.
Lan, Y. Q., Zhang, C., Xiao, J. H., Zhuo, Y. H., Guo, H., Peng, W., & Ge, J. (2009). Suppression of IkappaBalpha increases the expression of matrix metalloproteinase-2 in human ciliary muscle cells. *Molecular Vision, 15*, 1977–1987.
Lee, B. L., Bathija, R., & Weinreb, R. N. (1998). The definition of normal-tension glaucoma. *Journal of Glaucoma, 7*, 366–371.
Lee, S. H., Sim, K. S., Kim, C. Y., & Park, T. K. (2019). Transduction pattern of AAVs in the trabecular meshwork and anterior-segment structures in a rat model of ocular hypertension. *Molecular Therapy - Methods & Clinical Development, 14*, 197–205.
Liu, P., Chen, W., Jiang, H., Huang, H., Liu, L., Fang, F., Li, L., Feng, X., Liu, D., Dalal, R., Sun, Y., Jafar-Nejad, P., Ling, K., Rigo, F., Ye, J., & Hu, Y. (2023). Differential effects of SARM1 inhibition in traumatic glaucoma and EAE optic neuropathies. *Molecular Therapy - Nucleic Acids, 32*, 13–27.
Liu, Y., & Vollrath, D. (2004). Reversal of mutant myocilin non-secretion and cell killing: Implications for glaucoma. *Human Molecular Genetics, 13*, 1193–1204.
Lo, W. R., Rowlette, L. L., Caballero, M., Ping Yang, M., Hernandez, R., & Borrás, T. (2003). Tissue differential microarray analysis of dexamethasone induction reveals potential mechanisms of steroid glaucoma. *Investigative Ophthalmology & Visual Science, 44*, 473–485.
Martin, K. RG., Quigley, H. A., Zack, D. J., Levkovitch-Verbin, H., Kielczewski, J., Valenta, D., Baumrind, L., Pease, M. E., Klein, R. L., & Hauswirth, W. W. (2003). Gene therapy with brain-derived neurotrophic factor as a protection: Retinal ganglion cells in a rat glaucoma model. *Investigative Ophthalmology & Visual Science, 44*, 4357–4365.
Martínez, T., González, M. V., Roehl, I., Wright, N., Pañeda, C., & Jiménez, A. I. (2014). In vitro and in vivo efficacy of SYL040012, a novel siRNA compound for treatment of glaucoma. *Molecular Therapy, 22*, 81–91.
Menaa, F., Braghini, C. A., Vasconcellos, J. P., Menaa, B., Costa, V. P., Figueiredo, E. S., & Melo, M. B. (2011). Keeping an eye on myocilin: A complex molecule associated with primary open-angle glaucoma susceptibility. *Molecules, 16*, 5402–5421.
Millar, J. C., Sundaresan, Y., Zode, G. S., & Clark, A. F. (2023). Viral vector-induced ocular hypertension in mice. *Methods in Molecular Biology, 2708*, 77–97.
Mittag, T. W., Danias, J., Pohorenec, G., Yuan, H.-M., Burakgazi, E., Chalmers-Redman, R., Podos, S. M., & Tatton, W. G. (2000). Retinal damage after 3 to 4 months of elevated intraocular pressure in a rat glaucoma model. *Investigative Ophthalmology & Visual Science, 41*, 3451–3459.
Moreno, M. C., Campanelli, J., Sande, P., Sánez, D. A., Keller Sarmiento, M. I., & Rosenstein, R. E. (2004). Retinal oxidative stress induced by high intraocular pressure. *Free Radical Biology & Medicine, 37*, 803–812.
Moreno-Montañés, J., Sádaba, B., Ruz, V., Gómez-Guiu, A., Zarranz, J., González, M. V., Pañeda, C., & Jimenez, A. I. (2014). Phase I clinical trial of SYL040012, a small interfering RNA targeting β-adrenergic receptor 2, for lowering intraocular pressure. *Molecular Therapy, 22*, 226–232.
Murphy, C. C., Burnett, C. A. M., Spry, P. G. D., Broadway, D. C., & Diamond, J. P. (2003). A two centre study of the dose-response relation for transscleral diode laser cyclophotocoagulation in refractory glaucoma. *British Journal of Ophthalmology, 87*, 1252.
Mutsaers, S. E., Bishop, J. E., McGrouther, G., & Laurent, G. J. (1997). Mechanisms of tissue repair: From wound healing to fibrosis. *The International Journal of Biochemistry & Cell Biology, 29*, 5–17.
Newman, Nancy J, Patrick Yu-Wai-Man, Prem S Subramanian, Mark L Moster, An-Guor Wang, Sean P Donahue, Bart P Leroy, Valerio Carelli, Valerie Biousse, Catherine Vignal-Clermont, Robert C Sergott, Alfredo A Sadun, Gema Rebolleda Fernández, Bart K Chwalisz, Rudrani Banik, Fabienne Bazin, Michel Roux, Eric D Cox, Magali Taiel, José-Alain Sahel, and the LHON REFLECT Study Group. 2022. 'Randomized trial of bilateral gene therapy injection for m.11778G>A MT-ND4 Leber optic neuropathy', *Brain*, 146: 1328-41.
Newman-Casey, P. A., Robin, A. L., Blachley, T., Farris, K., Heisler, M., Resnicow, K., & Lee, P. P. (2015). The most common barriers to glaucoma medication adherence: A cross-sectional survey. *Ophthalmology, 122*, 1308–1316.
Nieuwenhuis, B., Laperrousaz, E., Tribble, J. R., Verhaagen, J., Fawcett, J. W., Martin, K. R., Williams, P. A., & Osborne, A. (2023). Improving adeno-associated viral (AAV) vector-mediated transgene expression in retinal ganglion cells: Comparison of five promoters. *Gene therapy, 30*, 503–519.
Nishijima, E., Honda, S., Kitamura, Y., Namekata, K., Kimura, A., Guo, X., Azuchi, Y., Harada, C., Murakami, A., Matsuda, A., Nakano, T., Parada, L. F., & Harada, T. (2023). Vision protection and robust axon regeneration in glaucoma models by membrane-associated Trk receptors. *Molecular Therapy, 31*, 810–824.

Noecker, R. S., Dirks, M. S., Choplin, N. T., Bernstein, P., Batoosingh, A. L., & Whitcup, S. M. (2003). A six-month randomized clinical trial comparing the intraocular pressure-lowering efficacy of bimatoprost and latanoprost in patients with ocular hypertension or glaucoma. *American Journal of Ophthalmology, 135*, 55–63.

Nucci, C., Di Pierro, D., Varesi, C., Ciuffoletti, E., Russo, R., Gentile, R., Cedrone, C., Pinazo Duran, M. D., Coletta, M., & Mancino, R. (2013). Increased malondialdehyde concentration and reduced total antioxidant capacity in aqueous humor and blood samples from patients with glaucoma. *Molecular Vision, 19*, 1841–1846.

O'Callaghan, J., Cassidy, P. S., & Humphries, P. (2017). Open-angle glaucoma: Therapeutically targeting the extracellular matrix of the conventional outflow pathway. *Expert Opinion on Therapeutic Targets, 21*, 1037–1050.

O'Callaghan, J., Darragh, E., Crosbie, P., Cassidy, S., Sherwood, J. M., Flügel-Koch, C., Lütjen-Drecoll, E., Humphries, M. M., Reina-Torres, E., Wallace, D., Kiang, A.-S., Matthew Campbell, W., Stamer, D., Overby, D. R., O'Brien, C., Tam, L. C. S., & Humphries, P. (2017). Therapeutic potential of AAV-mediated MMP-3 secretion from corneal endothelium in treating glaucoma. *Human Molecular Genetics, 26*, 1230–1246.

O'Callaghan, Jeffrey, Conor Delaney, Merissa O'Connor, Joseph van Batenburg-Sherwood, Martin Schicht, Elke Lütjen-Drecoll, Natalie Hudson, Sorcha Ni Dhubhghaill, Peter Humphries, Chris Stanley, Annahita Keravala, Thomas Chalberg, Matthew S. Lawrence, and Matthew Campbell. 2023. 'Matrix metalloproteinase-3 (MMP-3)–mediated gene therapy for glaucoma', *Science Advances*, 9: eadf6537.

Oddone, F., Roberti, G., Micera, A., Busanello, A., Bonini, S., Quaranta, L., Agnifili, L., & Manni, G. (2017). Exploring serum levels of brain derived neurotrophic factor and nerve growth factor across glaucoma stages. *PLoS One1, 12*, e0168565.

Oh, D.-J., Martin, J. L., Williams, A. J., Russell, P., Birk, D. E., & Rhee, D. J. (2006). Effect of latanoprost on the expression of matrix metalloproteinases and their tissue inhibitors in human trabecular meshwork cells. *Investigative Ophthalmology & Visual Science, 47*, 3887–3895.

Okeke, C. O., Quigley, H. A., Jampel, H. D., Ying, G. S., Plyler, R. J., Jiang, Y., & Friedman, D. S. (2009). Adherence with topical glaucoma medication monitored electronically the Travatan Dosing Aid study. *Ophthalmology, 116*, 191–199.

Osborne, A., Wang, A. X. Z., Tassoni, A., Widdowson, P. S., & Martin, K. R. (2018). Design of a novel gene therapy construct to achieve sustained brain-derived neurotrophic factor signaling in neurons. *Human Gene Therapy, 29*, 828–841.

Osborne, A., Khatib, T. Z., Songra, L., Barber, A. C., Hall, K., Kong, G. Y. X., Widdowson, P. S., & Martin, K. R. (2018). Neuroprotection of retinal ganglion cells by a novel gene therapy construct that achieves sustained enhancement of brain-derived neurotrophic factor/tropomyosin-related kinase receptor-B signaling. *Cell Death & Disease, 9*, 1007.

Overby, D. R., Bertrand, J., Tektas, O.-Y., Boussommier-Calleja, A., Martin Schicht, C., Ethier, R., Woodward, D. F., Daniel Stamer, W., & Lütjen-Drecoll, E. (2014). Ultrastructural changes associated with dexamethasone-induced ocular hypertension in mice. *Investigative Ophthalmology & Visual Science, 55*, 4922–4933.

Ozdemir, G., Tolun, F. I., Gul, M., & Imrek, S. (2009). Retinal oxidative stress induced by intraocular hypertension in rats may be ameliorated by brimonidine treatment and N-acetyl cysteine supplementation. *Journal of Glaucoma, 18*, 662–665.

Pang, I.-H., Fleenor, D. L., Hellberg, P. E., Stropki, K., McCartney, M. D., & Clark, A. F. (2003). Aqueous outflow-enhancing effect of tert-butylhydroquinone: Involvement of AP-1 activation and MMP-3 expression. *Investigative Ophthalmology & Visual Science, 44*, 3502–3510.

Panieri, E., Pinho, S. A., Afonso, G. J. M., Oliveira, P. J., Cunha-Oliveira, T., & Saso, L. (2022). NRF2 and mitochondrial function in cancer and cancer stem cells. *Cells, 11*.

Patil, S. V., Kaipa, B. R., Ranshing, S., Yogapriya Sundaresan, J., Millar, C., Nagarajan, B., Kiehlbauch, C., Zhang, Q., Jain, A., Searby, C. C., Scheetz, T. E., Clark, A. F., Sheffield, V. C., & Zode, G. S. (2024). Lentiviral mediated delivery of CRISPR/Cas9 reduces intraocular pressure in a mouse model of myocilin glaucoma. *Scientific Reports, 14*, 6958.

Pattabiraman, P. P., Inoue, T., & Rao, P. V. (2015). Elevated intraocular pressure induces Rho GTPase mediated contractile signaling in the trabecular meshwork. *Experimental Eye Research, 136*, 29–33.

Pease, M. E., McKinnon, S. J., Quigley, H. A., Kerrigan-Baumrind, L. A., & Zack, D. J. (2000). Obstructed axonal transport of BDNF and its receptor TrkB in experimental glaucoma. *Investigative Ophthalmology & Visual Science, 41*, 764–774.

Porter, K. M., Epstein, D. L., & Liton, P. B. (2012). Up-regulated expression of extracellular matrix remodeling genes in phagocytically challenged trabecular meshwork cells. *PLoS One1, 7*, e34792.

Quigley, H. A., Addicks, E. M., Green, W. R., & Maumenee, A. E. (1981). Optic nerve damage in human glaucoma. II. The site of injury and susceptibility to damage. *Archives of Ophthalmology, 99*, 635–649.

Quigley, H. A., & Broman, A. T. (2006). The number of people with glaucoma worldwide in 2010 and 2020. *The British Journal of Ophthalmology, 90*, 262–267.

Quigley, H. A., McKinnon, S. J., Zack, D. J., Pease, M. E., Kerrigan-Baumrind, L. A., Kerrigan, D. F., & Mitchell, R. S. (2000). Retrograde axonal transport of BDNF in retinal ganglion cells is blocked by acute IOP elevation in rats. *Investigative Ophthalmology & Visual Science, 41*, 3460–3466.

Ramachandran, P. S., Lee, V., Wei, Z., Song, J. Y., Casal, G., Cronin, T., Willett, K., Huckfeldt, R., Morgan, J. I. W., Aleman, T. S., Maguire, A. M., & Bennett, J. (2016). Evaluation of dose and safety of AAV7m8 and AAV8BP2 in the non-human primate retina. *Human Gene Therapy, 28*, 154–167.

Ramkumar, V., Jhaveri, K. A., Xie, X., Jajoo, S., & Toth, L. A. (2011). Nuclear factor κB and adenosine receptors: Biochemical and behavioral profiling. *Current Neuropharmacology, 9*, 342–349.

Ren, R., Li, Y., Liu, Z., Liu, K., & He, S. (2012). Long-term rescue of rat retinal ganglion cells and visual function by AAV-mediated BDNF expression after acute elevation of intraocular pressure. *Investigative Ophthalmology & Visual Science, 53*, 1003–1011.

Rodriguez-Estevez, L., Asokan, P., & Borrás, T. (2020). Transduction optimization of AAV vectors for human gene therapy of glaucoma and their reversed cell entry characteristics. *Gene Therapy, 27*, 127–142.

Rönkkö, S., Rekonen, P., Kaarniranta, K., Puustjärvi, T., Teräsvirta, M., & Uusitalo, H. (2007). Matrix metalloproteinases and their inhibitors in the chamber angle of normal eyes and patients with primary open-angle glaucoma and exfoliation glaucoma. *Graefe's Archive for Clinical and Experimental Ophthalmology, 245*, 697–704.

Rotchford, A. P., Jayasawal, R., Madhusudhan, S., Ho, S., King, A. J., & Vernon, S. A. (2010). Transscleral diode laser cycloablation in patients with good vision. *British Journal of Ophthalmology, 94*, 1180.

Salvetat, M. L., Pellegrini, F., Spadea, L., Salati, C., & Zeppieri, M. (2023). Pharmaceutical approaches to normal tension glaucoma. *Pharmaceuticals, 16*, 1172.

Scherer, W. J. (2002). A retrospective review of non-responders to latanoprost. *Journal of Ocular Pharmacology and Therapeutics, 18*, 287–291.

Schey, Kevin L., Zhen Wang, Jamie L. Wenke, and Ying Qi. 2014. 'Aquaporins in the eye: Expression, function, and roles in ocular disease', *Biochimica et Biophysica Acta (BBA) - General Subjects*, 1840: 1513-23.

Schlötzer-Schrehardt, Ursula, Jürgen Lommatzsch, Michael Küchle, Anastasios G. P. Konstas, and Gottfried O. H. Naumann. 2003. 'Matrix Metalloproteinases and Their Inhibitors in Aqueous Humor of Patients with Pseudoexfoliation Syndrome/Glaucoma and Primary Open-Angle Glaucoma', *Investigative Ophthalmology & Visual Science*, 44: 1117-25.

Shepard, A. R., Millar, J. C., Pang, I. H., Jacobson, N., Wang, W. H., & Clark, A. F. (2010). Adenoviral gene transfer of active human transforming growth factor-{beta}2 elevates intraocular pressure and reduces outflow facility in rodent eyes. *Investigative Ophthalmology & Visual Science, 51*, 2067–2076.

Sidjanin, D. J., McCarty, C. A., Patchett, R., Smith, E., & Wilke, R. A. (2008). Pharmacogenetics of ophthalmic topical β-blockers. *Personalized Medicine, 5*, 377–385.

Sit, S. T., & Manser, E. (2011). Rho GTPases and their role in organizing the actin cytoskeleton. *Journal of Cell Science, 124*, 679–683.

Sommerfeld, M. T., Schweigreiter, R., Barde, Y. A., & Hoppe, E. (2000). 'Down-regulation of the neurotrophin receptor TrkB following ligand binding. Evidence for an involvement of the proteasome and differential regulation of TrkA and TrkB'. *Journal of Biological Chemistry, 275*, 8982–8990.

Spiga, M.-G., & Borrás, T. (2010). Development of a gene therapy virus with a glucocorticoid-inducible MMP1 for the treatment of steroid glaucoma. *Investigative Ophthalmology & Visual Science, 51*, 3029–3041.

Starr, C., & Chen, B.o. (2023). Adeno-associated virus mediated gene therapy for neuroprotection of retinal ganglion cells in glaucoma. *Vision Research, 206*, Article 108196.

Stone, E. M., Fingert, J. H., Alward, W. L. M., Nguyen, T. D., Polansky, J. R., Sunden, S. L. F., Nishimura, D., Clark, A. F., Nystuen, A., Nichols, B. E., Mackey, D. A., Ritch, R., Kalenak, J. W., Randy Craven, E., & Sheffield, V. C. (1997). Identification of a gene that causes primary open angle glaucoma. *Science, 275*, 668–670.

Su, Wenru, Zuohong Li, Yu Jia, and Yehong Zhuo. 2014. 'Rapamycin is neuroprotective in a rat chronic hypertensive glaucoma model', *PLoS One*, 9: e99719.

Sulak, R., Liu, X., & Smedowski, A. (2024). The concept of gene therapy for glaucoma: The dream that has not come true yet. *Neural Regeneration Research, 19*, 92–99.

Sun, D., Zhan, Z., Zeng, R., Liu, X., Wang, B., Yang, F., Huang, S., Li, Y., Yang, Z., Su, Y., & Lan, Y. (2022). 'Long-term and potent IOP-lowering effect of IκBα-siRNA in a nonhuman primate model of chronic ocular hypertension'. *iScience, 25*, Article 104149.

Surgucheva, I., Weisman, A. D., Goldberg, J. L., Shnyra, A., & Surguchov, A. (2008). Gamma-synuclein as a marker of retinal ganglion cells. *Molecular Vision, 14*, 1540–1548.

Takahashi, H., Noda, S., Imamura, Y., Nagasawa, A., Kubota, R., Mashima, Y., Kudoh, J., Oguchi, Y., & Shimizu, N. (1998). Mouse Myocilin (Myoc) gene expression in ocular Tissues1. *Biochemical and Biophysical Research Communications, 248*, 104–119.

Takahashi, K., Igarashi, T., Miyake, K., Kobayashi, M., Yaguchi, C., Iijima, O., Yamazaki, Y., Katakai, Y., Miyake, N., Kameya, S., Shimada, T., Takahashi, H., & Okada, T. (2017). Improved intravitreal AAV-mediated inner retinal gene transduction after surgical internal limiting membrane peeling in cynomolgus monkeys. *Molecular Therapy, 25*, 296–302.

Tan, C., Jia, F., Zhang, P., Sun, X., Qiao, Y., Chen, X., Wang, Y., Chen, J., & Lei, Y. (2021). A miRNA stabilizing polydopamine nano-platform for intraocular delivery of miR-21-5p in glaucoma therapy. *Journal of Materials Chemistry B, 9*, 3335–3345.

Tan, C., Song, M., Stamer, W. D., Qiao, Y., Chen, X., Sun, X., Lei, Y., & Chen, J. (2020). miR-21-5p: A viable therapeutic strategy for regulating intraocular pressure. *Experimental Eye Research, 200*, Article 108197.

Tanito, M., Kaidzu, S., Takai, Y., & Ohira, A. (2016). Association between systemic oxidative stress and visual field damage in open-angle glaucoma. *Scientific Reports, 6*, 25792.

Tektas, O.-Y., & Lütjen-Drecoll, E. (2009). Structural changes of the trabecular meshwork in different kinds of glaucoma. *Experimental Eye Research, 88*, 769–775.

Teng, H. K., Teng, K. K., Lee, R., Wright, S., Tevar, S., Almeida, R. D., Kermani, P., Torkin, R., Chen, Z. Y., Lee, F. S., Kraemer, R. T., Nykjaer, A., & Hempstead, B. L. (2005). ProBDNF induces neuronal apoptosis via activation of a receptor complex of p75NTR and sortilin. *The Journal of Neuroscience, 25*, 5455–5463.

Tervo, D Gowanlock R, Bum-Yeol Hwang, Sarada Viswanathan, Thomas Gaj, Maria Lavzin, Kimberly D Ritola, Sarah Lindo, Susan Michael, Elena Kuleshova, and David

Ojala. 2016. 'A designer AAV variant permits efficient retrograde access to projection neurons', *Neuron*, 92: 372-82.
Tham, Y. C., Li, X., Wong, T. Y., Quigley, H. A., Aung, T., & Cheng, C. Y. (2014). Global prevalence of glaucoma and projections of glaucoma burden through 2040: A systematic review and meta-analysis. *Ophthalmology, 121*, 2081–2090.
To, C. H., Kong, C. W., Chan, C. Y., Shahidullah, M., & Do, C. W. (2002). The mechanism of aqueous humour formation. *Clinical & Experimental Optometry, 85*, 335–349.
Toney, L. M., Cattoretti, G., Graf, J. A., Merghoub, T., Pandolfi, P. P., Dalla-Favera, R., Ye, B. H., & Dent, A. L. (2000). BCL-6 regulates chemokine gene transcription in macrophages. *Nature Immunology, 1*, 214–220.
Toris, C. B., Yablonski, M. E., Wang, Y. L., & Camras, C. B. (1999). Aqueous humor dynamics in the aging human eye. *American Journal of Ophthalmology, 127*, 407–412.
Tshilenge, K.-T., Ameline, B., Weber, M., Mendes-Madeira, A., Nedellec, S., Biget, M., Provost, N., Libeau, L., Blouin, V., & Deschamps, J.-Y. (2016). Vitrectomy before intravitreal injection of AAV2/2 vector promotes efficient transduction of retinal ganglion cells in dogs and nonhuman primates. *Human Gene Therapy Methods, 27*, 122–134.
Vittal, V., Rose, A., Gregory, K. E., Kelley, M. J., & Acott, T. S. (2005). Changes in gene expression by trabecular meshwork cells in response to mechanical stretching. *Investigative Ophthalmology & Visual Science, 46*, 2857–2868.
Wallace, D. M., Murphy-Ullrich, J. E., Crawford Downs, J., & O'Brien, C. J. (2014). The role of matricellular proteins in glaucoma. *Matrix Biology, 37*, 174–182.
Wan, X., Pei, H., Zhao, M.-J., Yang, S., Wei-kun, Hu., He, H., Ma, S.-q., Zhang, G.e., Dong, X.-Y., & Chen, C. (2016). Efficacy and safety of rAAV2-ND4 treatment for Leber's hereditary optic neuropathy. *Scientific Reports, 6*, 21587.
Wang, J. T., Medress, Z. A., Vargas, M. E., & Barres, B. A. (2015). Local axonal protection by WldS as revealed by conditional regulation of protein stability. *Proceedings of the National Academy of Sciences of the United States of America, 112*, 10093–10100.
Wang, J., Zhai, Q., Chen, Y., Lin, E., Gu, W., McBurney, M. W., & He, Z. (2005). A local mechanism mediates NAD-dependent protection of axon degeneration. *The Journal of Cell Biology, 170*, 349–355.
Wang, Q., Zhuang, P., Huang, H., Li, L., Liu, L., Webber, H. C., Dalal, R., Siew, L., Fligor, C. M., Chang, K. C., Nahmou, M., Kreymerman, A., Sun, Y., Meyer, J. S., Goldberg, J. L., & Hu, Y. (2020). Mouse γ-Synuclein Promoter-Mediated Gene Expression and Editing in Mammalian Retinal Ganglion Cells. *The Journal of Neuroscience, 40*, 3896–3914.
Webb, J. G., Husain, S., Yates, P. W., & Crosson, C. E. (2006). Kinin modulation of conventional outflow facility in the bovine eye. *Journal of Ocular Pharmacology & Therapeutics, 22*, 310–336.
Weinreb, R. N., Aung, T., & Medeiros, F. A. (2014). The pathophysiology and treatment of glaucoma: A review. *Journal of the American Medical Association, 311*, 1901–1911.
Wight, T. N., & Potter-Perigo, S. (2011). 'The extracellular matrix: An active or passive player in fibrosis?'. *American Journal of Physiology-Gastrointestinal and Liver Physiology, 301*, G950–G955.
Williams, P. A., Harder, J. M., Foxworth, N. E., Cochran, K. E., Philip, V. M., Porciatti, V., Smithies, O., & John, S. W. (2017). Vitamin B(3) modulates mitochondrial vulnerability and prevents glaucoma in aged mice. *Science, 355*, 756–760.
Wu, J., Bell, O. H., Copland, D. A., Young, A., Pooley, J. R., Maswood, R., Evans, R. S., Khaw, P. T., Ali, R. R., Dick, A. D., & Chu, C. J. (2020). Gene therapy for glaucoma by ciliary body aquaporin 1 disruption using CRISPR-Cas9. *Molecular Therapy, 28*, 820–889.
Xiong, W., MacColl Garfinkel, A. E., Li, Y., Benowitz, L. I., & Cepko, C. L. (2015). NRF2 promotes neuronal survival in neurodegeneration and acute nerve damage. *The Journal of Clinical Investigation, 125*, 1433–1445.
Yam, G.-F., Gaplovska-Kysela, K., Zuber, C., & Roth, J. (2007). Aggregated myocilin induces russell bodies and causes apoptosis: Implications for the pathogenesis of myocilin-caused primary open-angle glaucoma. *The American Journal of Pathology, 170*, 100–119.
Yin, Lu., Greenberg, K., Hunter, J. J., Dalkara, D., Kolstad, K. D., Masella, B. D., Wolfe, R., Visel, M., Stone, D., & Libby, R. T. (2011). Intravitreal injection of AAV2 transduces macaque inner retina. *Investigative Ophthalmology & Visual Science, 52*, 2775–2783.
Zeng, R., Li, J., Gong, H., Luo, J., Li, Z., Ou, Z., Zhang, S., Yang, L., & Lan, Y. (2020). Hyperbranched cationic glycogen derivative-mediated IκBα gene silencing regulates the uveoscleral outflow pathway in rats. *Biomed Research International, 2020*, 8206849.
Zhang, D., Vetrivel, L., & Verkman, A. S. (2002). Aquaporin deletion in mice reduces intraocular pressure and aqueous fluid production. *Journal of General Physiology, 119*, 561–569.
Zhao, J., Solano, M. M., Oldenburg, C. E., Liu, T., Wang, Y., Wang, N., & Lin, S. C. (2019). Prevalence of normal-tension glaucoma in the Chinese population: A systematic review and meta-analysis. *American Journal of Ophthalmology, 199*, 101–110.
Zhao, X., Ramsey, K. E., Stephan, D. A., & Russell, P. (2004). Gene and protein expression changes in human trabecular meshwork cells treated with transforming growth factor-β. *Investigative Ophthalmology & Visual Science, 45*, 4023–4034.
Zheng, Y. J., Dilbeck, M. D., Economides, J. R., & Horton, J. C. (2024). Permanent transduction of retinal ganglion cells by rAAV2-retro. *Experimental Eye Research, 240*, Article 109793.
Zode, G. S., Kuehn, M. H., Nishimura, D. Y., Searby, C. C., Mohan, K., Grozdanic, S. D., Bugge, K., Anderson, M. G., Clark, A. F., Stone, E. M., & Sheffield, V. C. (2011). Reduction of ER stress via a chemical chaperone prevents disease phenotypes in a mouse model of primary open angle glaucoma. *The Journal of Clinical Investigation, 121*, 3542–3553.